Faculty of Engineering

Department of Architecture and Built Environment

A Novel High Capacity Space Efficient Heat Storage System for Domestic Application

Elamin Awad, R. Mohamed

(BSc, MSc)

August 2018

Thesis submitted in partial fulfilment of the requirement leading to the award of Doctorate of Philosophy in Sustainable Energy Technology

Table of content

List of Figures

List of Tables

List of Publications

Publications in International Journals

1- **Elamin Mohamed**, Saffa Riffat, Siddig Omer; Low-Temperature Solar-Plate-Assisted Heat Pump: A Developed Design for Domestic Applications in Cold Climate; **International Journal of Refrigeration, Sep.2017**

2- **Elamin Mohamed**, Devrim Aydin, Saffa Riffat, Siddig Omer; Experimental Study of Utilizing Thermochemical Heat Storage System for Existing Homes in Cold Region; **Energy, and University of Nottingham eprint Press, Jan.2018**

3- **Elamin Mohamed**, Rami Zeinelabdein, Siddig Omer, Saffa Riffat; A comprehensive investigation of using mutual air and water heating in *DX-SAMHP* for the moderate cold climate. **Renewable energy, June.2018**

4- **Elamin Mohamed**, Saffa Riffat, Siddig Omer, Rami Zeinelabdein; Developed solar energy heating system design for low-temperature in domestic buildings applications. **Applied energy, *under review***

5- Rami Zeinelabdein, Siddig Omer, **Elamin Mohamed**; Free cooling using phase change material for buildings in hot arid climate. **International Journal of Low-Carbon Technologies, August.2018**

Publications in Conferences Proceedings

1- **Elamin Mohamed**, Saffa Riffat, Siddig Omer; A Novel High Capacity Space Efficient Heat Storage system for Domestic Applications, **SolarTR2016. Dec.2016**, **Turkey**,

2- **Elamin Mohamed**, Siddig Omer, Saffa Riffat; Experimental Study of Utilizing Thermochemical Storage for Sustainable Domestic Applications. **SET2015. June.2015, UK**.

3- **Elamin Mohamed**, Saffa Riffat, Siddig Omer; Low-Temperature Solar-Plate-Assisted Heat Pump: A Developed Design for Climate. **SET2016. Sep.2016, Singapore**.

4- **Elamin Mohamed**, Siddig Omer, Saffa Riffat; High Capacity of Efficient Thermal Heat Storage System for Existing Homes. **SET2017, July.2017 Italy**

5- Omar Amer, **Elamin Mohamed**; Buildings' Evaporative Cooling by Means of Heat Pipes and Porous Ceramic Tubes. **SET2017, July.2017 Italy**

6- Rami Zeinelabdein, Siddig Omer, **Elamin Mohamed**; Numerical Investigation of a Free Cooling Based Latent Heat Storage System for Buildings in Hot Arid Climate. **SET2017, July.2017 Italy**

Awards and Prizses

The winner of Vice-Chancellor's Medal **July.2018** for Exceptional Achievement

Statement of originality

I declare that this thesis has never been submitted to any institution in partial or complete form for the award of any diploma, degree, master or PhD. The work contained herein is the original contribution of the author of this thesis during his period of study at the university of Nottingham, UK. For any referenced work, the due citation and acknowledgement have been given to the original author/s of that specific work.

Elamin Awad, R. Mohamed

Acknowledgement

Behold: To Allah belongs whatever is in the heavens and the earth. Behold: Indeed the promise of Allah is true, but most of them do not know (Yunis: 55).

I would like to take this opportunity to express my gratitude to a number of people whom without their help this work would not have made it to the finishing line. Firstly, I would like to thank my two supervisors' Dr. Siddig Omer and Prof. Saffa Riffat for their kindly supervision, moral support, and guidance. I would also like to thank my colleagues at the department of Architecture and Built Environment for their encouragement and help. Many thanks especially to my mother and father and my family for their prayers.

Nomenclature

A_{coll}	area of the solar collector, (m^2)
A_{tank}	total heat transfer area of the wall of the water tank, (m)
COP h-sys (t)	heat pump coefficient of performance for air, (-)
COP h-sys, av	coefficient of performance (average) for air, (-)
COP h,w-sys (t)	heat pump coefficient of performance (air and water)
COP h,w-sys (t)	coefficient of performance (average) for air/water (-)
COP effective	effectiveness coefficient performance of the system
Cold-air-in	inlet air temperature to the system, (°C)
C_{pw}	water specific heat capacity ($kJ \cdot kg^{-1}$ $°C^{-1}$)
D	refrigerant tube diameter, mm
D_i	inside refrigerant tube diameter, (m)
dt	variable time, per second, (t)
F'	collector efficiency factor, (%)
Hot-air-out	hot air gained by condenser, (°C)
hf_i	heat transfer coefficient, (-)
h_{refout}	refrigerant/Collector outlet enthalpy, ($kJ \cdot kg^{-1}$)
h_{refin}	refrigerant/ Collector inlet enthalpy, ($kJ*kg^{-1}$)
$HR_{, av}$	average of hot air rejected by condenser, (°C)
h_w	wind heat transfer coefficient, ($W \cdot m^{-2}$ °C)
$W_{\dot{m}}$	uncertainty in the mass flow rate of the water, (%)
$\dot{V}$	volume flow rate ($l \cdot s^{-1}$)
I_{coll}	intensity of the solar radiation, ($W \cdot m^{-2}$)
Inlet air, av	average of outdoor air temperature,(°C)
LPM	litre per-minute
M_W	water mass in the water tank (m^3)
N_u	Nusselt number (-)
P_r	Prandtl number (-)
P	Pressure, (bar)

Plate-inlet	fluid enters the collector, (°C)
Plate-out	fluid exits the collector, (°C)
$Q_{condenser\ air}$	condenser heat gained experimentally, (kW)
Q_W	heat gained at the *DHWT*, (kW)
$Q_h\ (t)$	heat exchange rate in the plate condenser, (kW)
$Q_{evaporator}$	evaporator heat gained experimentally, (kW)
Q_{solar}	collector's heat gained theoretically, (kW)
$Q_w\ (t)$	condenser gained heat delivered by a heat pump (water), (kW)
R_e	Reynolds number (-)
T_a	ambient temperature, (°C)
T_2	outlet collector's temperature, (°C)
T_3	discharge compressor temperature, (°C)
T_{room}	room temperature, (°C)
U_L	Collector's heat losses, ($W_* m^{-2}$ °C)
$U_{L,t}$	water condenser heat losses, ($W_* m^{-2}$ °C)
V	compressor's displacement, ($m^3{}_* h^{-1}$)
W_{comp}	compressor's work, (W)
$W\ (t)$	system input power, (W)

Abbreviations

DHWT	water temperature at domestic hot water tank
HR	room heating
LPM	litre per-minute
L	litre
LHS	latent heat storage system
P	pressure
SHS	sensible heat storage system
TES	thermal energy storage system
THS	thermochemical heat storage system

Greek symbols

$\dot{m}$	mass flow rate,
$\dot{m}_r$	refrigerant mass flow rate,(kg s^{-1})
$\dot{m}_{coll\_ref}$	refrigerant mass flow rate, (kg s^{-1})
η_{coll_ref}	collector efficiency, (%)
η_{comp}	compressor's efficiency, (%)
$\check{T}$	mean temperature in collector/evaporator, (°C)
ρ	fluid density (kg·m^{-3})
f_{comp}	compressor's frequency (Hz)
α	collector's adsorption rate (-)
τ	operating period of duration, per-second, (s)

Subscripts

after-comp	fluid temperature after being compressed
after-cond	fluid temperature after being condensed
hot-rif	hot refrigerant at heat exchanger plate
hot-water	hot water at heat exchanger plate
h-sys	heating space system
h-sys,av	heating space average
refout	refrigerant collector outlet
refin	refrigerant collector inlet
coll	collector's
air-ave	an average of out-door air temperatures
solar	enthalpy calculation via modelling
ref	refrigerant
comp	compressor
tank	Water tank
room	heated room area
av	Average
a	Ambient temperature
w	water
r	Refrigerant/fluid
(t)	time, per second

Abstract

Solar energy assisted heat pump (*SAHP*) and Direct Expansion Solar Assisted Heat Pump (*DX-SAHP*) systems are among the promising means of reducing the consumption of fossil fuels for heat production in residential building applications. The research in this thesis introduces a novel system that integrates solar energy, THS storage, and *DX-SAHP.* The objective is to develop an efficient heating system for existing homes in the cold climatic region which is sustainable and acts as an alternative to the conventional high energy loss domestic water and space heating systems.

One of the prospective techniques of producing and storing of thermal energy is the application of thermochemical materials. Storage of heat in salt hydrates provides an efficient and compact way of storing energy. Hence, the properties of salt hydrates that determine the storage capacity are being investigated. An experimental test has undertaken to assess the effect of integrating the new design of thermochemical storage materials with a solar-assisted multifunctional heat pump system. This research presents a novel design that involves the integration of *DX-SAMHP* and a hot water tank with a thermochemical sorption jacket. Investigations have been carried out to determine a suitable temperature range for household heating systems. Expanded Vermiculite (host matrix) and $CaCl_2$ (hygroscopic salt) have been used as composite material in an adsorbent reaction jacket for a domestic water tank. The new design has a total volume of 20 kg of V/$CaCl_2$, which can store the thermal energy with a complete reaction. The results show the high capability of the tested materials to enhance the domestic heating system performance when applied in cold regions. The feasibility of the designed system for residential space and water heating is also demonstrated. The maximum energy density obtained through the discharging process is 565 kJ/kg. It is also revealed that the coupling of thermochemical heat storage and heat pump increases the thermal production capacity by 1.166 kWh during the discharging process.

Chapter 1. Introduction

1.1. Introduction

In a typical UK residential region and its family homes, the energy used for domestic hot water and space heating comprises more than 61% of its yearly energy needs. In addition, it has subsequently become crucial to unveil more and more sustainable ways for covering the wide range of energy for consumers' demand. Furthermore, up to 50 % of pollutants and carbon dioxide emissions of the domestic houses originate from space heating and over 20 % from hot water heating for homes (Energy Saving Trust, 2010). In 2012, the energy used in homes accounted for more than a quarter of energy use and carbon dioxide emissions in the United Kingdom. More energy is used in housing than either road transport or industry,and housing presents a major opportunity to reduce energy use and CO_2 emissions (Jason and Ian, 2013).

According to the research studies, the reduction of energy consumption and CO_2 emissions are attributed to buildings. Hence, it is evident that an alternative energy source is required to control the greenhouse effect which can reduce the need for fossil fuel. The utilization of renewable energies, and their wider exploitation in the near future raises challenges and opportunities regarding their integration into energy supply systems and buildings. The objective of reducing energy demand in domestic buildings is not only to reduce the energy consumption of the houses with passive design methods but also to design equipment that integrates energy requirements with active techniques and renewable energy technologies (Heap, 1979).

On one hand, the success of the energy supply may be judged by its availability, quality and the cost of the service together with the capability of installations in the buildings. Moreover, the buildings require being adapted to the worst weathers and higher temperatures as climate change take effect. On the other hand, these requirements also entail that these zero-carbon houses will encompass a range of zero or low-carbon on or out-door power generation technologies, zero or low-carbon hot water and heating space technologies (Energy Saving Trust, 2010). Therefore, achieving zero-carbon space heating and water heating confers a disparate set of industrial challenges to the manufacturer and this is a very demanding objective, which necessitates novelty.

The heat pumps are promising means and their applications have been attributed to their widespread use, generally dictated by the necessities of the market where house-owners need air conditioning throughout the year, heating during winter and cooling in summer months. Therefore, heat pumps in their reversible form are capable of fulfilling these requirements and therefore have been developed over a period of time. Heat pumps are also reliable and to some extent cost-effective in terms the price of equipment (Bureaue, 2006). The aims of their applications are to enhance the heating capability as well as reducing the operating and capital costs to a reasonable level. In Europe, the rate of installation remains relatively low due to both the lack suitable equipment and the associated accessories as well as other economic factors. In the UK the heat pump is seen as the most promising system for family dwellings and due to climatic conditions (Government, 2008).

A packaged heat pump must not only be capable of delivering the air conditioning and space heating demands but also desirable to utilize the heat pump to fulfill at least part of the domestic hot water requirements which is considerably governing the widespread acceptability and boosts the application of heat pumps. The most common practical heat storages are water and latent heat of fusion storage media both of which are centered around their ability to store sufficient heat for practical domestic requirements, based on the influence of storage temperature on the heat pump coefficient of performance (Wright, 2008).

The volume capacities of materials play a key role in choosing the storage system and have a direct bearing on the performance of the heat pump for domestic and water heating. These have also been associated with attractive sources of energy and materials which are not harmful to the environment in conjunction with the supplementary electricity energy. The choice of material in which energy may be stored relies on the temperature at which it is to be provided and on the amount of energy to be stored. Thus, the running cost of direct supplement electric heating has led to a search for alternative sensible heat storage solutions if solar energy can be utilized effectively to fulfill the rapidly fluctuating energy requirements (Khudhair and Farid, 2004).

Consequently, space heating and water heating functions will become more significant as the trend towards low energy homes rises, with the hope that this would provide for a fully integrated system, based mainly on heat pumps. Another function which heat pump could play, under which this may become increasingly beneficial , is in the recovery of exhaust air and upgraded waste heat in domestic houses. This would be feasible with the aim of achieving more energy savings.

Large numbers of new heat pumps are presently available for use. However, although these systems are comparatively efficient, a major role still have to be played to investigate and do experiments to improve their performances. Economic viability has stayed a profound problem, and the insufficiency to offer satisfactory performance as constant heat output, substantially impaired the performance. They are susceptible to seasonal temperature variations especially in cold weather which always entails some considerations and innovation to counteract this deficiency (Ding and Riffat, 2013).

1.2. Statement of the problem:

In 1892 William Thomas, the first Baron Kelvin, considered the heat pump as simply a heat engine in reverse. The engine heat recovery ejects heat from a high-temperature source and discharges it to a low temperature. The heat pump needs a work input to reject heat from a low temperature and deliver it to a higher temperature (Heap, 1979). On the one hand, it becomes evident, the device that collects low temperature from the external heat source to deliver it at a higher grade heat would be ideal for the purpose of domestic hot water and space heating (Reay and Mac Michael, 1986). Heat pump systems at high performances have the capacity to develop thermal comfort at lower energy expenses and minimize CO_2 emission for low carbon dwellings.

Heat pumps are available in different sizes and shapes and there are two prevalent types; vapour compression types (compression cycle) and absorption types (absorption cycle). However, the vapour compression types are the most popular operating cycles and are used for domestic space/hot water heating in buildings. Most vapour compression heat pumps are using electric powered motors for their input work.

The solar air source heat pump technologies are well established and have recently been drawing extensive attention for their great potential energy-savings, environmental friendliness and high efficiency (Chua et al., 2010). In 2008, there were 650,000 heat pump units installed in Sweden whereas 895-2150 in the UK (Greening and Azapagic, 2012) . Traditionally, it is self-evident that the overall coefficient of performance (COP) for ground/air source heat pumps is higher than air/air source heat pumps owing to a quasi-stationary temperature of the ground in winter period as shown in Figure 1.1 when heating is highly needed (Wright, 2008). However, there are two main problems associated with ground/air source heat pumps: high borehole drilling and operating costs (Kjellsson et al., 2010).

When the heat pump is used for heating domestic buildings, a typical air-source heat pump has a marginal COP of 2.0 to 3.0 at the beginning of the heating season and then lessens gradually under bad weather conditions which substantially impair the COP (Ding et al., 2004). On average, the impacts for the air-source heat pump (ASHP) are 82% higher than from the boiler and 73% for the Ground-source (GSHP) and water-source heat pumps (WSHP) (Greening and Azapagic, 2012).

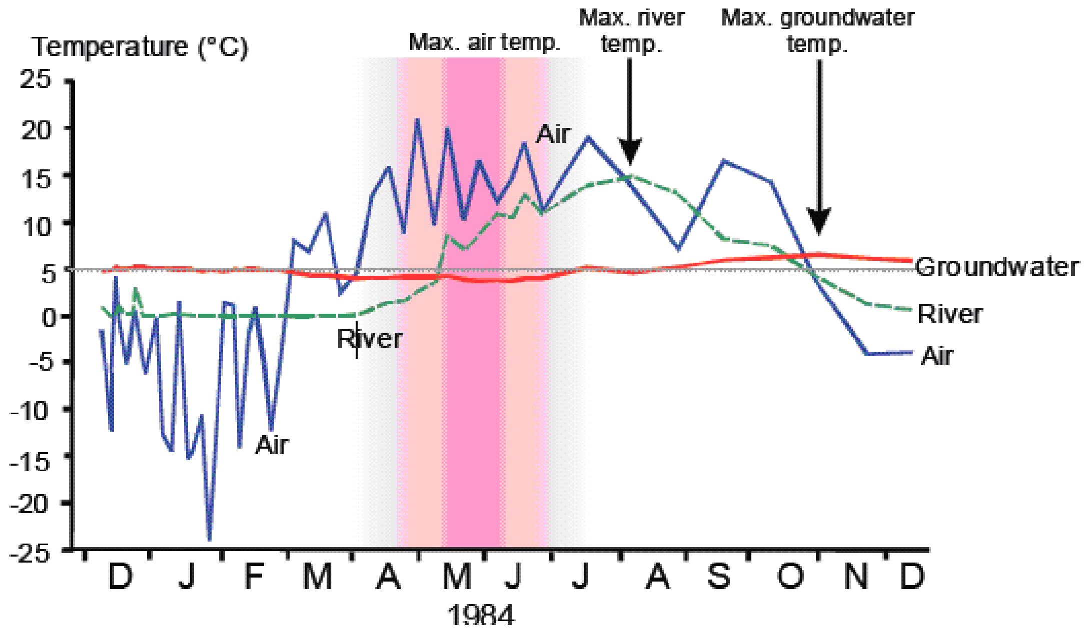

Figure 1.1. Variation in temperature of air, the river and shallow ground water at a site in Norway, through one year (BRE 2005)

The COP of the heat pump relies on several factors such as temperature difference between heat output at the heat pump's condenser and the ''lift'' heat input at the evaporator. Thus, the heat pump COP decreases as heat are transferred from the source to its destination, or increases according to temperature differences. Space and domestic water heating, therefore, experience a mismatch between heat supply and demand, as temperature changes, hence reducing the heat pump's COP. The situation is induced by the nature of the type of heat source as it changes due to external ambient temperature based on the season (Figure 1.1). Although a solar air-source heat pump is utilized to warm a house on a severe winter day, it requires more work to transfer the same quantity of heat indoors. This practically happens at around - 5°C out-door temperature. Consequently, the measures to enhance the COP of air-source heat pump are vital to broaden their utilization on low carbon homes in Europe and the free zero-dioxide emission houses in UK.

Virtually, air has recently been considered to be one of the most effective heat sources for heat pump operation on the vapour compression cycle, as it provides great potential to improve the heat pump systems to perform efficiently (Kong et al., 2011). As a disadvantage, air presents certain difficulties, due to fluctuations and variable of the ambient temperature and frost formation on the evaporator hence limiting its use.

Moreover, the unpredictability and the volatile nature of the source of energy, in addition to the required capability to store the collected energy and provide it within the periods of absence of the source, are one of the most important requirements to be considered. (Elamin, 2017) demonstrated the possibility of utilizing relatively inexpensive Thermal Energy Storage (TES) technology combined with a heat pump for residential buildings purposes without necessitating additional heating. It is revealed that this could eliminate the need for reheating process, thereby substantially reducing the cost of water/space heating system.

On the other hand, the challenge lies in maintaining the heat gained via integration of a periodic process between heat pump device and its attached hot water tank as long as possible for multiple domestic demands. This needs further consideration in terms of the selection of suitable collectors, working fluid, sizing of components and emphasizing specific configurations required to design the innovative thermal hot water storage tank in order to achieve greater efficiency and lower heat dissipation.

1.3. The aim of the Research

The main aim was to modify the heating system performance of the existing homes throughout the winter time in cold climate region. Firstly , the aim was to develop the solar-air source heat pump system for multiple uses to cover sufficiently the rapid heating demand from the beginning of the heating season to the end of coldest days. Secondly, it was intended to develop the solar-air heat pump's evaporator/collector to make use of the potential domestic waste heat and low-grade energy, and to reduce the direct bearing of frost formation. Thirdly and finaly it was aimed to improve the thermal storage density of the existing Domestic Hot Water Tank (DHWT) to assist the solar-air heat pump to enhance its COPs as well as ensuring a constant temperature during the severe winter period.

1.4. Objectives of the Research

In order to fulfil the above aims, the following aspects had to be independently investigated, therefore, the overall objectives of this research were:

I. To minimize the use of non-premium space by allowing minimal intrusion into existing residential areas, and this was done by using the existing central pipe system;
II. To develop the solar-air source heat pump by enabling the system to provide multifunctional heating requirements for residential buildings;
III. To enhance the coefficient of performance of the solar-air source heat pump system by improving the evaporator/absorber efficiency;
IV. To reduce the frost effects on the evaporator/absorber;
V. To provide higher energy density storage by examining comprehensive characteristics of storage materials that have the ability to store either sensible or latent heat, offering a distinct heat storage advantage over other systems to enhance the DHWT heating capacity;
VI. To minimize the heat loss or residual heat from the proposed system and,
VII. To reach a maximum invariably thermal comfort level.

The aimed novel outcomes of the research were:

- The use of non-premium house space (house attic area) to install the proposed heating system components;

- The use of the multifunction's heat pump system concept to provide alternative's space and DHW heating for existing homes in cold climate;

- The use of a ternary interior and exterior evaporator/collector for the Direct Expansion-Solar Assisted Multifunctional Heat Pump (*DX-SAMHP*) to efficiently absorb from indoor (waste heat) and outdoor (sun) heat or the ambient air at a low temperature with high COP in winter period;

- The implementation of an innovative thermal energy storage with thermochemical reaction Jacket (adsorption system) enclosed within the DHWT for a single home;

- The combination between *DX-SAMHP* system and thermochemical heat storage system in one unit for heating purposes.

1.5. Scope of the research

In order to successfully achieve the above targets, the research scope was divided into ten separate phases including :

- The review of the background and literature of previous work in residential solar and air heat pumps' performances.
- Experimental study on Air-to-Air heat pump performance in a single house;
- The 'modelling and simulation of the system using MATLAB software to test the capability and limitation of the cycle using different working fluid standards to ensure reasonable performance;
- The construction and investigation of a Direct Expansion Solar Assisted Heat Pump (*DX-SAHP*) system with the new concept of evaporator/absorber.
- The design and mathematical modeling of a developed DX-SAHP system for multifunctional heating purposes.
- The fabrication and examination of an experimental testing on *DX-SAMHP*.
- The validation of the theoretical results with laboratory experiments.

- The construction and examination of small-scale experimental rig to validate the concept of charging and discharging of the novel thermochemical storage tank's jacket during the heating season.
- The fabrication and analysis of a field-scale experimental setup to evaluate the actual thermochemical storage jacket combined with the developed *DX-SAMHP* system.
- The discussion of the enhancements and the influence of the combined *DX-SAMHP* with the novel (adsorbent) jacket for thermal hot water storage tank on the household's heating system.

1.6. Novelty of the research

This research has the following novelty attributes:

- The use of ternary interior and exterior evaporator/collectors which can efficiently absorb heat at a low energy grade and temperature for satisfying the heating demands of a domestic building during the heating season without resort to any auxiliary heating apparatus.
- The idea of using thermochemical material to enhance the thermal density of the DHWT is novel.
- The combination of *DX-SAMHP* system with thermochemical heat storage system (adsorbent jacket) to enhance the heating performance of single home are also novel.

This novel system illustrates an excellent opportunity to contribute towards a high level of sustainability and can also magnify the space and water heating market for systems using heat pumps.

1.7. Methodology

The research work encompasses the following principal stages:

- **Stage 1: Back Ground and Literature Review**

A literature review has undertaken to collect related information on the use of heat pumps and thermal heat storage technologies from the published research works to help understand the capability of such systems and to enhance the performance of the existing heating system for domestic applications.

- **Stage 2: Testing using Single-Attic heat pump in the laboratory**

From the literature review, it has been established that an air-to-air heat pump (Single-Attic) has been used as an air source heat pump for heating the space in a single house.

- **Stage 3: Assembling and testing of DX-SAHP for single home**

A DX-SAHP system was designed and assembled in the laboratory to investigate its thermal performance with the developed evaporator/collectors for only air space heating. The system under different evaporation temperatures was studied to determine the optimum performance.

- **Stage 4: Mathematical modelling with thermodynamic analysis and laboratory testing of the proposed DX-SAMHP system**

Mathematical modelling has been utilized to evaluate the performance of the system under different operating conditions including solar irradiation and water flow for multifunctional heating purposes (only space heating, space and water heating and only water heating). Experiments were conducted to validate the results acquired from the theoretical modelling.

- **Stage 5: Synthesising of nominated 'thermochemical storage materials' and testing the selected composites using a lab-scale Rig**

The energetic material test has been applied, and lab-scale rig designed and constructed for effective material testing to examine the performance of the selected composite and to determine the suitable materials for a new adsorbent reaction jacket, out of the tested materials. The design and construction have been carried out also to investigate the feasibility of the proposed jacket to enhance the thermal capacity of the DHWT. Preliminary tests were conducted and comparisons made to use the results for the next stage.

- **Stage 6: constructions of the DX-SAMHP system combined with a novel adsorbent Jacket for field testing**

The work was carried out on ternary evaporator/collector combined with *DX-SAMHP* connected to DHWT jacketed with thermochemical heat storage.

A field test was undertaken to validate the jacket's performance under 'charging and discharging cycles and to assess the performance of the novel system in severe winter period. In this stage, the thermal performance of the jacket has also been independently evaluated in terms of; its efficiency, the energy delivered to the domestic hot water tank and the total energy obtained by the composite material under cyclic tests.

1.8. Structure of the thesis

This thesis is composed of ten chapters and the chart in Figure 1.2 indicates the relation between them as well as the research plan.

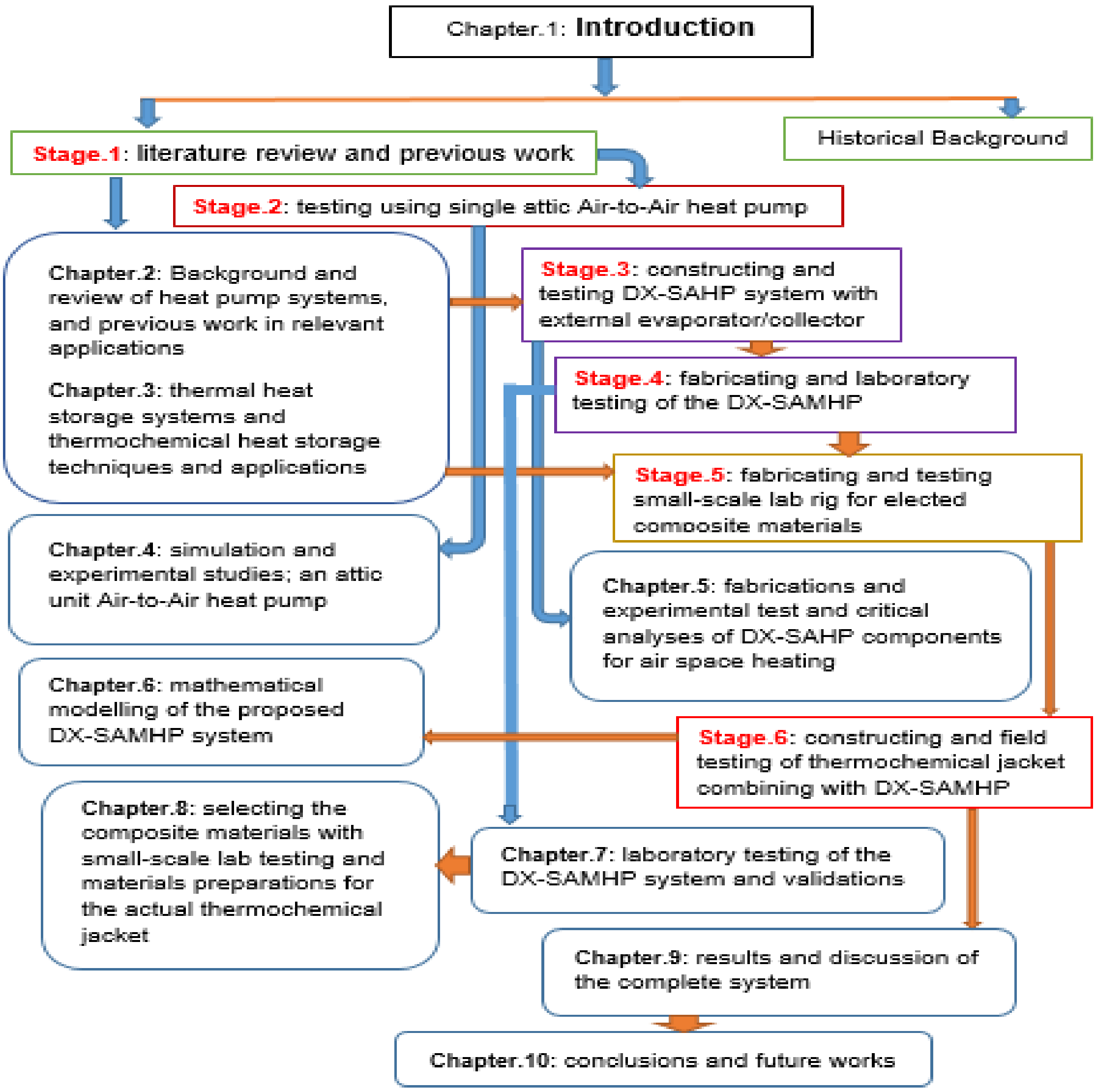

Figure 1.2. The Chart illustrates the relation between proposed chapters and research stages

The rest of the thesis is therefore organized as follow:

- **The first chapter** covers the introduction to the research with motivation, the project aims, objectives and the scope. The approach and methods to achieve the set aims and objectives are also stated.
- **The second chapter** covers the background of the research and outlines previously published theories and concepts that are necessary to understand technologies relevant to this research. It also covers

previous researches conducted to enhance the heat pump performance such as integration of evaporator/collector within multimode pump design, which permit the system to operate efficiently at low grade energy.

- **The third chapter** provides a review of past works on thermal storage technologies and the impact of high density thermal storage techniques on enhancing the thermal performance of the storage systems for building applications. This chapter also expounds the thermochemical heat storage technologies including the concepts, designs, and types. Much emphasis is mainly put on to materials, open/closed sorption applications and the use of thermochemical storage to improve the energy efficiency of heat pumps in domestic buildings with reduced effect of seasonal variations.
- **The fourth chapter** presents the mathematical modelling and laboratory experiment on an attic air-to-air heat pump. The evaporating and condensing temperatures using different working fluids are analysed.
- **The fifth chapter** presents the work on laboratory experiment of a DX-SAHP system with new evaporator/collector concept for space heating purpose.
- **The sixth chapter** describes the mathematical modelling done on the proposed *DX-SAMHP* system for the main five components (evaporator/collector, compressor, condensers, heat exchanger and expansion valve) under different operating conditions. The chapter also compares the thermal performance of a different system operating modes.
- **The seventh chapter** concentrates on the fabrication, and the laboratory experimental set-up, procedure, and operation of a *DX-SAMHP* system. The design and analyses for the main elements are explained in terms of the cycle of the refrigerant loop as well as describing other ancillary components (sight glasses, receiver and liquid

line dryer filter). The performance of the system under different operation conditions is also covered based on experimental results. The chapter also explains the validation of experimental results with theoretical works.

- **The eighth chapter** describes the process of selecting and analysing of thermochemical candidate materials for the proposed thermochemical jacket. Small-lab scale experiments set up and its findings are presented. The chapter has also covered the synthesis of composite materials and its preparation for the next stage.
- **The ninth chapter** includes the description of the design and construction processes of the proposed thermochemical reaction jacket. It also provides experimental and theoretical analyses of the combined system (*DX-SAMHP*) and thermochemical jacket) with the results and discussion.
- **The tenth chapter** is about the conclusions and future works. It summarizes the conducted research works and how the research aims and objectives were achieved. The effects and benefits of combining the heat pump technology with novel heat storage system are elaborated, on top of the suggestions and recommendations for future system improvements.

Chapter 2. Background and Overview of Heat Pump Systems

2.1. Background and Overview of Heat Pump and its Performance

2.1.1. Introduction

In 2008, the European and the UK introduced a policy aimed at decreasing carbon emission and improving energy efficiency in existing and new buildings (Government, 2008). Climate change is a critical challenge for the society today since it has an effect on all areas including dwellings (DCLG, 2008).

In 2012, it was reported that the building energy consumption for housing as well as commercial and public administration sectors in the UK was 502 TWh and 197 TWh, representing 29.1% and 45%, respectively. However, for transport and industry, it is 35% and 17% respectively (Figure 2.1) (Jason and Ian, 2013).

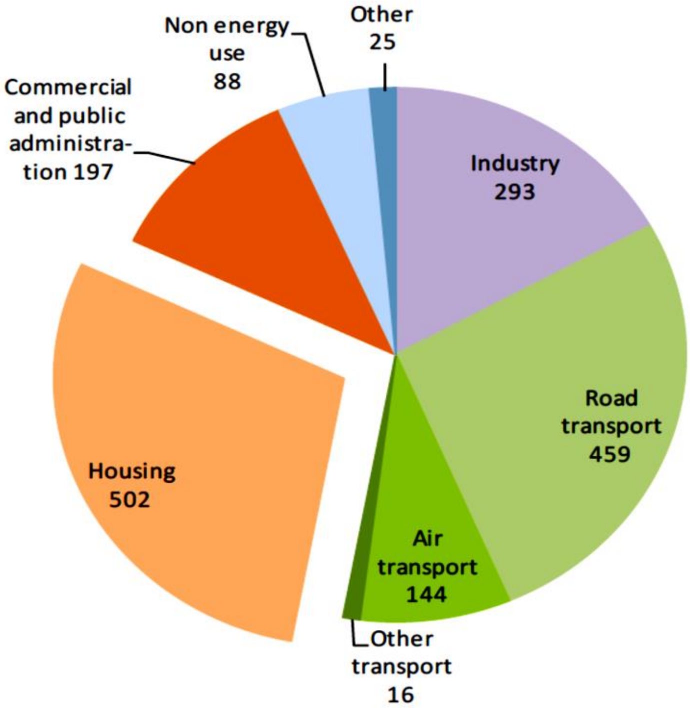

Figure 2.1. The energy consumption per sector for UK (Jason and Ian, 2013).

According to statistics the most of the energy consumed is for domestic space heating which is was 60 % of overall domestic consumption in 2012 (Figure 2.2). This is due to the growth of in the number of UK households at about 11 % and a 9 % raise in population since 2000-2013 (ECUK, 2014). To achieve thermal comfort and lifestyle requirements of households in dwellings, most of the UK's families utilize energy from fossil fuel combustion.

Figure 2.3 illustrates the domestic energy comsumption by fuel which has significantly changed since 1970 with 68 % natural gas. The generation of energy from these fossil fuels is prone to produce carbon dioxide (CO_2) along with other contaminated pollutants such as SO_2, PFCs, HFCs, CH_4 and Nitrogen oxides (N_2O). This creates extra critical issues including air pollution and global warming.

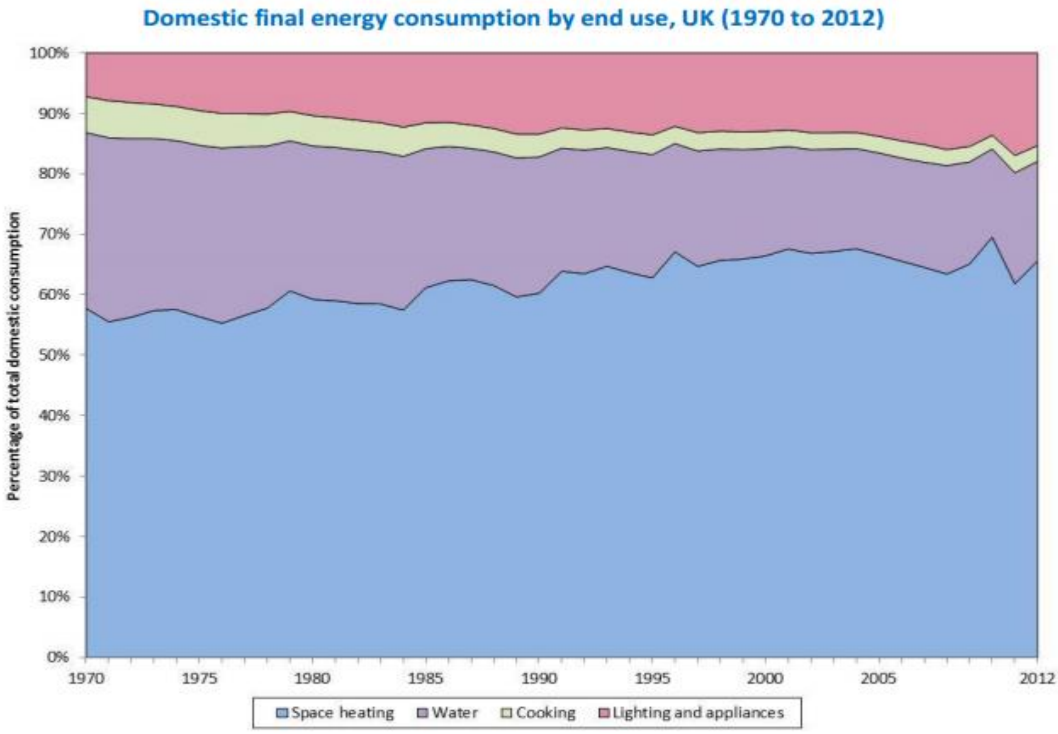

Figure 2.2. Source: DECC, ECUK (2014)

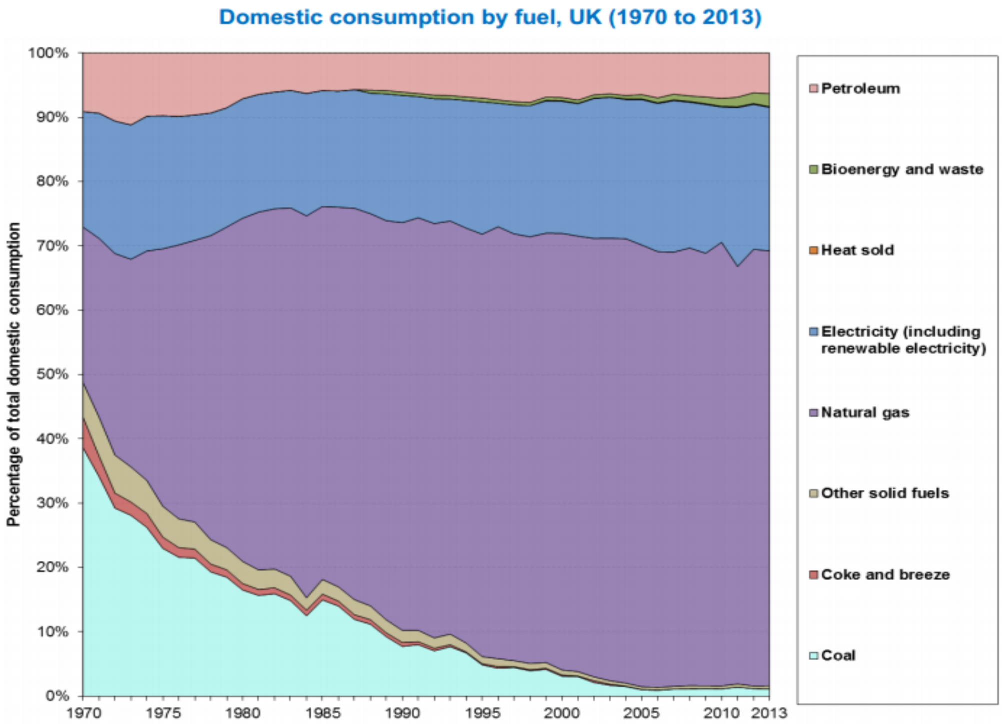

Figure 2.3. Source: DECC, ECUK (2014)

Developing heating system and a thermal heat storage that can contribute to achieving zero-carbon buildings i.e 100 % Carbon footprint mitigation, against a baseline of existing building usage of typical dwellings in the UK. Cutting carbon dioxide emitted from buildings and reducing the use of fossil fuel by increasing the exploitation of renewable energy resources can be done. Since, the low-energy solutions for domestic hot water generation and house heating systems are investigated broadly.

There are several ways which can be used to considerably generate energy at home from renewable energy technologies, for example, solar heating systems, wood-burning stoves and the use of heat pumps. Traditionally, renewable energy technology is costly due to high initial investment cost. However, energy technologies for generating heat like biomass boilers and heat pump, the UK government announced the tariff levels for Renewable Heat

Incentive scheme (RHI) in July 2013. Therefore, families which can generate heat using renewable energy technology are guaranteed to receive pay-back.

Heat pumps release about 0.17 to 0.21 $kgCO_2/kWh_{th}$ which is less than that of a gas-fired boiler (Figure 2.4). Therefore, they have a major role to contribute to the low-carbon levels in the UK in future with the possiblity to achieve zero or low-carbon heating system for the approved code homes (WYATT, 2004). Comparing to other domestic heating systems (Table 2.1), the Heat pump systems have the ability to improve the level of thermal comfort at lower energy costs as well as decreasing the level of CO_2 emission up to 100 % if renewable energy resources are used as the fuel source. It is also important to note that The Environmental Protection Agency (EPA), reported Air-Solar Heat Pump (*ASHP*) as one of the highest promising heating technologies.

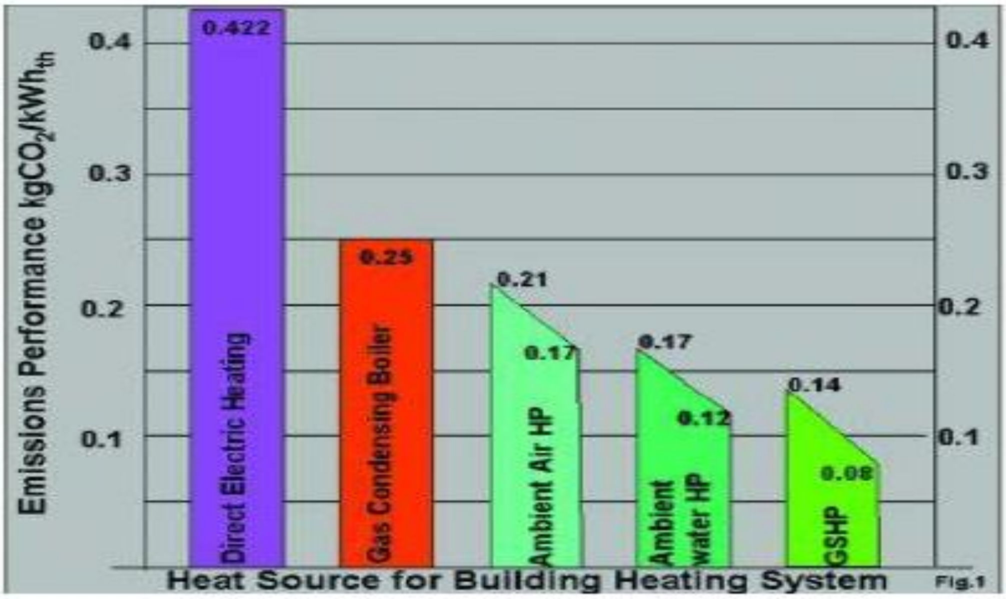

Figure 2.4. Heat Pumps Achieve lower CO_2 emissions with other forms of heating systems, source: (WYATT 2004)

Table 2.1. Implications of different domestic heating systems

Technologies /fuels	*Advantages*	*Limitations*
Natural gas	*Most environmental fossil fuel, especially when burned in a high efficiency boiler with heat recovery*	*-requires a gas network* *-Produces CO_2 when burning*
The oil boiler	*-Can use a similar system to the gas boiler* *-Does not require a network*	*-Expensive compare to others* *-Require a storage tank* *-Produces CO_2 when burning*
Electrical heating	*-efficient heating system* *-environmental friendly when electricity is generated from low carbon sources* *- works efficiently if the house or building is well insulate*	*- when electricity is generate from fossil fuel Produces CO_2 when burning* *-electricity is more expensive compare to gas* *-renewable energy power* [illegible]
	sufficient heating demand *-could be use for both heating and cooling* *-not generates CO_2 if renewable energy is use to supply the compressor and circulating pump*	
Micro CHP (Combined Heat and Power)	*-produces electricity and heat from one fuel*	*- use natural gas, or biomass* *-requires matching heat and electricity demand* *-produce too much heat for well insulated building* *- Produces CO_2 when burning*
District heating	*-very good for cold climates* *- the investment is justify if the buildings are well insulated*	*- Produces CO_2 when burning* *- with a central CHP plant is only efficient in (compact) cities where buildings have a sufficient heat demand* (Yumus, Cengel, & Michael, 1998)
Coal stoves	*-Produces comfortable heat atmosphere* *-Fairly good efficiency*	*-CO_2 emission are high* *-old technology*
Biomass (wood or wood pellets)	*-may be consider as renewable*	*- CO_2 emission when burning* *-lack of wood pellets distribution points*
Solar thermal energy	*-solar water boiler can be combined with low temperature heating for good efficiency* *-not produces CO_2 emission*	*-low efficiency* *-requires good sun*

2.2. Fundamental Principle of heat pumps

2.2.1. Heat Pumps

A heat pump is a mechanical device that utilizes an external power to transfer heat energy from a lower temperature heat source to higher one. For heating purposes in the residential sector, the heat pump can provide three-fold of energy or more towards the hot water and space heating/cooling than high-grade energy, making it an attractive energy technology for future zero-carbon houses.

It is generally working under many principles which are classified according to shapes, sizes, and aims of the application as given in Table 2.2. The vapour compression cycle and absorption cycle are the most well-known among them the types heat pumps. Although the most feasible and reliable technologies are the thermochemical heat pumps and thermoelectric heat pumps, the first type of operation cycle is quite popular and widely used in building heating applications. A heat pump is composed of four main components including; evaporator, compressor, condenser and expansion valve in a refrigeration loop. There are additional components such as a receiver, filter, dryer and sight glasses and others categorised as auxiliary accessories (Figure 2.5).

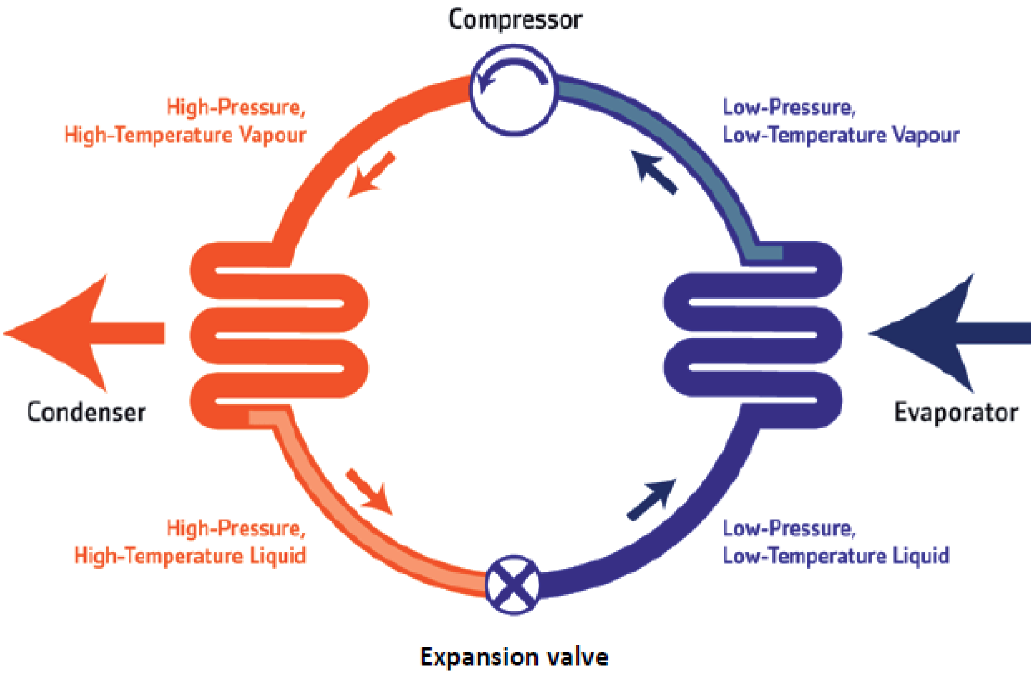

Figure 2.5. Heat pumps working loop

The four thermodynamic steps followed to achieve a particular cycle are as follow (Figure 2.6);

I. Evaporation; when the heat source temperature at evaporator is higher than the temperature of the working fluid, it will continuously absorb heat from the heat source (Air/Ground/Water), and the refrigerant provides energy, taking into account of changes in temperature. The evaporated liquid leaves the evaporator when it reaches its saturation curve.

II. Compression; when the vapour enters into the compressor in the saturated phase, it is compressed by raising its temperature and pressure where it goes into a super-heated form.

III. Condensation; the heat carried by the vapour in this process is rejected to the heat sink or water medium so that the vapour returns to the liquid phase at the end of the condenser outlet.

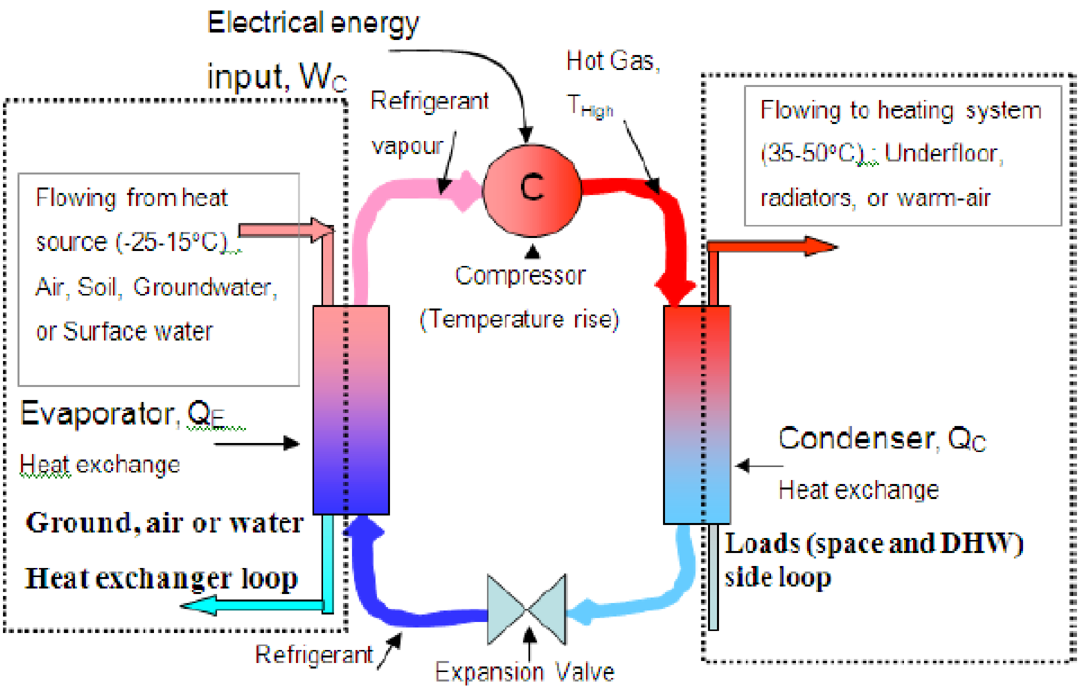

Figure 2.6. Thermodynamic model of heat pump vapour compression cycle

IV. Expansion valve; by passing through a capillary tube (throttling isenthalpic), both the temperature and pressure of the flow refrigerant drops below the heat source temperature or starting point by expanding the saturated liquid to evaporator pressure. So, the evaporator enters as a low-quality (liquid and vapour) saturated mixture and then leaves the evaporator to re-enter the compressor and the cycle is repeated.

Some of the work in this section is focused on the *ASHP* for domestic hot water and space heating in terms of enhancing the efficiency and performance whereas the other work concentrates on the review of *ASHP* as well as the essential theories to understand its operation.

2.2.2. Heat pump theory

The purpose of this section is to address the basic theoretical background of the heat pumps. This is aimed at appreciating the limitations of the air source heat pump which are not only imposed by the laws of nature but also caused by mechanical or engineering problems and challenges.

Table 2.2. Classification of heat pumps for heating in the buildings

Heat source	**Heat carrier**	**Term used to classify the heat pump**	**Description used by heat pump suppliers**
Water *(lake, river, or sea)*	Warm water	Water to water heat pump	Ground soil or Underground water–GSHP
Water *(lake, river, or sea)*	Warm air	Water to air heat pump	
Air *(ambient or exhaust air)*	Warm water	Air to water heap pump	Air source heat pump (ASHP)
Air *(ambient or exhaust)*	Warm air	Air to air heat pump	
earth *(ground or rock)*	Warm water	Soil to water heat pump	Ground source heat pump –GSHP
earth *(ground or rock)*	Warm air	Soil to air heat pump	
Solar radiation	Warm water	Solar radiation to water heat pump	Solar heat pump (or solar assisted heat pump-SAHP)
Solar radiation	Warm air	Solar radiation to air heat pump	

In a refrigerant cycle as depicted in Figure 2.6, the heat pump necessitates a work input (Wc) to eject the heat from the low temperature side (Q_E) (evaporator) which is transferred to the high temperature (Q_H) (condenser) i.e. heat is delivered isothermally in the ideal case at high temperature (via compressor) and it is collected isothermally (at low temperature through the expansion valve).

2.2.3. Ideal Vapour-Compression Cycle

The Pressure-enthalpy diagram defines the properties of thermodynamic for the refrigerant and the performance of equipment that is in use. In practice, it might not be probable to precisely control the condition of the refrigerant. However, in the ideal cycle, the refrigerant enters the compressor after leaving the evaporator as saturated vapour. The Temperature-Entropy (T-S) and

Pressure-Enthalpy (P-h) diagrams can clearly demonstrate the four processes of the refrigerant as shown in Figure 2.7

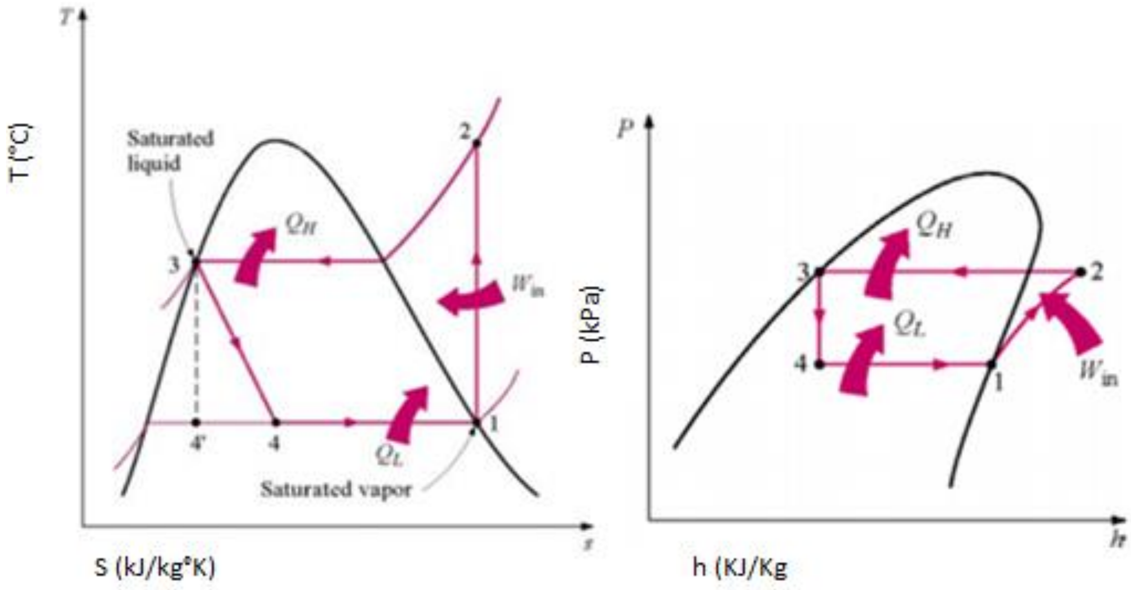

Figure 2.7. Ideal heat pump cycle in the T-s, P-h diagram under vapour

2.2.4. The working fluids of the Heat pumps

A refrigerant is a liquid used for transferring heat in a heat pump cycle. The role of the refrigerant is to absorb heat during evaporation process at low pressure and low temperature and remove heat during condensation at a higher pressure and a higher temperature. It is crucial to carefully select the refrigerant as it determines the optimal performance of the heat pump. Therefore, the refrigerant should have a zero Ozone Depletion Potential (ODP) and a relatively smaller Global Warming Potential (GWP) not only for environmentally friendly purpose but also for good physical thermodynamic properties and energetic performances. Thus, the desired refrigerant must be compatible with the vapour compression cycles and should have a high volumetric refrigeration capacity, suitable for domestic heat pump system operation. The thermo-physical Specifications of Refrigerants are shown in Table 2.3.

Table 2.3. Thermo-physical Specifications of Refrigerants

Name	Composition (wt, %)	Tc (°C)	NBT	Glide (°C)	GWP (CO_2=1)	ODP (R_{11}=1)	Psat At 0°C (bar)	Psat At 45°C (bar)	SCD X10^4 (kJkg^{-1})
R22		96	-40.8		1700	0.055	5.00	17.30	2.40
R134A		106	-26.1		1300	0	2.90	11.60	3.73
R404A	R-125/143a/134a (44/52/4)	72.1	-46.5	0.8	3700	0	6.15	20.60/ 20.70	2.06
R410A	R-32/125(50/50)	73.2	-52.7	0.1	1900	0	7.99/ 8.01	27.26/ 27.33	1.60
R407C	R-32/125/134a (23/25/52)	86.0	-43.7	7.2	1600	0	4.6/ 5.70	17.50/ 19.00	2.00

2.3. Performance rating of heat pumps

2.3.1. Coefficient of Performance (COP)

The COP is the ratio of useful heating or heating impact (Q_H) or cooling provided to the required work (Wc). This ratio indicates the efficiency of the machine by expressing the heating or cooling input power proportion to energy consumed (output).

2.3.2. Carnot heat pump COP:

The Carnot cycle consists of two isentropic and dual reversible isothermal processes. It is operating at the given temperature limits offering a maximum thermal efficiency theoretically between the evaporator and the condenser as shown in Figure 2.8. It is also employed as a standard which can be compared with the actual vapour compression cycle.

Equations for Carnot heat pump cycle are include (Yunus A. Cengel and Boles, 2011):

Heating Carnot COP:

$$COP_h = \frac{Q}{W} = \frac{T_H}{T_H - T_C} \tag{2.1}$$

Cooling Carnot COP:

$$COP_C = \frac{Q}{W} = \frac{T_C}{T_H - T_C} \tag{2.2}$$

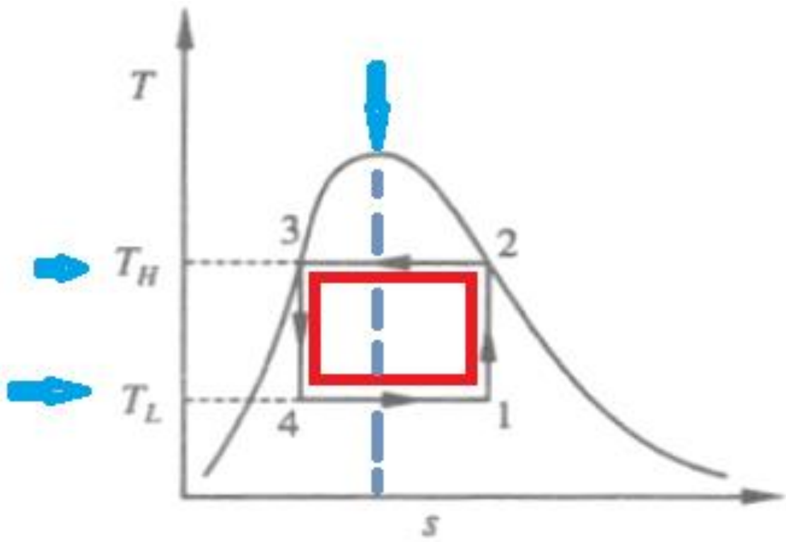

Figure 2.8. Revers Carnot Cycle

For heat pump cycle, operating within two regions at temperatures T_{high} (condenser), T_{low} (evaporator); when the evaporator temperature increases, the COP also increases as a result. This characteristic is also exhibited by actual heat pump system.

Therefore, the success of heat pump applications for residential sector depends on the reliable, cheap, and comparatively high temperature heat source. However, the COP of the heat pumps relies on many factors such as the temperature of the low energy source, actual temperature, the distance between heat exchangers and most importantly the evaporator temperature heat source. Hence, it is important to concentrate on the design of the evaporator to improve the COP of *ASHP* for space heating and domestic hot water.

2.3.3. The effectiveness of the heat pump

The effectiveness is defined as the ratio of the reverse Carnot cycle COP to the actual COP of the heat pump, typically in the range of 20-25 % for a typical heat pump cycle system. Therefore, the computation of the COP provides a measure to assess the effectiveness of the system by converting a small amount of work into useful energy which can be used for water or space heating. The Seasonal Performance Factor (SPF) of the heat pump can be converted into the Performance Energy Ratio (PER) by defining it as the useful heating energy divided by the amount of fossil fuel or the efficiency of the energy generation multiplied by the COP. In such case using an electric motor or including auxiliary energy (fan, pumps), the range of efficiency for generating power in the UK is approximately 43.9 %. When the grid losses of about 2 % are deducted the net power efficiency becomes 41.9 % (Yunus A. Cengel and Boles, 2011)

$$PER = \frac{\text{Useul heat delivered by heat pump}}{\text{Primary energy consumed}} \tag{2.3}$$

$$\text{PER} = \text{COP} * \eta_{\text{Power Generation}} \tag{2.4}$$

For the auxiliary equipment involved in operating the system, $COPs$ can be computed as follow:

$$COP_{effective} = \frac{Q_{cond}}{W_{elec}} \tag{2.5}$$

The coefficient of performance cycle is:

$$COP_R = \frac{Q_1}{W} = \frac{h_1 - h_4}{h_2 - h_1} \tag{2.6}$$

Where; The parameters in the equations above are described according to Figure 2.8 as follows;

Process 4-1: (evaporator) $h_4 + Q_1 + 0 = h_1,$ $Q_1 = h_1 - h_4$

Process 1-2 (compressor) $h_1 + 0 + W = h_2,$ $W = h_2 - h_1$

Process 2-3 (condenser) $h_2 + Q_2 + 0 = h_3,$ $Q_2 = h_3 - h_2$

Process 3-4 (throttle valve) $h_3 + 0 + 0 = h_4,$ $h_3 = h_4$

By using the refrigerant mass flow rate factor, the COP can be calculated as follow:

$$\mathrm{COP} = \frac{Q_{cond}}{W_{comp}} = \frac{m_r \cdot (h_2 - h_3)}{m_r \cdot (h_2 - h_1)} = \frac{h_2 - h_3}{h_2 - h_1} \tag{2.7}$$

Therefore, the SPF can be summarized as:

$$\mathrm{SPF} = \frac{heat\ energy\ output\ (kWh)}{Total\ input\ energy\ (kWh)} \tag{2.8}$$

Chapter 3. Literature Review of Heat Pump Systems and Thermal Energy Storage Systems

3.1. Types of heat pumps

There are different types of heat pumps which employ various heat sources and available in numerous shapes and sizes, made for different building structures, and those configured to operate in the closed vapour-compression cycle which is categorised based on the heat source and sink.

3.1.1. Air-to-Air heat pump

The air-to-air heat pumps extract heat from ambient outside air by natural convection to warm the indoor area or transfer heat reversely in summer. This pump type is the most popular used in domestic homes. However, because of low capital cost and easy installation, air-to-air heat pumps can also be utilized in commercial buildings. Figure 3.1 illustrates a typical ASHP unit operating in heating and reverse cooling mode.

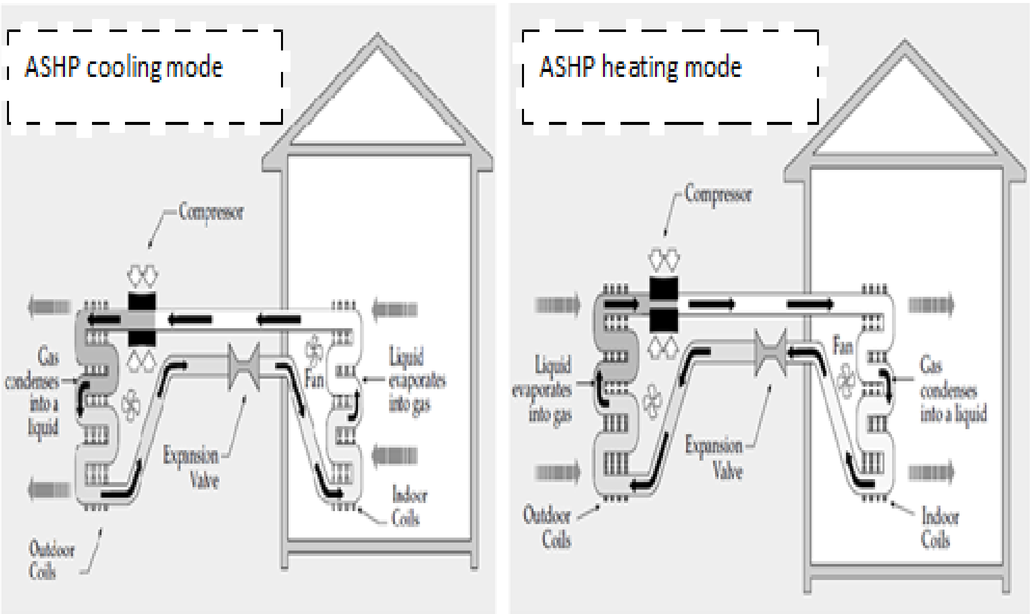

Figure 3.1. ASHP heating and cooling modes, source: NREL DOE/GO-102001-1113 FS143

3.1.2. Air-to-Water heat pump

This type is quite operates differently from the air-to-air heat pump, in that the refrigerant-to-water heat exchanger is installed as a part of the condenser. When water is heated up, heat is removed from it to the ambient. The working cycle of this heat pump is shown in Figure 3.12.

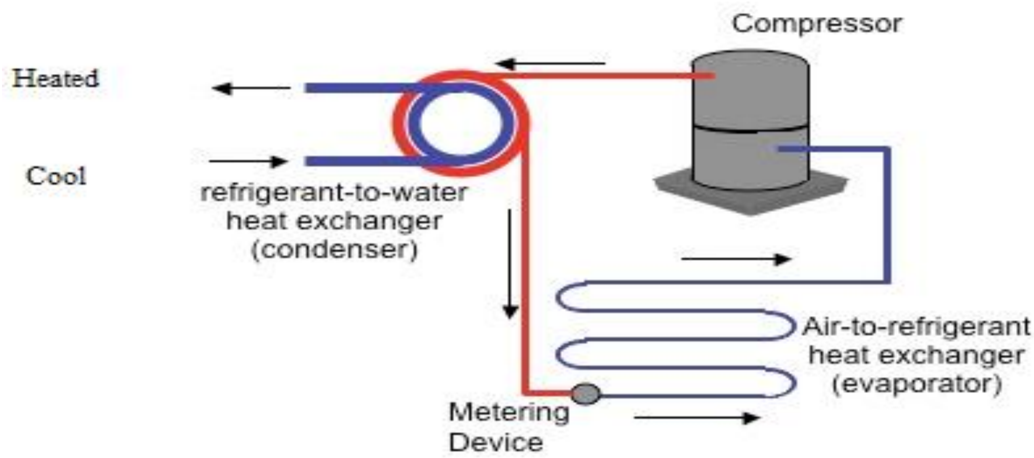

Figure 3.2. Heating cycle of Air-to-Water heat pumps (Eugene, 2014).

3.1.3. Water-to-Air heat pump

This type of heat pump depends on water and the sink as the heat source and utilizes the air to deliver heat for space heating. Various types of water-to-air heat pumps use heat sources which include, surface water, groundwater, waste water and an internal source. Figure 3.3 shows the water-to-air heat pump working cycle in the heating mode.

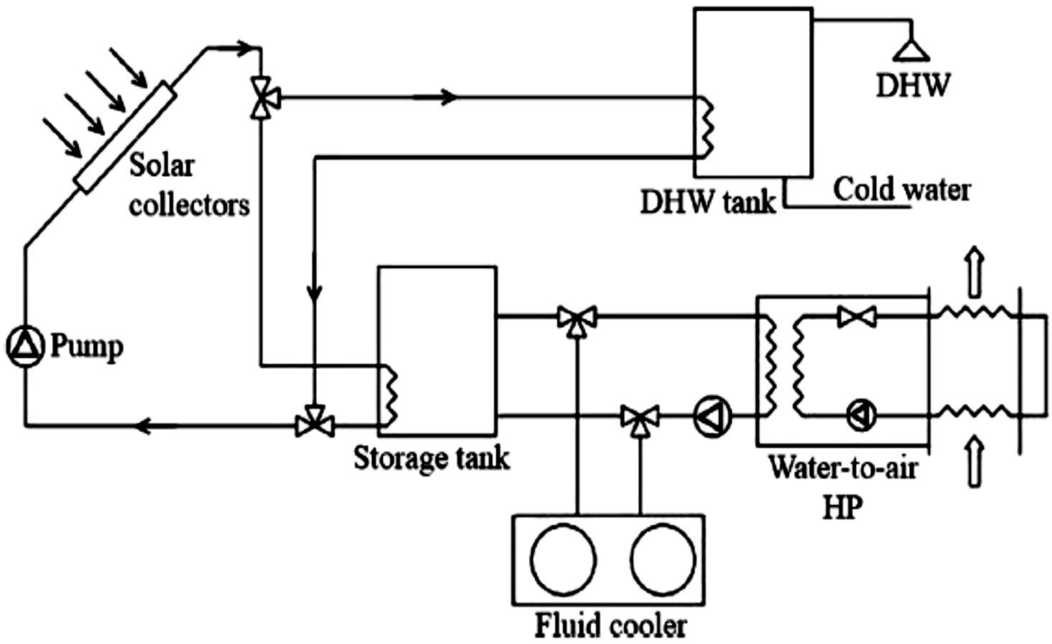

Figure 3.3. Water-to-Air heat pump working cycle (heating mode) (Sarbu and Sebarchievici, 2016).

3.1.4. Water-to-Water heat pump

For this heat pump, water is used as the sink and heat source as illustrated in Figure 3.4. the switching between cooling and heating can be applied in the water circuit rather than refrigeration circuit. Therefore, owing to pollution problem at the evaporator, it is necessary to apply an indirect path for heat exchange.

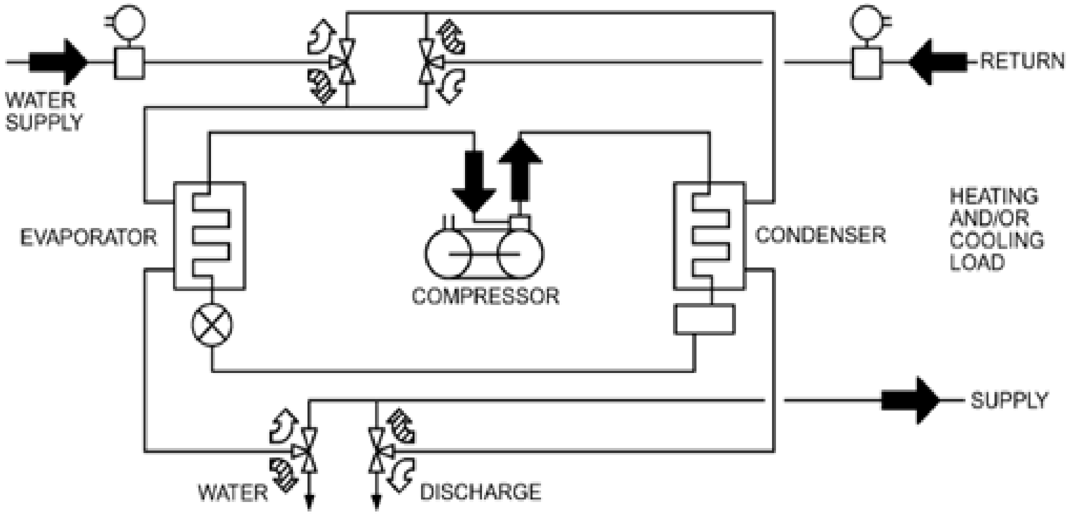

Figure 3.4. Heating-Cooling mode of Water-to-Water heat pump(Li et al., 2007).

3.1.5. Ground-water heat pump

This heat pump is known as an open-cycle heat pump system that drives water from a drilling well. When the heat is transferred inside, water is discharged into another well rather than being distributed through the system. Practically this choice is viable where sufficient water supply and environmental legislation are met. Therefore, an intermediate heat exchanger is a good choice to prevent erosion. Figure 3.5 depicts this system.

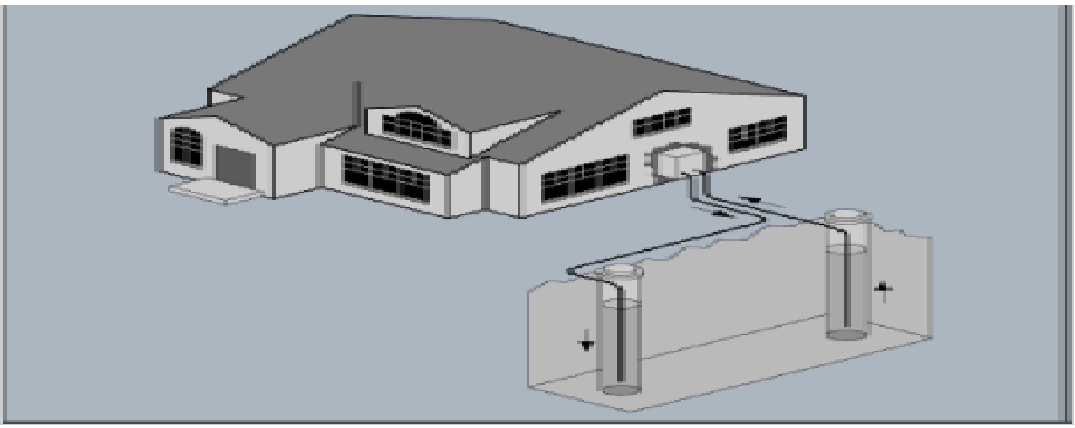

Figure 3.5. The open-cycle ground-water heat pump system (WBDG, 2016).

3.1.6. Ground-Source Heat pump systems GSHP

This type of heat pump is basically utilizing the ground as the sink and heat source. In the working cycle, the direct expansion system is varied from a refrigerant-to-water evaporator along with the vertical or horizontal slinky pipes fitted underground. A vertical loop system is usually applicable for commercial buildings as shown in Figure 3.6. However, the initial capital is relatively low, with minimal environmental effect. The horizontal loop system is undesirable if it is desired to use heat pump with a considerable size.

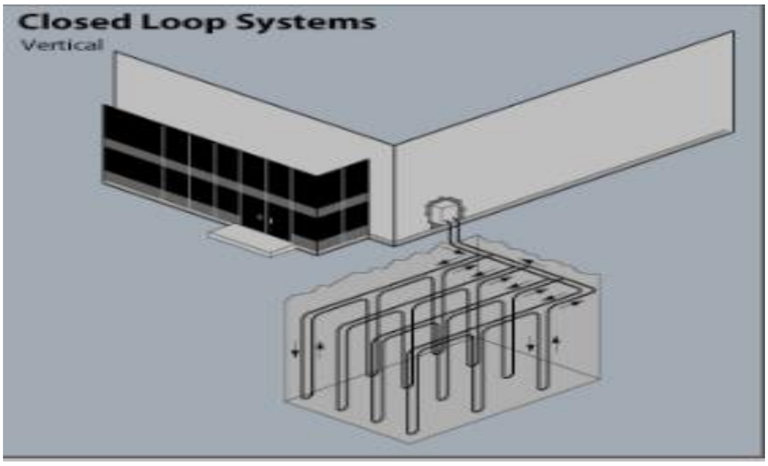

Figure 3.6. The Vertical GSHP system (WBDG, 2016).

For small applications, a horizontal cycle system indicated in Figure 3.7 is preferable because it has the lowest initial investment cost. Also, the efficiency of the system is seasonally lower due to a lower ground temperature in winter.

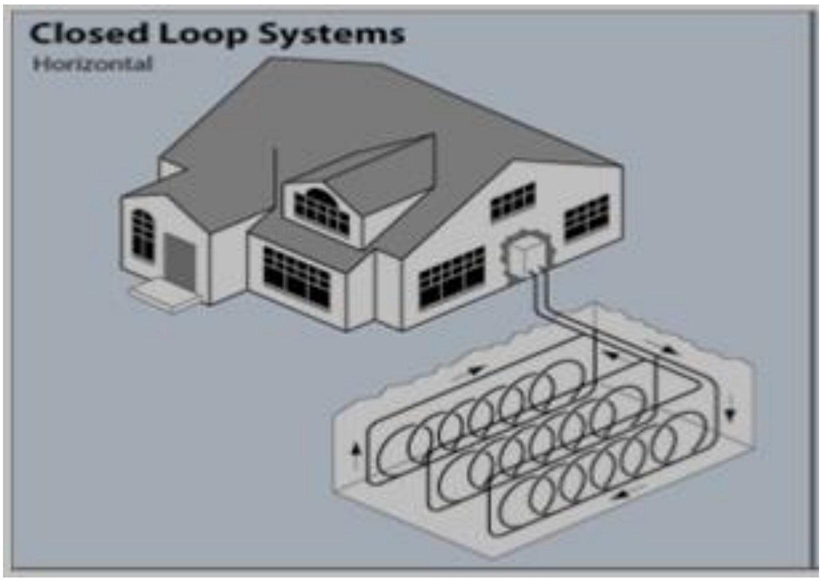

Figure 3.7. The Horizontal GSHP system (WBDG, 2016).

A surface-water system is cheaper and more practical since the building is near to lake or pond. A chain of convoluted pipes must be positioned under the source of water in order to sufficiently meet the quality criteria i.e. in terms of the specifiedvolume and depth as shown in Figure 3.8.

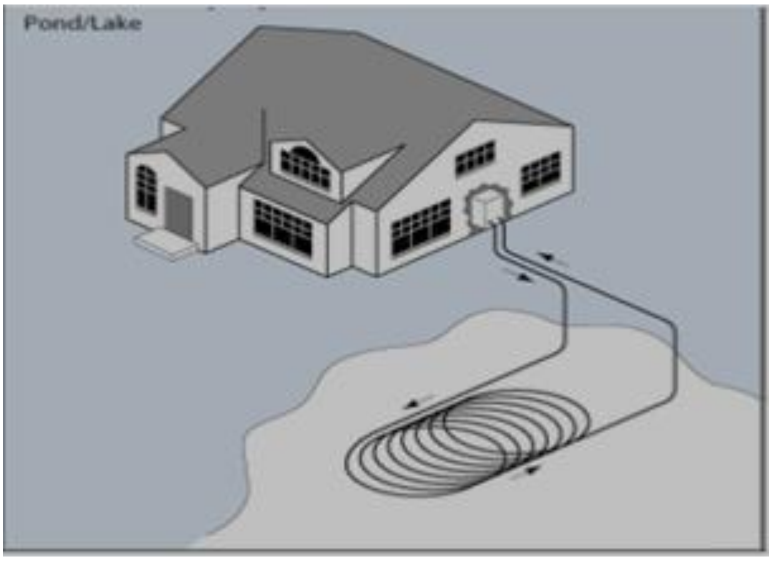

Figure 3.8. The Surface-water heat pump system (WBDG, 2016).

If the efficiency of heat transfer is improved, a direct expansion (DX) GSHP system is working by removing the requirement of having of the intermediate heat-transfer fluid and circulation pump, together with the fluid-to-refrigerant heat exchanger.This is achieved by installing the copper coils underground for direct exchange of heat with the ground and the refrigerant. As a result, it requires a good ambient environment like a good soil type and a considerable amount of refrigerant, such as underground water to achieve bettter COP and longer life span of the system. Figure 3.9 demonstartes the working principle of the DX-GSHP system.

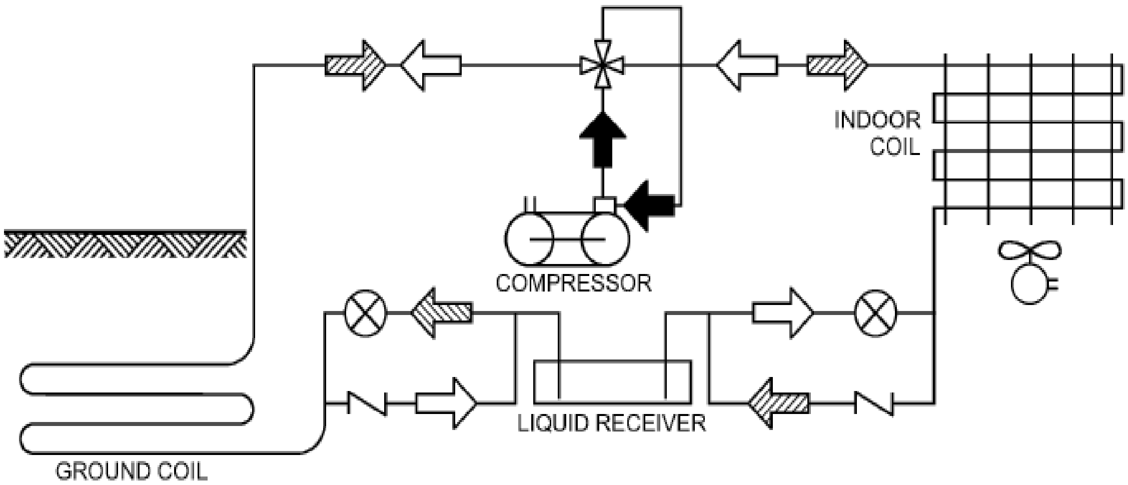

Figure 3.9. Cooling/heating mode in DX-GSHP system

3.1.7. Hybrid heat pump system

In the hybrid system, the heat source is a combination of solar technology and other heat sources such as air. This heat pump has higher COP with a free heat source and CO_2 emissions are reduced since solar energy is used. It produces hot water and heating supply during the year by utilzing less space. During sunlit periods, the evaporator/collector uses hybrid heat source which comprises of solar energy and air.

According to conducted experimental study, it was noted that the average daily COP attained by the heat pump is 4.0 %, whereas the average daily energy efficiency could reach 61-82 %, in circumstances where solar radiation is strongly available. Figure 3.10 displays a solar-assisted heat pump (*SAHP*) utilizing direct expansion in the evaporator.

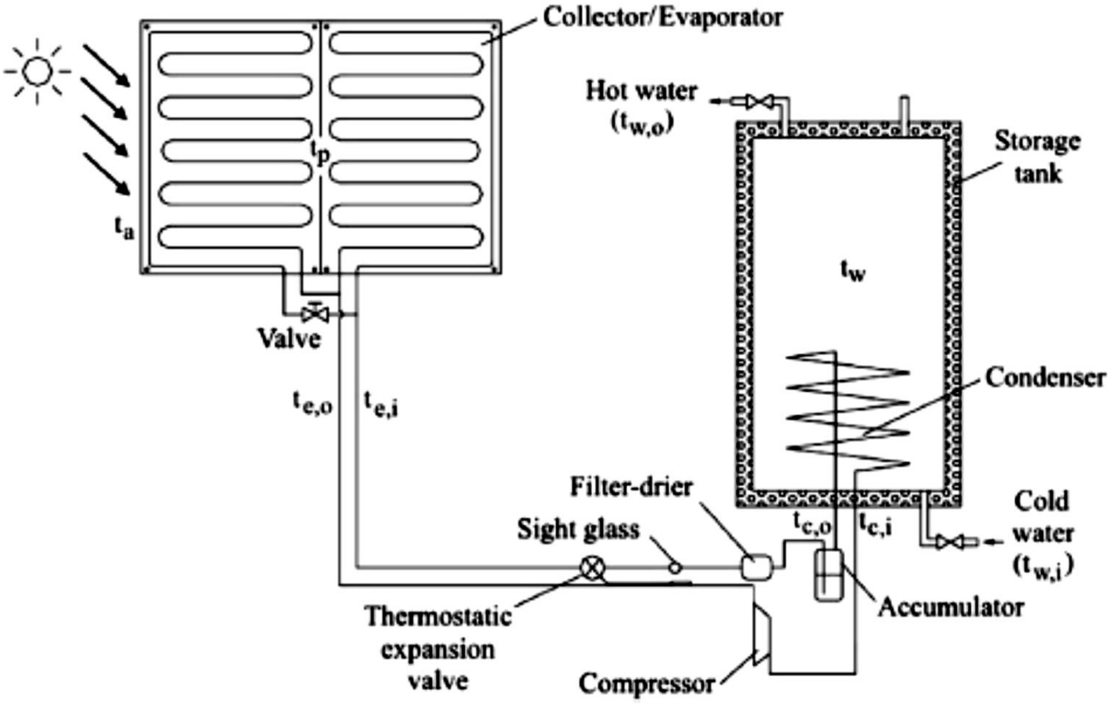

Figure 3.10. Schematic diagram of (*SAHP*) system circuit (Sarbu and Sebarchievici, 2017).

3.2. Past works on Heat Pumps

In the previous few decades, there are several theoretical and experimental studies conducted, with much attention put on improving the efficiency of the heat pump system. Nevertheless, numerous research has concentrated on improving the COP of heat pumps.

The application of residential heat pump for space heating started in the 1940s in the UK, and more investigation into improving its efficiency continued gradually. Thereafter, with continued deterioration of energy sources, environmental degradation coupled with an aim towards sustainability, the goal of reducing maintenance, system costs and to reduce ground for more research on heat pump technologies. Most of the reports came out to conclude that with the assistance of external power heat pump systems, there were possiblity of using natural and waste heat sources for dwelling space heating purposes.

Ground Source Heat Pump (GSHP) or geothermal heat pumps systems, typically have higher average efficiency among heat pump technologies because they draw heat at a relatively constant temperature from the ground soil. In 2016, Sarbu and Sebarchievici (2016) have stated that the applications of GSHPs for cooling and heating has experienced an annual increase of about 10-12 % because they have high energy performance and are environmentally friendly. Qi et al. (2014) have continuously monitored a GSHP system situated in Germany, in which the thermal performance of the system has been investigated. They achieved a much higher energy efficiency of about 80 % in summer, whereas the COP was up to 3.9 during the winter period. Sivasakthivel et al. (2014) investigated the GSHP system in terms of energy savings and CO_2 reduction potential, in which the study provided a profound analysis about to what extent India could benefit from this technology, where energy savings of 13-48 % were achieved during cooling and space heating respectively, while the annual reduction in electricity was 67-80 %. According to findings, it was concluded that the application of GSHP results in the decrease of CO_2 emission with 24-54% annually. The study concentrated on using Taguchi method to predict the COP and optimize the operating parameters. Therefore, it has also been found that at the evaporator inlet, the dryness fraction is the major influencing parameter, and under ideal conditions, the maximum values of COP obtained are 4.25 and 3.32 for heating and cooling operations respectively while the highest median value of COP is 3.92.

Another study analyzed a hybrid GSHP system as a new method for reducing the size of heat exchangers in order to minimize the exhaustion problem which typically happens on conventional GSHP systems. (Rad et al., 2013) have conducted a research in Canada to examine the feasibility of a GSHP hybrid system that utilise the solar/collector as a heat source. Through the use of TRANSYS simulation software, it was indicated that the utilization of solar thermal energy storage results in a significant reduction in the Ground Heat Exchanger (GHX) length with the net value of 3.7-7.6 % which is less than for the conventional GSHP systems. Regarding the economic predictions, (Alavy et al., 2013) examined the factors that directly influence the implemenation of the hybrid GSHP systems through sensitive analysis by varying the system sizes. It was concluded that the application of a small size of GSHP system could lead to the increase in the annual operation costs resulting into a long payback period, though it was observed that the the system was still more economical in relation to the other systems which depend of grid electricity.

A laboratory building test was also conducted to examine the thermal performance of thehybrid GSHP systems in Shanghai (Fan et al., 2014). The the results show that, throughout ten consecutive years, the average temperature of the soil increased gradually from 19.07°C to about 26.32°C by the end of the tenth year. Subsequently, the temperature variation of the soil produced a decline in the COP from 4.65 to 3.89 during summer time, but it increased from 3.27 to 3.48 in winter period. (Lee et al., 2014) studied and focused more on the transient performance characteristics of the hybrid GSHP systems in which it was revealed that the systems reached the optimum fluid flow rate of 8 kg min^{-1} (FFR), and a set-point temperature of up to 30°C. For the optimum condition, the average COP of the GSHP system increased by 7.2 % compared with the typical conventional GSHP systems.

It is an undeniable fact that the overwhelming majority of the heat pumps found on the market are either air source systems or ground source. However, water has the potential to be utilized as an energy source. Making use of water as reliable energy source comes with various benefits over the other energy sources. It is evident that, water has a higher capabiliy to transmit heat than air or the ground source. In comparison with the ground source, the utilization of water eliminates digging problem associated with the boreholes or trenches, thereby decreasing the initial investment costs. In addition, the COP of the heat pumps improved, with water as a heat source, due to the high return temperature obtained from the heat pumps compared to air or ground sources.

(Oh et al., 2014), conducted a study on a heat pump with a raw water source, for a vertical water treatment building by using TRNSYS simulation program. In the raw water source heat pumps system, the average $COPs$ of 3.76 and 4.79 were achieved under heating and cooling modes respectively. It was observed that the nature of climate has a significant impact on the power consumption of the heat pumps. In another research, the performance of Sea Water Heat Pumps (SWHPs) was noted to improve in terms of its energy efficiency by optimizing the design of the water-intake system (Wang et al., 2012). It was found out that the rate of energy saving, the reduction in the speed of water delivery water quite influences the energy efficiency. In 2010, Shi and Xue analyzed a water source heat pump to accurately control the analytical model of unsteady speed hermetic scroll compressor. Their analytical model effectively depicts the changeable speed features and regulated refrigerant flow rate in order to meet the target of increasing the energy efficiency (Xue and Shi, 2010).

(Lee et al., 2012), have carried out a study centred on the thermodynamic performance of R32/R152a refrigerant for SWHP. In comparison to HCFC 22, the COP of the R32/R152a mixture is 15.8 % higher and the compressor power is 13.7 % lower than that of HCFC 22. The SWHP systems are considered as candidate systems for coastal areas for cooling and heating purposes. However, the Simulation analysis done by (Zheng et al., 2014), proved that pumped water temperature is extremely affected by the seawater source temperature. Furthermore, the temperature of pumping will increasingly increase in winter period and decline during summer time due to the decrease in the pumping flow rate.

ASHP is another kind of heat pumps which extracts heat from low ambient temperature air and raises it by using the heat pump components to a higher temperature. The absorbed heat from the air at low temperature via fluid passes through a compressor from where its temperature is boosted to a higher temperature and later transmited into hot water and heating space for domestic use. Despite the efficiency of *ASHP* being lower because of low ambient temperature and low solar irradiation level, it has various advantages over ground or water source heat pump, including lower maintenance costs and easy installation. The *ASHP* system has the capability to offer domestic hot water at about 80°C and to be used for central heating.

(Hewitt et al., 2011) attempted to develop an air source heat pump and incorporate them into the dwelling building. In order to achieve higher COP when employing cold air as the energy heat source and to providing water with a temperature of up to 60°C, an expansion turbine was used instead of a conventional expansion valve, with an economical vapour injection compressor., The efficiency of *ASHP* that works at low ambient temperature was examined by implementing an assistant throttle apparatus which is a capillary that was twisted compactly around the compressor in the bypass cycle (Wang et al., 2011). The apparatus was used as an ancillary tool that can reuse the compressor surface heat. As a result, the heat capacity of ASHP achieved was three times that of the conventional compressor, consequently improving the work efficiency to more than 35 % at the operating condition of -10 °C.

In another development, (Cabrol and Rowley, 2012) through a comparative transient simulation analysed several building fabric properties in different UK locations by using TRNSYS numerical modelling of ASHP coupled with a floor-embedded heating system with Phase Change Material (PCM) as an insulation material. Annually, the air source heat pump system produced a COP of 4.0 for a mild climate and 3.5 for the colder climate. The use of PCM and thinner floor slab enhanced the stability of the temperature during the heating season, raised the comfort level and decreased the risk of overheating during the summer period in well insulated buildings. Elsewhere, a study was carried out for many sites in Italy by assessing the effect of different operating conditions, such as relative humidity and ambient air temperature on the energy performance of *ASHP* systems (Vocale et al., 2014). The findings highlighted that the monthly average COP can be reduced with a high valume of air and relative humidity (RH>80 %) by up to 17 % under outdoor air temperature in a range of 0-6°C. The whole season reduction (SCOP) between 1.51 % and 21.67 % was considered and the hourly simulation assessment indicated that the reduction of COP can reach up to 20 % in wet locations.

The simulation and experiment studies on a low-temperature *ASHP*, operating in a thermal buffer zone (TBZ) were carried out by using a climate chamber, with the COP observed for different climatic conditions (Touchie and Pressnail, 2014). The results indicated that the operation of an "off-the-shelf" *ASHP* under a TBZ can improve the COP in the cold weather. The developed model offered a sensible forecast of the *ASHP* performance working under 10°C, with a balcony used as a case study. (Li et al., 2014) investigated the energy consumption in both *ASHP* and GSHP on the concept of "warm energy" and "cool energy" through theoretical and quantitative analysis. The analysis of the exergetic characteristics of both *ASHPs* and GSHPs indicated that *ASHPs* is less than GSHPs in terms of energy consumption due to a lower temperature difference between heat source and heat sink. Another feasibility study was performed on the dual source heat pump by utilizing air and waste heat in electric vehicles.(Ahn et al., 2014). The experimentally results revealed that the COP for the dual heat source mode at the temperature is 0°C was 9.3 % while the heating capacity reached 315 %.

DX-SAHP system is regarded as one of the variants of *SAHPs* , incorporating solar energy and the heat pump in order to improve the energy performance. The working fluid from the expansion valve passes through the capillary tubes of the evaporator, which is evaporated by a solar radiation and the surrounding air. Afterwards, the saturated vapour is compressed through the compressor, which raises it to a high temperature and pressure so that it can be changed to the condensation phase. The condensed fluid then ejects heat and turns into water, with the ejected heat passed through the speeding fan so as to warm the indoor spaces while the liquid temperature and pressure is decreased and crosses the thermostatic expansion valve with cycle repeated. The modification of the collector/evaporator not only leads to efficient use of solar energy but can also result in the reduction of the system cost (Elamin, 2017). However, the solar irradiation is affected by mainly seasonal latitude and the climate change, leading to the variation in the system performance. Several studies have also concentrated on the performance improvement of solar-air heat pumps for practical applications. In 2008, an overview was conducted by (Kara et al., 2008), with a detailed modelling of *DX-SAHP* which utilizes a flat-plate solar collector/evaporator and a liquid R22 as a refrigerant with the system working in a surface area of 4 m². The authors observed that space heating systems need virtually a large area size of the collector unlike the water heating systems and that an air condtioner (A/C) system is also needed to provide higher heat energy. The obtained COP was recorded in the averaged of 1.5 to 9.0, which was greater than that of the traditional heat pumps with 2.3 to 3.0.

The authors presented an experimental study to determine the operating parameters of a *DX-SAHP* through a theoretical model for heating application parameter (Moreno-Rodriguez et al., 2013). The results from the prototype indicated that a solar collector with a surface area of 5.6 m^2 and a compressor rated at 1100 W, is influenced by the level of solar radiation, ambient temperature, and air. The solar radiation and the ambient temperature have a significant effect on the operation performance of the equipment. The COP from experiment varies between 1.9 and 2.7. By adding a domestic DHWT system, the COP ranged between 1.7 and 2.9, which is lower than the theoretical values of 1.85 to 3.1, while the temperature reached 51°C over the operating cycle. A quite similar research was done by (Banister et al., 2014) on SAHP implemented for DHWT, with a slightly different objective of identifying the weaknesses and strengths as well as the accuracy of a "TRNSYS model ".The results demonstrated agreement between the experiment and simulation.

A numerical study was presented by (Molinaroli et al., 2014), which examined the energy characteristics of a *DX-SAHP* by employing R407C as a working fluid for space heating. The results of the steady state heat pump through mathematical model are explained with various simulations carried out so as to anylase the five major influencing factors including; solar radiation, outdoor ambient temperature, solar field surface coefficient of the heat pump, collector efficiency and the heat capacity of the compressor. The results indicated that the COP is significantly affected by solar radiation and ambient temperature (in the range of 2.2°C and 4.3°C), but it is independent of solar field surface. The solar collector showed a high efficiency rate ranging from 50 to 149 % due to reduced collector heat losses and lower evaporation temperature. The authors recommended a variable compressor speed as a necessity to meet the building heating demand. An investigation of *SAHP* was conducted under a severe cold weather for space heating purposes by (Liu et al., 2014). The system design procedure and operation modes were presented and the COP was assessed under field test conditions and simulation by using TRNSYS software. The results show that the solar fraction and solar collector efficiency on identical heating days is 66 % and 51 % respectively. The *SAHP* technology system provided the lowest heating costs and a decrease in energy consumption of up to 55 % in comparison with existing gas/boiler heating systems.

A study focused on the exergy efficiency and performance characteristics of *SAHP* in winter period was accomplished experimentally in Turkey. The outcome of study emphasized that the COP may increase if there is a decrease in exergy loss in the evaporator. The exergetic efficiency of the system was found to be 65.6 % whereas the COP obtained was 3.08 with the exergy loss of the solar collector of 1.92 kW (Dikici and Akbulut, 2008). By using the life cycle cost Gagrani et al (Chaturvedi et al., 2014) researched about the possibility of energy saving and boosting the economic performance of *DX-SAHP* for water heating applications in low temperature conditions by using the life cycle cost analysis. The life cycle cost reached the minimum value when the solar collector area and compressor displacement capacity were at their ideal conditions. Hence, it was concluded that the life cycle cost of *DX-SAHP* systems can be decreased by using the most effective collector area. In addtion, an experimental evaluation of *DX-SAHP* systems for water heating was done by assessing the operating performance of the system under zero solar radiation conditions in a climate chamber where the results indicated that the COP was 3.23 at water temperature of 14-55C° and ambient air temperature of about 21.9°C, whereas the power consumption of the compressor was 279 to 478 W. Therefore, the *DX-SAHP* system has the capability to operate at higher COP values even for different severe conditions.

Wang et al (Li et al., 2007) carried out an experiment for *DX-SAHP* for water heating with the system incorporating a 4.20 m^2 type solar collector/evaporator operating with an R22 type as a working fluid and a compressor with a power rating of 0.75 kW as well as a 130 ltr water tank. The experimental results show that the COP of the system was 6.61 when the average temperature of the water was between 13.4°C and 50.5°C with an average ambient temperature of of 20.6°C and at a solar radiation intensity of 955 $W \cdot m^{-2}$. The average value of seasonal COP and collector efficiency was observed to be 5.25 and 108 % respectively.

3.3. Working Fluid Selections

Over the last decade, hydro-chlorofluorocarbons (HCFCs) and chlorofluorocarbons (CFCs) were vastly used in air conditioning applications and refrigeration. However, HCFCs and CFCs were banned by a universal protocol (1997) due to their ozone depletion potential which could result in more global warming. Accordingly, hydro-fluorocarbons (HFCs) were progressed as the replacement for HCFCs and CFCs. Although HFCs were not able to cause harm to ozone layer it was discovered that they have a considerable potential to cause global warming. Consequently, it was also banned to be used along with other refrigerants which involve fluorinated greenhouse gases with 150 or higher. Most recently alternative combinations of working fluids such as Difluoromethane/Pentafluoroethane and Tetrafluoroethane mixtures are used as a substitute to HCFCs, CFCs, HCFCs, and HFCs.

In 1997, R407c was suggested to be an alternative for R22 which was also phased out due to its negative impact on the environment. Therefore, R407c seemed to be a promising refrigerant with good thermodynamic properties that could provide the same refrigerant load to those working under vapour-compression circuit (Greco et al., 1997). Which is composed of three refrigerants compositions; R32, R125, R134a and its chemical formula is zeotropic mixture ($CH_2F_2/CF_3\text{-}CHF_2/CF_3\text{-}CH_2F$)

3.4. Thermal Energy Storage System (TES)

Energy storage systems are very important as effective storages and sources of renewable energy, which can be used when needed. In many parts of the world, the direct solar radiation is regarded as the most prospective energy source. Moreover, an energy storage system not only reduces the mismatch between demand and supply but also improves the reliability and the performance of the energy systems by playing a key role in energy conservation. This therefore minmizes the probability of energy wastage. Thus, in order to store energy as internal change, it is suggested to select one of the various suitable techniques such as latent heat, sensible heat and thermochemical or a combination of them. The major techniques used for solar thermal energy storage are summarized in Figure 3.11.

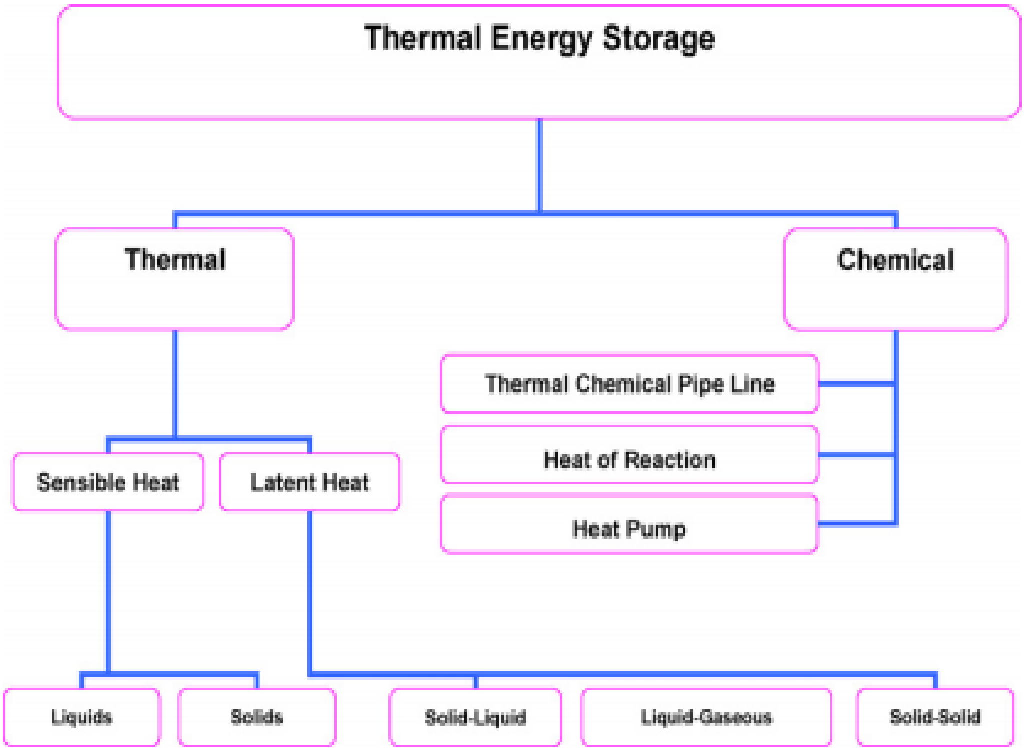

Figure 3.11. Different types of solar thermal energy storage (Balasubramanian et al., 2010).

3.4.1. Sensible heat storage (SHS):

In this type of storage, thermal energy is stored by raising the solid or liquid temperature. SHS system uses heat capacity and the change in the temperature of the material during the operating process for charging and discharging of the system. The quantity of stored heat depends on the specific heat storage medium. Hence, when the temperature varied, the amount of storage material is also changed accordingly. Water is reported to be one of the commonly used storage media because of its availability, cheaper and has high specific heat.

The popular technique of storing sensible heat is the water tanks. The sensible heat storage media are centred on either solid or liquid and not subject to a phase change when heat energy is removed or injected into them. Therefore, they are instead prone to temperature change. The solar energy systems need effective methods to store surplus heat collected during periods of sunlight, which is subsequently utilized when there isn't enough sunshine or later use.

Traditionally, the concept of storing heat in form of sensible heat was being used in most of the low temperature implementations, for example, water was utilised as a storage medium typically by raising its temperature for later use. It has been found that sensible heat is affected by boosting the temperature of the storage medium. Therefore, it is preferable for the storage medium to have high heat capacity, long-range steadines under thermal cycling, and most significantly, low cost consideration (Hasnain, 1998).

3.4.2. Latent heat storage (LHS):

The latent heat storage (LHS) technique operates by heat absorption or release during which the storage material is subjected to phase change from liquid to gas or solid to liquid and vice-versa. Phase change material (PCM) and its variants are considered recently as the most popular and attractive LHS system due to their high energy storage density at a steady temperature, but they are faced with containment problems in thermal storage systems that limit their application. To solve this problem, it is necessary to separate the heat transfer medium for transmiting energy from the source to PCM and from PCM to the load. Another challenge is that they have low thermal diffusivity and also require special design for PCM containers (Sharma et al., 2009).

In 1983, (Abhat, 1983) gave a helpful classification of the types of materials which were used at that time, their characteristics, pros and cons to determine the behaviour of these materials for thermal energy storage, as seen in Figure 3.12. The organic and inorganic heat storage materials are categorized as inorganic salt hydrates, paraffin, fatty acids and eutectic compounds.

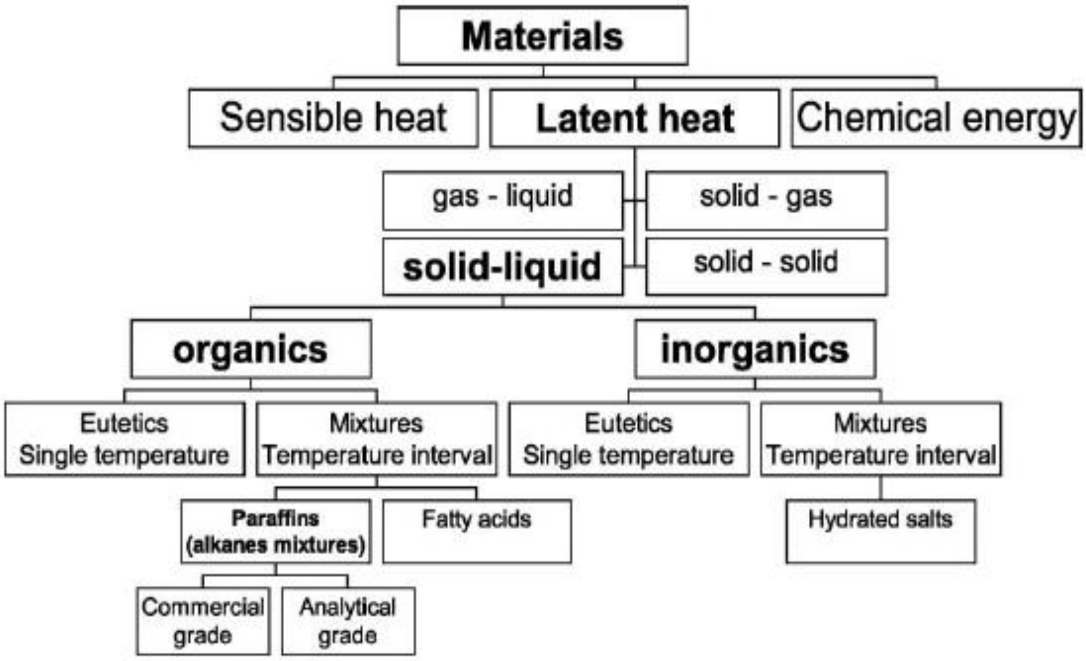

Figure 3.12. Classifications of energy storage materials (Xu et al., 2014).

A study has focused on the review of sensible and latent heat storage methods for water and space heating applications where the the basic principles and definitions were also discussed. It was stated that there was a growing interest in the development of latent heat storage technology due to the operational advantages, lower weight, higher storage capacity per unit and smaller systems size as well as a lower temperature variation. The review demonstrated that the choice of PCM as a material played a magnificent role in terms of heat transfer mechanisms. It is worth to note that the latent heat storage systems are considered in two major directions, namely heat exchanger and phase change materials research. The PCMs, such as salt hydrates have a promising possibility for low temperature thermal energy storage applications. Hence, there is need to conduct experimental work on their thermophysical properties (Hasnain, 1998). Another work was carried out about the background of thermal energy storage with solid-liquid phase change (Zalba et al., 2003). The review focused on three aspects; materials, heat transfer and its TES applications. With respect to thermophysical properties, the enthalpy-temperature curves presented as indicated in Figure 3.13 whereas the stability with respect to the corrosion of molten salts was investigated. With regard to the heat transfer analysis, the authors stressed that the use of exergy is essential in understanding the thermodynamic conduct of (TES) system.

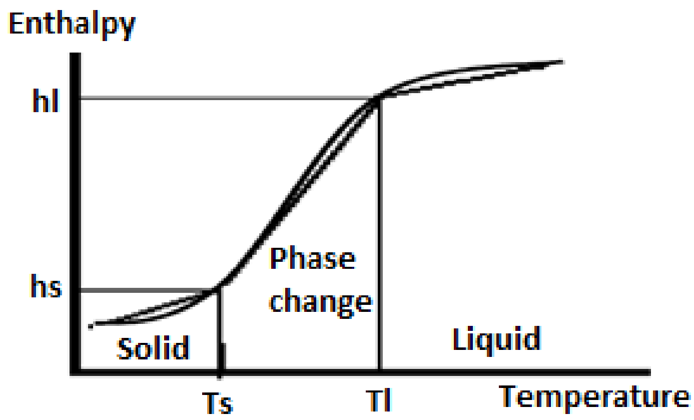

Figure 3.13. Enthalpy variations with temperature

An experimental study was conducted by (Khudhair and Farid, 2004) on building walls to enhance human comfort and maintaining the desirable temperature for a longer period of time by directly capturing energy from the ambient temperature. The study investigated the thermal energy storage systems by integrating PCMs in which the materials were used in different building parts among other the floor, concrete and the ceiling. It was concluded from the study that the PCM walls and other building components had higher thermal mass with the ability to capture a greater amount of solar radiation and are capable of minimizing the influence temperature swing inside the building. In the same study, the selected materials were cheap and had a moderately large thermal energy density. It has been noted that the hydrated salts (inorganic compounds) have relatively higher conductivity (0.5 $W{\cdot}m^{-1}°C^{-1}$) and larger energy volumetric storage density (350 $MJ{\cdot}m^{-3}$) but experience two obstacles; phase segregation and supercooling and thus require the use of thickening agents and some nucleating. The crystallization temperature of the hydrated salts was 30 to 50°C making them highly receptive for solar energy heating applications (Farid et al., 2004).

3.4.3. Thermochemical heat storage (THS)

This storage mainly depends on absorbed and released energy by reforming and breaking the molecular bonds in a completely chemical and reversible reaction. In such a case, the stored heat depends on the quantity of storage material, the bounds of conversion and the endothermic heat reaction (Ding and Riffat, 2013). Figure 3.14 explains the classification of chemical TES which is can be categorised generally into thermochemical and chemical energy storage. Thermochemical storage systems are also classified as open and closed systems. The open system with desiccant work and heat storage can work on adsorption process in order to complete the sorption process (at atmospheric pressure). On the other hand, the closed systems based on a closed running fluid circuit that is separated from the atmosphere (vacuum pressure). In this case, two processes in a closed system can be defined; absorption and adsorption (Weber and Dorer, 2008). Frequently, it may be difficult to distinguish between the phrases like ‘’thermochemical storage’’, ‘’chemical storage’’ or ‘’sorption storage’’ which differ depending on a particular author. Figure 3.15 shows the classification of sorption and chemical storage (N’Tsoukpoe et al., 2009).

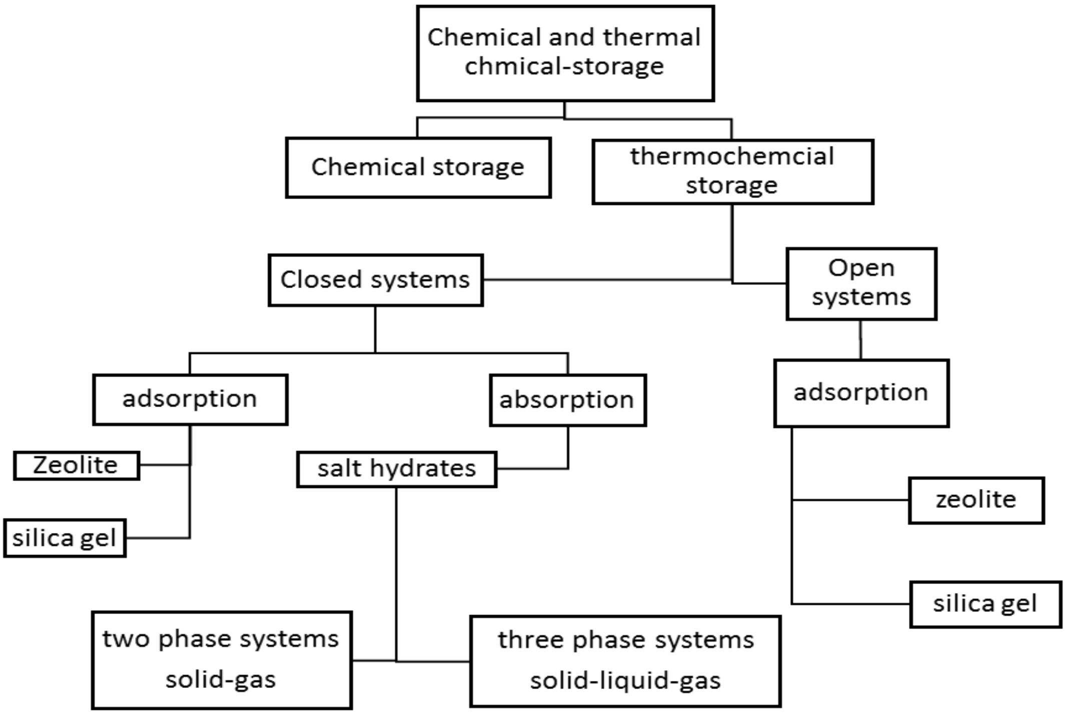

Figure 3.14. Classification of chemical and thermochemical storage (Bales et al., 2005).

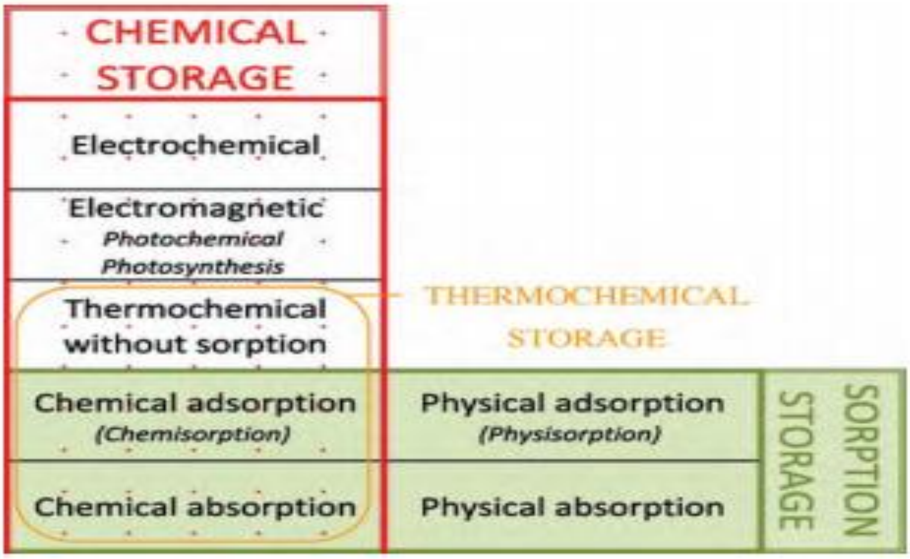

Figure 3.15. Chemical storage and sorption storage classification (Yu et al., 2013).

Sorption generally contains both adsorption and absorption both of which involve the physical transfer of a volume of energy or mass and can be utilised to collect the vapour or gas (sorbate) in condensate status by a substance (liquid or solid), which is referred to as (sorbent). Based on the bonding type, the sorption can be classified as chemical and physical sorption. Therefore, the state of dissolution or permeation of volume or mass of energy (absorbate) into another energy volume (absorbent) is called absorption (Inglezakis and Poulopoulos, 2006). Chemically, the process of transfering the sorption components in a fluid phase onto a solid adsorbent surface is called adsorption (Wang et al., 2009). The processes of sorption which are devoted to storage can also be classified as open and closed systems. Open systems as discussed before, operate under atmospheric pressure and the vapour is rejected into the atmosphere. The only material component which is used is water, but the isolated materials from the fluid are circulated in the closed system. Furthermore, closed systems have the capability to provide a higher output temperature for heating application purpose in comparison with an open system (Hauer, 2008). Sorption is also used in the solar refrigerant, and waste heat recovery for promoting heat pump technology (Demir et al., 2008), (Wang et al., 2009). Thus, adsorption is the transfer of an accumulated volume onto the surface or mass of energy or adsorbate onto the adsorbent surface to produce a large amount of heat (Aveyard and Haydon, 1973). Adsorption is divided into two types: chemical adsorption (chemisorption or solid/gas chemical reaction) and physical adsorption (physisorption).

The Thermo-Chemical Materials (TCM) or Thermo-Chemical Reaction Materials (TCRM) process is a reversible chemical reaction which has higher storage density close to that of biomass used in sorption storage systems. Many research studies on various storage systems have proved the potential and effectiveness of utilizing of TCM in storing heat and it has been proved to be one of the promising methods which are efficient and economical. The different TES materials, their reaction temperature and densities which are regarded as the major factors for selecting these materials are indicated in Figure 3.16.

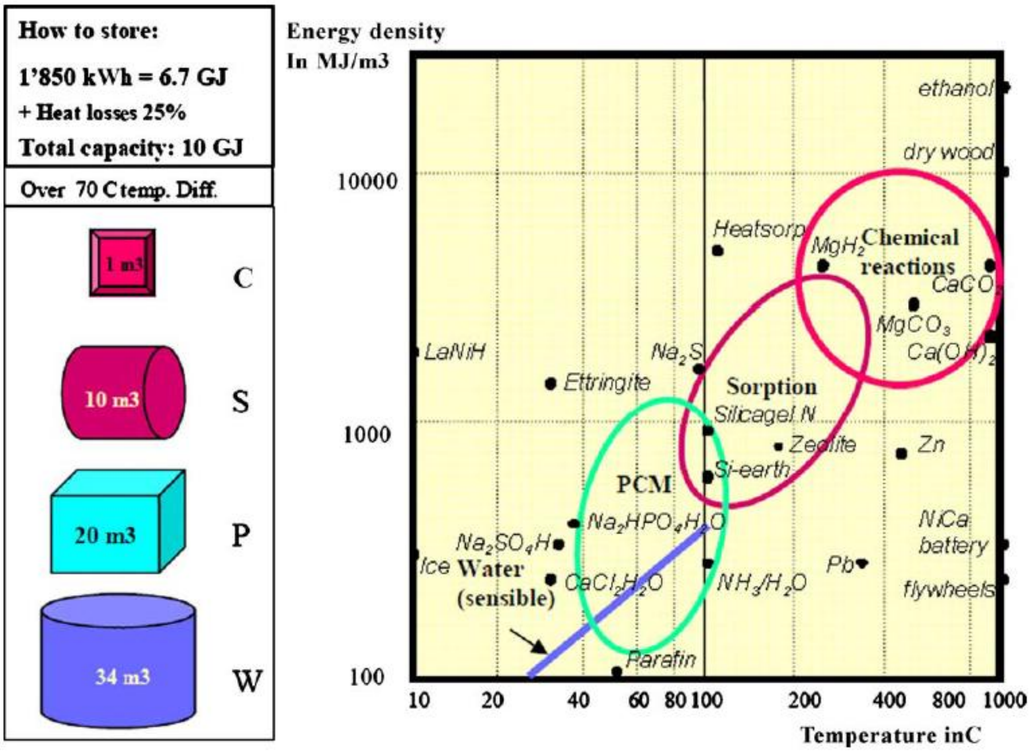

Figure 3.16. Different TES materials and their features

3.4.4. Sorption thermal storage systems

The use of reversible chemical reaction can be realised by chemisorption processes. Sorption is the physical or chemical bonding of a gas, with a solid (adsorption) or a liquid (absorption). During sorption, heat is released and can be used for heating. The process of adsorption and absorption on the surface of solid materials is illustrated in Figure 3.17. Adsorption indicates the bond between the liquid or gaseous phase of the component onto the inner surface of a porous material. Practically, the Sorption process cannot take place untill the sorbent connects with the sorbate. Hence, bonding energy can be stored. The entropy and heat are released to the environment instead of being stored in the vessels. These characteristics make the sorption thermal storage for solar energy storage applications as the most promising option.

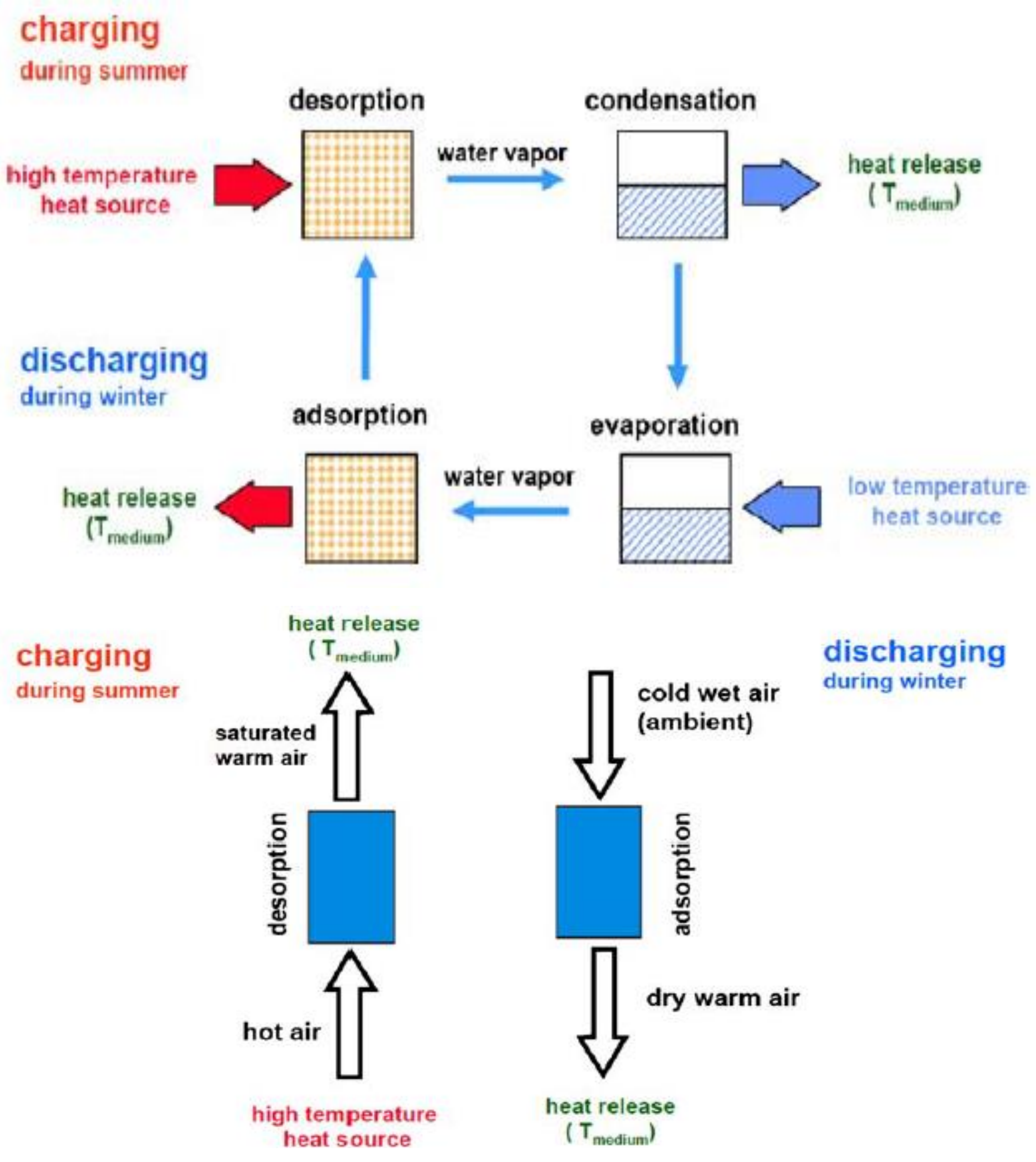

Figure 3.17. The process of desorption and adsorption on the surface of solid materials (N’Tsoukpoe et al., 2009).

Accordingly, sorption mechanisms are classified into four categories; solid sorption, liquid sorption, chemical reaction and composite materials as indicated in (Figure 3.18). The comparative research compared sorption systems and pointed out that internal substances of the closed loop system are dissociated from the steam of heat transport, providing an output temperature higher than an open loop system. However, this also requires high temperature throughout the process of the cycle. The study stated clearly that in terms of overall performance, the closed system was found to be satisfactory.

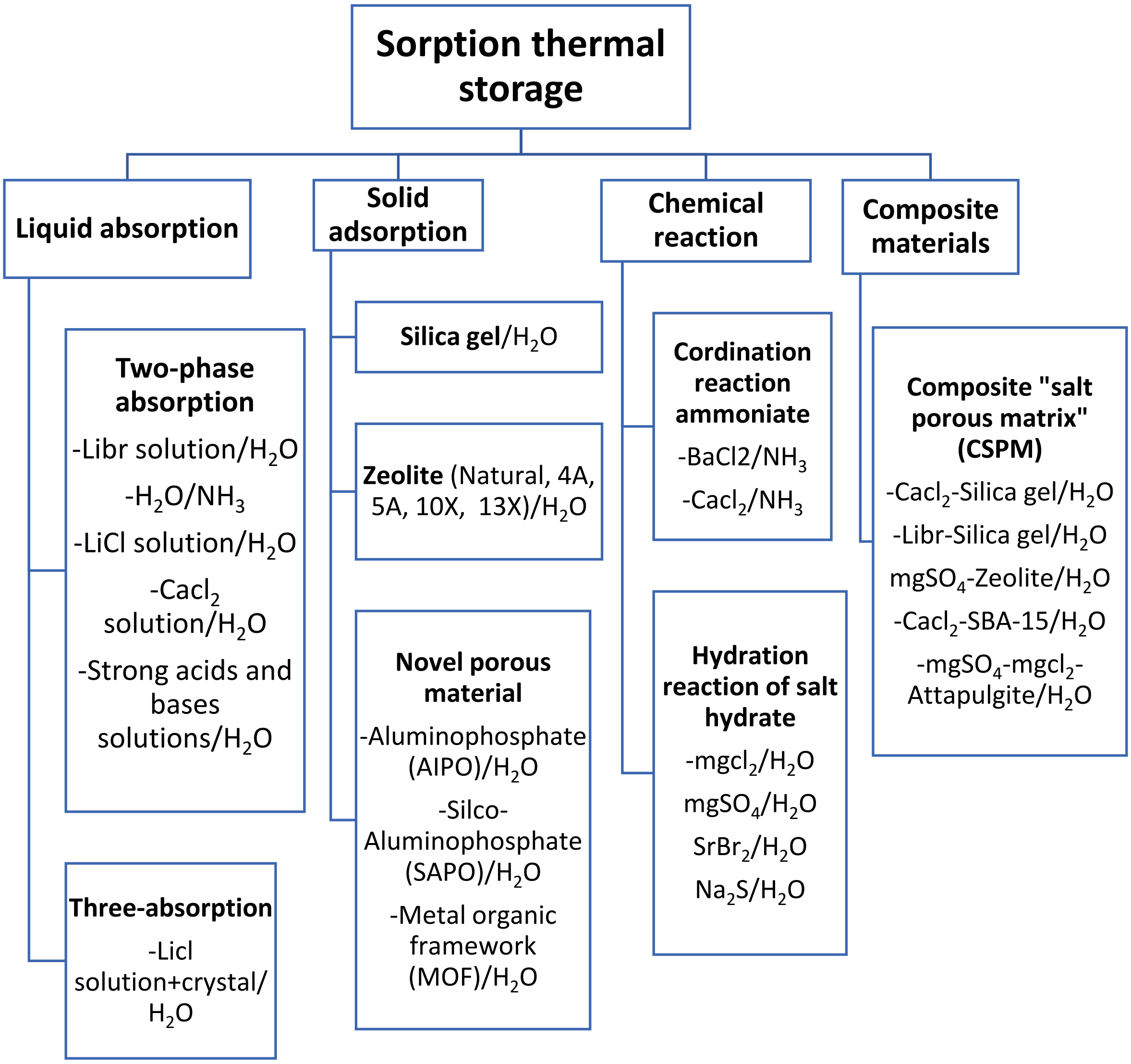

Figure 3.18. Sorption thermal storage classifications and new porous materials (Yu et al., 2013).

The sorption process basically comprises of two type of reactions; hydration and coordination reaction reactions. The hydration reaction involves the reaction salt hydrate with water while coordination is the reaction of ammoniate with ammonia. The water vapour or ammonia is derived from metal ions which compose to coordinate bonds. To promote the use of sorption systems, a group of composite sorbents, known as composite “salt porous matrix” (CSPM) has recently been adopted for sorption heat pump, energy storage applications and cooling. Hence, there are two components of sorbent; one of them is a host matrix including among other; expanded vermiculite, silica gel, and aerogel alumina, and the other is called inorganic salt such as LiCl, $CaCl_2$, $MgCl_2$, $MgSO_4$, Ca $(NO3)^2$, $LiNO_3$ etc.These are arranged in form of the matrix pores as indicated in Figure 3.19 and Figure 3.20. However, hot water is still employed as a storage medium as well as an aquifer, duct and gravel water (Yu et al., 2013).

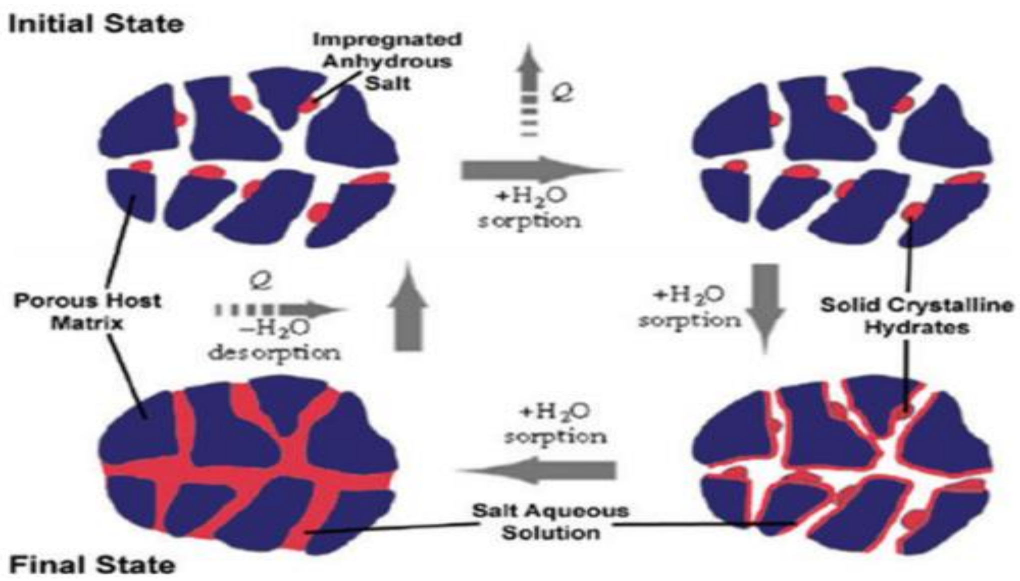

Figure 3.19. Scheme of water sorption on Selective Water Sorbents (SWS) (Aristov, 2007).

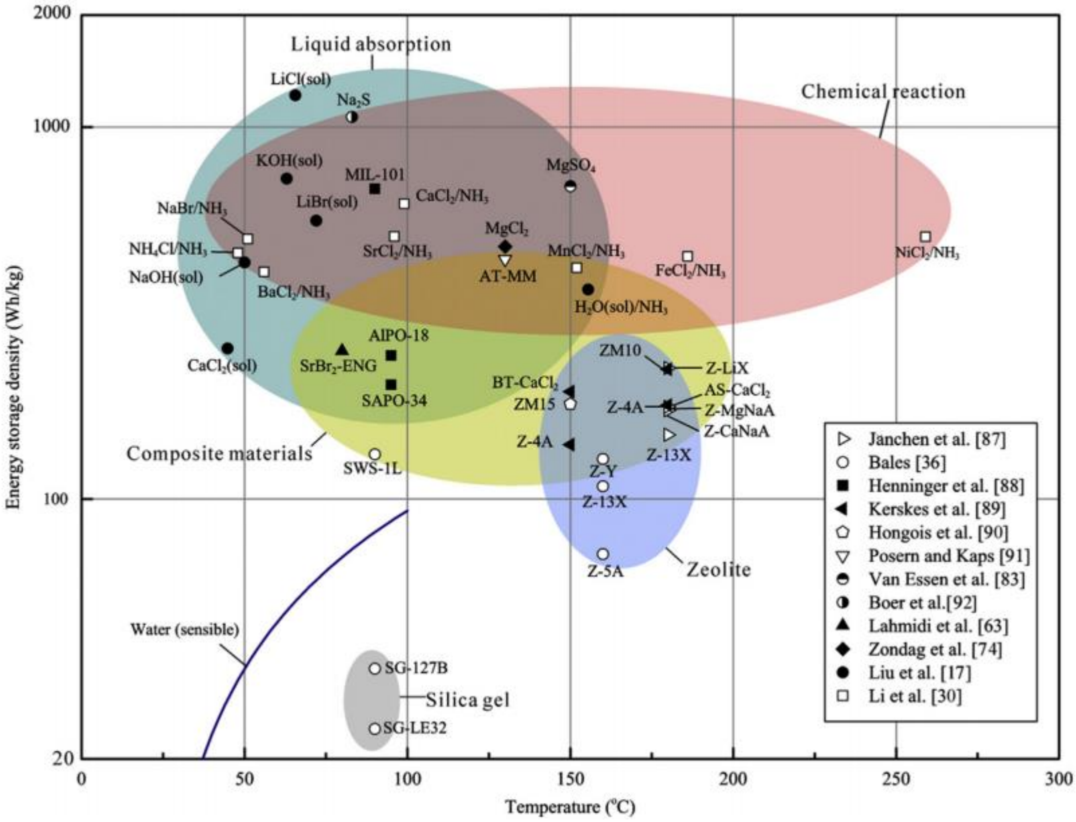

Figure 3.20. Energy storage densities of sorption materials (Yu et al., 2013).

The storage materials have a magnificent role to play in improving the sorption thermal storage systems. The major criteria for choosing the appropriate materials include; low charging temperature, low energy heat losses, high energy storage density, low cost; low price per kWh of heat energy stored, good heat and mass transfer properties, thermal stability without deterioration, higher sorbate and should be easy to handle (Wongsuwan et al., 2001). Several studies revealed that the salt hydrates can generally be considered as suitable TCMs. It is, however, necessary that these salts are integrated with a considerable amount of water into their lattice crystals if they are employed for solar heat storage in summer to dehydrate for a long time during storage until the stored heat is used in winter or when needed (Visscher and Veldhuis, 2005).

A composite material $MgSO_4.7H_2O$ was examined using an open system reactor and water vapor extracted from the ambient air, where the results indicated the power provided was practically not sufficient. Thus, it was recommended that the selected material requires being distributed over a larger exchange surface in order to react at a suitable rate so that it can release greater thermal power. The study also aimed at effectively use the power density or heat transfer of $MgSO_4.7H_2O$ by utilizing various porous matrixes to distribute this salt while mantaining as high energy density as possible. The finding revealed zeolite/$MgSO_4$ composite is more satisfactory than others (Hongois et al., 2011).

To choose a solid for thermochemical storage the volumetric energy densities of $CaCl_2$, $MgCl_2$, $MgSO_4$ and Na_2S are ranked as the most promising candidates for this purpose because of their operation conditions and other requirements. However, problems associated with the physical and chemical stability of the salt hydrates may be solved by encapsulating the salt with water permeable polymers (Trausel et al., 2014).

3.4.5. Principles of Thermochemical and Sorption Storage System:

Thermochemical and sorption storage systems are used as the reversible physical-chemical reaction to store energy. In order to provide the stored heat back for use, exothermic (synthesis reaction) is taking place as;

$$AB + \text{heat} \leftrightarrow A + B \qquad (1)$$

In this reversible reaction, the thermochemical materials (TCMs) are used to store solar energy seasonally during the warm period for use during the cold season. The TCM has recently demonstrated satisfactory heat storage capacity for a long period of time. With influence of heat supply, the TCM ‘C’ can dissociate into component A and B. I.e;

$$C + heat \leftrightarrow A+B \qquad (2)$$

The compounds AB is defined as a sorption working pair, sorption couple or reactants, whereby the combination between A (sorbate) and B (sorbent) is formed to heat release (exothermic reaction) and thus energy can be stored as a chemical energy with negligible thermal losses (Faninger, 2004).

The thermochemical energy storage cycle is composed of three major processes; (i) charging process, which requires the energy source for dissociation of C compound and this is called endothermic reaction. (ii) Storing; after the charging process, A and B will be formed and are both stored. (iii) Discharging process, where the combination between A and B in the exothermic reaction will push material C to regenerate, and recovered heat energy is released from this stage. These three processes are demonstrated in Figure 3.21.

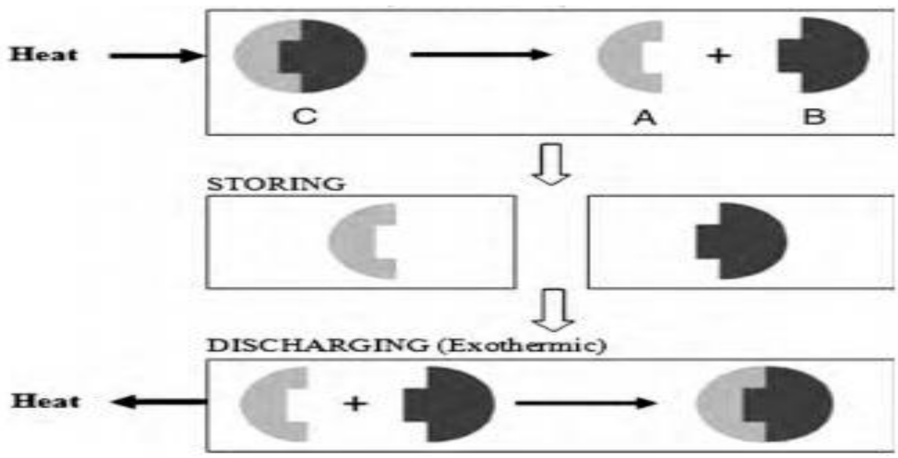

Figure 3.21. THS cycle: charging, storing and discharging (Yu et al., 2013).

3.4.6. Thermochemical-sorption open and closed systems

The combination of sorbent and sorbate is also called a working pair. There are two operating modes of the thermochemical-sorption system; open and closed system. In an open system, the reactive solid bed passes through a moist air flow at atmospheric pressure. Research reveals that the open system is cheap and a simpler reactor (Yu et al., 2013). Alternatively, in a closed thermochemical system, the salt reacts with pure water vapour at vacuum pressure. Hence, with the closed system, the design components need to be careful consideration. In the thermochemical-sorption storage, the promising concept for low-temperature is the closed sorption (Hadorn and Agency, 2005). This is mainly due to the heat output from the sorption materials, adsorb/absorb vapour of a solute which releases the enthalpy of absorption/adsorption. The main operating condition for the typical closed sorption storage system is that it must be evacuated before any operation. Therefore the materials absorbed or adsorbed are called sorption martials or sorbent. The substance that has been sorbed is referred to as a sorbate, and it is described as a working fluid or solute before it is sorbed. A study based on the second law and sensitivity analysis has identified the working modes and the main limitations of each method as well as the ways to address these challlenges. In terms of gas supply, a thermochemical-sorption storage system under the base of a hydration reaction could operate in two ways; at atmospheric pressure with moist air (open system) or at vacuum pressure with pure vapour about 1000pa (closed system) (Jähnig et al., 2006).

Apart from the operating pressure, the open or closed working modes may have other differences. For an open system, the steam is supplied by moist air coming from the ambient environment. In this case, however, the water of ambient air cold, therefore, have low partial pressure due to winter weather conditions. So, it would have to be humidified before passing it inside the reactor. The closed operating mode needs a heat source and an evaporator to generate steam for the hydration phase. It should be noted that a heat exchanger is essential to collect/supply the reaction heat in the closed system. Alternatively, in an open mode the thermochemical reactor, the reactive gas, and the heat transfer fluid are combined in a single flow (Stitou et al., 2004).

The closed sorption storages and heat pump absorption are utilized in similar processes. They, however, vary in the operation sequences. An actual heat pump works through two closed circulation cycles at the same time. The loop with the running fluid captures the heat in the evaporator at low temperature and ejects it in the condenser-absorber at a higher temperature. The sorbent loop is regenerated to increase the concentration of the sorbent, with heat provided at high temperature. Both the closed cycles simultaneously work at the same time. The heat storage cycles are not closed and the processes work in a sequential order. As result, the vessel is needed to store the intermediate products. The regenerator may be used as an absorber while condenser as an evaporator (Weber and Dorer, 2008).

Over the last decade, some recognised programmes have drawn some attention to show the relevance and feasibility of long term energy storage of solar energy in particular and have concluded that the stored latent and sensible heat cannot be used in materials over long-term periods. In chemisorption systems, due to negligible heat losses during the storage and the recovery of heat, it is necessary to store energy in chemical form to overcome this problem. Therefore, high capacity heat storage of smaller volume is practically promising especially for the buildings that integrate long-term and seasonal storage for dwelling heating (Michel et al., 2014). An experimental research was carried out for energy generation with solar energy storage and a solid-gas reaction heat transformer applied to upgrade the temperature to the middle grade heat. Solar energy and waste heat were considered to provide high capacity heat storage, which worked together to contribute to the high temperature of middle-grade heat to save energy through various thermal processes including chemical reaction, heat transfer, adsorption, and absorption, as well as the electrical process like a vapour compression heat pump. The researchers have mentioned that the advatanges of solid-gas reaction are not only its high heat storage capacity but also the upgrading of the middle-grade temperature as well as its dual role of storing and releasing the heat enegy via thermo-chemical reactions together with the absorption and adsorption refrigeration (Yu et al., 2008).

3.5. Working principle of thermochemical based heat pump systems

The the performance of the thermochemical heat pump (TCHP) was analysed for the energy storage system. The relationship between the pressure of the system and the equilibrium pressure analysed experimentally. Where it was deduced that these two pressures can be predicted at different water vapour content to design the TCHP system. It was also suggested that the solar panel could be incorporate to charge the desiccant throughout the adsorption process (Tahat et al., 1995). Another study concentrated on the performance of solar-assisted TCHP, where it was observed that the performance will decrease due to the reduction in the energy of condenser and the efficiency of drying (Fadhel et al., 2010). A mixture of materials comprising of expanded graphite, $Mg(OH)_2$ and calcium chloride for TCHP was evaluated in which it was concluded that the composite materials have higher hydration reactivity and dehydration rate at 200°C when compared with other materials (Fadhel et al., 2011).

The heat pumps with heat storage maybe utilised in different kinds of heating applications. In cold climate, the ambient source efficiency of a heat pump is highly required to have more heat for use during this period. Therefore, it is better to complement the heat pump with extra heat from storage rather than to utilising many or large capacity heat pumps. The stored heat energy may be used at a time when it is required. The nature of the heat storage determines the operating costs of the heat pump and thus the capital cost of the heat strorage systems should be optimized (Heap, 1979). So, it is essential to evaluate the value of heat storage for the heat pumps by considering the storage potential and the cost of materials for thermal storage. Consequently, the selection of the material for thermal storage depends on the amount of energy that has to be stored and the temperature at which it is to be supplied. In the context of utilizing heat pump with TCM, the volume of materials required to store sufficient heat energy for domestic buildings demand can be high and costly for large scale applications. The domestic storage tank may thus be heated by heat energy ejected from the condenser of heat pump for different heating purposes or to the heat exchanger with assistance of TCM storage.

The heat storage systems are commonly combined for water and space-heating for buildings applications. The storage system for hot-water use is usually designed to accommodate the unsteady heat demand of consumers. Heat pumps thus may be used in association with heat storage in a variety of heating applications. In cold climate regions, naturally, the ambient source of heat may have the insufficient capacity or heat pump efficiency is reduced. Hence, it may be a priority to supplement it with heat energy the storage system rather instead of using a heat pump with a large capacity which might be expensive (Reay and Mac Michael, 1986).

3.6. Aim and objectives of the proposed system

The main aim for proposing this system is to enhance the existing households heating performance in cold climate region. By utilizing generated heat from the collected diffuse solar and surrounding low grade heat energy, which can be used for space and hot water heating purposes. Meanwhile, the purpose of the thermochemical heat storage is to boost and maintain the hot water temperature at the desired level. The objective of this study is to investigate experimentally the performance of the novel design of the *DX-SAMHP* system while using low grade heat and the potential of incorporating the thermochemical reaction jacket into the DHWT to improve the overall heating performance of a single domestic home.

3.6.1. Description of the proposed system

The proposed system comprises of the *DX-SAMHP* unit coupled to the ternary evaporator panels. The *DX-SAMHP* system may makes use of the off-peak electricity which in most cases cheaper than at peak time or by utilizing energy generated from PV panel. The system also has an existing DHWT enclosed within a new adsorbent thermochemical jacket as shown in Figure 3.22.The thermochemical jacket is made of a high energy density composite of salt impregnated vermiculite, which uses the reversible reaction of salt and moisture vapour to produce heat. The expected reaction in the jacket is based on a single DHWT configuration which employes the existing central heating system pipes to supply heat for household use. The DHWT contains an immersion heater connected to the hot water supply which based on *DX-SAMHP* for energy supply to the tank.

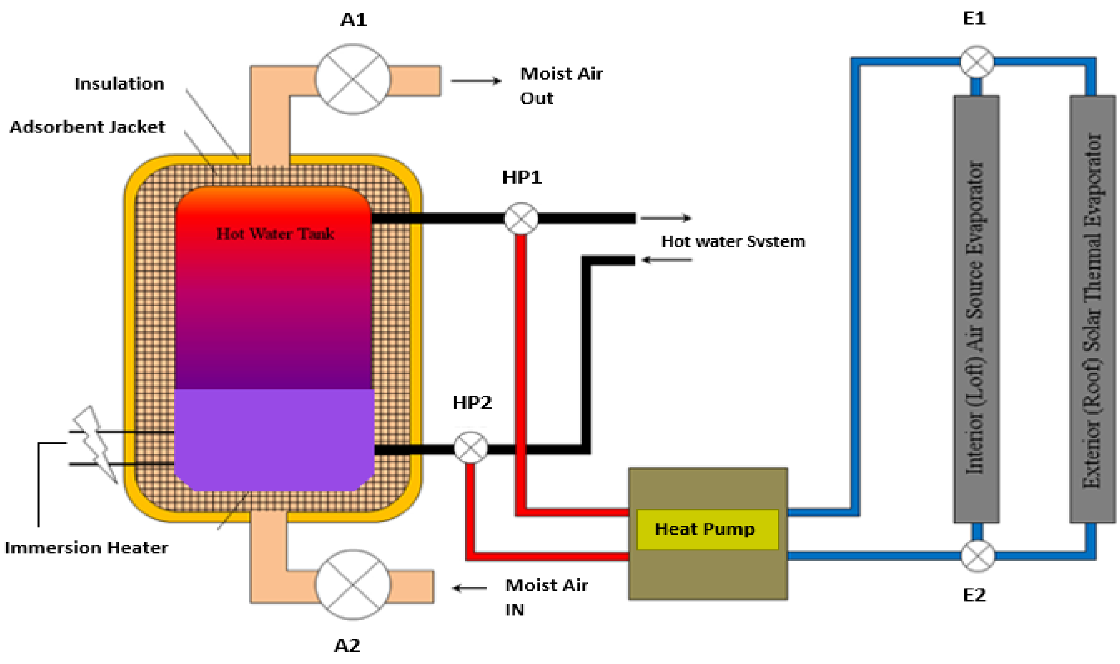

Figure 3.22. A schematic diagram of the main components of the proposed system

For evaporator panels (collectors), two solar thermal evaporators could be mounted externally on the roof and another placed internally in the loft space of the house. A refrigerant R407C is selected to be circulated through the aluminium panels. The refrigerant can collect the solar radiation, ambient temperature and/or waste heat and carrying the heat energy to the *DX-SAMHP* unit via pipes (blue). The selection of the most efficient evaporator panel to use at any given time can be intelligently controlled via valves E1 and E2. A water pump can then circulate a cold water from the water cylinder into the condenser-heat exchanger (HP1) after which the hot water returns back to the cylinder through red pipe and valve (HP2). This flow continues until the water in the cylinder reaches 50ºC or above. Once this is achieved the *DX-SAMHP* can go into standby.

When required, the composite material in the jacket may be discharged by opening valves A1 and A2, passing moist air from the interior of the house (e.g. for showering, cooking etc.) through the adsorbent jacket. The thermochemical reactions (chemical and sorption) of the composite material can thus be utilised for direct air heating of the hot water in the DHWT by restricting air movement at valve A2, depending on the user demand.

Using off peak electricity at night time which is in most cases less costly, the immersion coil is powered to heat up the composite material in the reaction jacket, when valve A1 is opened to allow moisture to be desorbed and release heat through the material's pores or interstices. The desorption of moisture from the composite material is referred to as the 'charging' cycle. Thermal regulation controls the DHWT water flow to ensure that adequate temperature is achieved during the charging stage. When the composite material is fully charged, the valve A1 is closed, and the hot water in the DHWT is stored and ready for use.

All these components are suggested to be situated internally within the attic space of the house as portrayed in Figure 3.23, for three main reasons but not exhaustive:

1) The refrigerant is heated using waste heat inside the house via internal collector/evaporator while carries the heat energy back to the heat pump unit. This would also maximize the use of non-premium space allowing minimal intrusion into existing residential areas.
2) Reduce the disruption and noise of *DX-SAMHP*'s compressor and diminish the refrigeration pipe works, to minimize the heat loss.
3) As the system utilizes thermochemical reaction with the salt stored in the cold 'dehydrated' state, such a place prevents moisture from hydrating the salt.

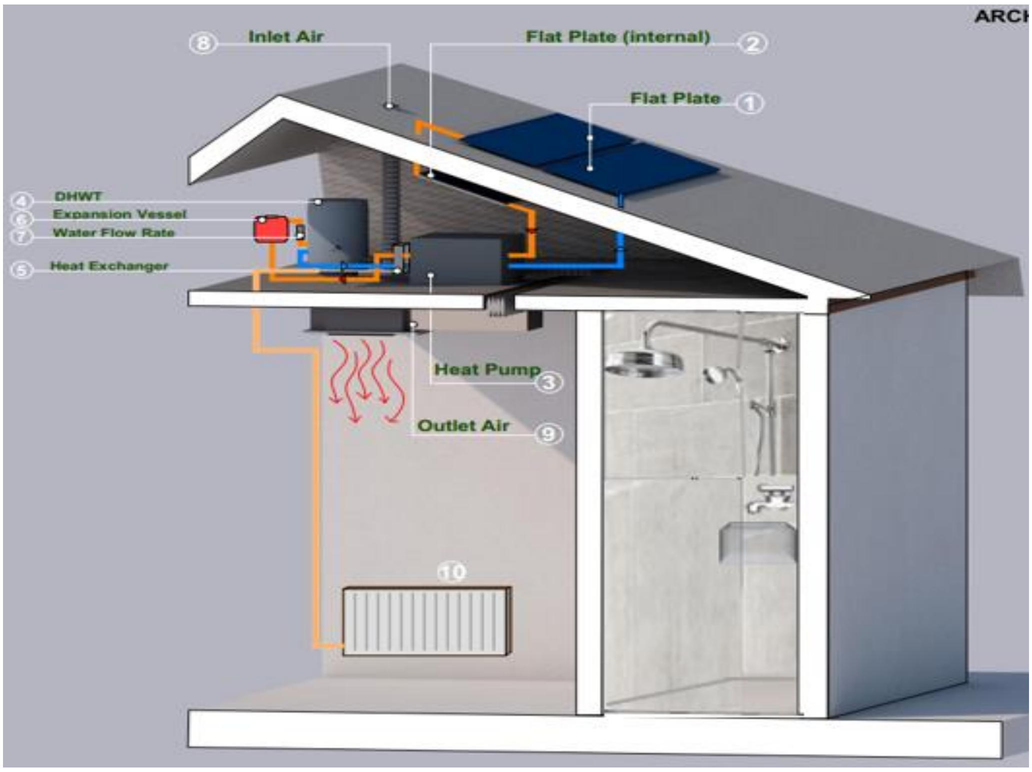

Figure 3.23. The proposed system installation on top of the roof for the building

Chapter 4. Numerical and Experimental Analysis on Performance of the attic Air-to-Air Heat Pump System Under Cold Climatic Conditions

The air has attracted attention as an effective heat source. *ASHPs* are considerably cheaper and easy to install in residential buildings. The purpose of this chapter is to study the thermal performance of air heating system for domestic space heating in typical houses in the cold region. The main purpose is to improve thermal comfort of the homes and reduce the Carbon footprint ffrom these houses. In this regard, an attic (air to air) heat pump, which could be installed in an existing home's loft for space heating is used. The study evaluates the use of a single heat source for space heating in domestic buildings. In addition, it is aimed to minimize the costly space required for the heating system in the domestic house.

4.1. Description and Data Acquisition of the ASHP system

The *ASHP* consists of an attic unit that contains four main components: the evaporator, condenser, an expansion valve (capillary tubes) and the compressor with the refrigerant of type R134A running inside as a working fluid as depicted in Figure 4.1.

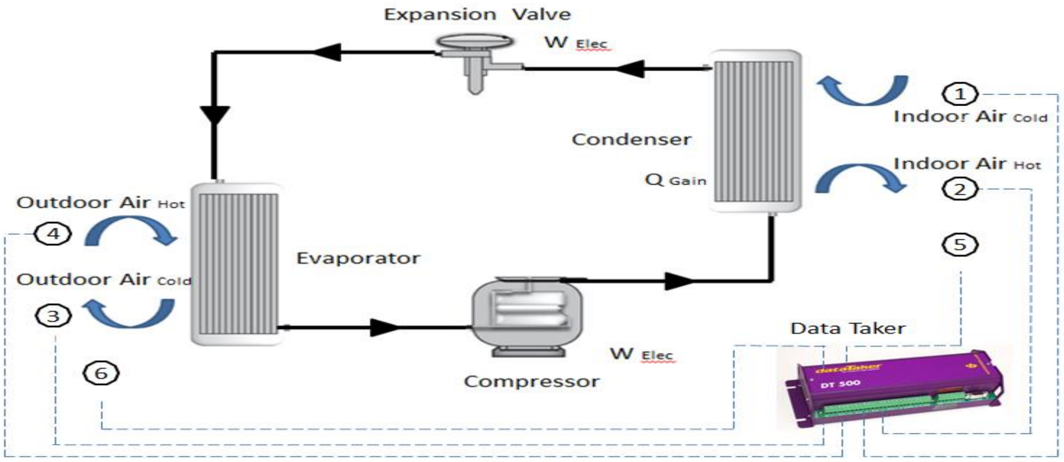

Figure 4.1. The schematic diagram of the *ASHP*

Two fans are operated alongside the evaporator and the condenser for exchanging heat through air circulation. At the evaporating end, the indoor air is sucked in and blown out directly from the inlet and outlet respectively. The components are numbered based on the sequence of operation from 1 to 6 in Figure 4.1. The unit is installed indoor, and interior/exterior airflows are designed as exhibited in Figure 4.1, (1, 2, 3 and 4), so that the temperatures of these points can be monitored. A data taker is used to record the data (5). The recorded data is recorded on the computer (6) and kept for analysis.

4.2. Operation and Principle of *ASHP* System

The *ASHP* system using reverse carnot cycle principle can be simplified as the system that can carry heat to specific area from low-temperature heat source whereas consuming a small amount of electrical power. When the *ASHP* is in operation, the fluid enters the evaporator with low temperature, extracts heat from the available outdoor air to evaporate, and at the exit of evaporator becomes a low-pressure vapor. Consequently, the compressor compresses the fluid and raises the temperature and pressure. Subsequently, the high temperature and pressure vapour pass into the air condenser, which is condensed to become a liquid during this process, where the rejected is utilized to heat the indoor air. Lastly, after the throttling process via the capillary tube (expansion valve), the fluid experiences a sharp pressure drop before entering the evaporator to continue with another cycle.

4.3. Experiment set up and procedure of *ASHP* System

Figure 4.2 shows, the preparation of *ASHP* system test. A digital power meter is utilized between the plug and the socket to measure the power consumption and the voltage of the compact unit as indicated in Figure 4.2 (a). The two flexible ducts at the entrance and the exit of the condenser are connected to the outside of the laboratory to faciliate the condensation process as displayed in Figure 4.2 (b). A number of thermocouples (type T) are connected to measure the temperatures. A hand-held anemometer was used to measure the outlet air flow rate at the condensation fan in order to assess the thermal performance of *ASHP* and the other operational parameters. The remaining technical specifications of the tested *ASHP* system and the test procedure are presented in Table 4.1. The testing of *ASHP* system took place in three typical days; 20th, 19th, and 12th of November 2014 during rainy, cloudy and sunny days respectively. The system was operated from 9:50.am until 16: 20pm for 6.5 hours. The data taker recorded the data each at one second intervals for raw data to be analyzed.

(a) Power meter (b) *ASHP* test set-up

Figure 4.2. Testing rig of *ASHP* system

Table 4.1. System technical specifications

Model: Tongyi *KR25*			
Heating Capacity	2.7kW	Input current (cooling)	4.36A
Cooling Capacity	2.5kW	Max input power (heating)	1.22kW
Voltage	220V~	Max input current (heating)	5.54A
Frequency	50Hz	Max input power (cooling)	1.15kW
Input power (heating)	1.02kW	Max input current (cooling)	5.22A
Input current (heating)	4.6A	Design pressure	≤4.2MPa
Input power (cooling)	0.96kW	Refrigerant: R134A	800g

4.4. Results and discussions of experimental test

The purpose here is to clarify the effects of parameter variations on the performance characteristic of the *ASHP* system. Figure 4.3 displays the overall thermal performance trend of the *ASHP* system, showing the operating temperatures of different components. It is observed that the indoor temperature remained relatively constant at the desired level of up to 25°C during a specified period. It is also indicated that the average value of the evaporating temperature is about 15°C while the produced hot indoor air temperature is in the range of 23°C-25°C. Meanwhile, the condensing temperature varied between 45°C-55°C corresponding to an outdoor temperature between 18°C and 22°C. It is noticed that the outdoor temperature has an obvious effect on the evaporator temperature, and hence on the condensation as well.

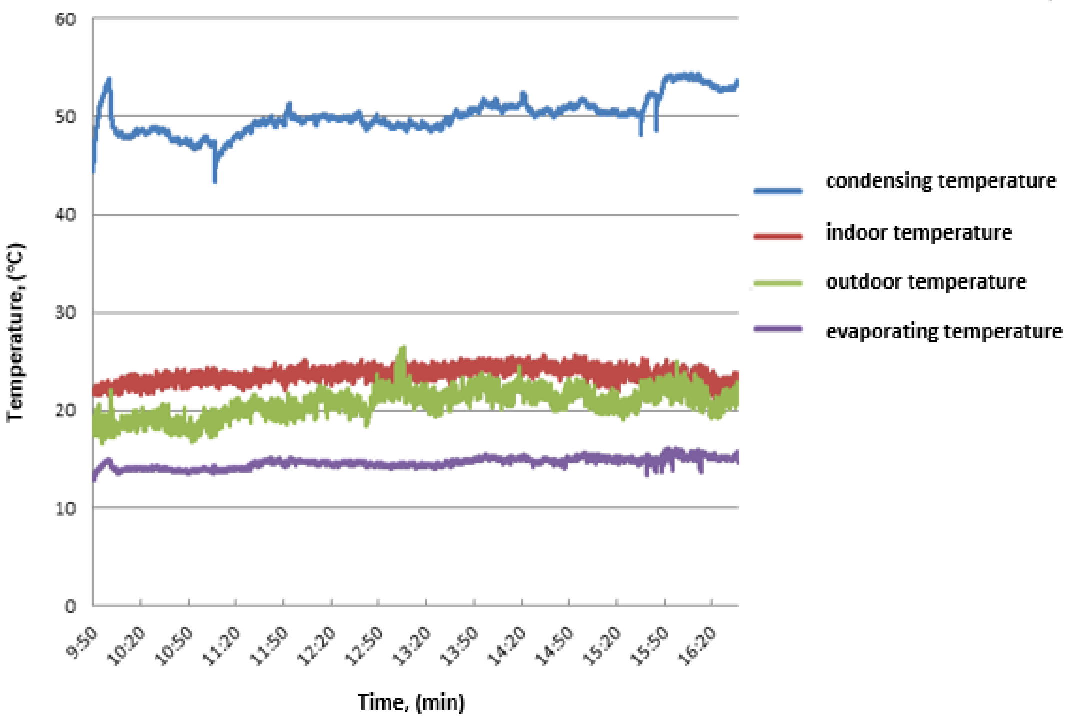

Figure 4.3. The effects of parameter variations on the performance characteristic of the *ASHP* system

The power consumption from the power meter was recorded once every 30 minutes as shown in Figure 4.4. The graph also presents the heating capacity of the system and the power consumption for the duration of the indicated time. It is observed that in the early morning the highest thermal energy is up to 7.5 kW. The reason for this is that the temperature of sthe evaporator in the early morning is relatively lower than the ambient temperature. This allows the evaporator to accumulate the useful heat and transfer it from the ambient to the evaporator. Therefore, one can note that the power consumption of the system decreases as the outdoor temperature drops and it rises as the outdoor temperature increases (Figure 4.3 and Figure 4.4).

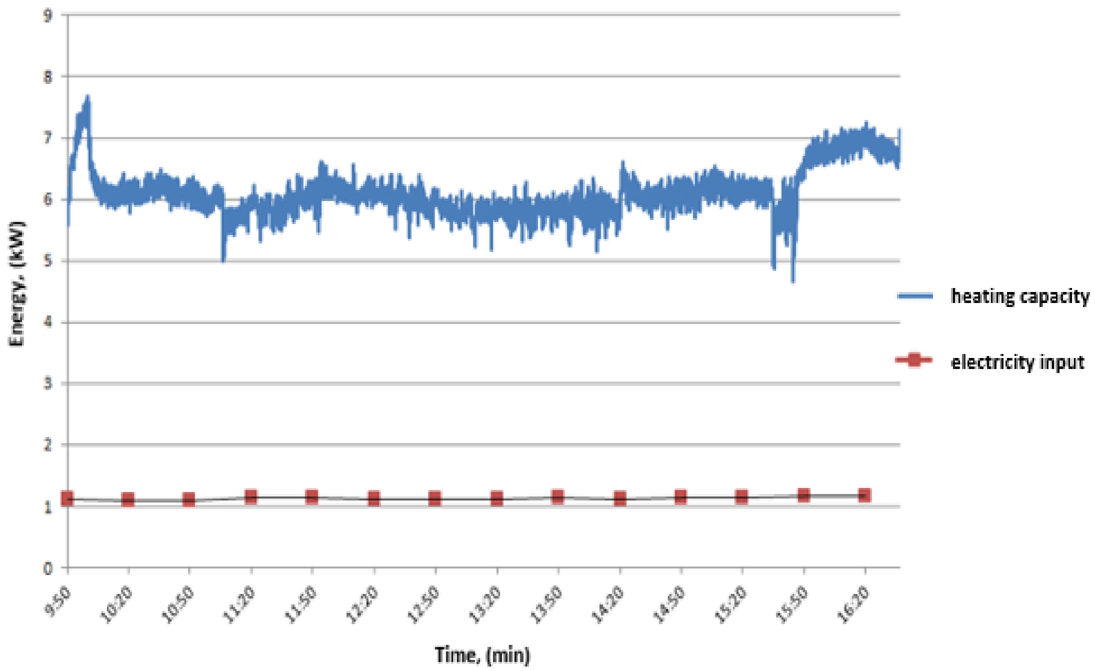

Figure 4.4. The influence of electricity consumption on the heat gain and performance

The velocities of air are measured experimentally at chosen locations from the center of the outlet to the boundaries using equation 1:

$$ṁ_{air} = \rho * V * A \quad (1)$$

where $ṁ_{air}$ is the air mass flow rate; ρ is the density of flowing air 9 (kg·m^{-3}); V is the air flow velocity (m·s^{-1}); and A the flow area (m^2) with the average calculated value of 9.5 m·s^{-1}.

The thermal energy gained by the system was calculated using equation 2:

$$Q_{H\_air} = ṁ_{air} * C_{p\_air}(T_{out} - T_{in}) \tag{2}$$

where Q_{H_air}, is the heat gained by the air condenser (kW); C_{p_air} (kJ·kg^{-1}·°C^{-1}) is the specific heat capacity of air; T_{out} and T_{in} (°C) are the system's outlet and inlet air temperatures respectively.

The COP ofheating (COP_H) of the system was determined using equation 3:

$$COP_{H-sys}(\tau) = \frac{Q_{H\_air}(\tau)}{W\ (\tau)} \tag{3}$$

where Q_{H_air}, is the air heat exchange rate in the condenser; while W, is the system power input within the specified duration period (τ).

As a result, the system achieved the highest COP_H 4.9 in the early morning, and the lowest value of 3.6 at 15:35.pm within the operating period as shown in Table 4.2.

Table 4.2. The experimental coefficient performance of *ASHP* system

Operating Time	9: 50.am	10:20 am	11:10 am	12:00 pm	13:20 pm	14:35 pm	15:35 pm	16:10 pm
COP	5.5	4.5	3.8	4.0	3.9	4.2	3.6	5.1

It should be noted that the system COP was mainly due to the power consumed by the compressor and other electrical apparatus. Thus, the system can take advantage of the low off-peak energy rates set by the utility to reduce the system energy consumption cost.

4.5. The instruments and measuring tools accuracy

An anemometer for air velocity type (DVA 30) with uncertainty ±1 % was used to measure the system inlet and outlet airflow rate. The airflow rate was measured at various points inside the system's ducts to ensure the uniform flow and air measurement. The temperatures were measured using T-type thermocouples with the uncertainty of ±0.4 % as shown in Table 4.3. All the data was recorded using a data logger (4V4R2-Type) with Data taker (DT600-Type), recording at the one-second interval with the accuracy ±0.1 %.

Table 4.3. The specifications of the experimental instruments

Parameter	Range	Accuracy	Measuring apparatus
Temperature (°C)	-200°C +200°C	Special-limits error ± 0.4 (%) ±0.1°C	T-type thermocouple
Power meter (kW)	0-4kW, 13A, 220-250Vr, 50/60Hz	± 1(%)	Digital wattmeter, Primera-Line PM 231 E
Airflow rate (m/ps)	1013mb, 0.00399-90m^2 At 20°C	±1(%) of reading, ±1 digit	Anemometer DVA 30 VT
Data Taker	From 1 second	±0.1(%)-of recording digits	DT600,with DeLogger4V4R2

4.6. Modelling and simulation analysis of *ASHP* system

In order to validate the experimental work on the present *ASHP* system, modeling and simulation were carried on the system for alternative R407C as replacemnet for R134A refrigerant. A MATLAB program was developed and written on the basis of the mathematical model.The thermal performance and the theoretical COP of the system can be obtained by computing the enthalpy changes in the compression and the condensation phases of these two refrigerants. The input data included; the enthalpy saturated liquid, enthalpy saturated vapor, enthalpy superheated, and entropy vapor at each temperature. The thermal properties of the refrigerants are obtained from the refrigerant manufacturer 'DuPont Suva'.

4.6.1. Modeling and thermodynamic analysis of the *ASHP* system

4.6.1.1 Compressor model

The compressor power (W_{comp}) can be calculated in terms of the enthalpy changes of the refrigerant at the inlet and outlet of the compressor, and It can be determined from equation 4:

$$W_{comp} = m_r(h_2 - h_1) \tag{4}$$

4.6.1.2 Evaporator and condenser model

The absorbed energy rate at the evaporator and the condenser can be determined in terms of the refrigerant enthalpy changes as presented in equation 5 and 6.

$$Q_{evap,ref407\mathrm{C},134A} = m_r \cdot (h_1 - h_4) \tag{5}$$

$$Q_{cond,ref407\mathrm{C},134A} = m_r \cdot (h_2 - h_3) \tag{6}$$

where h_1, h_2, h_3,and $h_4$are the enthalpy changes at the respective specific refrigeration cycle states.

However, in this *ASHP* system test, the actual heating and cooling capacities are attained using equation 7 and 8 by measuring the air mass flow rate, and the air temperature difference at both the inlet and outlet of the evaporator and the condenser.

$$Q_{evap,air} = m_a \cdot c_p \cdot (T_{air,out} - T_{air,in}) \tag{7}$$

$$Q_{cond,air} = m_a \cdot c_p \cdot (T_{air,out} - T_{air,in}) \tag{8}$$

4.6.1.3 Coefficient of performance of ASHP system

The relationship between the power consumed by the compressor and the rejected heat by the condenser is defined as the COP of the *ASHP system*, which can be determined from equation 9:

$$COP = \frac{Q_{cond}}{W_{comp}} = \frac{m_r \cdot (h_2 - h_3)}{m_r \cdot (h_2 - h_1)} = \frac{h_2 - h_3}{h_2 - h_1} \tag{9}$$

However, the COP defined in equation (9) only takes into account the enthalpy changes of refrigerant for the theoretical situation. In a real operation, some auxiliary apparatus, such as the fan, refrigerant pump, electronic control devices, the consumed electrical power to run the system must be computed. Hence, the previous equation can be replaced by the effective COP equation as:

$$COP_{effective} = \frac{Q_{cond}}{W_{elec}} \tag{10}$$

4.6.2. Simulation analysis of the *ASHP* system

In this study, the theoretical model and simulation of the alternative refrigerant are applied to assess the working fluid based on the reversed Carnot cycle and the heat transfer laws. The flowchart of the simulation program is described in Figure 4.5. The operatings stages of the systems include; evaporator outlet (T_e), compressor outlet and condenser outlet (T_c) respectively.After inputting the evaporating and condensing temperature, three essential parameters h_1, h_2, and h_3 at the operation stages can be imported into the software from the thermodynamic property chart. If the evaporating temperature is higher than 19.85°C (328K) and condensing temperature is over 55.85°C (293K), the simulation will be automatically stopped, otherwise, it continues by incrementing the temperature to T_e + 1°C and T_c + 1°C. The $COPs$ and the corresponding temperature variations are recorded and the results are discussed.

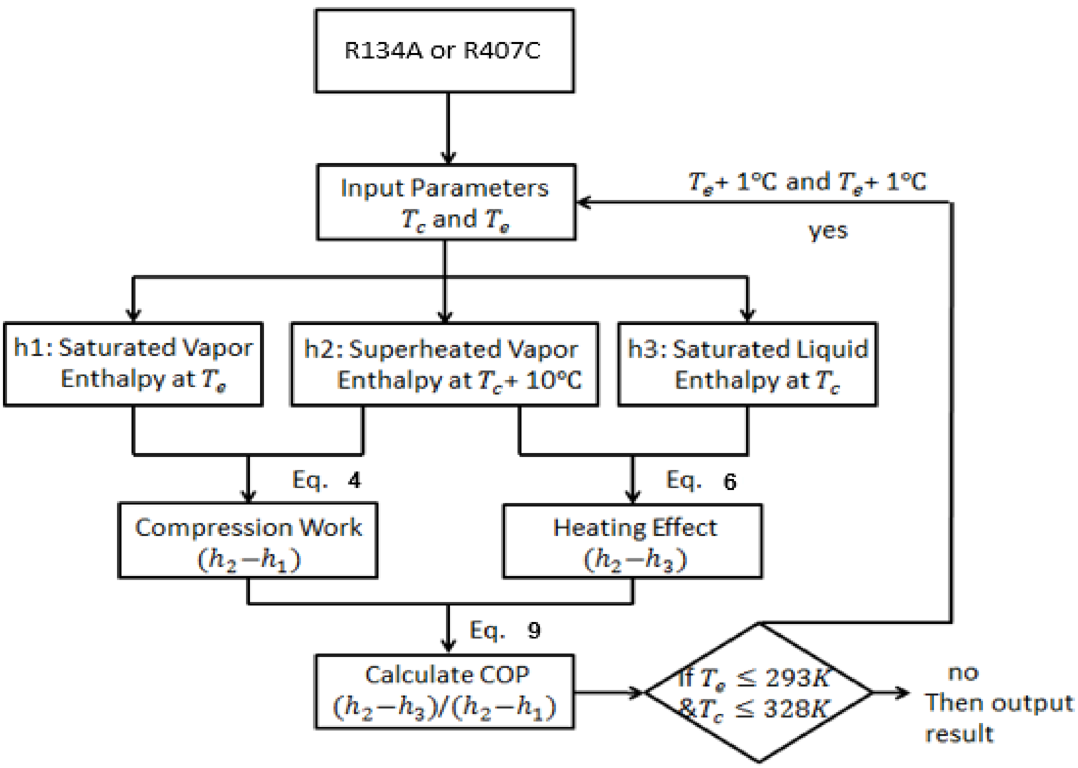

Figure 4.5. Flow chart of the simulation program

Based on the selected refrigerants, the *ASHP* cycle can be analyzed in order to assess the refrigerant's thermodynamic behavior. Figure 4.6 portrays the Temperature-Entropy (T-s) diagram of the system, which comprises of four processes; (i) the compression process to condensing the fluid and raising its pressure in the compressor (1 to 2s practically or 1 to 2 theoretically); (ii) the isobar condensation process for saturation of the fluid in the liquid state in condenser (2 to 3); (iii) isenthalpic expansion process via the capillary tube or expansion valve at temperature T_{EXV}, (3 to 4); and (iv) the constant isothermal evaporation process when the fluid is flowing via the air-cooled evaporator. For this application, due to the external conditions, the condensation temperature is constant while the evaporation temperature varies. Therefore, the moddeling and simulation are used to assess the operating conditions of the air temperatures.

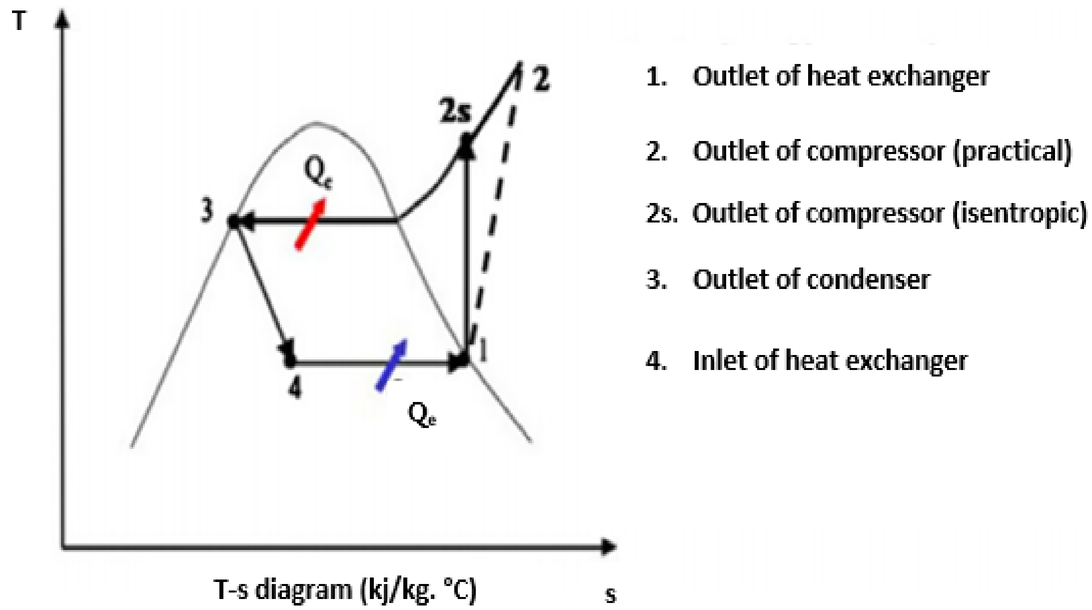

Figure 4.6. Indication of the *ASHP* thermodynamic cycle in T-s diagram

4.6.3. Modeling and simulation results with discussion for *ASHP*

The modelling and simulation were carried out with the aid of the refrigerant thermodynamic properties chart, through the computational software programme. A comparison of the COP and thermal performance between the prominent R134A and a substitute refrigerant R407C has also been done for the system. The theoretical COP of these two refrigerants was obtained by calculating the enthalpy change in the compression and condensation stages using equations the presented above. Table 4.4 indicates the gap between the practical and theoretical thermal COP of the *ASHP* system. The the difference in the results is attributed to the power consumption during experiment due to electronic devices, compressor, and other auxiliaries components as well as the laboratory environment and the uncertainties in the measuring instruments.

The electrical power consumption during the operating time wasnoted to be between 1.2 kW to 1.5 kW.

Table 4.4. Comparison between the practical and theoretical $COPs$ of the *ASHP* system

Operating Time	9:50 am	10:20 am	11:10am	12:00. pm	13:20 pm	14:35 pm	15:35 pm	16:10 pm
COP_{exp}	5.5	4.5	3.8	4.0	3.9	4.2	3.6	5.1
COP_{mod}	8.7	8.5	8.3	8.1	7.8	7.6	7.4	7.2

The simulation was also carried out within the range of condensing temperature changes from 25°C to 55°C, while the evaporating temperature was varied from 0°C to 20°C, within the experimental operating conditions of *ASHP* system. The difference between the COP of R134A and R407C under various condensing and evaporating temperatures are revealed in Figure 4.7 and Figure 4.8, respectively. In Figure 4.7, the condensing temperature changes from 25°C to 55°C, while the evaporating temperature is defined as 0°C.

In the simulation , the $COPs$ for both refrigerants drop steadily as the condensing temperature increases. Once the condensing temperature increases by 1°C, the $COPs$ of the two refrigerants decline at an average of about 3.5 %. The cause of this variation can be exaplined by analyzing the refrigerant thermodynamic cycle as exhibited in Figure 4.6 above. Since T_c increases whereas T_e remains unchanged, the compressor has to work at a higher rate to condense the fluid to raise its pressure up to the the isobar process (from 2 to 3). Additionally, part of the heating effect is challenged at the same time. Also, the $COPs$ of R134A reamin constant and about 13 % higher than that of R407C which is attributed to its higher enthalpy vapor value.

Figure 4.8 demonstrates the variation of COP at the condensation temperature of 55°C. It is observed that the evaporating temperature increases from 0 to 20°C. It is also clear that with the rise of the evaporating temperature, the COP of these two refrigerants increases steeply, and COP variance also increases from about 19% at 0°C to nearly 22% at 20°C. As T_c and T_e become very close, the COP also increases in value. Therefore, the compressor consumes less power as the evaporating temperature increases. Besides, the impact of evaporating temperature on COP is higher than that of the condensing temperature due to the sharper variation curve showed in Figure 4.8.

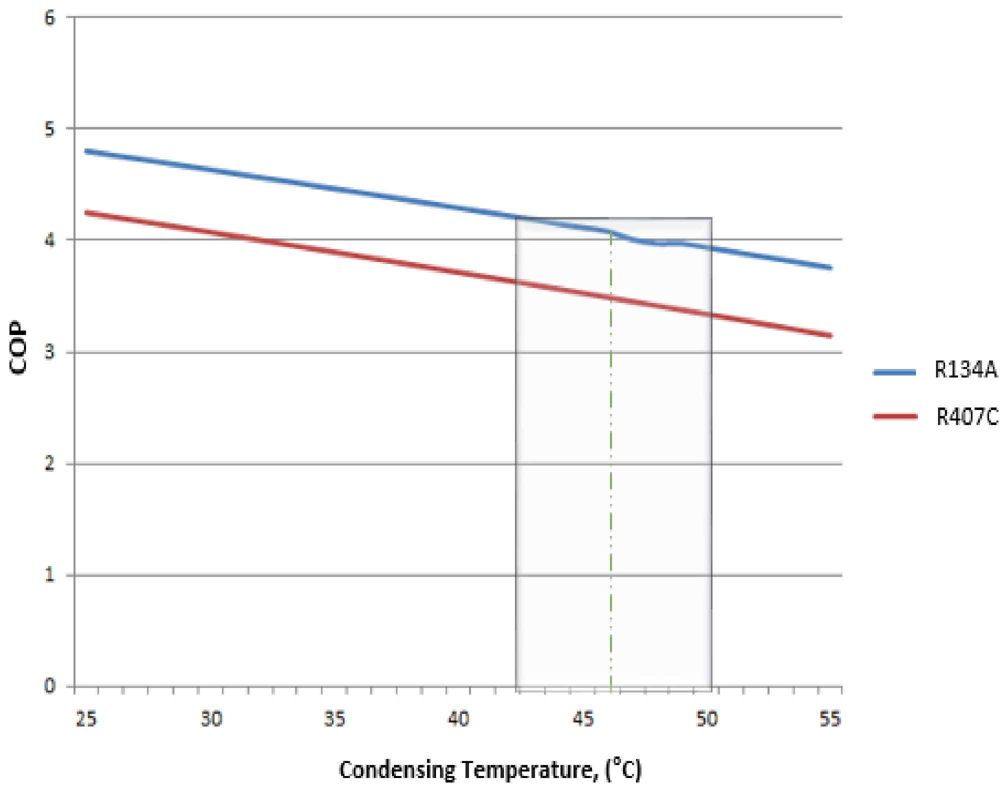

Figure 4.7. The variation of COPs for R407C and R134A under different condensing temperatures

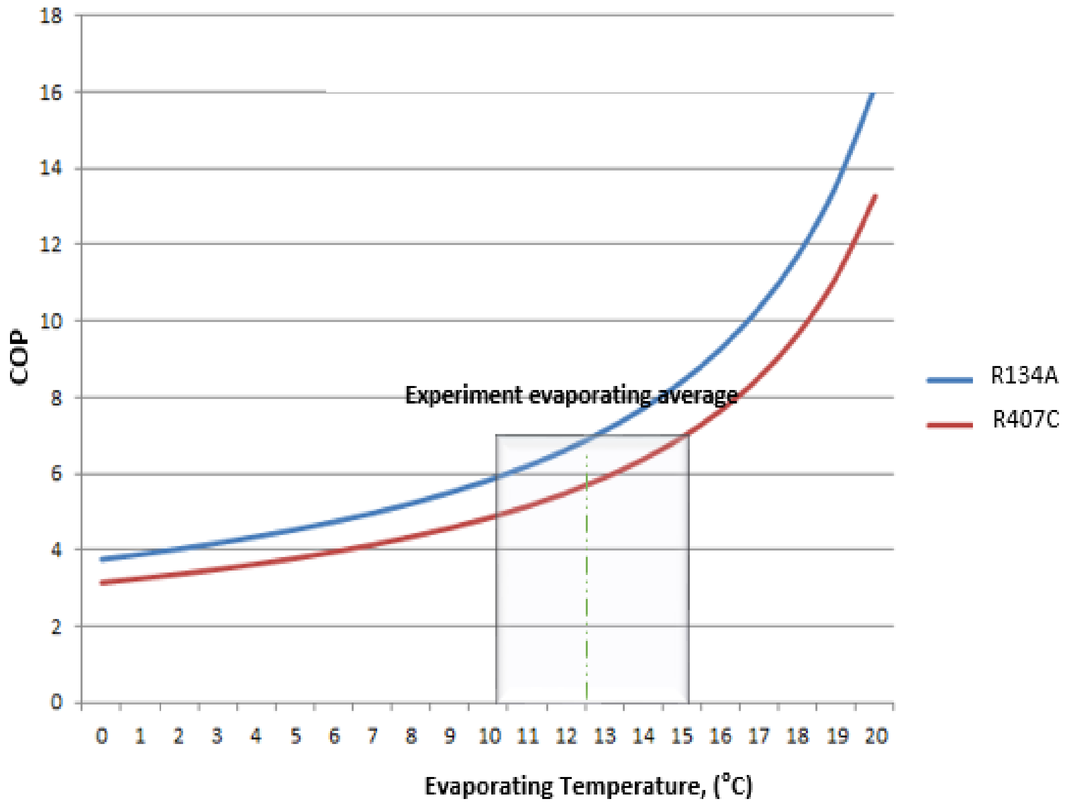

Figure 4.8. $COPs$ variation of R407C and R134A under different evaporating temperatures

Figure 4.9 and Figure 4.10 show a three-dimensional view of the simulated *COPs* as a function of T_e and T_c for R407C and R134A. The refrigerant R407C has lower values of COP, which increase from 3.15 to 18.77 within the simulation conditions. On the other hand, the R134A COP values vary between 3.75 and 21.41. The highest and lowest values of COP for both refrigerants occurs at the minimum temperatures (T_e = 20°C and T_c = 25°C) and the maximum temperature difference (T_e = 0°C, T_c = 55°C). This is due to the fact that, the smaller the temperature difference between T_e and T_c, the larger the COP of *ASHP* system, which is attributed to the reduced power consumption of the compressor. Furthermore, eventhough the difference between the evaporating and condensing temperatures are equivalent, the COP may be different because higher evaporating and condensing temperatures have a greater impact on COP value as tΔT remain the same.

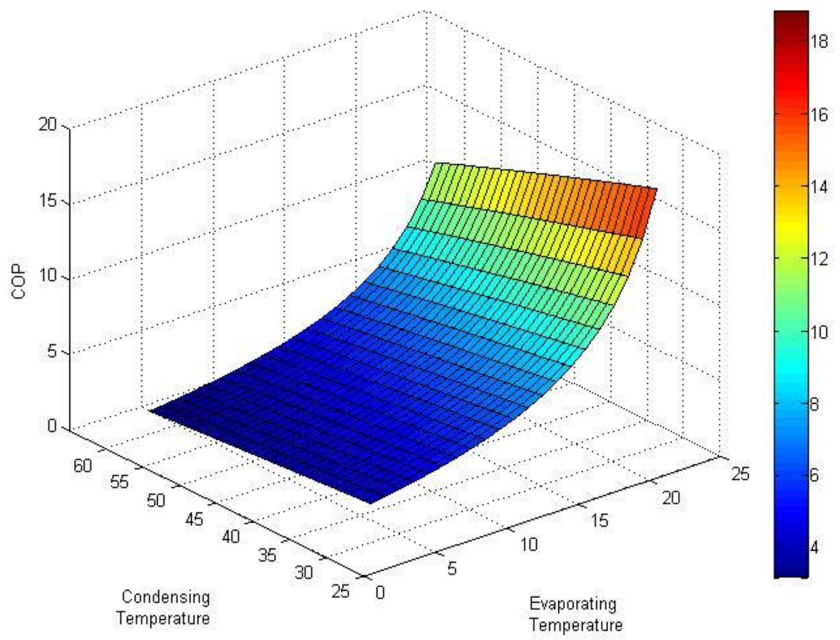

Figure 4.9. COP of R407C as a function of Te and Tc in modelling

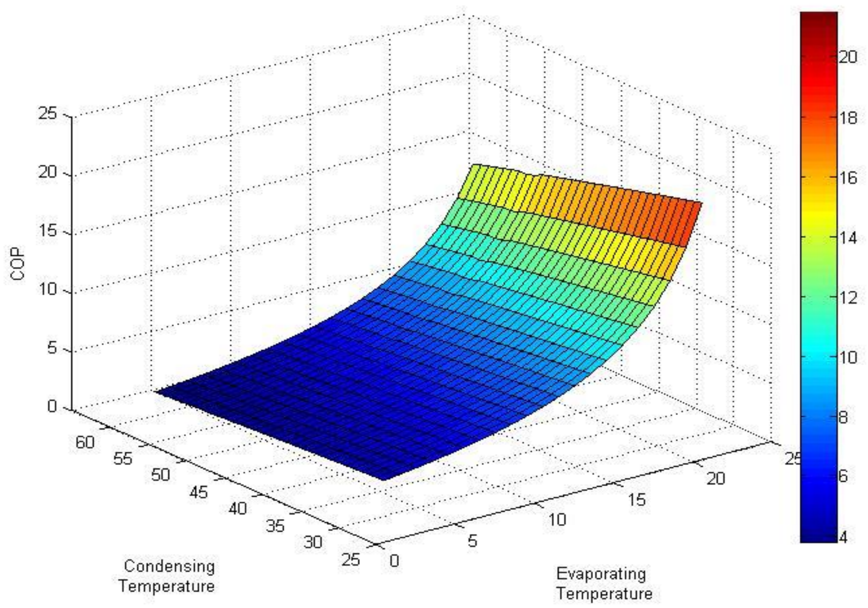

Figure 4.10. COP of R134A as a function of Te and Tc in modelling

To sum up, the COP of the *ASHP* system is mainly attributed to the difference between the temperature (temperature lift) of the low-grade air heat source and the output air temperature of the *ASHP* condenser. However, the differences between the temeparture of the heat exchangers and the temperature of of the useful heat output are also important. The ideal COP of *ASHP* is solely determined by the temperature difference and the condensation temperature. On the other hand, the simulation values can only determine the theoretical thermal performance variations but neglect the energy consumption of the auxiliary or supplementary system components and the expected energy loss.

4.7. Conclusion of Chapter 4

This chapter covered the concept of the *ASHP* system using Reverse Carnot cycle. The purpose of the work was to improve the air-to-air heat pump performance, in order to produce space heating that suitable for domestic applications and targeted users.The experimental work and mathematical model of the *ASHP* systemwith evaporation and condensation processes were described. The experimental and theoretical analyses that are crucial to understanding the mechanism of the heat pump by using only air as a heat source were presented. The simulations were conducted to compare the two working fluids in terms their thermal performance. The mathematical model was analysed and validated using the experimental results. The results have provided the significant factors that affect the COP of *ASHP*. Among those factors, the constant temperature of the low-grade air heat source at the evaporator was the most significant. But this is not to suppose that other factors are of lesser significance. However, due to the fluctuation in air temperature especially in the cold region, the *COP* of the system from the experiment was remarkably lower compared to the theoretical value. Therefore, hybridize the *ASHP* system with supplementary heat sources such as solar energy, domestic waste heat, etc. to assist quick recovery and to offer surplus heat are highly recommended. This could minimize the effect of delivered air to the evaporator and avoid the seasonal changes on the performance of *ASHP*. In the next work different technical arrangements can be implemented to improve the evaporative temperature effect on the system. Therefore, the next chapter will concentrate on the evaporator design, to improve the *COP* of *ASHP* system, which could allow the attic unit to operate efficiently.

Chapter 5. Development and Experimental Investigation on DX-SAHP System Performance Enhanced by Solar-Air Collectors

5.1. Development of *ASHP* system

In order to improve the thermal performance of the *ASHP* system and its, the quality of the low-grade air temperature at the evaporator should be enhanced. This can be achieved by allowing renewable energy sources to be iintegrated in the heat pump system. To meet the heating demand of the existing homes, technical arrangements can be applied as suggested from the previous chapter to improve the evaporation effect on the *ASHP* system. The aim here is to carry out an investigation on a solar/collector which is able to work with an air source heat pump) which is termed as a *DX-SAHP*. In this case, solar energy is collected together with the surrounding thermal sources which can satisfy the heating demand of the targeted homes, thereby enhancing the system performance. In this chapter, a proposed system is developed to achieve these requirements.

5.2. Description and main components of the proposed *DX-SAHP*

The proposed system has been designed and assembled in the University of Nottingham laboratory. It consists of two main parts; (a) the heat pump system and (b) solar panels, as shown in Figure 5.1.

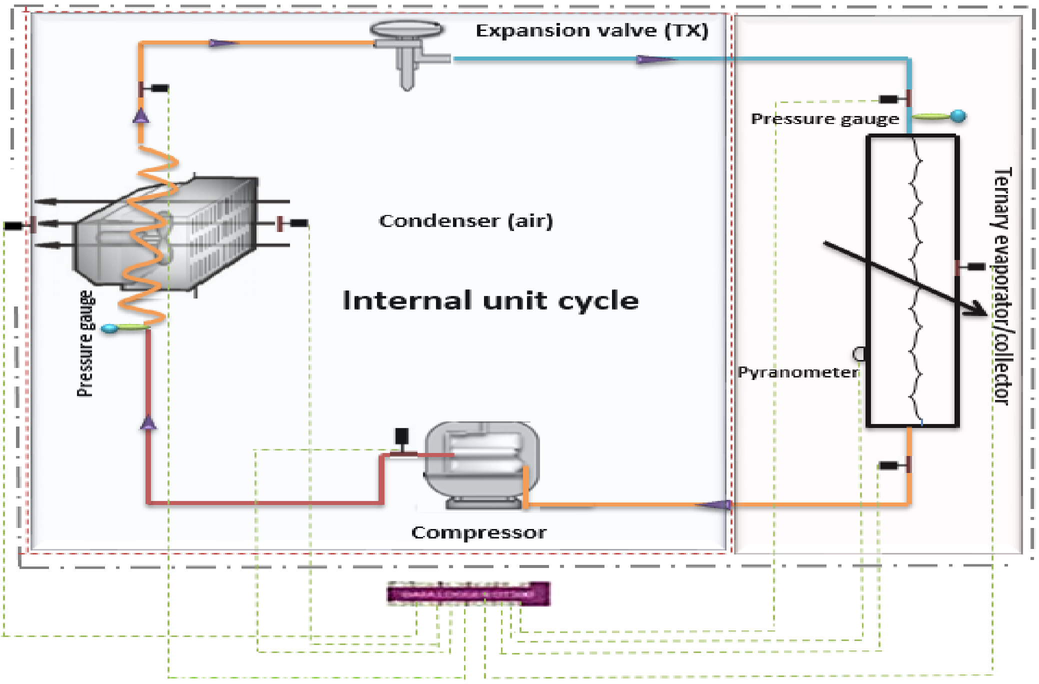

Figure 5.1. Schematic diagram of the proposed DX-SAHP system

a. The Heat Pump System

The purpose of the heat hump is to collect, enhance, and transfer the low grade temperature (heat energy) into useful heat. A compact heat pump (450 x 450 x 450 mm) is used that can be contained within the house's attic as demonstrated in Figure 5.2. A refrigerant substance has to be chirculated within these systems in a closed loop as exhibited above. There are four main components in this heat pump unit and four supplementary elements.

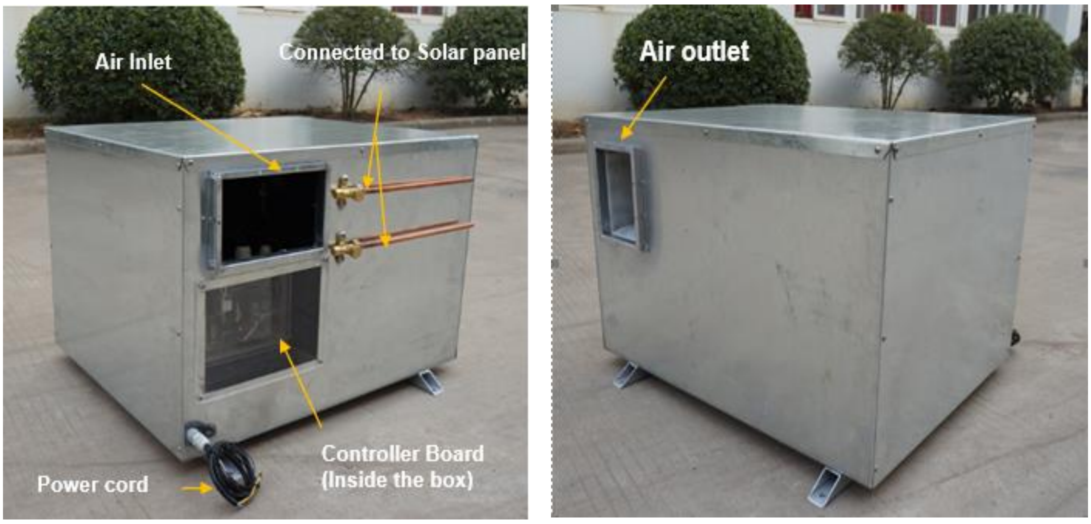

Figure 5.2. The heat pump unit

The four main components of the heat pump are:

I. The Compressor
II. The Condenser
III. The Expansion valve (TX valve), and
IV. The system controller board

I. The Compressor

In the refrigerant cycle, the compressor executes two functions. It receives the fluid from the collector/evaporator in a saturated vapour form, compresses it into the form of vapour and circulates the fluid around the cycle. The compressor used in this study is a Mitsubishi brand and is of electrical rotary hermetic-type as shown in Figure 5.3 and whose specification is dispalyed in Table 5.1. It can be adjusted by the internal frequency converter and has a volumetric displacement of 7.8 L/s.

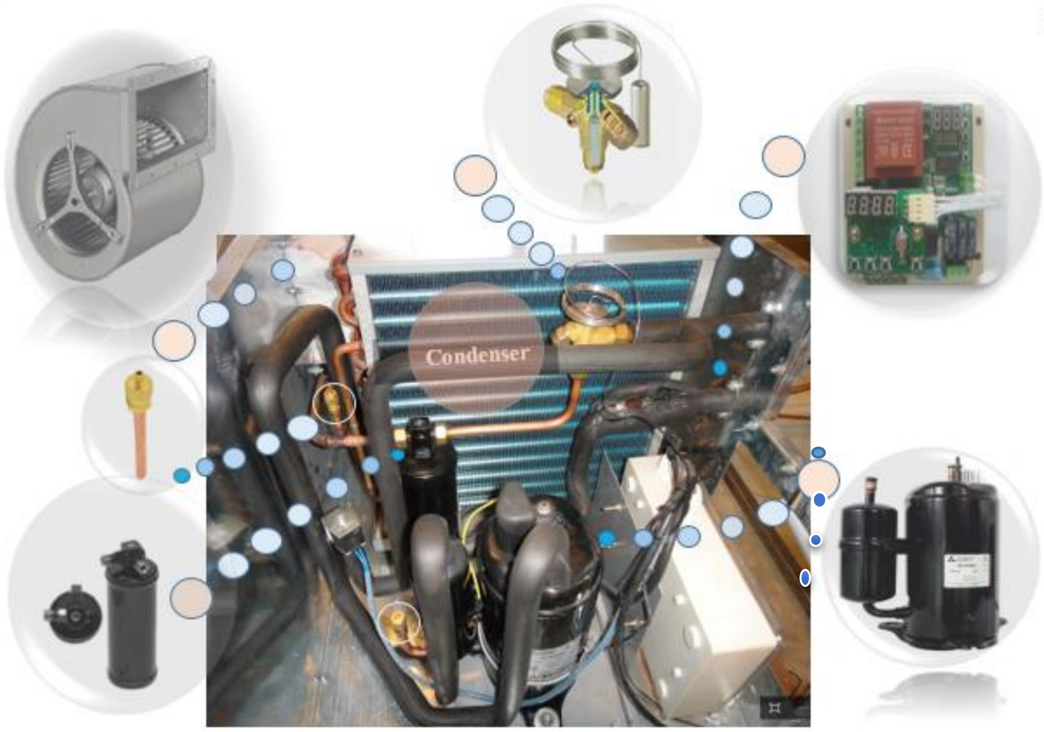

Figure 5.3. Heat pump's fundamental and supplementary components

Table 5.1. Specifications of the main components of the system

Elements	**Specification**
Compressor	Mitsubishi RE165VA
Compressor displacement ($\mathbf{VD}$)	7.84 L/s
Compressor rated input	800 *W* at (50 Hz) frequency
Condenser (air)	Finned coil 38.3 cm x 37cm with 4.2cm thickness
Centrifugal Blower (fan), for heat pump	A.C Inti-vibration (D4E225-CC01-54) ebm-papst type with airflow 2615 m^3/h
Expansion valve ($T_X v$)	T_X valve: Danfoss TZ2+1# 220/240V A.C, 50 Hz 15A
Sight glass & filter	2 in 1 Mitsubishi Type

II. The Condenser

The condenser (fan-driven condenser) receives the refrigerant at a high temperature after being compressed by the compressor. When passed via a condenser, it gives up its heat, and the vapour becomes condensed liquid which flows back to the collector. The produced heat exchanged between the refrigerant and air source can be used for heating purposes. The condenser used in this study is made of a copper tube with aluminium fins with heat transfer area of about 1417.1 cm^2 The operation of the compressor enforce the liquid to circulating around the refrigeration cycle, extracting heat from the collector/absorber and dump it to the condenser.

III. Thermostatic Expansion Valve (T_X valve)

An orifice or capillary tube between the collector/evaporator and condenser operates in two functions; it causes a sudden drop of the refrigerant pressure, and expand it into the collector/evaporator at low temperature to allow the refrigeration to evaporate at low pressure. It provides cooling load or extracts heat from the load. It can also respond to heat load changes on the evaporator by regulating the liquid flow by raising or reducing it in the collector/evaporator. Figure 5.3 also shows the expansion valve used for this experimentation (Danfoss TZ2+1# type) with the external equaliser and fix orifice. It has a sensing bulb linked to the outlet of the collector/evaporator. The function of this bulb is to detect the suction line temperature and send an electrical signal to the expansion valve, permitting it to adjust the flow rate. It is also called the refrigerant control mechanism, because it ensures that all the liquid is changed into vapour and the gas return to the compressor with ± 10°C additional superheated, and not having any liquid content.

IV. The system control board

The control board is an electrical digital device which controls the power supply to the compressor and other apparatus such as the the fan, pump, electrical valves, etc. in order to regulate the frequency and speed. It also governs the signals between bulb's sensors and heat pump devices (T_Xv, compressor, etc.), by using temperature detectors. The unit is designed for single-phase and its power rating is 220/240V AC, 50 Hz 15A with inner frequency converter (see: Figure 5.3).

The four supplementary elements are:

1. Centrifugal Blower (fan)
2. Receiver (accumulator)
3. Sight glass and liquid line filter
4. Digital controller

1. Centrifugal Blower (fan)

The centrifugal unit executes two functions; it draws the cold outdoor air into a heat exchange surface (condenser), cooling down the condenser, and rejects the heat out for heating space. The fan used for this research is an anti-vibration centrifugal blower (Appendix-A (1 and 2).

2. Receiver (accumulator)

The receiver is attached to the compressor to keep the accumulated excess refrigerant from the condensate line when the refrigerant flow to collector/evaporator is reduced due to the limitation of the expansion valve because of its size as depicted in Figure 5.3.

3. Sight glass and liquid line filter

The sight glass or viewing window is fixed along the liquid line filter (2 in 1) for viewng the refrigerant level in the system. The filter can absorb a small quantity of water, and catch small particles such as copper chips and welding debris.

4. Digital controller

The digital cabinet is the unit which controls the electric and electronic operational processes of the heat pump. The components of the heat pump receive control signals and commands from this unit. The controller records all the operational information of the systems components as well as the surrounding conditions and responds accordingly.

b. Solar panels (collector/evaporator)

The proposed heat pump consists of a normal roof mounted bare ternary, soft aluminium flat-plates. The flat-plates are formed by integrating bare aluminium solar-collectors which are connected in series as shown in Figure 5.4 to absorb heat from the surroundings or other heat sources. The insulation is placed at the back of the collectors to prevent the unnecessary loss of heat to the sorounding. This un-glazed plate collector is used as a heat source acting as the absorber/evaporator. The sheets are painted with a black cover for transferring heat to the flowing refrigerant and for an effective absorbsoption of the solar irradiation. The piping network design is aranged between the three aluminium plates so thatthe lumped collectors form an over-pressurizing network to create a cycle for circulating the the fluid within the fins. The aluminium plates are also bonded together, with each plates having a thickness of 2 mm and the inner diameter of the tube is 12.7 mm with the total piping length of 25 m.

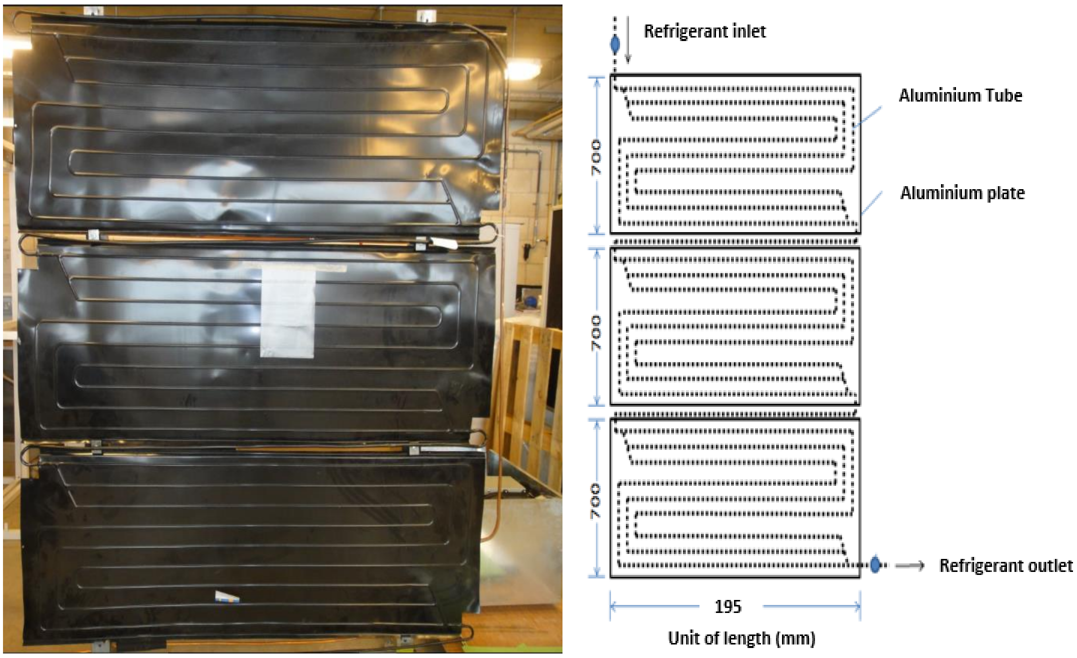

Figure 5.4. Collector/evaporator of the heat pump system

5.3. Fabrication and construction of the proposed *DX-SAHP* system

The three assembled collectors are fixed to the carrier by nuts and clips, using galvanised screws as shown in Figure 5.5. Both the charging and suction lines are placed near the heat pump box in order to avoid oil formation traps. Since a shorter runninglength of the refrigeration loop offers better system performance, the unit is located in close proximity to the panels. Thus, 9 m is considered in this study as the maximum length between the heat pump and panels since it is a relatively shorter distance in principle. In this study, the tube to the inlet of the evaporator is 7.9 mm ($^{5}/_{16}$") and is connected to the evaporator outlet with 12.7 mm ($^{1}/_{2}$") length. After connecting the solar panels to the heat pump system, Nitrogen is flushed through the pipe and panels to clear out any remaining fragments caused by the welding and connection work. Subsequently, pressure testing and evacuating of the evaporator/collector as well as the pipework is then conducted at a pressure between 1700 to 2000 kPa to ensure there are no leakages of the pipe joints.

Finally, the system is filled with a refrigerant R407C of 2.8 kg via the fitted service valve. At the end of this action, the heat pump system is connected to the solar panels (collector/evaporator), to complete the construction of the *DX-SAHP* air heater for space heating purposes.

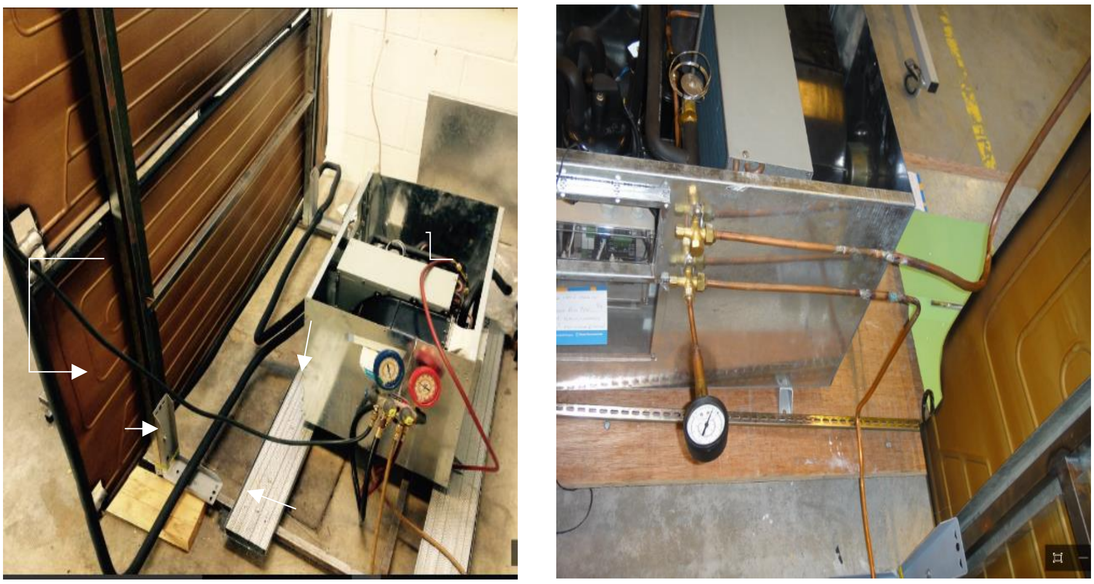

Figure 5.5. Heat pump system and solar panels connections

5.3.1. Experimental work on the heat source

In this study, to simulate solar insolation under laboratory conditions, an artificial portable light source combining metal-halide and thirty tungsten halogen floodlights source is assembled as shown in Figure 5.6. The use of a solar simulator is to deliver a controllable indoor sunlight for the system collector. In this regard, unevenness values obtained for most of the points were found less than 9%, which is in a good agreement with the British Standards values for the indoor solar simulator. This adjustable light illuminates with the wavelength ranging between 360 to 2500 nm, and power rating of 0 to 400 $W{\cdot}m^{-2}$ controled by a regulator switch which to maintains the solar irradiance variations evenly, to cover an area of 4.22 m^2 (Figure 5.6 and Figure 5.7).

Figure 5.6. Solar simulator and light regulator

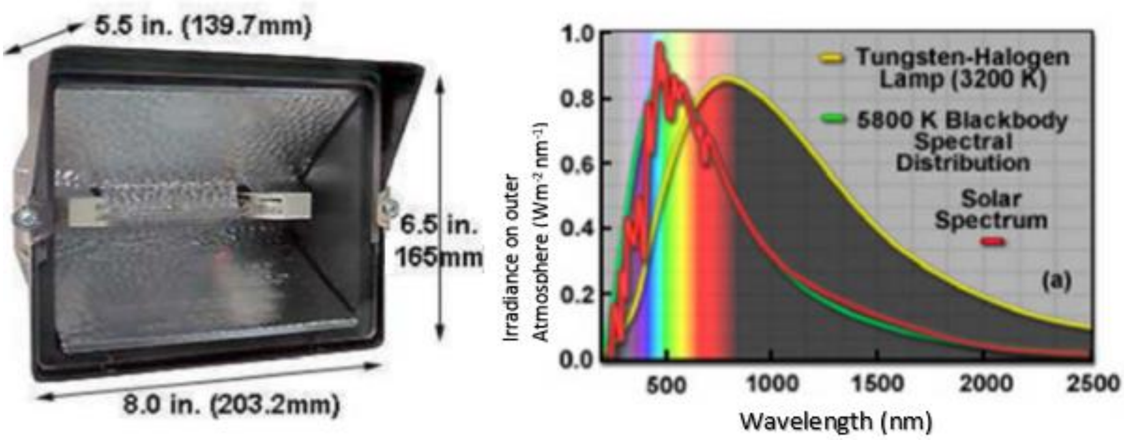

Figure 5.7. Tungsten halogen lamp specification

5.4. Operation procedures and experimental setup

The *ASHP* systemis designed by integrating the bare ternary aluminium solar-collectors connected in series. These collectors are integrated into the structure of a house roof, where the working fluid flowing inside the evaporator/collector absorbs the solar energy and the surrounding heat at low temperature. The proposed system was designed to provide domestic space heating throughout the cold season when space heating is essential. The test was carried out during the months of December, January and February in the laboratory at the University of Nottingham, UK. As part of the test control strategy, the test was conducted only from 23:00.pm to 06:00.am under the the lowest outdoor temperatures, to ensure that the system would relatively be under quasi-steady conditions for all tests. During the test, air is provided to the system from the ambient via inlet 'flexible duct' as shown in Figure 5.8. Meanwhile, the collector which acts as the evaporator is placed indoor up-right in the laboratory to simulate the solar irradiation.

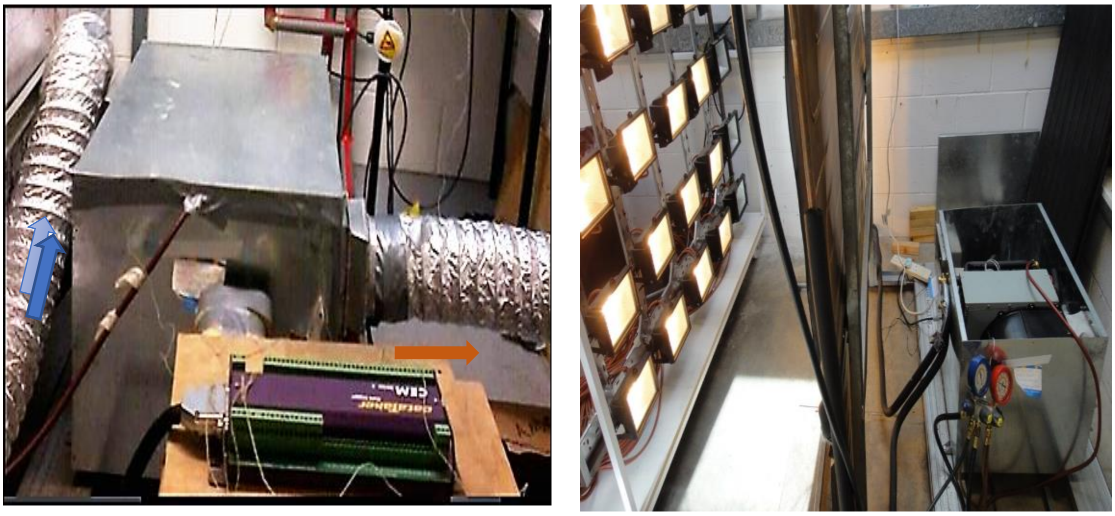

Figure 5.8. Experimental set-up of the DX-SAHP system

Once the system is switch-on, the refrigerant is filled through the solar collector (evaporator/collector). When the refrigerant is in avapour state from the compressor, it enters the heat exchanger directly at a high temperature and pressure. For this application, the heat exchanger (finned coil tube) works as an air-condenser. Meanwhile, the outlet-air duct with the assistance of the centrifugal fan dissipates the heat to the domestic space. The temperatures sensors were positioned thermocouples to measure the system inlet/outlet air temperature. The solar intensity was adjusted from 57 to 200 W·m^{-2} to investigate its influence on the system thermal performance. A solar pyranometer was mounted on the evaporator/collector to maintain consistency of solar irradiance, as the collector surface temperatures, and the refrigerant temperature was being monitored. The pressure gauges and flow meter were clamped on the pipe to measure the pressure and the refrigerant mass flow rate respectively. An electronic power meter was utilised to monitor the system energy consumption. The system was operated within a specified test period for each case. All the measuring processes were monitored by a computer-based data-acquisition system. The collected data was recorded at the one-second interval by the data logger and stored on the computer ffrom which the data analysis was performed.

5.5. Measuring tools and instrument’s accuracy

A series of thermocouples (‘T’ and ‘K’ Type) were used to measure the ambient (indoor/outdoor) temperature, the system (inlet/outlet) airflow, and the refrigerant temperatures with toleance of± 0.1°C and error of ± 0.4 % as demonstrated in Figure 5.9 (a). The thermal camera with a resolution of 50 pixels was used to evaluate the frost formation on the collector/evaporator as shwon in Figure 5.9 (b).

(a) (b)

Figure 5.9. Thermocouples T Type (a), and thermal camera (b)

The solar pyranometer, type SP Lite 2 silicon (SP lite2 compares to *ISO* 9060) type with a sensitivity of 60 to ± 100 μV $w^{-1} \cdot m^{-2}$ and uncertainty error of ±1.0 % displayed in Figure 5.10 (a), was used in these tests to maintain the consistent of solar radiation while covering the entire surface area of the collector/evaporator in the range of 0-800 $W \cdot m^{-2}$. The pressures were measured at the low and high-pressure side of the system cycle. A yellow jacket prssure gauge (steel case Type) in the range of 0.5-55 bar was used with an accuracy of up to ± 1 % (Figure 5.10 (b)).

(a)

(b)

Figure 5.10. Pyranometer (a), and pressure gauge (b)

The airflow rate at the system inlet and outlet ducts were measured by using an anemometer, type DVA-30VT with the uncertainty of ± 1% as shwon in Figure 5.11 (a). The refrigerant's mass flow rate was also measured using an ultrasonic mass flowmeter, type Katronic T-flow 200 with an accuracy of ± 0.5 %, clamped on the pipe as indicated in Figure 5.11 (b).

(a) (b)

Figure 5.11. Anemometer (a), and ultrasonic mass flowmeter (b)

The energy consumption of the whole system including the electrical apparatus and fan were measured using a digital power meter of type (Primera-Line PM 231 E) with an accuracy of ± 1 % (Figure 5.12 (a)). Then all parameters by a data taker (DT-600) connected to DeLogger programmer (4V4R2) with an accuracy of ± 0.1% as shwon in Figure 5.12 (b). The specifications of all the instruments and their parameters are presented in Table 5.2.

(a) (b)

Figure 5.12. Digital power meter (a), and Data taker type DT-600 (b)

Table 5.2. Specifications of the measuring tools

Parameter	Range	Accuracy	Measuring apparatus
Temperature (°C)	-200°C +200°C	Special limits error ± 0.4 (%), ±0.1°C	K- and T type thermocouple
Pressure: suction/discharge lines	0.5-55 bar	±1 (%)	3-1/8” steel case-Pressure gauge
Irradiation ($W{\cdot}m^{-2}$)	0-800 $W{\cdot}m^{-2}$	±5 (%) 400-to-1100 nm	SP Lite 2 Silicon Pyranometer.Sensitivity 60 to ±100 $\mu Vw^{-1}{\cdot}m^{-2}$
Power meter (kW)	0-4 kW, 13A, 220-250Vr, 50/60Hz	± 1 (%)	Digital wattmeter, Primera-LinePM231 E
Refrigerant Mass flow rate ($kg{\cdot}s^{-1}$)	0.001-1 $kg{\cdot}s^{-1}$	±0.5 (%)	Ultrasonic clamp-on pipe-mass-flowmeter Katronic T flow 200
Airflow rate (m/ps)	1013mb, 0.00399-90m2-At 20°C	±1 (%) of reading, ±1 digit	Anemometer DVA 30 VT
Data Taker	From 1 second	±0.1(%) of recording digits	DT600,with DeLogger4V4R2

5.6. Results and discussion

5.6.1. Measuring results

In the present study, the performance of the developed *ASHP* system was evaluated for space heating during the cold season, where thesystem was subjected to provide heating for the room. The system was tested on the coldest days over the period from December to early February under the same environmental conditions. Each test was repeated three times in order to verify the validity and accuracy of the results under the chosen environmental condition. Thereafter, the average value of 40 measurements from 23:00 pm to 06:00 am with an interval of 1 min was computed. The comparsion between the laboratory condition and actual weather condition was based on British Standard Institute (BSI) 13612-1:2014 for testing and performance standard. The average daily-outdoor air temperature ($T_{air,av}$) was ranging from 6.5 to 8.5°C and a solar simulator used to beam light on the collector with solar radiation intensities of 57, 100 and 200 W·m^{-2}.

Figure 5.13 shows the measured data of the system components in the absence of solar irradiation under certain climatic conditions. It is observed that the evaporator/collector temperature (T_{plat_inlet}) is always lower than the indoor (T_{room}), and ambient temperature ($T_{ambient}$). This allows the fluid to absorb heat at low temperature rather than reject it to the ambient. Therefore, it is proved that the system is capable of delivering space heating at the desired temperature of up to 26°C without solar radiation.

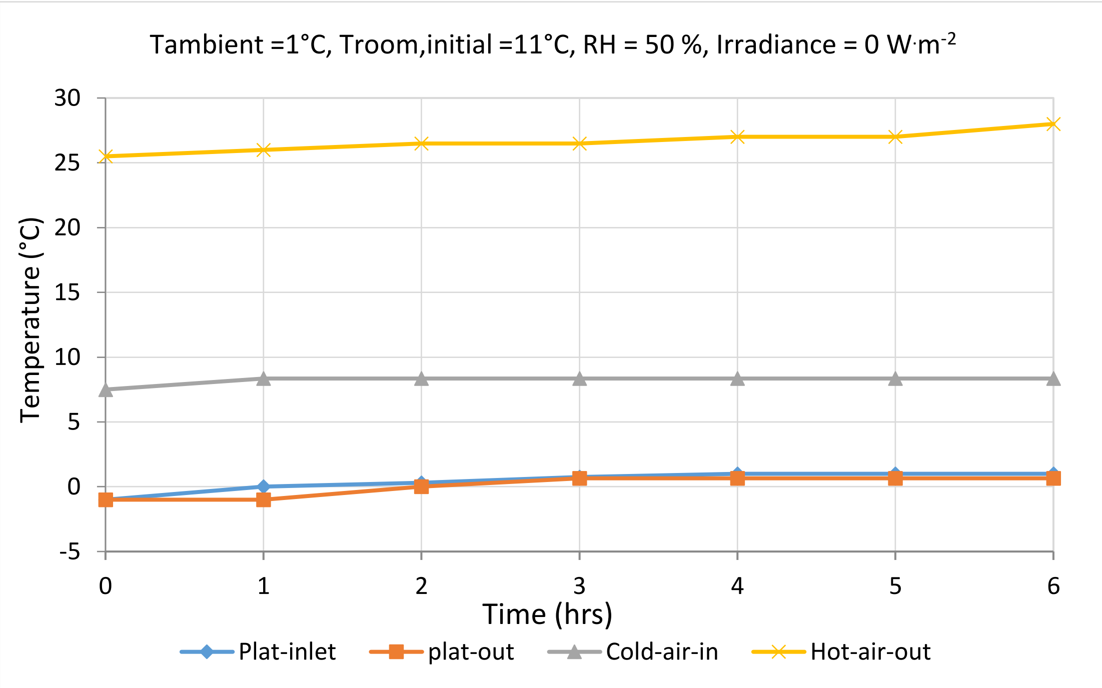

Figure 5.13. The system thermal performance without solar irradiance

When the environment is stable, the system can reach a quasi-operational-state after about 20 min. Under the outdoor temperature of 6, 7 and 8°C, the evaporation temperature is found to be -1°C, 0°C and 1°C, respectively. The test is repeated three times to examine the system behaviour under the same conditions. The results reveal that the increase of T_{room} is not significant on the system thermal performance. However, the system outlet hot-air $(outlet_{air,av})$ increases by 5%, corresponding to 1°C increase in T_{room} as indicated in Table 5.3.

Table 5.3. The system thermal performance without solar radiation for space-heating

Solar.radiation (W·m^{-2})	T_{room} (°C)	$outlet_{air,av}$ (°C)	$inlet_{air,av}$ (°C)	$press_l$ (bar)	$press_h$ (bar)
0	18.4	24.9	7.48	1.1	09.8
0	19.2	26.6	8.23	1.3	10.0
0	19.0	25.0	8.5	1.1	10.3

Figure 5.14 illustrates the influence of different solar irradiation intensities on the system thermal performance. The experiments are carried out under the solar radiations of 57,100 and 200 W·m^{-2}, and the indoor temperature of 18.4°C and 20.1°C as exhibited in Table 5.4.

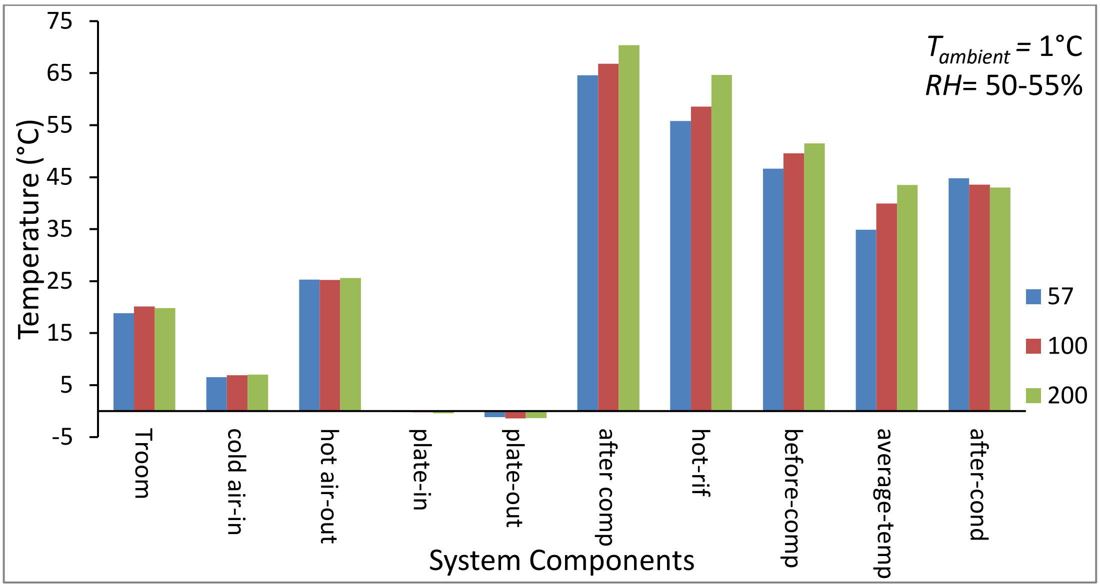

Figure 5.14. The influences of the operating parameters on the system thermal performance

Table 5.4. The system thermal performance with different solar radiations

Solar.radiation W·m^{-2}	T_{room} (°C)	$outlet_{air,a}$ (°C)	$inlet_{air,a}$ (°C)	Compressor (kW)	$press_l$ (bar)	$press_h$ (bar)
57	18.8	25.3	6.6	0.95-1.101	1.3	11.4
100	20.1	25.4	6.9	0.87-0.99	1.4	11.5
200	19.8	25.6	7.5	0.81-0.95	1.5	11.6

The results show that the system performance is much enhanced with the increase in solar irradiation as observed in the figure above where the performance of the system is high at the highest solar irradiance of 200 W/m^2. The incorporation of solar irradiation, therefore, can effectively increase the evaporator/collector temperature (plate-in/plate-out). It is observed that when the evaporator temperature increases, both the system (suction/ and charging line pressures increase but the compressor energy consumption rises due to increasing in solar intensity. This in return triggers a rise in the refrigerant temperature, resulting in an increase in the condensing heat exchange rate (*hot-rif*) under the four experimental conditions.

5.6.2. The effect of frost accumulation on the surface of the collectors

The risk of frost formation on the external collector/evaporator (absorber) in winter can limit the use of the *ASHP. Because of the*icing of the absorber plates of the *ASHP* system, the COP of the system reduces. Therefore, there is need to use advanced technology to overcome this problem. Meanwhile, it is essential that measures are taken to increase the temperature of the collector/evaporator. Therefore, an alternative collector/evaporator for *ASHP* is developed in order to reduce the frost accumulation during the cold season, by using a Direct Expansion (DX) flat plate absorber.

In general, for a fan-driven ASHP, the frost layer will arise on the evaporator and increase the thermal resistance between the evaporator and air. As a result, the evaporator and its heat exchanger rate decline, leading to a reduction in the system; COP and heating capacity, in addtion to blocking the airflow. Therefore, it is paramount to consider the the mechanism that can stop the frost formation by studying a *DX-SAHP* system.

Here, the influence of solar irradiation/non-solar irradiation on frosting formation and heat performance on the collector's surface is to investigate with the aid of a thermal camera. The data collected from monitoring collectors are frequently analysed to determine if the frosting values are within acceptable tolerances. The three flat plates and the pipe work are thermally pictured during the experiment where Figure 5.15 shows the refractory performance of the plates. It can be noticed that after 30 min, the surface of the absorber plates and the outlet of the copper pipe are covered by a layer of frost. The evaporator/collector is also frosted and as the experiment continues, the frosting becomes more prominent as indicated in Figure 5.15, A (6-8). However, with the presence of solar radiation above 90 Wm^{-2}, the frosting is reduced. Thus, with solar rradiation of 100 and 200 $W{\cdot}m^{-2}$ the evaporator is mildly frosted (Figure 5.15, A (3-4)). By monitoring the refractory performance over time, the hot spots (red colour) on the thermal image depicts the mainstream of hot refrigerant inside pipe works, when the fluid is absorbing the heat and passes it successively through the plates to the heat pump unit as demonstrated in Figure 5.15.

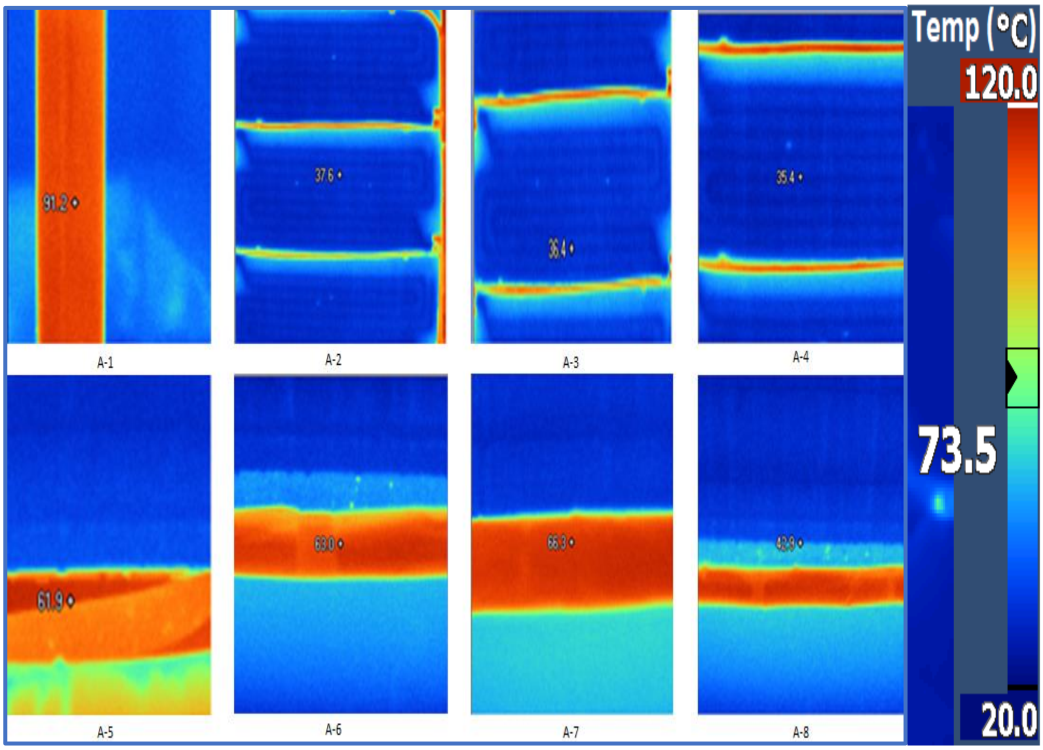

Figure 5.15. Collector/evaporator's refractory performance

A dark blue spot on the thermal image indicates that the panels remain cold in order to absorb the surrounding heat at lower temperature conditions. The lighter blue colour demonstrates the frosty and cold area throughout the plates and system components when the ambient temperature is 5°C or higher. (Yiqiang et al., 2000) reported that, for the air source heat pump, the frosting condition occurs when the relative humidity is above 67% and the ambient temperature is between -12.8 and 5.8°C. In the present *DX-SAHP* system, when the relative humidity was 45-60% and the ambient temperature is up to 6°C, the water vapour from the ambient air condensed on the evaporator cold surface, from which the freezing of the water dews was started while the frost spots were being accumulated.

In short, frost occurs on the surface of a collector when the relative humidity is above certain values between 60 and 75%, and the ambient temperature is between 6 and 7°C, without solar irradiance. With the presence of solar radiation, mild frost is formed on the evaporator as illustrated earlier, thus the operating of the system is not highly affected, hence the heating performance is still not affected significantly. Accordingly, the *DX-SAHP* system could operate efficiently with a mild level of frost under low solar irradiation conditions.

During the tests, the heating capacity absorbed via the evaporator/collector (Q_{evap}) and the ejected heat by the condenser ($Q_{cond_{air}}$) were calculated experimentally using equation 11 and 12:

$$Q_{evap} = \dot{m}_{r_{rif}} * c_{p_{rif}} \left(T_{out.evapo} - T_{in.evapo}\right) \tag{5.1}$$

$$Q_{cond_{air}} = \dot{m}_{r_{air}} * c_{p_{air}} (T_{out.cond} - T_{in.cond}) \tag{5.2}$$

where $\dot{m}_{r_{rif}}$ is the mass flow rate of the refrigerant (R-407C); $c_{p_{rif}}$ is the specific heat capacity of R-407C; $T_{in.e\ vapo}$ and $T_{out.evapo}$ are the respective refrigerant temperature difference at both the inlet and outlet of the evaporator/collector. Meanwhile, $\dot{m}_{r_{air}}$ is the outlet air mass flow rate; $c_{p_{air}}$ is the specific heat capacity of air; and $T_{in.cond}$ and $T_{out.cond}$ are the temperature difference of air at the inlet and outlet of the condenser respectively.

During the experimental study, the energy consumption of the compressor ($Work_{comp}$) and other auxilliary power devices ($Work_{electrical}$) were displayed on the power-meter and recorded. The work of the compressor is also determined based on the efficiency of the compressor which is variable related to the fluid condition (entropy), and temperature of the collector outlet. Therefore the total power consumption ($Work_{consump}$) is calculated as;

$$Work_{consump} = \frac{Work_{comp} + Work_{electrical}}{\eta_{comp}} \quad (5.3)$$

η_{comp} can be determined from equation 14 as follows:

$$\eta_{comp} = \frac{T_{2i} - T_2}{T_{2a} - T_2} \quad (5.4)$$

where T_2 is the collector outlet temperature; T_{2i} is the isentropic (CTD calculated); and T_{2a} is the compressor discharge temperatures. These two temperatures (T_{2i} and T_{2a}) vary and can be calculated as;

$$T_{2i} = T_2 * \left[\frac{P_2}{P_1}\right]^{0.28571} \quad (5.5)$$

$$T_{2a} = T_2 \left[\frac{P_2}{P_1}\right]^{\left[\frac{n-1}{n}\right]} \quad (5.6)$$

Where $P_{2/}$ and $P_1$are the system high and low pressures respectively obtained by measurement from the test rig; $[n]$ is the ratio of the specific heat ofR-407C, which is 1.14.

The system *COP* is obtained by measuring $Work_{consump}$ and the thermal energy gained by the heat pump Q_H as;

$$COP_{heatpump} = \frac{Q_H}{Work_{consump}} \quad (5.7)$$

where Q_H is the thermal energy produced by the heat pump which is the condenser work $Q_{cond_{air}}$.

Figure 5.16 displays the heat gain of the evaporator and the condenser with the influence of solar radiation. The results show that the increase in solar irradiation has an effect on the evaporator temperature and hence on the *COP* of the system as shown in Table 5.5. The condensing heat exchanging rates under the four experimental conditions are also indicated. The average of $Q_{cond,air}$ is up to 3.16 kW in the whole experimental period, while the hot air temperature was 25-26 °C. T_{room} at different solar radiation intensities remained relatively the same, at the same experiment condtions as indicated in Table 5.5. As stated earlier, the power consumption of the compressor rises as the solar intensity increases. However, it is noted that after the solar intensity of 195 W·m^{-2} , the heat gained from the condenser drops as a result of superheating as shown in Figure 5.16.

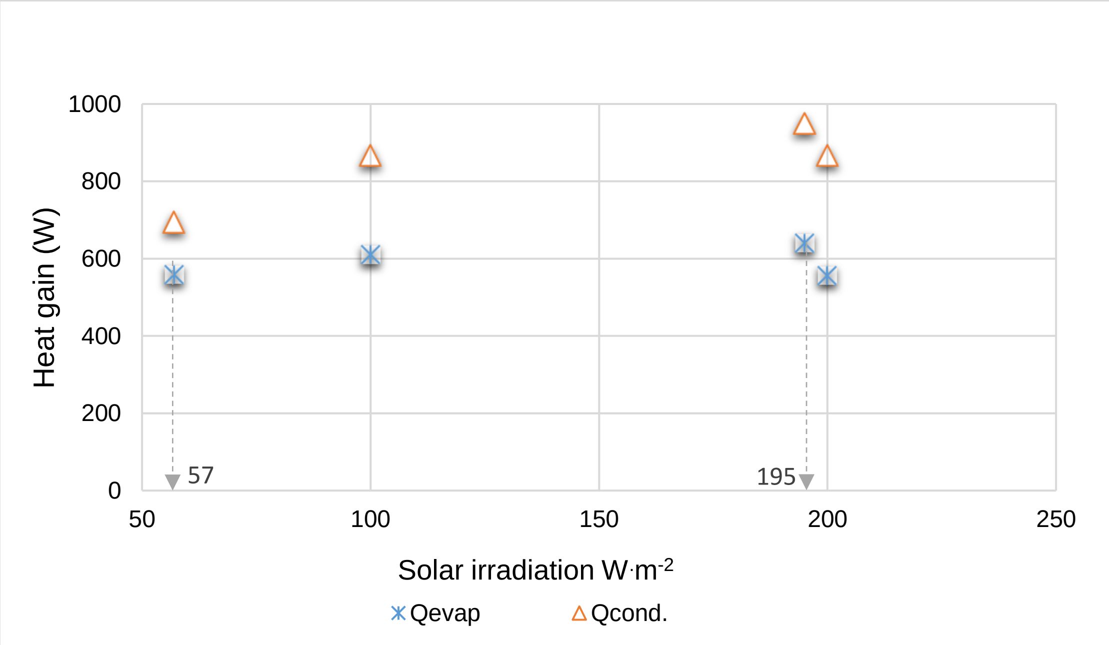

Figure 5.16. The influence of solar radiation upon the *DX-SAHP* system

It is worthy to mention that, in this case, the fluid was in the superheated vapour state at the exit of the collector panels, a situation which considerably decreases the mass flow rates of the refrigerant, thereby lessening the heat gain, the compressor consumption, and the fluid condensation at the heat exchanger.

Table 5.5. The influence of solar irradiation upon the system parameters

Solar.radiation W·m^{-2}	T_{room} (°C)	$inlet_{air,av}$ (°C)	$outlet_{air,\mathit{c}}$ (°C)	$Q_{cond_{air}}$ (kW)	$COP_{sys,ave}$
57	18.8	6.6	25.3	3.182	3.86
100	20.1	6.9	25.3	3.191	3.88
200	19.8	7.5	25.6	3.139	3.91

It also is obvious in Figure 5.17 that the *COP* of the system increases as the solar irradiation increases, However, as the condensing heat exchange rate increases, the energy consumption also increases and to some extent the *COP* decreses. The average specific values of the COP are 3.86, 3.88 and 3.91, corresponding to the solar radiation of 57 W·m^{-2}, 100 W·m$^{-2,}$ and 200 W·m^{-2} respectively as exhibited in Figure 5.18. It is noticed that the COP is improved as the solar radiation is increased.

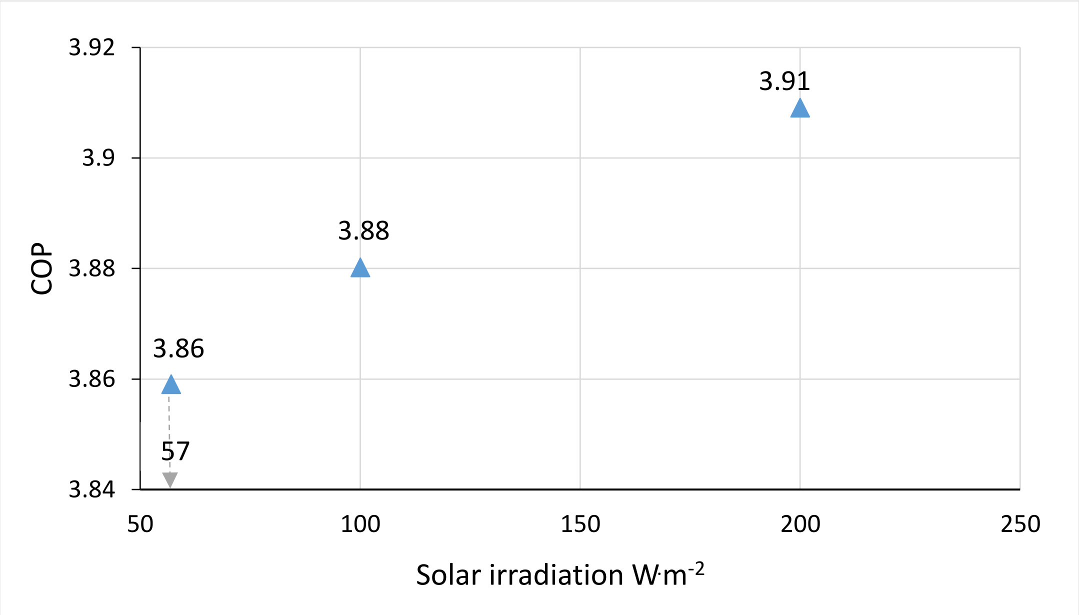

Figure 5.17. coefficient performance of the system at different solar irradiations

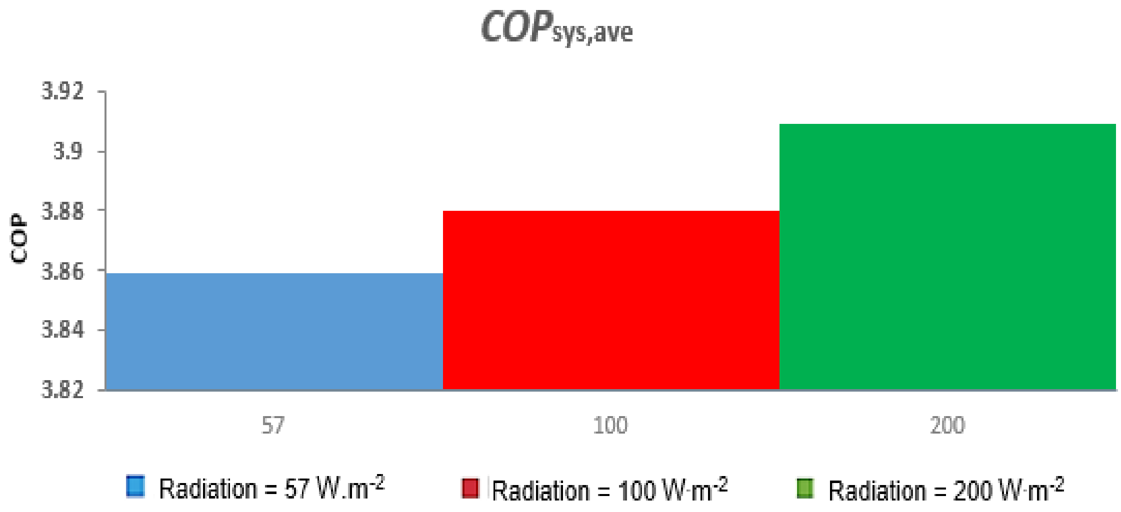

Figure 5.18. COP average of the system at different solar intensities

5.7. Comparison between the thermal performances of *ASHP* and the developed *DX-SAHP* systems

Table 5.6 and Table 5.7 show that the developed system performs much better than the previous *ASHP* system under the same evaporating and condensing temperatures. The *DX-SAHP COPs* are always higher than the *ASHP* system because of the evaporator/collector characteristics, whereby the system is able to absorb more heat from different heat sources.

Table 5.6. Thermal performances of ASHP and DX-SAHP systems at lower condensing temperature range

System Type	$T_{condensing}$	$T_{evaporating}$	T_{indoor}	$T_{outdoor}$	$T_{hot.air}$	COP
ASHP	25-55	0°C	22°C	21.5°C	22-23.5°C	3.2
DX-SAHP	25-55	0°C	19°C	1°C	25°C	3.8

Table 5.7. Thermal performances of ASHP and DX-SAHP systems at higher condensing temperagure range

System Type	$T_{condensing}$	$T_{evaporating}$	T_{indoor}	$T_{outdoor}$	$T_{hot.air}$	COP
ASHP	55+	0°C	22°C	21.5°C	22-23.5°C	2.5
DX-SAHP	55-65	-1°C	19°C	1°C	25°C	3.6

5.8. Conclusion of chapter-5

This chapter has presented the indoor thermal performance analysis of the developed *ASHP* system to provide space heating for existing homes in the UK when the atmosphere temperature in winter is about -5 to 1°C. The analysis was based on the steady-state thermodynamic vapour compression cycle. In all presented cases, tests were carried out at evaporator/collector temperatures less than the indoor-room temperature. In the meantime, the evaporator/collector was also tested by incorporating the solar system with the solar irradiances of 0, 57, 100, and 200 $W{\cdot}m^{-2}$, during simulation. During operation, the compressor receives the saturated vapour fluid from the absorber at low temperature and pressure and then delivers it to the condenser at higher pressure and temperature. The useful heat is rejected from the condenser with the assistance of a fan to satisfy the heating requirements of a residential building.

The developed system with ternary bare solar collectors has demonstrated efficient operation under low solar irradiance and frosting conditions. As a result, the *COP* of the developed system is enhanced by 44% compared to the previous system under the same evaporating and condensing temperatures. Subsquently, the developed system operates well under various solar irradiations and is capable of delivering hot air with the temperature of about 23°C to 26°C without requiring an additional or auxiliary heating device during the coldest days. The investigation also proved that the system can provide adequate space heating to satisfy the existing heating demand for the homes. However, the system can only provide space heating at this stage, without fulfilling domestic hot water requirements as well as not being able to provide sufficient heating during the peak time. Some technologies have been suggested to provide both space heating and domestic hot water requirements, which could be used to improve the present system. By employing these alternative technologies, it is possible to provide low-cost heat production for the existing homes in the UK. The combination of these technologies appears to be more attractive to increase the heat pump’s COP.

In the next chapter, the study will concentrate on the improvement of the current system in order to provide mutually domestic hot water and space heating while improving the total heating performance for residential building.

Chapter 6. Analytical modelling and system validation of Direct-Expansion Solar-Assisted Multifunctional Heat Pump system

6.1. Mathematical modelling and thermodynamic analysis

To predict the *DX-SAMHP* system performance under selected environmental conditions, analytical modelling was carried out using Matlab programme and spread sheet to evaluate the system performance. Numerical modelling was executed to predict the performance of the developed system under different operating conditions. Therefore, the size and dimensions of evaporator/collector of the system, the influence of the physical characteristics of the ternary absorber and main parameters were were also analyzed. The variable speed compressor and the expansion valve were also examined. The variable speed of the compressor was, achieved with a frequency converter by varying the frequency from 15 to 110 Hz. The fabricated condensers from the finned coil (copper tube and aluminium fin), immersed coil tube, and heat exchanger for the *DX-SAHP* model as well as their thermal heat gains and $COPs$ were also studied. The analytical results were then validated by the predicted and the experimental results.

In this study, the system was assumed to be operating at only lowest temperature hours during night-time and early morning, when the evaporating temperature was at least 5°C less than ambient temperature (indoor temperature). The evaporator/collector pressure was first assumed, and subsquently determined by simulating the evaporator/collector, compressor, condensers and the heat exchanger. The enthalpy and entropy states of the leaving refrigerant were precisely assigned. In cases, wherethe calculated differences are not within the tolerance limit, then the leaving refrigerant was amended and the same process repeated.

6.1.1. The evaporator/collector section

When the solar irradiation falls on the solar collector, the main part of the radiation ((I)*I*), strikes the electroplated aluminium absorber. Part of the solar radiation is absorbed by the working fluid and the remaining part is dissipated through the top and the bottom of the absorber plate to the surrounding. In other words, to compute the outlet temperature and the efficiency of the solar collector, first the heat losses to the surrounding should be calculated. The rate of useful energy extracted by the collector ($Q_{evap/coll}$) expressed as the rate of extraction under steady state conditions is proportional to the rate of useful energy absorbed by the collector. The relation between the absorbed heat and heat losses is expressed as follows:

$$Q_{evap/coll} = A_{coll} * \left[\propto I - U_L(T_p - T_a)\right] \tag{6.1}$$

$$= \mathrm{F}'\mathrm{A_{coll}}\left[\propto \mathrm{I} - \mathrm{U_L}(\check{\mathrm{T}} - \mathrm{T_a})\right] \tag{6.2}$$

where

Ac: solar collector surface area (m²)

$\propto$: the collector transmittance-absorptance product

I: the intensity of the solar radiation (W·m^{-2})

U_L: the collector overall loss coefficients (W·m^{-2} °C^{-1})

T_p: the collector/evaporator temperature (°C)

T_a: ambient (indoor) temperature (°C)

F': solar collector efficiency factor, which is dependent of the tube and the sheet

$\check{T}$: mean refrigerant temperature in the collector/evaporator (°C)

The heat gain of the evaporator/collector $Q_{evap/coll}$, and temperature ($T_{evap/coll}$) are predicted for the condensing temperatures between 35°C and 55°C, and the pressure drop in the collector is assumed to be less than 0.15 bar. However, under various climatic conditions, $Q_{evap/coll}$ is not always comparable to the solar energy absorbed by the refrigerant (Q_S), and the ratio between the total energy gain of the refrigerant and solar energy gain of refrigerant (f_S) would be different. Solar energy input ratio f_S and Q_S are defined as follows:

$$f_S = \frac{the\ solar\ energy\ gain\ of\ \ refrigerant}{the\ total\ energy\ gain\ of\ refrigerant} \tag{6.3}$$

and

$$Q_S = \frac{R_w}{R_w + R_n} \mathrm{Q_{evap/coll}} \tag{6.4}$$

Where R_w is the air side heat transfer resistance, and R_n is the refrigerant-side resistance including tube wall heat transfer.

For this study, it is not essential to develop a completely new analysis of the tube-sheet relation, Hottel-Whilliar-Blis (Klein et al., 2006) have developed the collector efficiency factor $\mathrm{F'}$ for the tube-sheet relation which can be computed by the following formula:

$$\mathrm{F'} = \frac{1}{\mathrm{W}\left[\frac{1}{[\mathrm{D+(W-D).F}]} + \frac{\mathrm{W.U_L}}{\mathrm{\pi D_i hf_i}}\right]} \tag{6.5}$$

Where W is the pitch between the serpentine tubes of the collector (mm); D is the outer tube diameter of the risers (mm); $\mathrm{D_i}$ is the inner tube diameter of the risers (mm); and F is the Fin efficiency factor of the collector plate and can be calculated as follows:

$$\mathrm{F} = \frac{\mathrm{tanh[m(W-D)/2]}}{\mathrm{m(W-D)/2}} \tag{6.6}$$

$$\mathrm{m} = \sqrt{\mathrm{U_L/k_m * \delta_m}} \tag{6.7}$$

where $\mathrm{k_m}$ is the thermal conductivity of the collector/evaporator flat plate ($W{\cdot}m^{-1}{}^{\circ}C^{-1}$) and δ_m is the thickness of the absorber collector/evaporator flat plate (mm). To obtain the Fin tubes internal heat transfer coefficient of two-phase flow in horizontal tubes, $\mathrm{h_{fi}}$ can be determined by(Charturvedi, 1982):

$$hf_i = \frac{N_u * k_{ref}}{D_i} \tag{6.8}$$

Thus, the definition of the Nusselt number must be applied, where N_u, is Nusselt number (a dimensionless parameter used in calculations of heat transfer between a moving fluid and a solid body); k_{ref}, is the refrigerant thermal conductivity (W·m^{-1} °C^{-1}); and D_i is the collector inner tube diameter (mm).To calculate the Nusselt number, Gnielinski correlation is used which is valid for $2300 \leq Re \leq 10^4$ and $0.5 \leq Pr \leq 2000$ (Mohamed et al., 2017). This correlation is expressed as follows:

$$N_u = \frac{(f/8)(R_e - 1000) * P_r}{1 + 12.7(f'/8)^{0.5} * (P_r{}^{0.6} - 1)} \tag{6.9}$$

Where f' is the Darcy friction factor for pipes in the superheated zone and can be obtained by Petukhov's-Popov formula by evaluating it (Sarbu and Sebarchievici, 2016):

$$f = (1.821g\ R_e - 1.64)^{-2} \tag{6.10}$$

Assuming that any quality change in the collector/evaporator is largely due to enthalpy change and neglecting the quality difference due to pressure drop, this is relatively acceptable for laminar flow in smooth pipes (Sarbu and Sebarchievici, 2016) where:

$$f' = \frac{1}{[0.790 I_n(R_e) - 1.64]^2} \tag{6.11}$$

The relation is valid for the Reynolds numbers between 2300 and 10^4, where Reynolds (R_e) and Prandtl's (P_r) numbers are described as follow:

$$R_e = \frac{4\dot{m}_r}{\pi . D_i . \mu_{rif}} \tag{6.12}$$

$$P_r = \frac{\mu_{rif.} C_{p_{rif}}}{k_{rif}} \tag{6.13}$$

Where $\mathrm{R_e}$ is in terms of mass flow rate in any riser ($\dot{m}_r$); ($\mathrm{\mu_{rif}}$) is the refrigerant viscosity (kg·m^{-1}·s^{-1}); and $\mathrm{k_{rif}}$ is the thermal conductivity of the fluid (W·m^{-1}·°C^{-1}).

The overall heat loss coefficient of the collectors/plates $\mathrm{U_L}$ is the sum of the top ($\mathrm{U_t}$), bottom ($\mathrm{U_b}$), and the edge ($\mathrm{U_e}$) loss coefficients, which is attributed to the radiation and convection heat transfer from the top, bottom and edge of the collector to the surrounding environment. By assuming that the losses of the collectors/plates occur to a common sink temperature $\mathrm{T_a}$, the parameter $\mathrm{U_L}$ can be summarised as follow:

$$\begin{aligned} \mathrm{U_L} &= \mathrm{U_t} + \mathrm{U_b} + \mathrm{U_e} \\ &= h_r + h_c \end{aligned} \tag{6.14}$$

Where $\mathrm{U_t}$ is the heat loss coefficient from the top/plate; $\mathrm{U_b}$ is the heat loss coefficient from the bottom/plate; $\mathrm{U_e}$ is the heat loss coefficient from the edges of the collector, but for this study, the edge's heat losses are out of scope; h_r and h_c are the heat transfer coefficients due to radiation and convection respectively. By using the analysis given by (Duffie and Beckman, 1980), h_r between the collectors/plates and the sky temperature (T_{sky}) can be computed. Assuming that T_{sky} is the same as T_a, and that the front and back of the collector are at the same temperature:

$$h_r = \varepsilon\sigma(T_p^2 + T_a^2)(T_p + T_a) \tag{6.15}$$

Where ε is the collector's emissivity (0.9), and σ is the Stefan-Boltzmann constant (5.7x10^{-8} W·m^{-2}·C^{-4}).

As the wind speed is very low in this study, free convection condition dominates, hence h_c can be determined using the dimensional equation(Watmuffj, 1985):

$$h_c = 2.8 + 3.0v \tag{6.16}$$

where ν, is the wind speed (m·s^{-1}). An iterative process is used to compute the first value of $\mathrm{U_L}$ by assuming the initial mean plate $\check{\mathrm{T}}$ or $T_{evap/coll}$ to be 10°C and $\mathrm{F'}$ can be calculated.

Since $\check{\mathrm{T}}$ is expressed as the mean refrigerant temperature in the evaporator/collector, which can be assumed to be the same as the refrigerant's evaporating temperature ($T_{evap/coll}$) in the collector/evaporator, and from equation (6.1) and (6.2), $T_{evap/coll}$ can be defined as:

$$T_{evap/coll} = \frac{1}{F'}\ [T_P - (1 - F') + T_a)] \qquad (6.17)$$

The collector model is used to determine the value of the collector outlet temperature $\mathrm{T_p}$ for the given values of ambient temperature $\mathrm{T_a}$, $\mathrm{I_{coll}}$, refrigerant properties of h_{rifin} and (h_{rifout}), as well as the heat pump parameters such as the specific volume of the fluid at the outlet of the collector ($\mathrm{V_1}$) in addition to the compressor displacement volume rate (VD). The outlet fluid temperature $\mathrm{T_p}$ can be calculated through the steady state energy balance on the collector, which is expressed as:

$$\frac{\mathrm{VD}}{\mathrm{\nu_1}}(h_{rifout} - h_{rifin}) = \mathrm{F'A_{coll}} * [\mathrm{I_{coll}}(\tau \propto) - \mathrm{U_L}(\mathrm{T_p} - \mathrm{T_a})] \qquad (6.18)$$

From the above equation equation (6.18), $\mathrm{T_p}$ can be computed as:

$$\mathrm{T_p} = \mathrm{T_a} + \frac{\mathrm{I_{coll.}(\tau\alpha)}}{\mathrm{U_L}} - \left(\frac{\mathrm{VD}}{\mathrm{\nu_1}}\right) * \frac{(h_{rifout} - h_{rifin})}{\mathrm{U_L.F'.A_c}} \qquad (6.19)$$

For the Nottingham city (UK location), the $\mathrm{T_a}$ value is incorporated over a given month and those assumed values of enthalpies at the refrigerant h_{rifout} (state points 2) and h_{rifin} (state point 1) which are modelled and computed from the polynomial fit for the refrigerant's properties will be explained later in the modelling result section.

However, $Q_{evap/coll}$ may also be calculated by means of the amount of heat absorbed by the fluid passed through the evaporator/collector ($\dot{m}_{coll\_rif}$). This can be expressed in terms of thermodynamic enthalpy change of the fluid from inlet, h_{rifin} to outlet, h_{rifout} of the the the evaporator/collector and defined as follows:

$$Q_{evap/coll} = \dot{m}_{coll\_rif}(h_{rifout} - h_{rifin}) \tag{6.20}$$

Where $\dot{m}_{coll\_rif}$ ($kg \cdot s^{-1}$), is the refrigerant's mass flow rate in the evaporator/collector, and will be explained in the next section.

The efficiency of the evaporator/collector ($\eta_{coll_{rif}}$) is necessary to be determined to evaluate the thermal performance of the collector and can be computed as:

$$\eta_{coll\_rif} = \frac{Useful\ energy\ gain\ by\ the\ collector,\ \mathrm{Q_{evap/coll}}}{Solar\ energy\ available\ on\ collector\ plate, Acoll\ , \mathrm{I_{coll}}} \tag{6.21}$$

or

$$\eta_{coll\_rif} = \frac{Q_{evap/coll}}{\mathrm{I_{coll}} * A_{coll}} \tag{6.22}$$

6.1.2. The compressor section

The compression vapour of the refrigerant is assumed to be a polytropic process, so the compressor work, $\mathrm{W_{comp}}$ or compressor power, $\mathrm{W_{power}}$ for a given compression ratio P_2/P_1 can be determined from (Cleland, 1994):

$$W_{comp} = \frac{P_1 v_1}{\eta_{comp}}\left(\frac{k}{k-1}\right)\left[\left[\frac{P_2}{P_1}\right]^{\frac{k-1}{k}} - 1\right] = \dot{m}_r\left(h_{rifout} - h_{rifin}\right) \tag{6.23}$$

Where $\mathrm{P_{2,}}$ and $\mathrm{P_1}$ are the condensing (high-side) and evaporating (low-side) pressures (bar), which can be determined via the refrigerant's thermodynamic polynomial chart; η_{comp} is the compressor efficiency; $[k]$ is the ratio of specific heat, which is 1.14 for R407C; $\dot{m}_r$ is the system mass flow rate (kg·s^{-1}); h_{rifin} and h_{rifout} are the refrigerant's temperature at the compressor's inlet and outlet respectively.

$\mathrm{W_{comp}}$ dependents on η_{comp}, and it is a variable related to fluid's state (entropy) and the temperature of the collector outlet fluid $\mathrm{T_p}$ or h_{rifin} (enthalpy). η_{comp}, can be expressed as:

$$\eta_{\mathrm{comp}} = \frac{\mathrm{T_{pi}} - \mathrm{T_p}}{\mathrm{T_{pa}} - \mathrm{T_p}} \tag{6.24}$$

The η_{comp} is calculated through simulation through multiple iterations , and its value also depends on the fluid state arising out of $\mathrm{T_p}$ variation. The variations occur very rapidly since T_{pi} (CTD calculated) and T_{pa} are isentropic, each with variable temperature, whereby:

$$\mathrm{T_{pi}} = \mathrm{T_p} * \left[\frac{\mathrm{P_2}}{\mathrm{P_1}}\right]^{0.28571} \tag{6.25}$$

$$\mathrm{T_{pa}} = \mathrm{T_p}\left[\frac{\mathrm{P_2}}{\mathrm{P_1}}\right]^{\left[\frac{\mathrm{n}-1}{\mathrm{n}}\right]} \tag{6.26}$$

where, $\mathrm{n} = \mathrm{k}$, and determine the fluid's temperature after compression $(\mathrm{T_3})$ or h_{rifout} $\mathrm{T_3}$ can be expressed as follows:

$$\mathrm{T_3} = \mathrm{T_p}\left[1 + \frac{\left[\frac{\mathrm{P_2}}{\mathrm{P_1}}\right]^{\frac{[\mathrm{k}-1]}{\mathrm{k}}} - 1}{\eta_{\mathrm{comp}}}\right] \tag{6.27}$$

Since the compressor under consideration is a rotary hermetic variable speed compressor, the fluid mass, $\dot{m}_r$ circulated and pumped by the compressor is given as:

$$\dot{m}_r = \frac{N * \mathrm{V_D} * \eta_v}{60 * \mathrm{v_1}} \tag{6.28}$$

Where *N* is the number of rotations; η_v is the volumetric efficiency of the compressor, and $\mathrm{V_D}$ for a reciprocating compressor type can be expressed as:

$$\mathrm{V_D} = \frac{S_c N * \pi * D_i^2}{4 * 60} \tag{6.29}$$

6.1.3. The condenser (air) section

The maximum heat gain received at the inlet of the condenser (air) can be evaluated from the compressor outlet temperature $\mathrm{T_3}$. $Q_{cond_{rif}}$ can be calculated in terms of the change of the enthalpy on the refrigerant side from the inlet ($h_{cond_{rif,in}}$) to outlet ($h_{cond_{rif,out}}$) of the condenser as follows:

$$Q_{cond_{rif}} = \dot{m}_{rif}(h_{cond_{rif,out}} - h_{cond_{rif,in}}) \tag{6.30}$$

$$Q_{cond_{rif}} = \dot{m}_{rif} * C_{p,rif}(T_{cond_{rif,out}} - T_{cond_{rif,in}}) \tag{6.31}$$

On the air side of the condenser, the heat gain from the refrigerant can be estimated as:

$$Q_{cond_{air}} = \dot{m}_{air} * C_{p,air}(T_{cond_{air,out}} - T_{cond_{air,in}}) \tag{6.32}$$

Where $C_{p,air}$ is the specific heat coefficient of the air; $T_{cond_{air,out}}$ and $T_{cond_{air,in}}$ are the respective estimated air temperatures at the outlet (rejected hot air) and inlet (delivered cold air) of the condenser; while $\dot{m}_{air}$ is the mass flow of the air and can be estimated as:

$$\dot{m}_{air} = \rho * \mathrm{V} * \mathrm{A} \tag{6.33}$$

Where ρ is the density of the flowing air ($kg \cdot m^{-3}$); V is the mean airflow velocity ($m \cdot s^{-1}$) and A is the flow area (m^2).

From section two and three, since the COP of the system ($COP_{DX-SAMHP}$) is dependent on the thermal energy produced by the system ($\mathrm{Q_H}$), which is the condenser work, and inversely dependent on compressor's work, the $\mathrm{COP}_{DX-SAMHP}$ can be calculated from:

$$COP_{DX-SAMHP} = \frac{\mathrm{Q_H}}{\mathrm{Work_{comp}}} \tag{6.34}$$

For the system space-only mode, the $COP_{DX-SAMHP}$ at any time instant (t) can be expressed as:

$$COP_{DX-SAMHP} = \frac{Q_{cond_{air}}(t)}{W_{comp,fan}(t)} \tag{6.35}$$

6.1.4. Heat exchanger and submerged condenser in DHWT section

For a well-insulated heat exchanger plate, the ejected heat from the refrigeration cycle is completely taken away by a water cycle loop i.e:

$$\dot{m}_w.\mathrm{C}_{pw}\left(T_{out,w} - T_{in,w}\right) = (UA)_{h\,x} \times LMTD \tag{6.36}$$

Where $\dot{m}_w$ (kg·s^{-1}), is the water mass flow rate in the heat exchanger plate; $T_{out,w}$ and $T_{in,w}$ are the water temperatures at the outlet and inlet of the plate heat exchanger respectively; $(UA)_{h\,x}$ is the overall heat transfer coefficient in the plate heat exchanger; while $LMTD$ (log mean temperature difference) is expressed as (Chyng et al., 2003):

$$LMTD = \frac{\left(T_{out,R} - T_{in,w}\right) - (T_{in,R} - T_{out,w})}{In\left[\left(T_{out,R} - T_{in,w}\right) - (T_{in,R} - T_{out,w}\right]} \tag{6.37}$$

Where $T_{in,R}$ and $T_{out,R}$ are the refrigerant R407C temperatures (R) at the inlet and outlet of the plate heat exchanger (°C) respectively. Therefore, the condenser energy balance can be obtained, assuming no heat losses, as:

$$\dot{m}_R\ (h_{R,in} - h_{R,out}) = (UA)_{h\,x} \times LMTD \tag{6.38}$$

The temperature distribution in the water side along the flow direction can be expressed as:

$$T_{h\,x,,w}(\mathrm{z}) = \frac{T_{out,w} - T_{in,w}}{In\ (L+1)}\ \mathrm{In}(z+1) + \ T_{in,w} \tag{6.39}$$

Where $T_{h\,x,,w}$ is the water temperature in the plate heat exchanger (°C) and (z) is the plate exchanger vertical distance (m).

The modulation of the plate heat exchanger starts from an estimated initial water temperature in the DHWT and by predicting a water outlet temperature at the plate heat exchanger $T_{out,w}$. The plate heat exchanger mass flow rate $\dot{m}_w$, is first calculated from equation (6.37) using the identified temperature distribution in the DHWT and plate heat exchanger. A new outlet water temperature at the plate heat exchanger $T_{out,w}$ then can be determined using the mass flow rate $\dot{m}_w$ and $Q_{h\,x}$ attained from the energy balance relation:

$$Q_{c.hx} = \dot{m}_w C_{pw}\left(T_{out,w} - T_{in,w}\right) \tag{6.40}$$

Where $Q_{c.hx}$ is the condenser heat rate (W), as a function of the plate heat exchanger and DHWT condenser as parameter.

The condenser heat rate $Q_{c,wt}$ at the DHWT can also be predicted when a serpentine copper tube is used for DHWT condenser (submerged heat transfer coil). Like the collector/evaporator, the condenser copper tube can also be divided into sections equal to enthalpy difference. Supposing that the DHWT is non-stratified, the energy balance can be obtained with the immersed condenser as follows:

$$Q_{c,wt} = M_w C_{pw} \frac{dt_w}{d_\tau} = \dot{m}_r (h_3 - h_4) - U_{L,t} A_t (T_{w,out} - T_{w,in}) \tag{6.41}$$

Where $Q_{c,wt}$ is the condenser heat gain, which is released and transferred into the DHWT by the condenser; M_w is the water mass in the water tank; C_{pw} is the water specific heat, while $T_{\mathrm{w,in}}$ and $T_{w,out}$ are the inlet and outlet water temperature respectively. Within an operating test period of the duration τ; h_3 and h_4 are the refrigerant's specific enthalpies at the inlet and outlet of the condenser respectively; $U_{L,t}$ is the total heat loss coefficient of the tank and A_t is the total heat transfer area of the wall of the water tank.

For the system space-and-water heating mode, the $COP_{DX-SAMHP}$ at any time instant (t) can be expressed as follows:

$$COP_{DX-SAMHP} = \frac{Q_{cond_{air}}(t) + Q_{cond_{water}}(t)}{W_{comp,fan,pump}(t)} \tag{6.42}$$

$$= \frac{\int_0^{\tau} Q_{cond_{air}}(t)\,dt \; + \; \int_0^{\tau} Q_{cond_{water}}\,(t)dt}{\int_0^{\tau} W\,(t)dt} \tag{6.43}$$

For water heating-only mode, since the thermal energy produced by the system $(\mathrm{Q_H})$, is only from the $Q_{cond_{water}}$, the $COP_{DX-SAMHP}$ at any time instant (t) for this mode can also defined as:

$$COP_{DX-SAMHP}(t) = \frac{Q_{cond_{water}}(t)}{\mathrm{W}\,(t)} \tag{6.44}$$

$$= \frac{\int_0^{\tau} Q_{cond_{water}}\,(t)\,dt}{\int_0^{\tau} W_{comp,pump}\,(t)\,dt} \tag{6.45}$$

6.1.5. Thermostatic expansion valve section

An orifice thermodynamic expansion valve is modelled, through which the refrigerant is extended from condensing to evaporating pressures, and the mass flow rate of the liquid passing through it can be computed as:

$$\dot{m}_r = \mathrm{C_v A_0}\sqrt{2_{\mathrm{\rho i,I}}\Delta \mathrm{P}} \tag{6.46}$$

Where $\mathrm{C_v}$ is the liquid flow coefficient, which depends on the degree at which the valve is opened, it reaches its maximum value when the valve is fully open $\mathrm{C_v} = 0.02005\sqrt{\mathrm{\rho i, I}} + 0.634\mathrm{v_0}$ which is evaluated empirically (Wile, 1935). Additonally, $\mathrm{A_0}$ is the minimum flow area across the orifice; $\mathrm{v_0}$ is the refrigerant specific volume at the outlet valve; $\mathrm{\rho i}$ is the density of the liquid, and can be calculated at the inlet valve; while $\Delta\mathrm{P}$ is the pressure variation across the orifice valve.

For an isenthalpic process in the expansion device:

$$\mathrm{h}_4 = \mathrm{h}_1 \tag{6.47}$$

Where; h_4 and h_1 are the respective refrigerant's specific enthalpies at valve inlet and outlet.

6.2. The results of refrigeration's cycle design

It is important to determine the optimal size of the heat pump during design because oversized systems operate with lower efficiencies, and may lead to excessive running cost. For system planning, components must be designed to interact optimally in order to ensure reliable operation and high performance levels. Therefore, to achieve quasi-steady condition of the heat pump by means of constant temperature and condensation, the work should be sufficiently enough to meet the minimum requirement for the heat pump, hence allowing it to operate reversibly and with higher COP values. In the current study, analytical investigations were carried out to examine the thermodynamic performance of the heat pump and the experimental tests were conducted to validate the mathematical model of the developed system.

The working fluid R407C evaporates at a temperature T_{EV} (S2) by extracting heat from the surrounding and the available solar irradiation. It is then compressed and gives up its latent heat. Subsequently, the fluid condenses at higher temperature T_{CO} (D3) in the first condenser for space heating and another portion is immersed inside DHWT for water heating purpose, where an external heat exchanger plate is used to extract heat from the fluid to heat the water as shown in Figure 6.1.

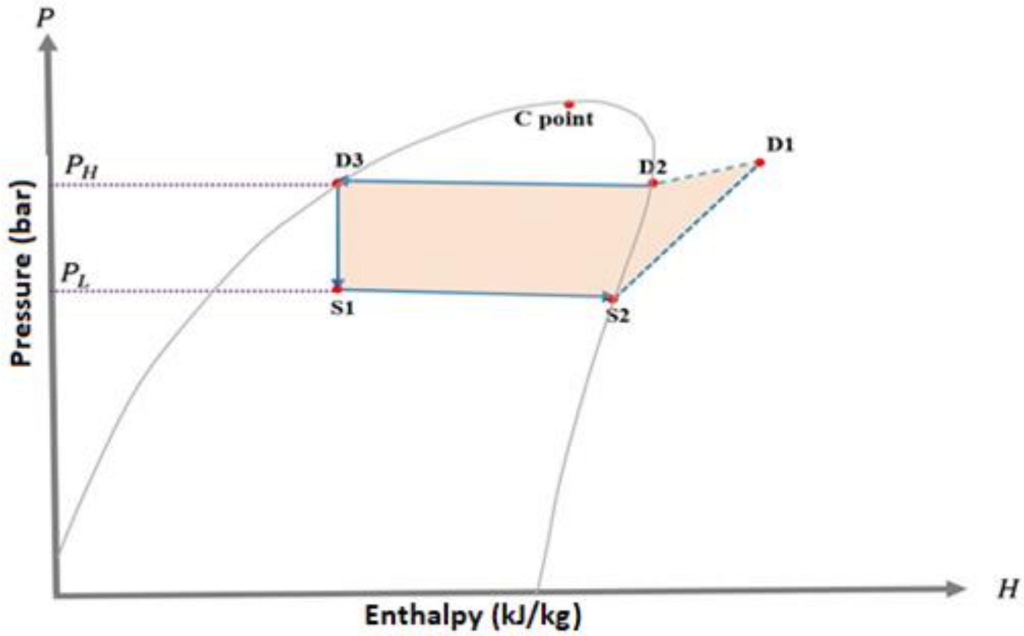

Figure 6.1. DX-SAMHP refrigeration cycle [Pressure/Enthalpy diagram (kJ/kg)]

The condensed liquid is then expanded adiabatically and irreversibly through an expansion valve and is throttled into the evaporator/plate to complete the cycle. The heat pump cycle is the reverse of the power cycle and can be illustrated with reference to R407C pressure enthalpy diagram.

This *DX-SAMHP* system is designed to operate at the discharge line pressures (P_H) between 17 and 20 bar, and suction line pressure (P_L) of 3 to 4 bar as seen in Figure 6.2. The compression ratio (CR) of the corresponding pressures in the condensers and evaporator (P_{CO}/P_{EV}) is up to 5.1. The highest obtainable condensing temperatures are up to 45°C in ideal conditions which are relatively moderate. It is worthy to mention that, without solar irradiation, the evaporating and condensing process does not occur at a constant temperature inspite of the pressure of these transmissions being constant.

The cycle in Figure 6.1 and Figure 6.2 can be combined to evaluate the working fluid at S2 in form of saturated vapour at an evaporation temperature T_{EV} of -3.98°C.

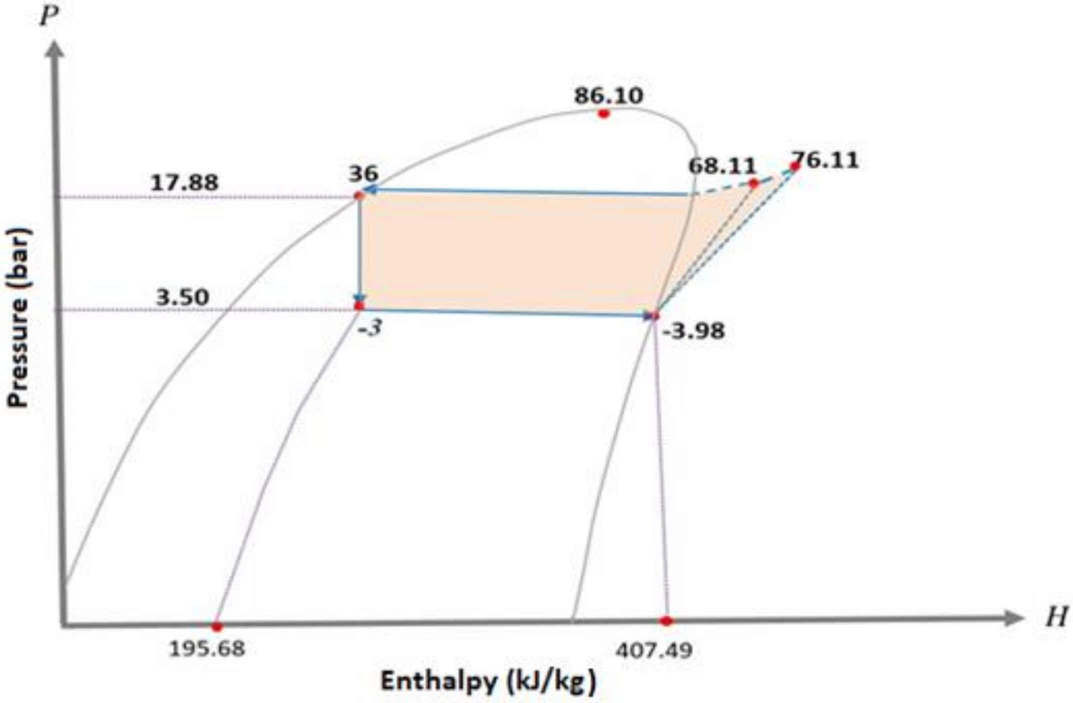

Figure 6.2. Enthalpy P-h diagram of the DX-SAMHP refrigeration cycle (kJ/kg)

The fluid is isentropically compressed to point D1 in the superheated vapour region. The superheat (HD1-HD2) is then removed and it is isothermally condensed from saturated vapour at D2 to saturated liquid at point D3 at a condensing temperature T_{CO} between 36-40°C. From D3, it is isenthalpically expanded to a mixture of liquid and vapour at point S1 to -3°C from which it is isothermally evaporated at a temperature of -3.98°C to point S2. Theoretically, the COP of a heat pump can be determined as COP = $[(H_{D1}- H_{D3})/ (H_{D1}-H_{S2})]$ = 3.8 where H, is the enthalpy per unit mass. Figure 6.3 presents the temperature changes in the designed refrigeration cycle of the *DX-SAMHP* system.

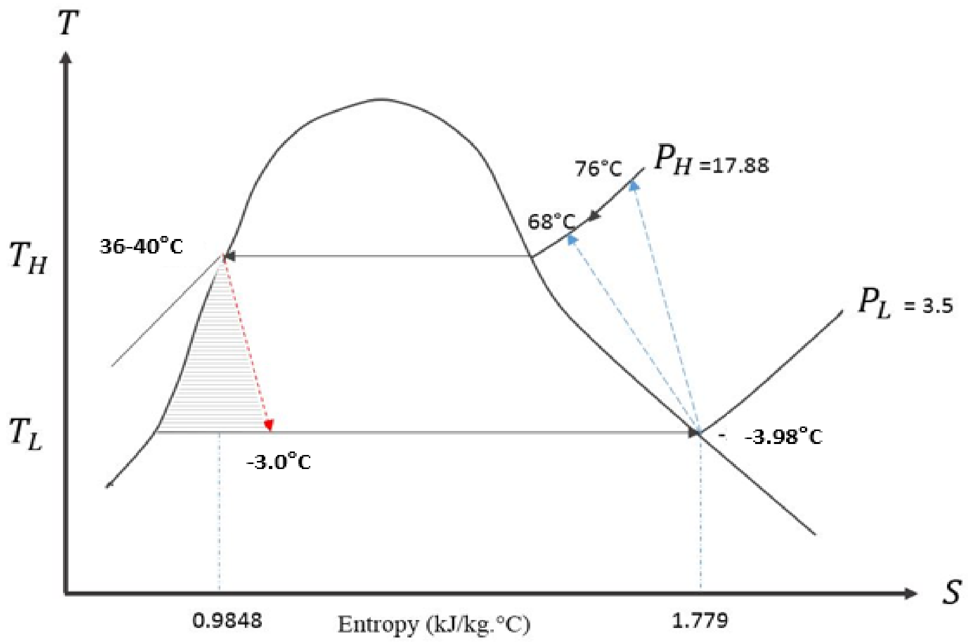

Figure 6.3. Entropy T-s diagram of the DX-SAMHP system (kJ/kg. °C)

It can be observed that the possible gross temperature lift (T_{CO}-T_{EV}) is graphically illustrated. The net temperature difference between TS2 and TD1 in the superheated vapour region is also depicted as well as the temperature variations in high and low pressure sides (T_H and T_L) among the system components that determine the evaporation T_{EV} and condensation T_{CO} temperatures.

Since the compression from point S2 to point D1 is at constant entropy, $\emptyset S_2 = \emptyset D_1$, where ∅ is the entropy per unit/mass. The entropy values of ∆S are shown by the dotted downward lines to right and left, where $\Delta S = Cp \ \ln \frac{T_{S2}}{T_{S1}}$ and Cp, is the refrigerant heat capacity at constant pressure per unit mass. The graph also provides the fluid upper limit at which a condensing vapour heat pump can deliver heat energy. The working fluid is condensed at a temperature sufficiently below the critical temperature to provide an adequate amount of latent heat per unit mass.

6.3. Analytical results of the *DX-SAMHP* system

6.3.1. The effect of different solar irradiation on the evaporation heat capacity and condensation heat gain

Figure 6.4 shows how the air condenser heat capacity of the *DX-SAMHP* changes with the evaporator/collector heat capacity. From the graph, when the evaporation heat capacity increases due to the increase in solar irradiation, the condensation heat capacity also increase as expected. This is mainly due to the difference between the evaporator temperature and the condensing temperature. For the evaporation heat capacity between 932 *W* and 1622 *W*, the simulated condensation was between 1474 *W* and 2255 *W* respectively.

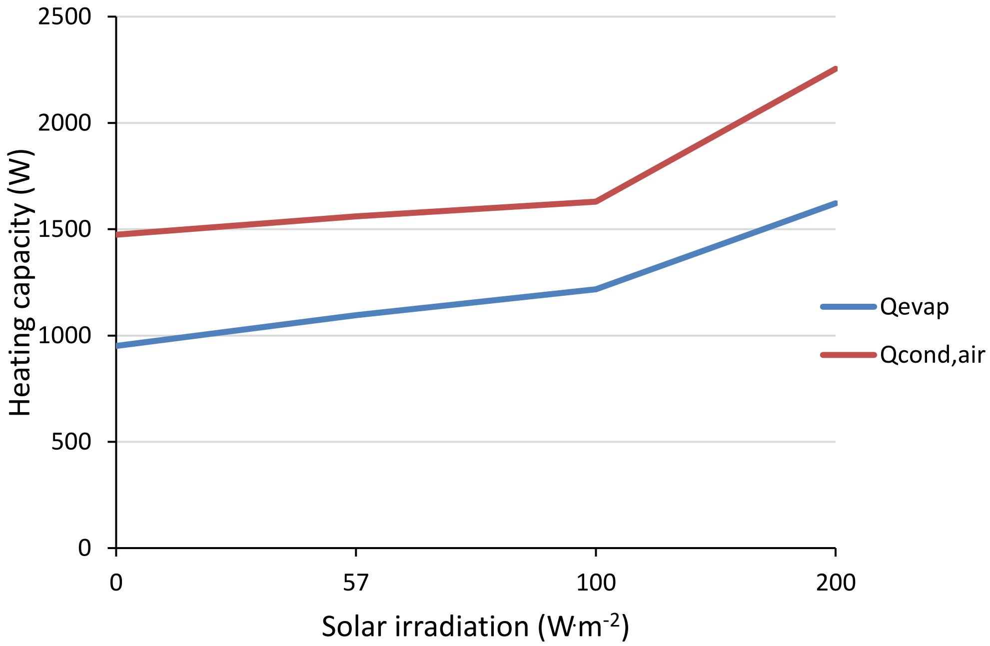

Figure 6.4. The influence of solar radiation on the system heat gain for space heating-only mode

6.3.2. The effect of the solar irradiation and water flow rate on the system's air condenser under space and water heating mode

Under space and water heating mode, the two condensers and evaporation heat gains were influenced by the increase in the water flow rate as well as the solar intensity as shown in Figure 6.5. From the graph, when the water flow rate increases, the heat capacities of the condensation and evaporation also increase. This is due to the increased heat exchange rate at both the condensers, whereby the working fluid is cooled down to a lower level on its way back to the evaporator.

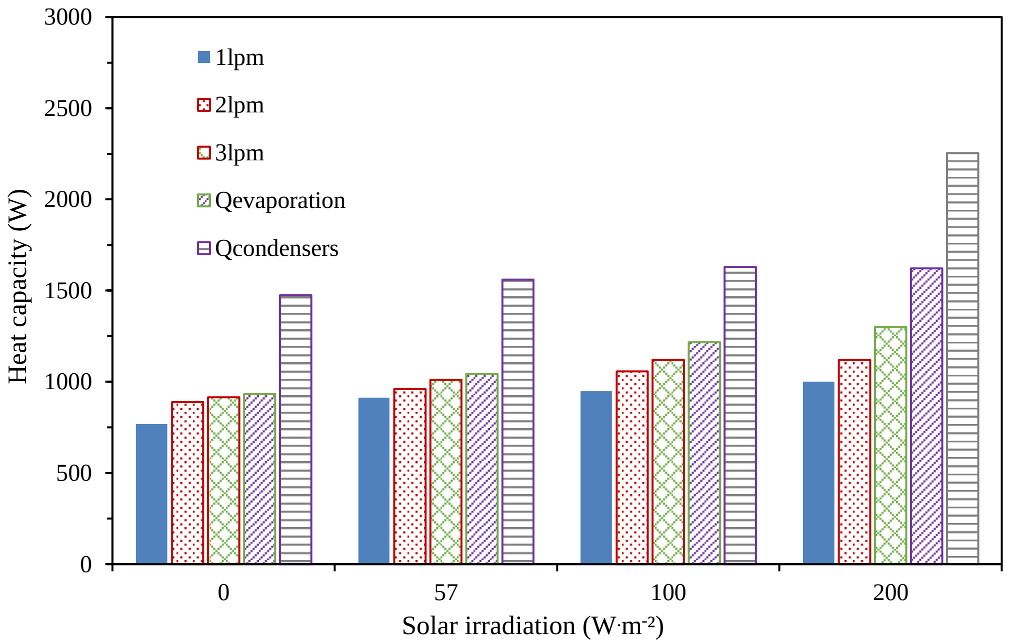

Figure 6.5. Solar radiation and waterflow rate influences on different parameters of the system

The effect of the waterflow rate on the air-side and water-side heat capacity under different solar radiations

Figure 6.6 illustrates how the heat gain of the condensers is affected by the increase of water flow rate as well as solar intensity. It is observed that when the solar radiation increases, the percentage of the heat capacity for the condensers also increases. On contrary, the lower the level of water flow, the higher the rate of heat capacity in the air-condenser side. This is attributed to the system's pipe designs cross section diameter and the speed of heat exchange rate at the water heat exchanger in the water-side loop. The highest simulated air and water heating percentages are 75 % and 25 % respectively under 200 W·m^{-2} solar radiation, and the lowest was 60 % and 40 % respectively under 0 W·m^{-2} solar intensity.

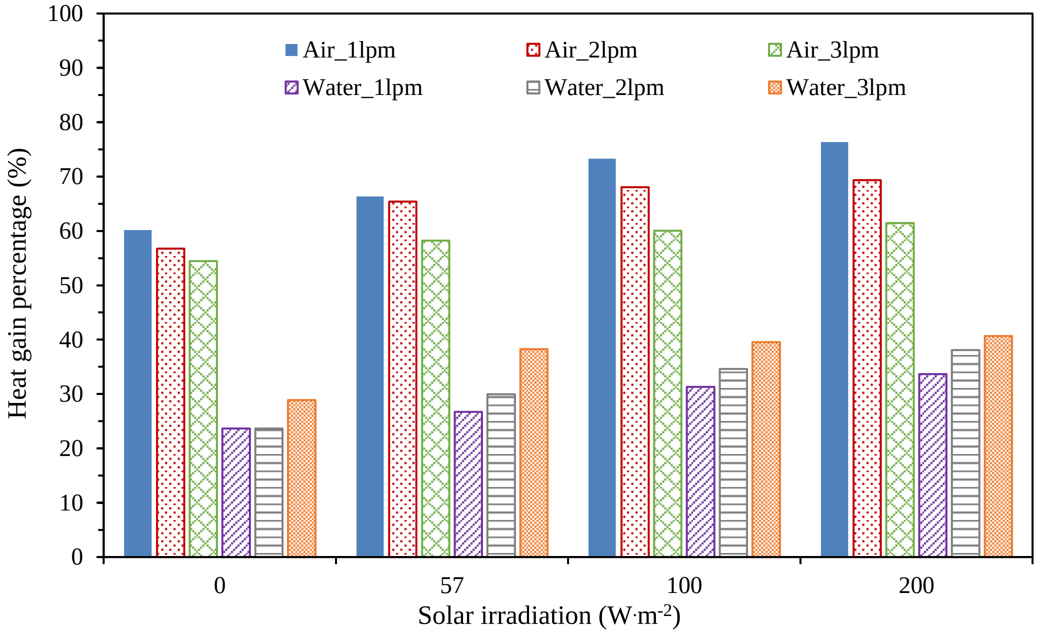

Figure 6.6. The percentages of heat gain between air and water condenser

6.3.3. The effect of space and water heating mode on the COP of DX-SAMHP system

Figure 6.7 shows the variation of $COPs$ of the *DX-SAMHP* system with solar irradiation and waterflow rate at the two condensers. Its is seen that when the solar radiation is increased, the COP raises which increases the heat capacity of both condensations accordingly as assumed. And when the water flow in the water loop increase, the COP of system raises as well as. The simulated COP was between 2.8 and 3.9, which indicates that the proposed system has higher performance compare to traditional ASHP and the existing DX-SAHP systems for the winter period.

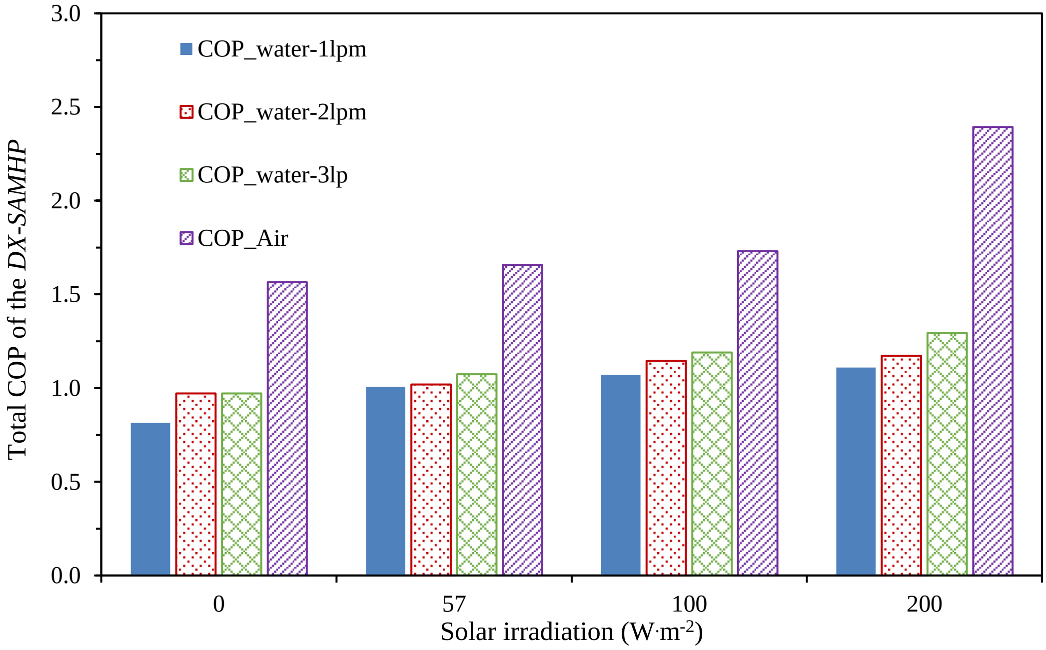

Figure 6.7. The total COP of the DX-SAMHP system

6.3.4. The effect of the working fluid on the performance of water-heating only mode

In this mode, the heat produced can be used only to heat the water in the DHWT, in situations where there is no need for space heating or in the summer season. The air-condenser's fluid line can be shut-down or eliminated in this mode. In this case, the compressor serves as the only one-way line to feed the refrigerant to the water-to-refrigerant heat exchanger. Meanwhile, the immersed coil tube (submerged condenser) ejects the heat to the domestic storage tank. The compressor is suggested to be shutdown once the water temperature in the tank exceeds the selected load temperature of 55°C from an initial temperature of 20°C.

The simulation model results presented in Figure 6.8 are taken within one-hour time at water-heating only mode, where the DHWT total volume is 200 ltrs for specified operation conditions in winter period.

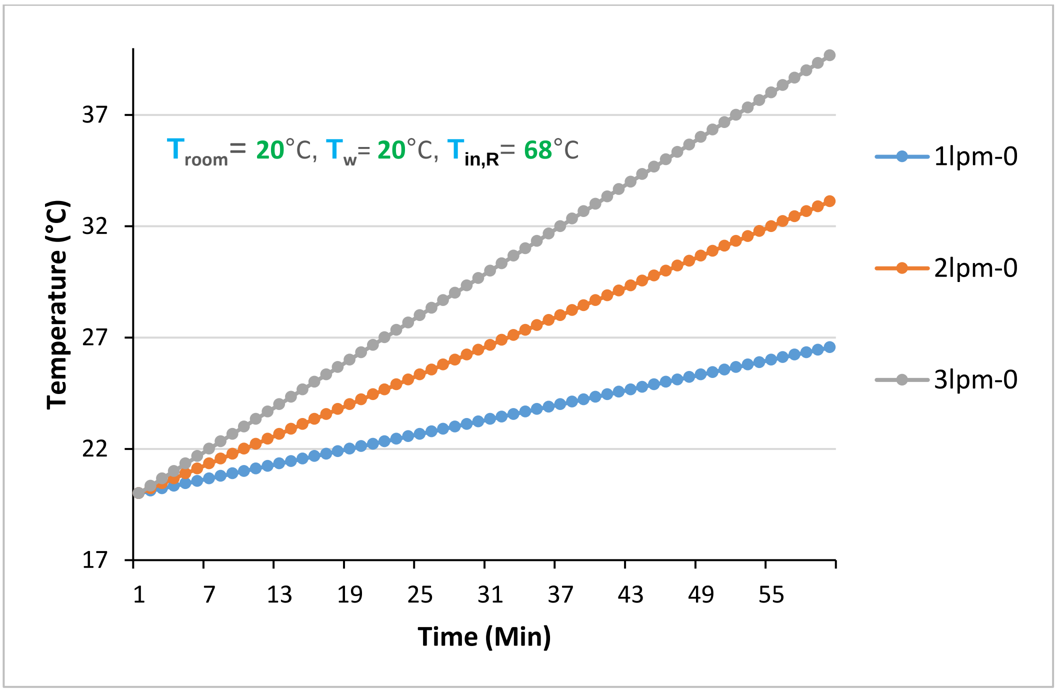

Figure 6.8. Water-heating-only mode performance under 0 W·m^{-2} and different water flow rates

Figure 6.8 and Figure 6.11 show the highest and lowest thermal performance of the mode while Figure 6.9 and Figure 6.10 present the mode performance under 57 and 100 W·m^{-2} solar irradiance. In these assessments, the system performance is governed generally by the change of the incident of solar insolation, indoor ambient temperature T_{room} and the water flow rate $\dot{m}_w$. Thus at lower values of T_{room} and solar intensity or $\dot{m}_w$, the longer time is needed to reach the required water temperature. However, it is necessary to note that, the performance of this mode essentially depends on the operation time (t)

and compressor capacity W_{comp}. A larger compressor capacity permits larger mass flow rate of fluid $\dot{m}_R$ at high temperature $T_{in,R}$, which leads to higher heating energy $Q_{c,wt}$, consequently resulting in a less value of (t) but with higher values of $COP_{DX-SAMHP}(t)$. From the graphs, the water heating rates are enhanced by 25%, 28% and 25% corresponding to the solar irradiances of 0, 57, 100 and 200 W·m^{-2} respectively at the water flow rate of 3l/min.

The simulation results indicate that for solar irradiation range of 0-57 W·m^{-2}, it takes 60 min to heat 200 ltrs of water from 20°C up to 40°C and 44°C respectively at 3l/min water flow rate. However, for solar irradiation of 100 and200 W·m^{-2}, it takes 50 and 45 min respectively to reach the desired hot water temperature of 50°C under the same operating conditions.

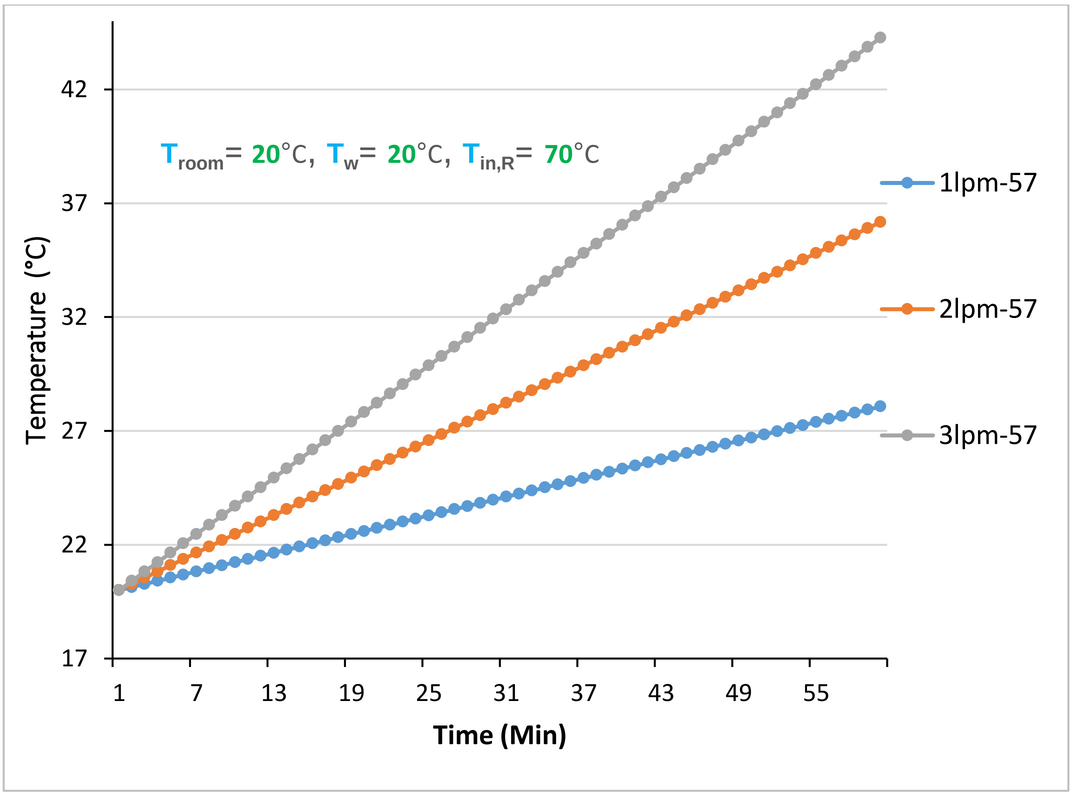

Figure 6.9. Water-heating-only mode performance under 57 W·m^{-2} and different water flow rates

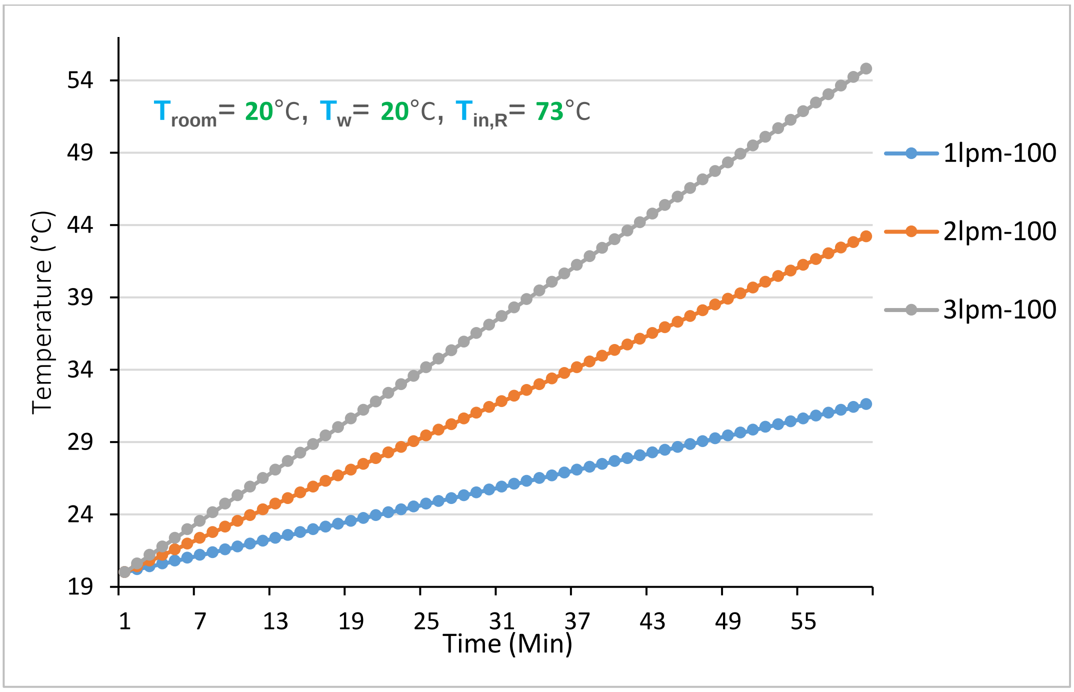

Figure 6.10. Water-heating-only mode performance under 100 W·m^{-2} and different water flow rates

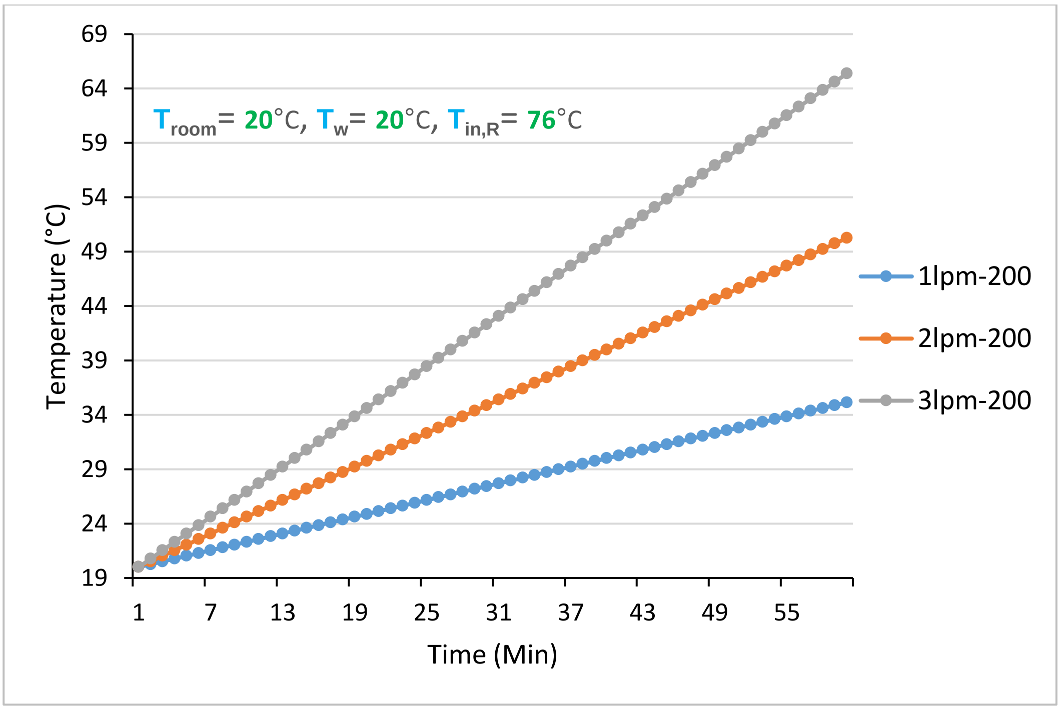

Figure 6.11. Water-heating-only mode performance under 200 W·m^{-2} and different water flow rates

6.4. Conclusion of chapter 6

In this chapter, the simulation was carried out using the Matlab software at different solar irradiations of 0 W·m^{-2}, 57 W·m^{-2}, 100 W·m^{-2}, and 200 W·m^{-2} under different air and water heating operating conditions to analyse the performance of the *DX-SAMHP* system. The thermal energy absorbed by the evaporator/collector, heat gain at both condensers, and the COP of the *DX-SAMHP* system were evaluated at different water flow rates. In addition, the effects of the air heating as the priority for designing the heat pump at different water flow rates on the system parameters were investigated. Moreover, the effects of the working fluid on the water heating only mode and its influence on the system thermal performance was also examined. The simulation results indicate that for solar irradiation range of 0-57 W·m^{-2}, more time is necessary to heat water than at solar irradiation of 100 and 200 W·m^{-2}, where 60 min are spent to heat 200 ltrs of water from 20°C up to 40°C and 44°C respectively at 3 l/min waterflow rate, whereas for 100 and 200 W·m^{-2}, only 50 and 45 min respectively are required to reach the desired hot water tempearture of 50°C under the same operating conditions. Meanwhile, the simulated $COPs$ were between 2.8 and 3.9, which indicates that the proposed system has higher performance compare to traditional *ASHP* and the existing *DX-SAHP* systems for the winter period.

Chapter 7. Experimental Investigation of he *DX-SAMHP* System

The aim of this chapter is to develop the *DX-SAHP* system by carrying out the experimental and analytical studies on the proposed Direct-Expansion Solar Assisted Multifunctional Heat Pump (*DX-SAMHP*) system to provide the existing homes with a multi-modes heating system.

7.1. Description and main components of the proposed *DX-SAMHP*

The system under consideration has been designed and constructed at the laboratory of the Department of Built Environment, University of Nottingham, UK, as shown in Figure 7.1.

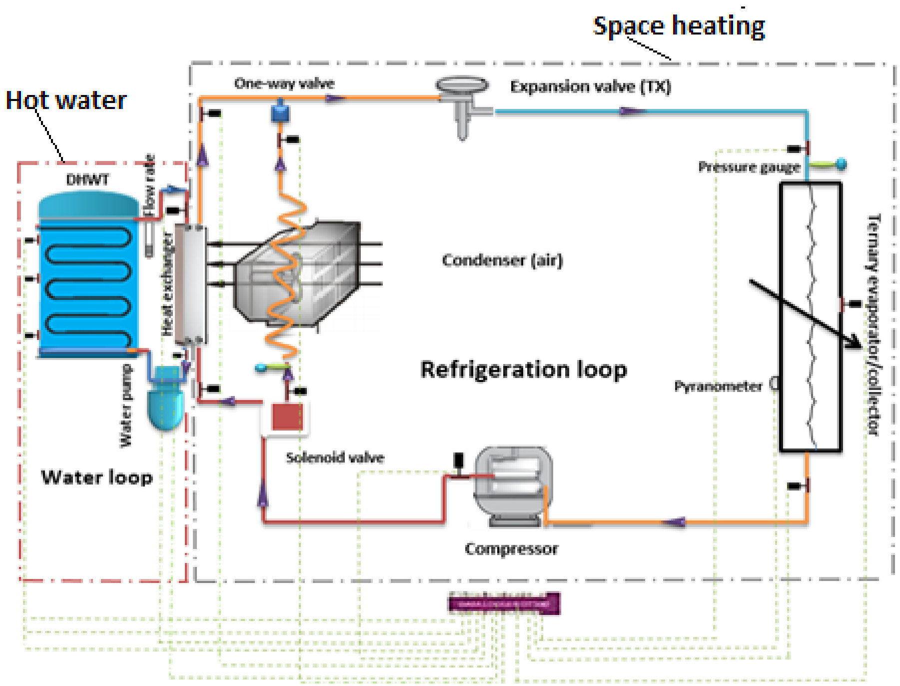

Figure 7.1. Schematic design of the proposed (DX-SAMHP) system

The proposed DX-SAMHP system mainly consists of an attic heat pump unit, a ternary aluminium coated flat-plates solar collectors, and a domestic hot water tank (DHWT). The heat pump unit comprises of; a refrigeration cycle, an air circulation unit, and a water loop as seen in Figure 7.1. The refrigeration cycle contains, a variable speed hermetic compressor, fan-coil units as an air-cooled condenser, water-to-refrigerant heat exchanger, and a thermostatic expansion valve. The water loop is made of a DHWT with an immersed condensing coil loop (water-cooled condenser), and the water circulating pump. Meanwhile, the air circulation unit contains the inlet/outlet ducts, assisted by the centrifugal fan. The supplementary elements are also added to the system to facilitate the operating cycle including; the expansion vessel, electronic control, water tank thermostat, and the solenoid valves as exhibited in Figure 7.1 and Figure 7.2.

The heat pump is coupled with three unglazed solar collectors, formed by integrating the bare ternary soft aluminium solar-collectors, which are connected in series as mentioned in chapter five. These collectors are used as the heat source and evaporator for the heat pump refrigeration cycle. Two solar plates are placed and integrated into the exterior structure of a house roof, with another plate mounted inside the house attic to absorb heat as illustrated in Figure 7.2.

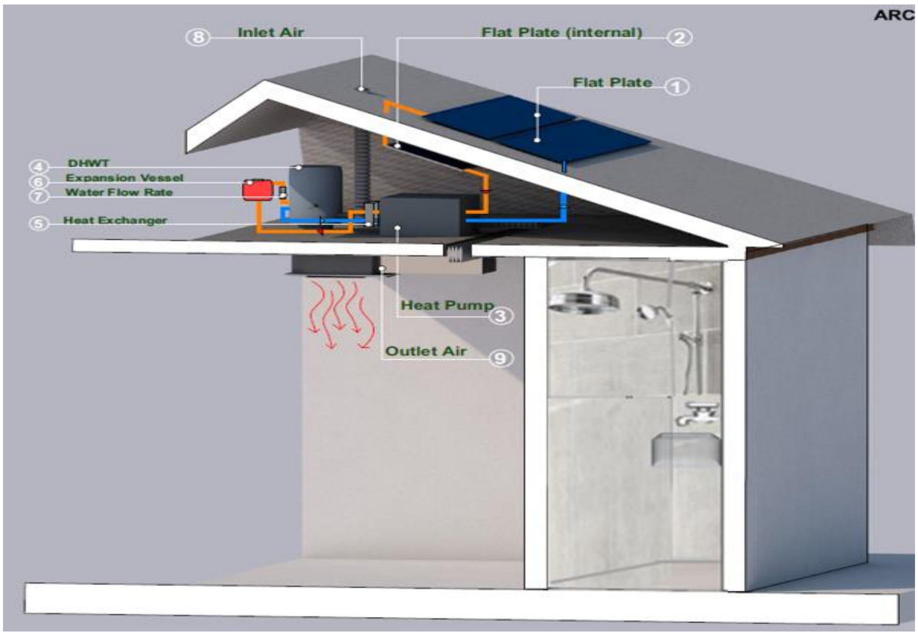

Figure 7.2. The proposed DX-SAMHP system for domestic application

7.2. Construction and fabrication of the *DX-SAMHP* system

Since the domestic buildings must have hot water as a basic requirement for use by the households particularly in winter-time, the system tested in chapter five is modified to satisfy this need. Therefore, the DHWT and other auxiliary apparatus were refabricated and added to the *DX-SAHP* system to come up with a *DX-SAMHP* system. For this to occurs, the hot water cycle is added to the system, and special consideration is put in place to give priority to space heating. Whereby the system can only heat the water storage when the output of the system exceeds the space heating requirements.Therefore, the space heating capacity is assumed to be greater than that of water heating. In other words, the diameter (cross-section) between air cooler and the compressor is set to be larger than the one between water-to-refrigerant heat exchanger. The electronic and electrical devices are also included to ensure the control and safetyof the entire operational processes. Therefore, the development of the *DX-SAMHP* system is based on the following assumptions:

(i) The system is at quasi-steady-state within the chosen time interval.

(ii) Excess of collector area to control superheated vapour at the inlet of the compressor.

(iii) The pressure drop in the collector, condenser as well as in the piping is negligible.

(iv) The refrigerant compression vapour is assumed to be polytropic.

(v) A considerable portion of the condenser surface area can be included in order to reduce the large temperature changes and pressure drops, so as to increase the *COP*.

(vi) The inner collector is added to absorb the indoor waste heat.

(vii) The domestic hot water tank is non-stratified.

(viii) Such improvements could increase the efficiency of *DX-SAMHP* and its thermal performance.

Additional refrigeration cycle to heat the water in the hot water tank, the conduction heat transfer between the two fluids (heat pump's refrigerant and the water) is utilized. Hence, the water-to-refrigerant heat exchanger is added, whereby the exchanger receives the refrigerant in gas form from the compressor and transfers heat to the water loop cycle. The heat exchanger used in this study is a plate heat exchanger type (SEWP 14 plates), made of stainless steel with a total area of 322 cm^2 as indicated in Figure 7.3. The refrigerant exchanges heat repetitively with water through the heat exchanger. The refrigerant condenses to liquid before it returns to the evaporator/collector.

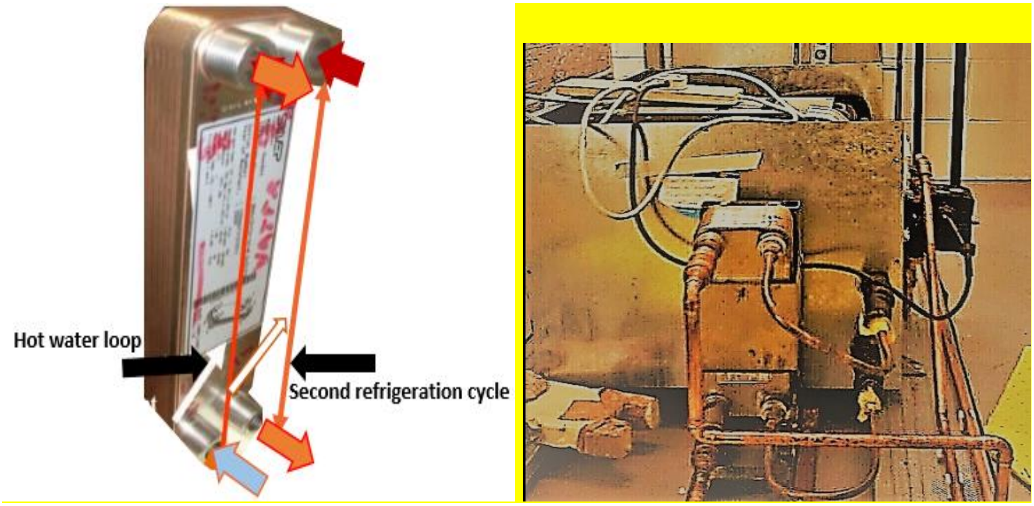

Figure 7.3. The fabricated water-to-refrigerant heat exchanger connections

7.2.1. Water loop and water circulating pump

The water loop consists of three main components; a water-to-refrigerant heat exchanger, a variable speed water pump, and an immersed coil-heater in the water tank as shwon in Figure 7.4. The heat exchanger is connected to DHWT through a circulating piping pump. The Auxiliary components such as the expansion vessel and the solenoid valve are also added to the loop for safety purpose to prevent any possible damage of the system due to high pressure (Figure 7.4 and Figure 7.5). The function of the expansion vessel is to absorb any pressure rise in the circulating water pipe and the water loop components. The vessel has two parts: one connects directly to the water system while the second is separated by a special diaphragm which contains air. The pressure rises as the volume increases whereas the diaphragm is displaced. Thus, when the water pump is switched on, the water is circulated d around the heat exchanger and the water tank coil, wheile heat is removed from the heat exchanger plates and transferred to the DHWT.

7.2.2. Electrical devices

Once the water tank temperature reaches the desired water temperature, the solenoid and the electrical valves receive the signals from the cylinder thermostat to close or redirect the refrigerant as indicated in Figure 7.5. The water pump used in this research is a variable speed type whereas the immersed coil-condenser is a traditional spiral cooper tube pipe (Table 7.1). The expansion vessel used is an elbi type with water pipe connections while the selected solenoid valve, made of stainless steel. All pipes are insulated to protect the system from condensed-water damage. The components and the specifications are given in Table 7.1

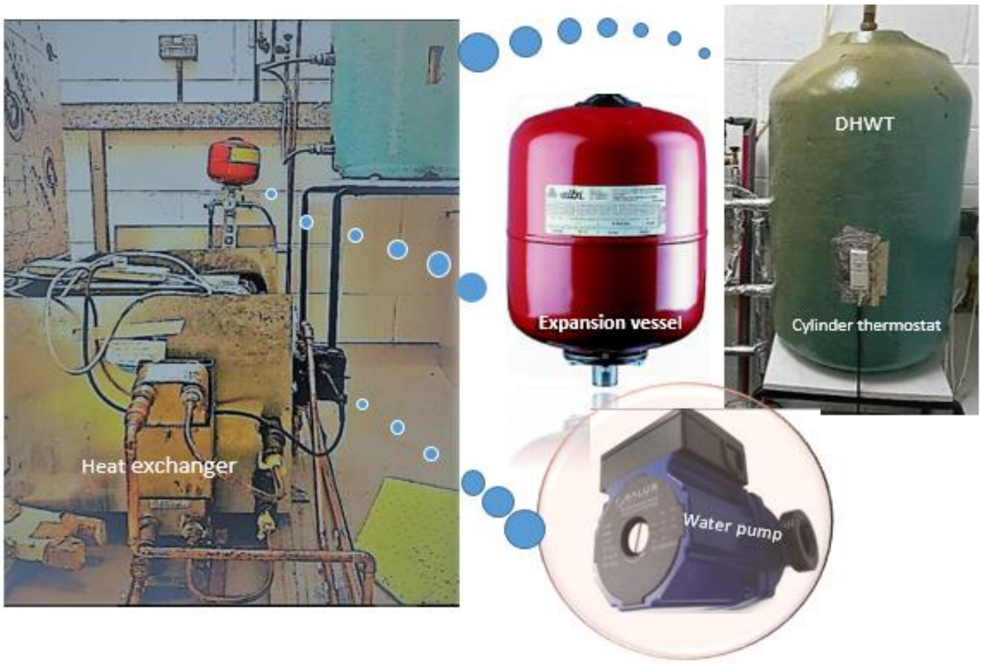

Figure 7.4. Main components of the water heating loop

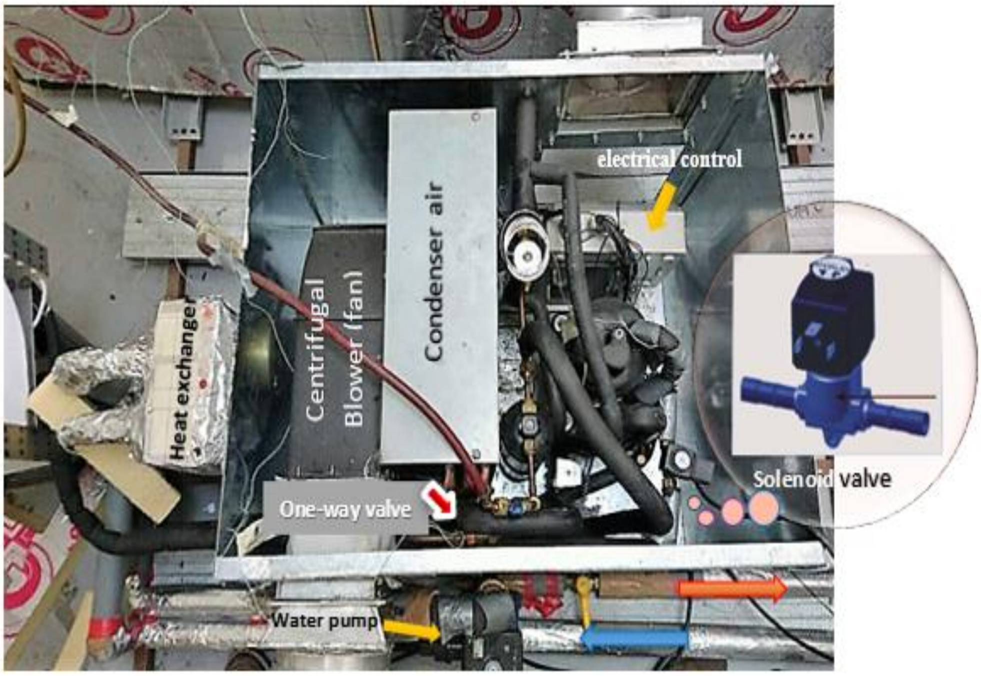

Figure 7.5. The control apparatus of the refrigerant cycle

Table 7.1. Specifications of the DX-SAMHP's additional components

Components	Type and Specification
Expansion Vessel	elbi type, (⅜") Max Seat-Teflon diaphragm, temp:99°C, Min temp:-10°C, Max pressure 6 bar
One and two way valve	RS Type, (⅜") refrigeration control valve
Solenoid Valve	SPORLAN(V10S/V23S), Pressure:0-35 bar, Max fluid temp: -40°C; +125°C, Max ambient temp:+40°C
Water pump	SALUS(V3F2) three speeds
Water-to-refrigerant heat exchanger	Plate's heat exchanger (SWEP): 14 plates 28cm x 11.5cm, with 9.0 thickness, Max temperature: 185°C, and Max pressure: 31 bar
Cylinder Thermostat	Wired cylinder: Drayton(HTS3), Setting range:50-80°C, A 230V AC

7.3. Operation procedures and experimental set up

A *DX-SAMHP* system is designed to operate within three modes, for heating a domestic building in winter period; Space heating only mode, hot water and space heating mode, and domestic hot water only mode. In order to assess the thermal performance of the new *DX-SAMHP* system, a number of experiments were conducted in the laboratory.

At the beginning of the test, once the compressor is turned -on, its speed is varried using a variable frequency drive until the operating temperature and pressure are reached as indicated in Figure 7.6. The evaporator/collector acts as the external heat source by using the indoor waste heat with or without the solar energy. A solar simulator is configured indoor to simulate the incident solar insolation on the surface of the collectors. A flexible luminous area positioned in parallel to the collector surface is exhibited in Figure 7.7. The solar irradiation (simulated light) is initially set at 57 $W{\cdot}m^{-2}$, and successfully increased to 100 and 200 $W{\cdot}m^{-2}$. During the experiment, when the solar irradiance falls on the solar collector, the main part of the radiation strikes the two aluminium absorber plates. Meanwhile, the outdoor cold air is sucked by the heat pump unit through a flexible duct into the system. After twenty-minutes, the system reaches a quasi-operational-state. A refrigerant receiver and an accumulator facilitate the refrigerant distribution within the system cycles. The system has two heat rejection modes, one of which uses a centrifugal fan to achieve space heating load. The energy rejected by this technique is exchanging the heat between the hot refrigerant and cold air. The DHWT is connected to the heat exchanger through the circulating pump to enable both space/water heating mode and domestic hot water only mode as indicated in Figure 7.6 and Figure 7.7. This helps to satisfy the space and water heating demand throughout the operation period. The water temperature at the DHWT is set constant at 55°C, with all simulated radiations. This is to maintain space and water heating demand throughout the operation period. After one hour the system shuts-down and the water circulating pump remains running to stratify the water tank. In the present experiment, the switching between these modes is accomplished by changing the valve positions and the on–off controls.

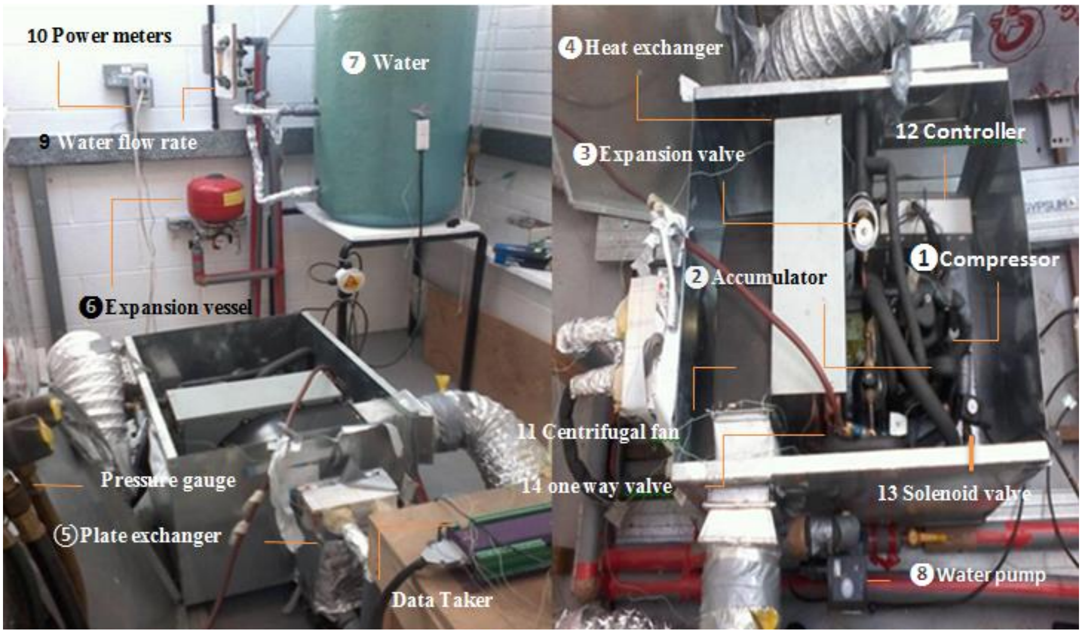

Figure 7.6. The DX-SAMHP system under experimental Set-up

Figure 7.7. Configuration of solar simulator with evaporator/collector and DX-SAMHP set-up

7.4. Data acquisition and processing system

The data acquisiation was used to measure different parameters including; the ambient/indoor temperature, relative humidity, the incident solar simulation and outdoor air temperature. In addition, temperatures of both refrigerant cycles and water loop monitored at different locations were also measured. The pressures of the refrigerant at compressor outlet, evaporator/collector inlet/outlet/surface and condenser were also measured. The electric power consumed by the different systems components such as the compressor, fan, pumps, electronic valves, etc. was also recorded.

7.5. Measuring Equipment's

The temperatures were measured with thermocouples, T, and K types as shown in Figure 7.8 (a). All thermocouples were calibrated in a high accuracy thermostatic bath using standard platinum resistance thermometer. In this study relative humidity and the thermal camera were also chosen to measure and evaluate the humidity and the component's refractory performance via humidity sensors with uncertainty of ±2 % respectively as shown in Figure 7.8 (b). The pressures were measured using two pressure sensors located at different points (outlet-collector, outlet-compressor, and outlet condenser) to monitor the suction and discharge lines as demonstrated in

Figure 7.9. Water flow rate

Table 7.2. A solar pyranometer was placed in the middle of the collector plates to measure the instantaneous simulated solar irradiance from zero to 200 $W{\cdot}m^{-2}$. The water flow meter was also fixed to determine the water cycle flow rate (l/min) with the uncertainty of ± 2 % as depicted in Figure 7.9. The refrigerant mass flow rate was measured using a clamp on pipe ultrasonic flowmeter. Electronic power meters e.g a digital power meter, were utilised to evaluate the energy consumptions of the compressor, and other components of the whole system including, a booster water pump, electrical valves, and the fan.

The major operating parameters were recorded during the testing period and stored on a personal computer via data acquisition at per the second interval using data logger.

(a) (b)

Figure 7.8. Sets of thermocouples K and T type (a), humidity sensors (b)

Figure 7.9. Water flow rate

Table 7.2. Specification of measuring equipment's

Parameter	Range	Accuracy	Measuring apparatus
Temperature (°C)	-200°C +200°C	Special limits error ± 0.4 (%), ±0.1°C	K- and T type thermocouple
Pressure: suction/discharge lines	0.5-55 bar	±1 (%)	3-1/8” steel case-Pressure gauge
Irradiation (W·m^{-2})	0-800 W·m^{-2}	±5 (%) 400-to-1100 nm	SP Lite 2 Silicon Pyranometer.Sensitivity 60 to ±100 μVw^{-1}·m^{-2}
Power meter (kW)	0-4 kW, 13A, 220-250Vr, 50/60Hz	± 1 (%)	Digital.wattmeter, Primera-LinePM231 E

Refrigerant Mass flow rate (kg·s^{-1})	0.001-1 kg·s^{-1}	±0.5 (%)	Ultrasonic clamp-on pipe-mass-flowmeter Katronic T flow 200
Airflow rate (m/ps)	1013mb, 0.00399-90m2- At 20°C	±1 (%) of reading, ±1 digit	Anemometer DVA 30 VT
Relative.Humidity humidifier sensor (%)	0-100 %	±2 (%) RH	SHT71.Standard/ Sensiron
Refractory performance	-20 to + 250°C	-	Thermal camera TiS10 9 Hz type, 5megapixel 640/480 resolution
Water flow rate (l/min)	0.5 l/min-5 l/min -10-100°C	± 2 (%)	Mass flowmeter /Polysulfone, F-44375

7.6. Experimental results and discussion

The experiments were carried out twice, earlier in winter 2016 and the latter in winter 2017. A series of consecutive and repetitive experiments were conducted for two fundamental operating modes during the cold season under typical Nottingham weather conditions; space heating only mode, and space and water heating mode. The experiments were executed indoor, but comparsions have been made between laboratory conditions and actual outdoor air temperature based on British Standard Institute/International Organisation for Standardization *BSI//ISO* 13612-1:2014 for testing and performance standard. The system was operated at night time and early morning hours from 23:00.pm until 06:00.am, targeting the coldest outdoor temperature of 4 to 8°C outdoor air temperature and 11 to 15°C of initial indoor temperature as well as 40 to 45 of relative humidity (*RH*). The solar irradiations of 57 to 200 W·m^{-2}, and various water flow rates were applied to investigate the capability of the new system. The wind speed factor was not considered in this study because it has no great influence on the system performance (Kong et al., 2011). Due to several tests, experiments were performed for one hour for each test. The system remained switched off for the rest of the day to ensure the same operating conditions for the all tests. Arithmetic average values of the measurements were then taken for analysis. Thereby the experimental results were later compared with analytical model.

7.6.1. Results of space heating only mode

In order to investigate the performance and capability of the developed *DX-SAMHP* system for space heating, outdoor temperatures, indoor temperatures, relative humidity, and the temperatures of heat pump components have been measured and recorded during the test period without using any ancillary heating apparatus. During the test, the outdoor air temperature was changing from 6.5°C to 7.5°C. It is observed that under solar irradiation of 57, 100 and 200 $W{\cdot}m^{-2}$, the evaporator/collector temperature ((plate-in and Plate-out) was negative as shown in Figure 7.10. This condition allows the evaporator/collector to harvest heat from solar energy and from the surrounding heat sources. The refrigerant leaves the evaporator/collector at a low temperature and in wet condition. This consequently results in uniform temperature distribution and maximizes the evaporator/collector capacity. It is clear that, with the increase of solar irradiation, the thermal performance of the heat pump also increases, leading to the increase in the system hot air outlet as illustrated in Figure 7.10 (Appendix-B).

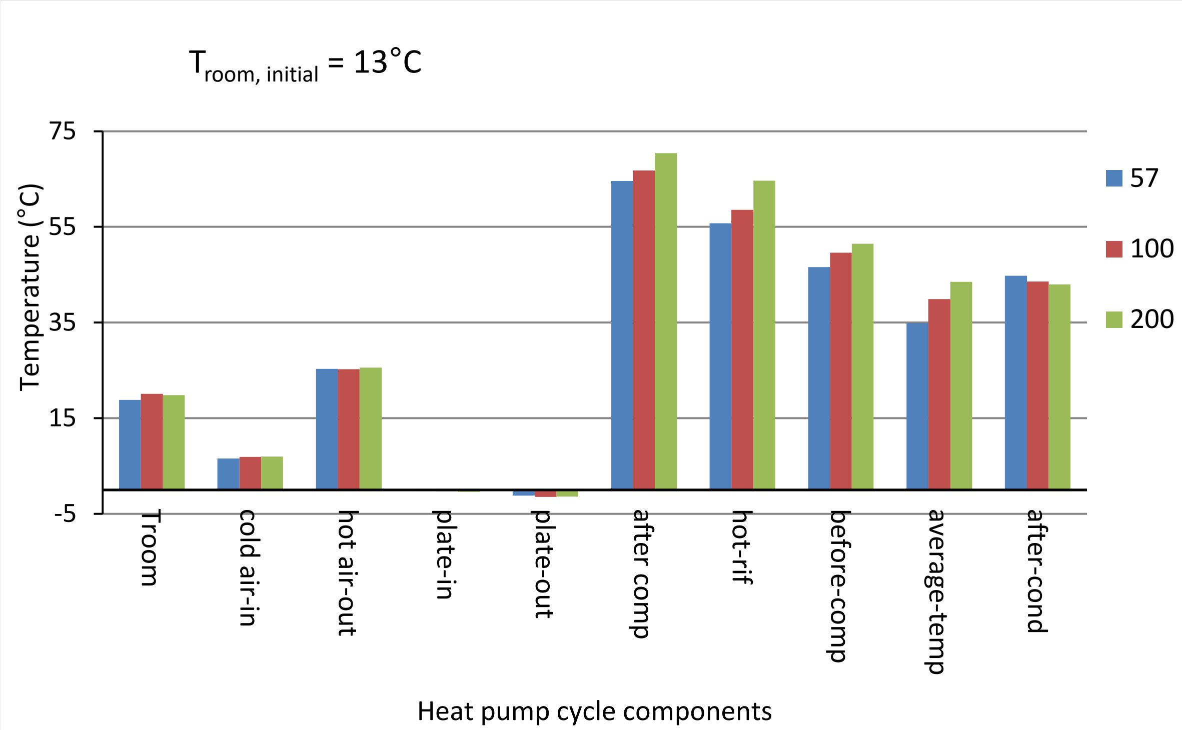

Figure 7.10. The influence of the solar irradiation on the system thermal performance

The experimental data are listed in Table 7.3 where it is shown that the average indoor temperature (T_{room}) varies from 18.8°C to 20.1°C. This little fluctuation is due to the inlet air differences. Meanwhile, the outlet hot air increases slightly as the solar radiation increases. It is observed that the increase in solar intensity slightly reduces the compressor work and the mass flow rate of refrigerant. This is because the increase in solar intensity leads to the rapid increase in the evaporating temperature, causing a reduction in the operation of the heat pump. It is also noticed that as the solar radiation increases, the system hot air increases and reaches its peak value of 25.6°C. Therefore, the room temperature is raised as the solar irradiance increases.

Table 7.3. The system thermal performance with different solar radiations

$Solar.radiation$ W·m^{-2}	T_{room} (°C)	$outlet_{air,av}$ (°C)	$inlet_{air,av}$ (°C)	$T_{room,initial}$ (°C)	$ŋ_{r_{rif}}$ (kg·s^{-1})
57	18.8	25.3	6.55	13.2	0.0330
100	20.1	25.4	6.90	15.0	0.0328
200	19.8	25.6	7.50	14.7	0.0324

To evaluate the performance characteristics of the *DX-SAMHP* under space heating- only-mode, the following equations were used to calculate the energy gain of the system's evaporation (Q_{evap}), condensation ($Q_{cond_{air}}$), and to assess the total *COP* of the *DX-SAMHP* system at any time instant (t);

$$Q_{evap} = \dot{ŋ}_{r_{rif}} * c_{p_{rif}} * \left(T_{out.evap} - T_{in.evap}\right) \qquad (11)$$

$$Q_{cond_{air}} = \dot{m}_{air} * C_{p,air} * (T_{out} - T_{in}) \qquad (12)$$

$$COP_{space.only.mode} = \frac{Q_{cond_{air}}\,(t)}{W_{comp}(t) + W_{electric}(t)} \qquad (17)$$

where eqaution (11) and (12) are already explained in chapter five; $Q_{cond_{air}}\,(t)$ is the heat exchanger rate at the condenser; $W_{comp}(t)$ and $W_{electric}(t)$ are the power input (for compressor, fan, electrical devices) to the heat pump at any time instant (t).

For the test period of duration (τ), COP_{average} is expressed as;

$$COP_{\text{average}} = \sum_{0}^{\tau} Q_{cond_{air}}\,(t)\,dt \Big/ \sum_{0}^{\tau} W_{comp}(t)\,dt + W_{electric}(t)\,dt \qquad (18)$$

The average input values of the solar irradiances and indoor heat, suggest that the thermal energy from solar energy and indoor surrounding heat account for 100%of the total energy obtained. The system was operated by either absorbing both solar energy and indoor heat simultaneously or by the only utilzingtheheat pump. The thermal energy used for space heating ($Q_{cond_{air}}$) was raised steadily from 3.139, 3.182, and 3.191 kW corresponding to solar radiations of 57, 100 and 200 W·m^{-2} respectively, in order to supply stable temperature to heat the space ($room$) as shown in Table 7.4.

Table 7.4. The DX-SAMHP thermal performance under space-only-mode

$Solar.radiation$ W·m^{-2}	T_{room} (°C)	$outlet_{air,av}$ (°C)	Q_{evap} (kW)	$Q_{cond_{air}}$ (kW)	COP
57	18.8	25.3	1.621	3.139	3.772
100	20.1	25.4	1.680	3.182	3.860
200	19.8	25.6	1.695	3.191	3.939

It is worthy to mention that, with low solar irradiation, the system is able to operate and provide sufficient space heating at a satisfactory temperature level of 25.3°C. The indoor heat was mainly transferred to the collector by natural convection, with adequate heat being provided. Figure 7.11 presents the performance characteristics of the *DX-SAMHP* system under space-only-mode, where the system temperatures versus the COPs for various solar irradiations are shown.

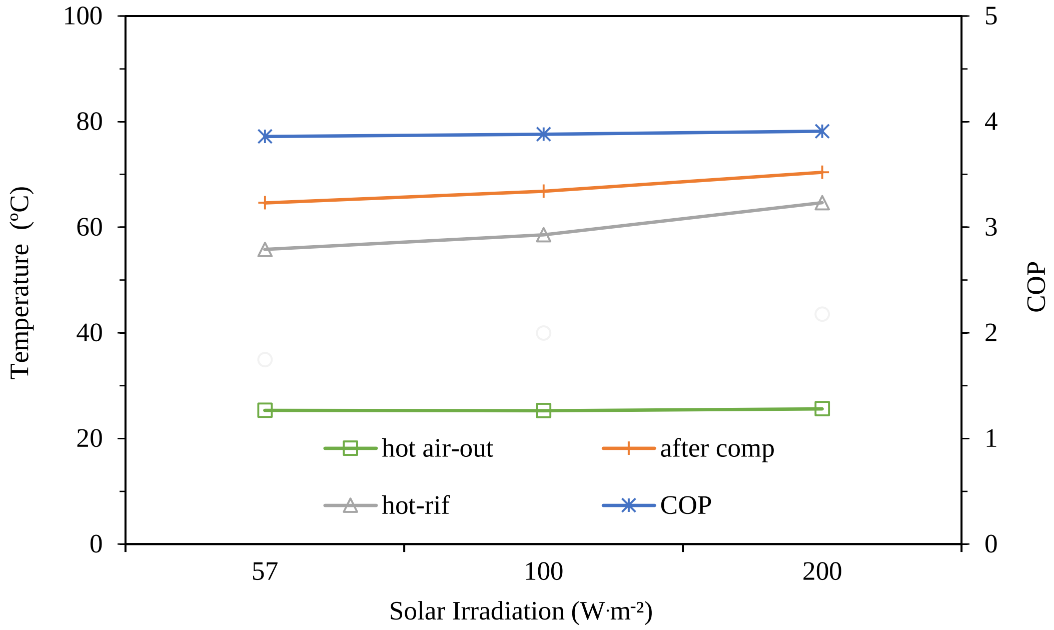

Figure 7.11. The Influences of the component's temperatures on *DX-SAMHP* performance characteristics under various solar radiations for space-only-mode.

(Huang and Chyng, 2001) indicated in their study of a solar source heat pump that the COP ranged from 2.5 to 3.7. (Kuang and Wang, 2006) stated in their work that, the COP of a multi-functional heat pump system was 2.1 in cloudy days for space-only mode and 3.5 in clear sunny days in winter. However, in the present study the obtained values of COP is much higher compared to traditional *DX-SAHP* and the above mentioned values. The highest COP achieved was 3.93 under 200 W·m^{-2} solar radiation whereas the lowest was 3.77 attained under solar irradiation of 57 W·m^{-2}.

7.6.2. Results of space-and-water heating mode

In this stage, space and water heating mode were implemented to investigate the performance of the developed *DX-SAMHP* system during the winter period. The performance of the system is carried out under varying solar irradiations, indoor (ambient) temperature, relative humidity, and water flow rate. A thermal storage water tank is utilised to store hot water for domestic use during the winter period. In this study, the total volume of the domestic hot water tank is about 200 litres, with a nominal temperature chosen to be 50°C. The heat rate gain at the condenser is plotted against the evaporated temperatures. The COP of *DX-SAMHP* system and the energy consumption of the compressor were also evaluated. Figure 7.12 shows the effect of the increase in solar irradiance on the system thermal performance. In the beginning, when the solar irradiation increases, the evaporator temperature increases, causing the evaporating pressure to rise as well as the refrigeration mass flow rate. Higher solar irradiation allows the temperature of the collector/evaporator plate ($\mathrm{T_p}$) to rise, which in turn raises the temperature difference between the indoor tempearture (T_{room}) and $\mathrm{T_p}$. The evaporator/collector plates often worked at temperatures lower than the indoor temperature, with values of -2.6, 0.5 and 1.8°C corresponding to the solar irradiations of 57, 100 and 200 W·m^{-2}. Therefore, when T_{room} is higher than $\mathrm{T_p}$, the collector/evaporator gains higher heat energy from both ambient and solar irradiations. However, a higher $\mathrm{T_p}$ results in the decrease in the temperature difference between $\mathrm{T_p}$ and T_{room} because of the decline in the heat transfer between the indoor temperature and collector/evaporator. It is obvious that by the end of the tests the system reaches its highest thermal temperature at 200 W·m^{-2} followed by 100 and 57 W·m^{-2} respectively.

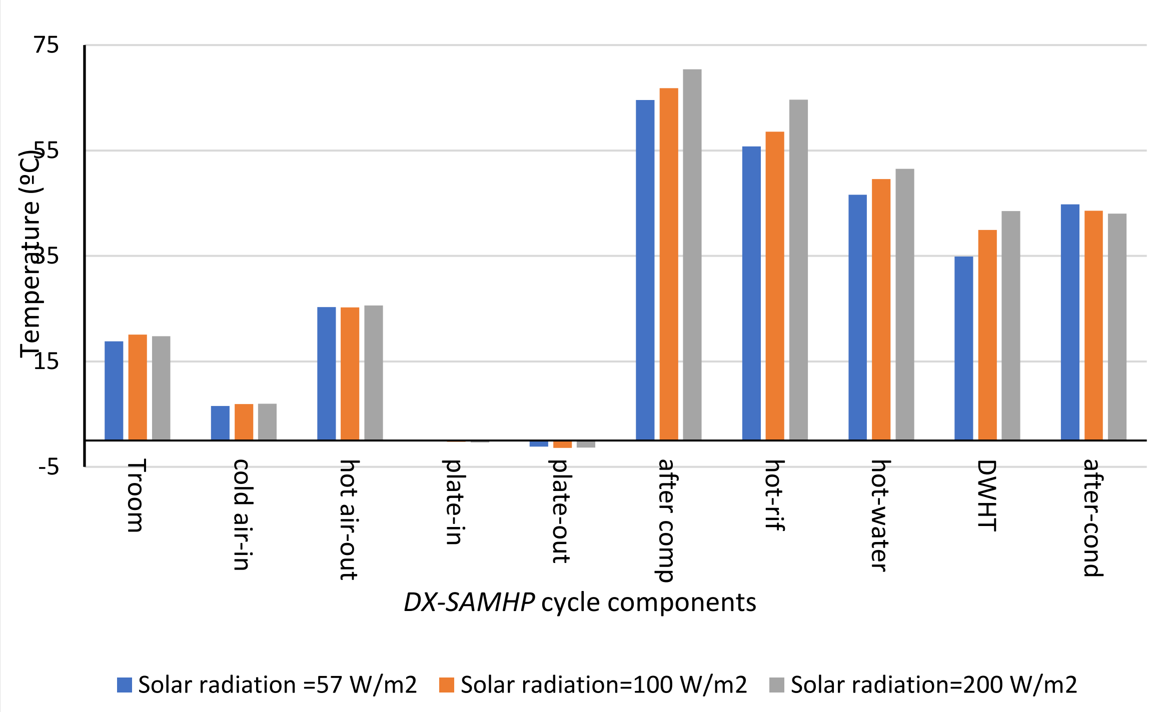

Figure 7.12. The influence of solar irradiations on the system for space-and-water heating mode

Figure 7.13 to Figure 7.15 shows the system performance under space and water heating mode without solar irradiation for the three water flow ratesof 1l/min, 2l/min, and 3l/min. Figure 7.13(a), Figure 7.14 (a) and Figure 7.15 (a) illustrate the average temperature of the components during the operating period. Similarly, Figure 7.13, (b), Figure 7.14 (b) and Figure 7.15 (b) indicate the monitored thermal behaviour of the system within the investigated time interval. The outdoor temperature was -1°C when the ambient temperature was in the range of 16.22°C to 17. 20°C. It is noted that the heat gain of the DHWT increase with time. It is also observed that, as water flow rate increases, the water tank temperature rate raises steadily to 4.5, 5.0 and 5.3°C for the specified testing time, corresponding to 1 l/min, 2 l/min, and 3 l/min respectively. however, the hot air production remained relatively constant at 24°C for all cases. It is noticed that the increase in water flow rate causes the system's total energy consumption to also increase. This is due to the rise the rate of operation of the water pump, rendering it to consume more energy. It is noted that the evaporating and condensing temperature remained practically at the samefor all tests. This is due to two reasons; (1) there was no support from solar irradiation to obtain a higher evaporating temperature of the refrigerant, (2) the indoor/ambient temperature T_{room} and relative humidity are maintained constant.

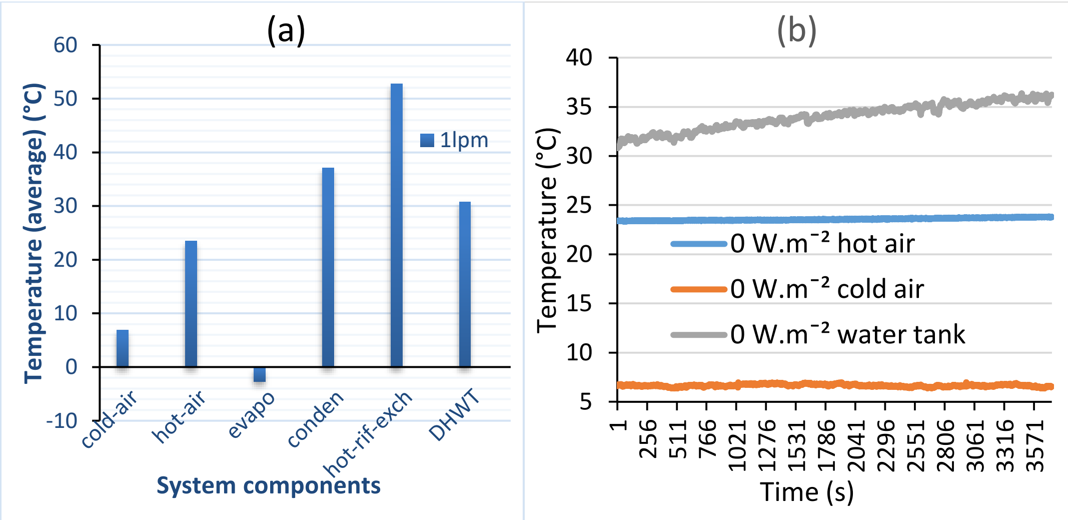

Radiation (W·m^{-2})	Water-rate l/min	Indoor Temp (°C)	outdoor Temp (°C)	compressor frequency (Hz)	R/H (%)	Comp pressure (bar)	Evapo pressure (bar)	Rate.of energy consump (W)
0	1	16.93	-1	35	29	18-19	3.4	934

Figure 7.13. System thermal performance without solar irradiation and (1 l/min) water flow rate

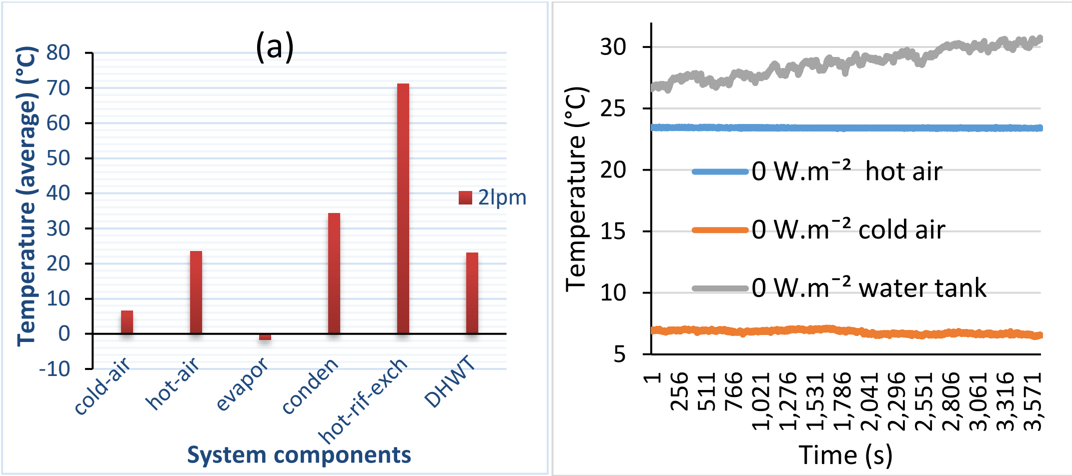

Radiation W·m^{-2}	Water-rate (l/min)	Indoor Temp (°C)	outdoor Temp (°C)	compressor frequency (Hz)	R/H (%)	Comp pressure (bar)	Evapo pressure (bar)	Rate.of energy consump (W)
0	2	17.2	-1	40	29.17	17.8	3.2	963

Figure 7.14. System thermal performance without solar irradiation and (2 l/min) water flow rate

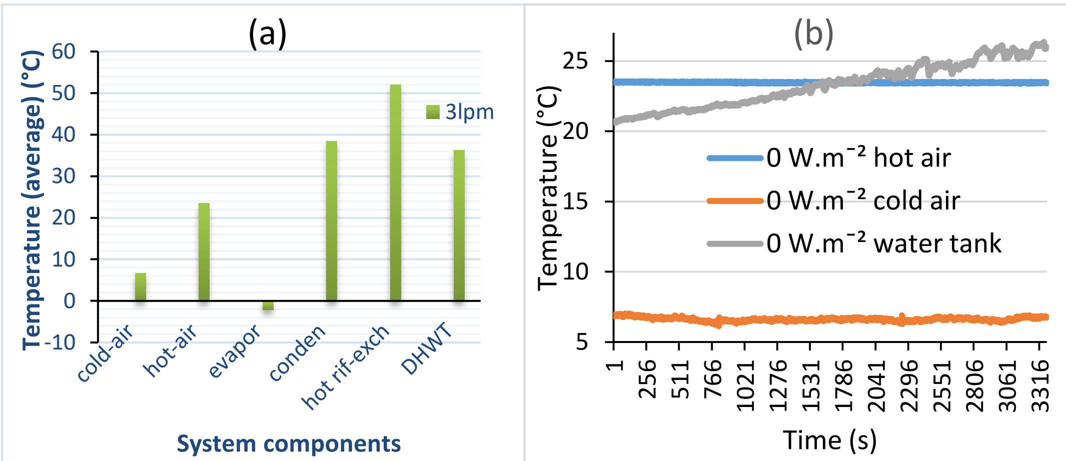

Radiation W·m^{-2}	Water rate (l/min)	Indoor Temp (°C)	outdoor Temp (°C)	compressor frequency (Hz)	R/H (%)	Comp pressure (bar)	Evapo pressure (bar)	Rate.of energy consump (W)
0	3	16.22	-1	30	30	18-20	3.5	1000

Figure 7.15. System thermal performance without solar irradiation and (3LPM) water flow rate

At a solar irradiation of 57 W·m^{-2}, the evaporator/collector was heated up, thereby increasing the evaporator temperature and influencing the temperature of the condenser to also increase. Hence, the average temperatures of the evaporator and the condensor were slightly increased by 2°C and 4°C respectively. Meanwhile, the average water temperature rate was increased by 22 %, 23 % and 24 % corresponding to 1 l/min, 2 l/min and 3 l/min water flow rates, while the delivered hot air for space heating reached its peak value of 25°C (Table 7.5 and Appendix B-1).

Table 7.5. System performance under 57 W.m-2 solar radiation and different waterflow rate

radiation W·m^{-2}	Water-rate (l/min)	Water increase rate (%)	Indoor Temp (°C)	Evaporating Temp (ave) (°C)	condens Temp (ave) (°C)	Hot Air Temp (°C)	Comp pressure (bar)	Evapo pressure (bar)	Energy Rate (W)
57 W·m^{-2}	1LPM	22	19	±1.0	39	25	18	3	941

radiation W·m^{-2}	Water-rate (l/min)	Water increase rate (%)	Indoor Temp (°C)	Evaporating Temp (ave) (°C)	condensing Temp (ave) (°C)	Hot Air Temp (°C)	Comp pressure (bar)	Evapo pressure (bar)	Energy Rate (W)
57W·m^{-2}	2LPM	23	17.2	±1.5	39	23.8	18-19	3.4	958

radiation W·m^{-2}	Water-rate (l/min)	Water increase Rate (%)	Indoor Temp (°C)	Evapo Temp (ave) (°C)	condens Temp (ave) (°C)	Hot Air Temp (°C)	Comp pressure (bar)	Evapo pressure (bar)	Energy Rate (W)
57W·m^{-2}	3LPM	24	18	±1.0	39	23.9	18-21	3.7	993

After one hour under 100 W·m^{-2} solar irrradiation, the system temperature gain at the DHWT was 7 to 8°C, resulting into the increase of the water flow rate as shown in Figure 7.16, Figure 7.17 and Figure 7.18. Therefore, the air temperature reached a maximum of 26.3°C for space heating in winter. It is clear that the increase in temperature at condenser has a similar trend with the solar irradiance and waterflow rates. In contrast, the collector/evaporator inlet temperature of -1 to -2°C and the compressor energy consumption rate were independent oof the time. However, although the condensing heat exchange rate and energy consumption raise with the increase in solar irradiance, the increase of the condensing temperature rate is somehow higher.

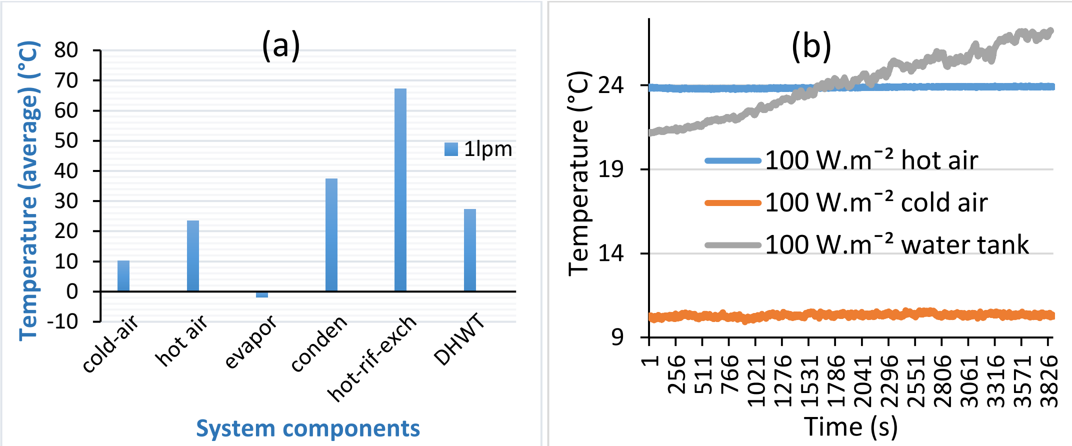

radiation	Water-rate	Indoor Temp	outdoor Temp	compressor frequency	R/H	Comp pressure	Evapo pressure	Rate.of energy consump
$W{\cdot}m^{-2}$	(l/min)	(°C)	(°C)	(Hz)	(%)	(bar)	(bar)	(W)
100	1	16.9	5	35	38.5	18-19	3.3	972

Figure 7.16. System thermal performance under 100 $W{\cdot}m^{-2}$ irradiation and 1 l/min waterflow rate

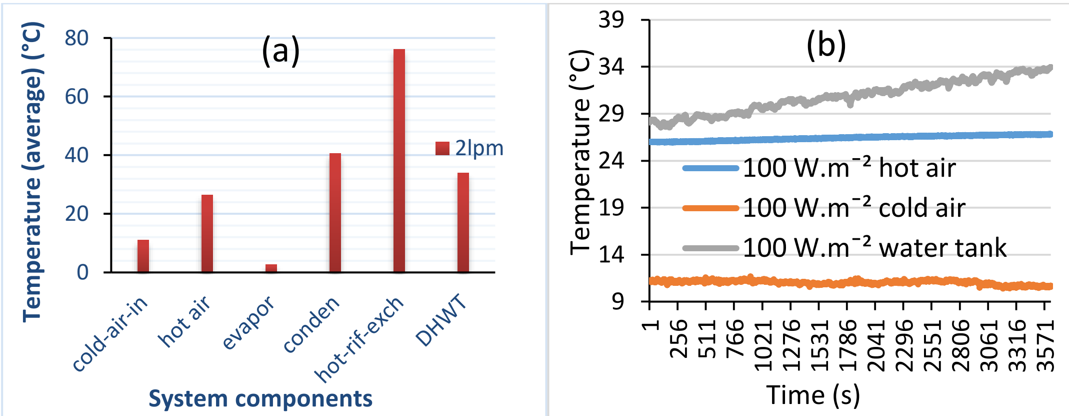

radiation	Water-rate	Indoor Temp	outdoor Temp	compressor frequency	R/H	Comp pressure	Evapo pressure	Rate.of energy consump
($W{\cdot}m^{-2}$)	(l/min)	(°C)	(°C)	(Hz)	(%)	(bar)	(bar)	(W)
100	2	18.2	5	35	28	20. 8	3.8	1015

Figure 7.17. System thermal performance under 100 $W{\cdot}m^{-2}$ irradiation and 2 l/min waterflow rate

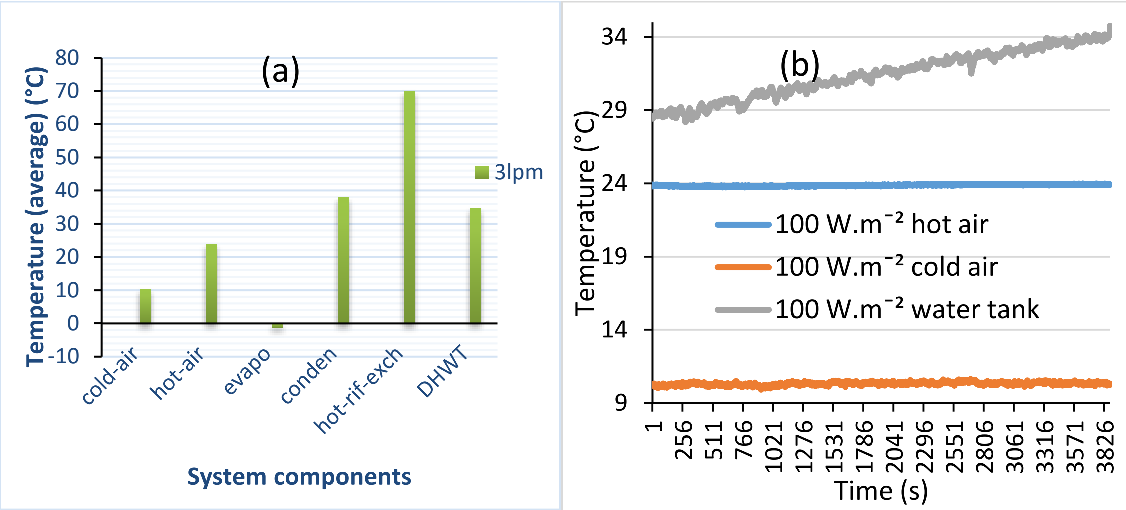

radiation W·m^{-2}	Water-Rate (l/min)	Indoor Temp (°C)	outdoor Temp (°C)	Compressor frequency (Hz)	R/H (%)	Comp pressure (bar)	Evapo pressure (bar)	Rate.of energy consump (W)
100	3lpm	16.6	6	30	38	18	3.5	1030

Figure 7.18. System thermal performance under 100 W·m^{-2} solar irradiation and 3 l/min flow rate

Figure 7.19 reflects that a significant enhancement in the system thermal performance achieved under 200 W·m^{-2} solar irradiation. The heat exchange rate at both condensers increased steeply, although the initial temperature was relatively high (23°C for hot air, and 30.8°C for water heating), while the waterflow rate was at the lowest level of 1 l/min. The results revealed that the temperature difference across the condenser water side reached up to 8°C during the specified operating period as shown in Figure 7.19 (a). Meanwhile, the outlet air temperature reached its peak of 26.6°C as shown in Figure 7.19 (b). This is attributed to the operating performance of a heat pump which is related to the temperature difference between the heat source temperature and the output temperature of the heat pump. Figure 7.20 illustrates the influence of the 3 l/min waterflow rate on the performance of *DX-SAMHP* system under 200 W·m^{-2} solar irradiation. It is detected that, compressor work rises slightly with the increment of relative humidity. The reason is that, when relative humidity raise, the condensing latent heat increases the evaporating pressure, resulting in rise of energy consumption.The average evaporating and condensing temperature was about 2°C and 46°C respectively as shown in Figure 7.20 (a).

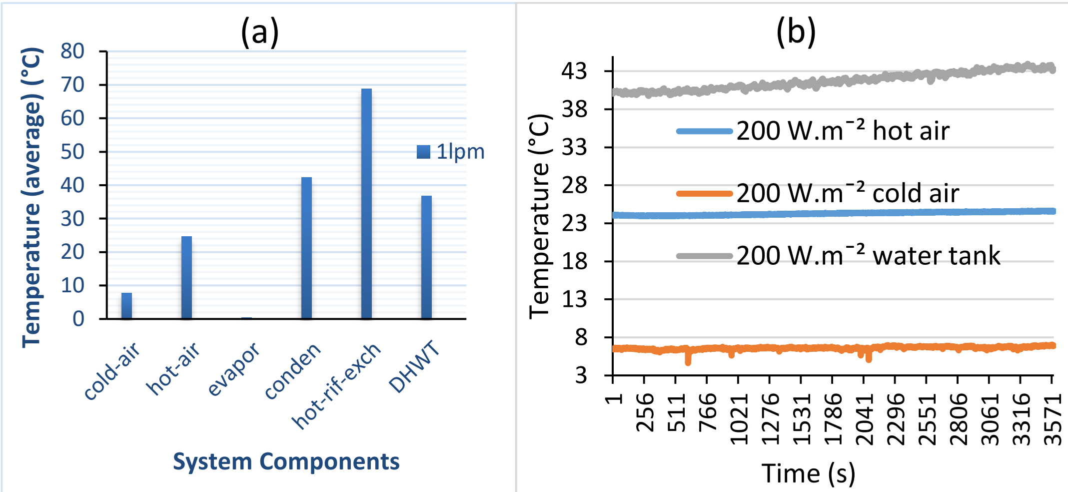

radiation W·m^{-2}	Water-rate (l/min)	Duration (hour)	Indoor Temp (°C)	outdoor Temp (°C)	compressor frequency (Hz)	R/H (%)	Comp pressure (bar)	Evapo pressure (bar)	Rate.of Energy consumption (W)
200	1lpm	1	22	0	30	31.8	23	3.89	1050

Figure 7.19. System performance under 200 W·m^{-2} solar irradiation and 1 l/min water flow rate

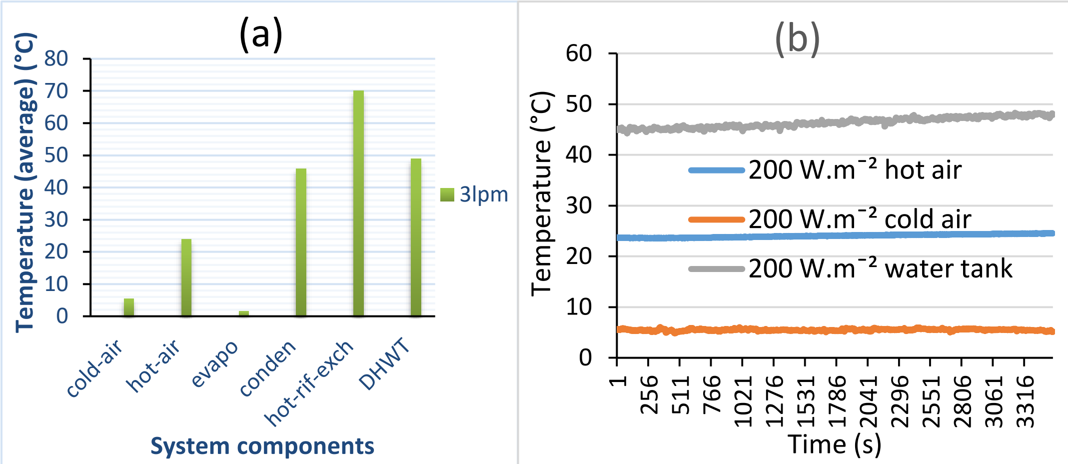

Radiation W·m^{-2}	Water-rate (l/min)	Indoor Temp (°C)	Outdoor Temp (°C)	Comp frequency (Hz)	R/H (%)	Comp pressure (bar)	Evapo pressure (bar)	Rate. of Energy consumption (W)
200	3lpm	21	1	35	26	23.5	4	1086

Figure 7.20. System performance under 200 W·m^{-2} solar irradiation and 3 l/min water flow rate

7.6.2.1 The effect of frost formation on *DX-SAMHP* system under space-and-water mode

In order to provide a comprehensive understanding of the operating conditions of the system, the thermal data are gathered and analysed to show the performance trend and component's characteristics during frost formation. It is important to note that frosting may bring problems such as interruption of space heating, and compressor's refrigerant flood back. The system compressor, air ducts, condenser and expansion vessel were monitored to evaluate the frost formation. The captured images using the heat camera were also used to detect the system expected heat loss areas, to determine the spots on which more insulation is needed throughout the system.

Figure 7.21, shows the refractory performance of the systemcomponents during the operational period. Atter monitoring refractory performance over time, the compressor was observed to be hotter than the other components as shown in Figure 7.21, B-2. Alternatively, the water-to-refrigerant heat exchanger (B-1), water pump (B-3), and the expansion vessel (B-6) were respectively warmer than the rest of other system components such as the water tank valve B-5. Figure 7.21, B-4 indicates the images of the hot and return water line in the water loop.

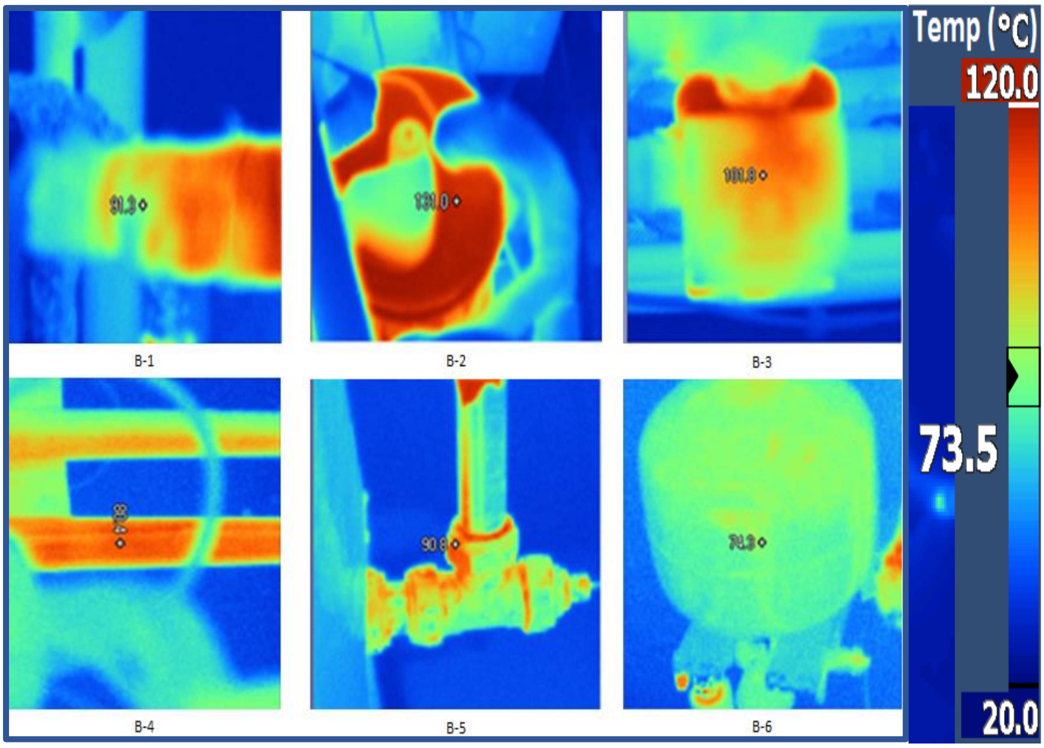

Figure 7.21. Refractory performance of the space-and-water heating mode components

It has been noted that solar irradiance of 100 $W{\cdot}m^{-2}$ can effectively prevent frosting with an ambient temperature of at least -2°C and relative humidity of about 85%. However, at solar irradiances of 200 $W{\cdot}m^{-2}$, the frost is totally overcome although the evaporator works at a temperature lower than the ambient temperature, with values of 0 to 1°C. Therefore, appropriate solar irradiation can solve the problem of frosting in the system. On the other hand, at the relative humidity of 50 %, no frost formation is detected whereas at 60%

frost is very thin. Nevertheless, it is observed that the system energy consumption rises slightly with the increase of the relative humidity. This is because when the relative humidity rises, the latent heat from condensing rises the evaporating pressure, resulting in the increase of the energy consumption of the system. Natural convection is forced within the pump and the fan when warm refrigerant rises and the cool refrigerant drops. Figure 7.22 reveals energy loss spots of different system components such as the mass flow meter(a) duct carriers (b), and heat pump's outlet air (c), which are responsible for the most of the heat losses. Besides, the outlet of the evaporator/collector (f), a solenoid valve (g), and water-to-refrigerant heat exchanger (k) should be considered for proper thermal protection.

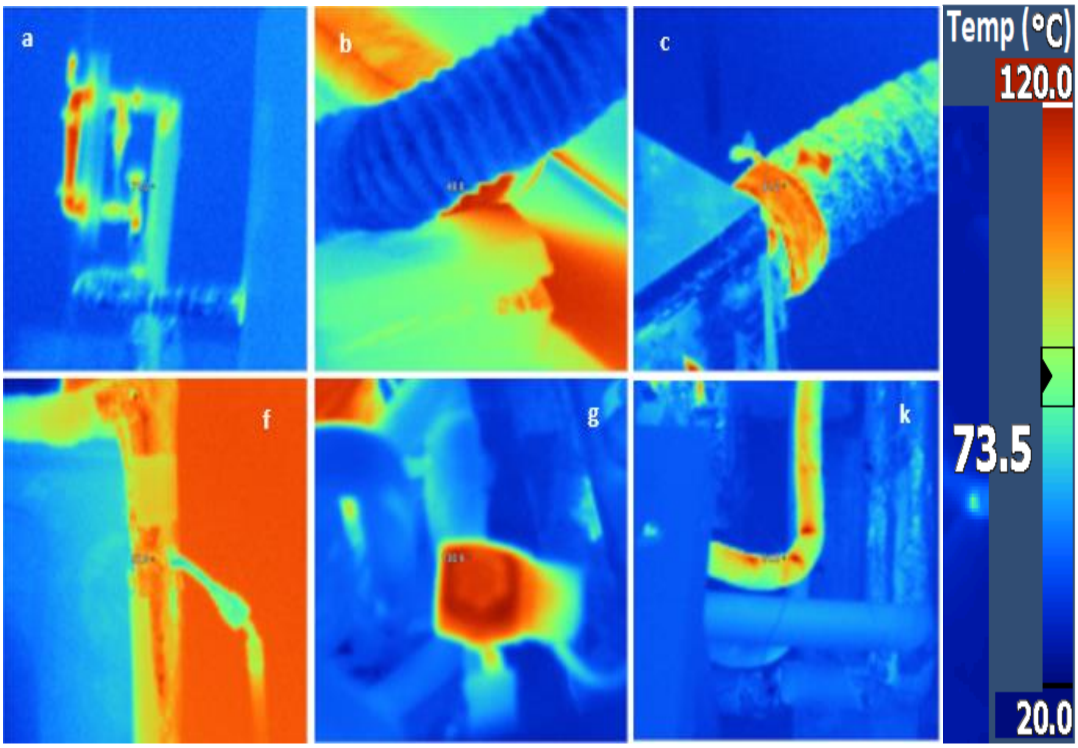

Figure 7.22. Refractory performance of the space-and-water heating mode components

7.6.2.2 Calculated parameters

The heat gain at the submerged condenser (water) of the *DX-SAMHP* system for space-and-water heating mode was also evaluated using:

$$Q_{water} = M_w * C_{pw} * (T_{w,out} - T_{w,in}) \tag{7.1}$$

Where Q_{water} is the heat gain of the condenser, which is released and transferred to the DHWT; M_w is the mass of water in the water tank, C_{pw} is defined as the specific heat of water; $T_{w,out}$ and $T_{w,in}$ are the outlet and inlet temperature of water respectively.

The COP for space and water-heating mode ($COP_{a,w-mode}$) is defined as follows (Kuang and Wang, 2006):

$$COP_{a,w-mode}(t) = \frac{Q_{cond_{air}}(t) + Q_{cond_{water}}(t)}{W\,(t)} \tag{7.2}$$

$$COP_{a,w-mode} = \frac{\int_0^\tau Q_{cond_{air}}(t)\,dt + \int_0^\tau Q_{cond_{water}}\,(t)dt}{\int_0^\tau W\,(t)dt} \tag{7.3}$$

$$COP_a = \frac{\int_0^\tau Q_{cond_{air}}(t)\,dt}{\int_0^\tau W_{comp,fan}\,(t)dt} \tag{7.4}$$

$$COP_w = \frac{\int_0^\tau Q_{water}(t)\,dt}{\int_0^\tau W_{comp,pump}\,(t)dt} \tag{7.5}$$

Where; $Q_{cond_{air}}(t)$ is the heat exchange rate at the air heat exchanger; $Q_{cond_{water}}(t)$ is the heat exchange rate at the water storage tank; $W\,(t)$ is the system power input; and (t) is the operating time of the system. The compressor work divided according to the percentage of useful energy gained by the both condensers. Figure 7.23 reveals that the system heat capacities $Q_{cond_{air}}$ and $Q_{cond_{water}}$increase when evaporation rises its capacity Q_{evap} , due to increase in solar irradiation. The minimum and maximum thermal energy obtained at the condenser($Q_{cond_{air}}$ and $Q_{cond_{water}}$) are 1474 *W* and 2255 *W*, corresponding to Q_{evap} of 932 *W* and 1622 *W* respectively. This implies that the increase in solar irradiation and water flow rate result in a higher condensation capacity. When the solar irradiance is increased from 0 W·m^{-2} to 200 W·m^{-2}, the heat capacity of the *DX-SAMHP* system is enhanced by 52.94 %. In contrast, when the water flow rate is varied from 1 l/min to 3 l/mn, the heat capacity also increases by 29.9 %.

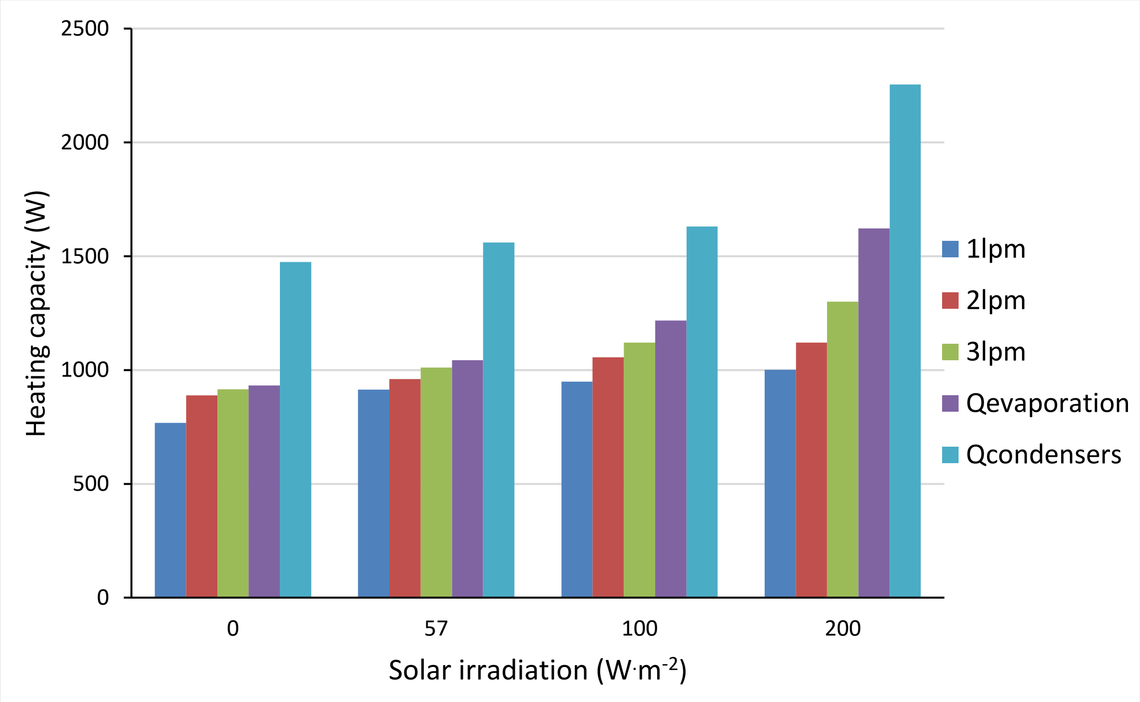

Figure 7.23. The DX-SAMHP performance under space-and-water heating mode test conditions

Figure 7.24 shows the percentages of heat energy delivered to the two condensers via a compressor under specific conditions. As mentioned earlier, since the priority of *DX-SAMHP* design was given to space heating, the air heating capacity is higher than the water heating capacity throughout the experiments.

It is also noted that, when the air heating capacity is increased with solar irradiance, the water heating capacity decreases. However, it is also observed that, with the increase of water flow rate, the air heating capacity decreases. In return, the water heating capacity rises with the increase of solar intensity and also increases with the rise of water flow rate due to the rate of heat exchange in the water-to-refrigerant heat exchanger. The average percentages of the air heating and water heatings are 70 % and 30 % respectively which are dependent on the solar radiation and water flow rate.

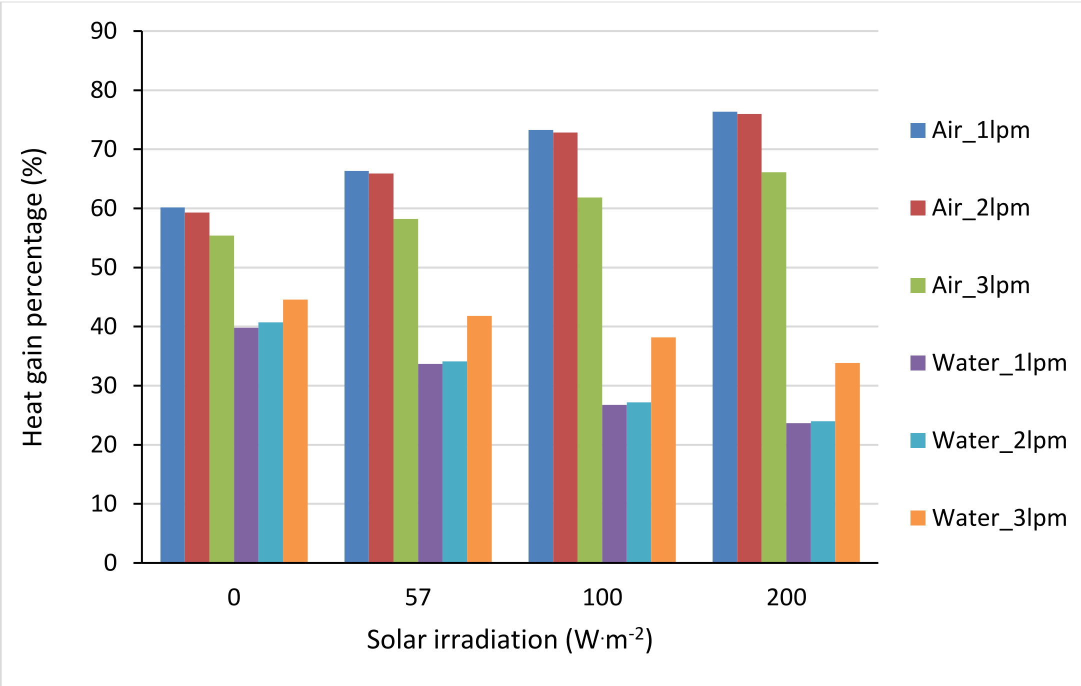

Figure 7.24. The system heating capacity percentages for both air and water condensers

Figure 7.25 shows the system COP for air and water heating mode ($COP_{a,w-mode}$) for each test. It is clear that $COP_{a,w-mode}$ increase with increase in solar an insolation and waterflow rate. As solar irradiance varies from zero to 200 W·m^{-2}, the total $COP_{a,w-mode}$ increases by 41.3 %. In contrast, when the water flow rate is boosted from 1l/min to 3 l/min, the $COP_{a,w-mode}$ increases by 16.65%. The highest value of $COP_{a,w-mode}$ achieved is 3.7 in the coldest days in winter for space-and-water heating mode whereas it is 2.5 with presence of solar radiation. In comparison, (Bi et al., 2004) reported that in cold season, the COP of the heat pump with solar energy as heat source was found to be 2.73. (Yumrutas and Kaska, 2004) demonstrated that for solar source heat pump for space heating system with energy storage tank, the COP value is about 2.5 for a lower source temperature and is up to 3.5 for a higher supply temperature.

Based on the obtained values in the present study, the $COPs$ of the developed *DX-SAMHP* system for both space heating only mode and space-and-water heating mode are higher than those for the conventional heat pump system by 35.5 % and 5.7 % respectively.

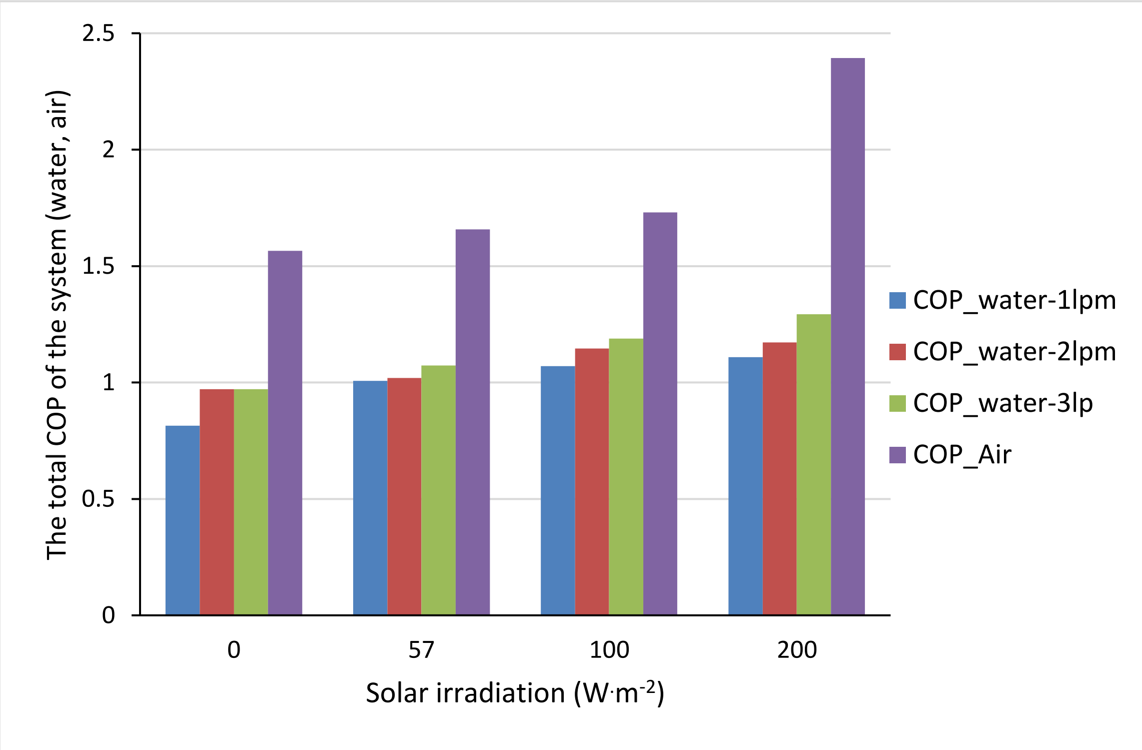

Figure 7.25. The system coefficient of performance under space-and-water heating mode

7.6.3. Uncertainty and experimental errors

Experimental errors and uncertainties can result from components, environmental conditions, calibration of the measuring instruments as well as reading errors. Therefore, error analysis is necessary to determine the accuracy of the experiments (Ozgener and Hepbasli, 2005). Each experimental case was repeated three times throughout the tests in order to obtain results within the appropriate error margins as compared to the values from the working fluid and thermodynamic equations. Arithmetic average values of the recorded data were then taken with an interval of 1 second to improve the accuracy of experimental measurements.

In this study, the uncertainty in the measurement of the mass flow rate of water at the inlet of the hot water tank as well as for the other parameters was measured and calculated in a similar fashion. Therefore, the uncertainty arising in determining the mass flow rate of water $W_{\dot{m}}$ may be found as (Holman and Gajda, 1994):

$$W_R = \left[\left(\frac{\partial R}{\partial x_1} w_1\right)^2 + \left(\frac{\partial R}{\partial x_2} w_2\right)^2 + \cdots + \left(\frac{\partial R}{\partial x_n} w_n\right)^2\right]^{1/2} \tag{7.6}$$

Where R is a given function of the independent variables; $x_1, x_2, \ldots x_n$ and $w_1, w_2 \ldots, w_n$ are the uncertainties of the independent variables.

where

$$\dot{m} = \rho\dot{V} \tag{7.7}$$

$$W_{\dot{m}} = \left[\left(\frac{\partial_{\dot{m}}}{\partial_{\rho}}\right)^2 w_{\rho}^2 + \left(\frac{\partial_{\dot{m}}}{\partial\dot{V}}\right)^2 w_{\dot{V}}^2\right]^{1/2} \tag{7.8}$$

Taking into account the uncertainty value of ±0.2% in the thermophysical properties (Hepbasli and Akdemir, 2004) and inserting the numerical values of uncertainty yields:

$$\frac{W_{\dot{m}}}{\dot{m}} = [(0.2)^2 + (5.208)^2]^{1/2} = 5.2\% \qquad (7.9)$$

The waterside capacity was consistent with the percentages determined for the water-to-refrigerant heat exchanger capacity, thus the present experimental setup was found to be appropriate. The $COPs$ of the *DX-SAMHP* system for water heating was calculated using equation equation (7.5). The relative error (RE) of the evaporating heat exchanger rate, COP and the evaporator temperature can be calculated as follows:

$$RE_{Qevaporator} = \frac{dQevaporator}{Qevaporator} = \frac{dQcondenser_{a,w} + \eta d\mathrm{W}_{\dot{in}}}{condenser_{a,w} - \ \eta d\mathrm{W}_{\dot{in}}} \qquad (7.10)$$

$$RE_{COP} = \frac{dCOP}{COP} = \left|\frac{1}{Qcondenser_{a,w}}\right| dQcondenser_{a,w} + \left|\frac{1}{\mathrm{W}_{\dot{in}}}\right| d\mathrm{W}_{\dot{in}} \qquad (7.11)$$

According to equation (7.10), the experimental RE_{COP}, is about 1.3 %. The maximum uncertainty of the power input and the heat capacity were determined to be 0.2 %, and ±3.7 % respectively, using the method suggested by (Holman and Gajda, 1994, A, 1966, Moffat, 1988b). The maximum uncertainties forpressures, temperatures, solar radiation, air velocity, and the compressor discharge temperature of the system are calculated using equation equation (7.11) and were found to be 5.2, 4.2, 3.9, 6.6, and 7.8 % respectively.

7.7. Comparison of theoretical and experimental results

The comparison between the predicted results through simulation of the proposed system and the experimental results is accomplished to validate the performance of the new system. The experimental values of COPs for the system ($COP_{DX-SAMHP}$) were compared with theoretical results, as exhibited in Figure 7.26.

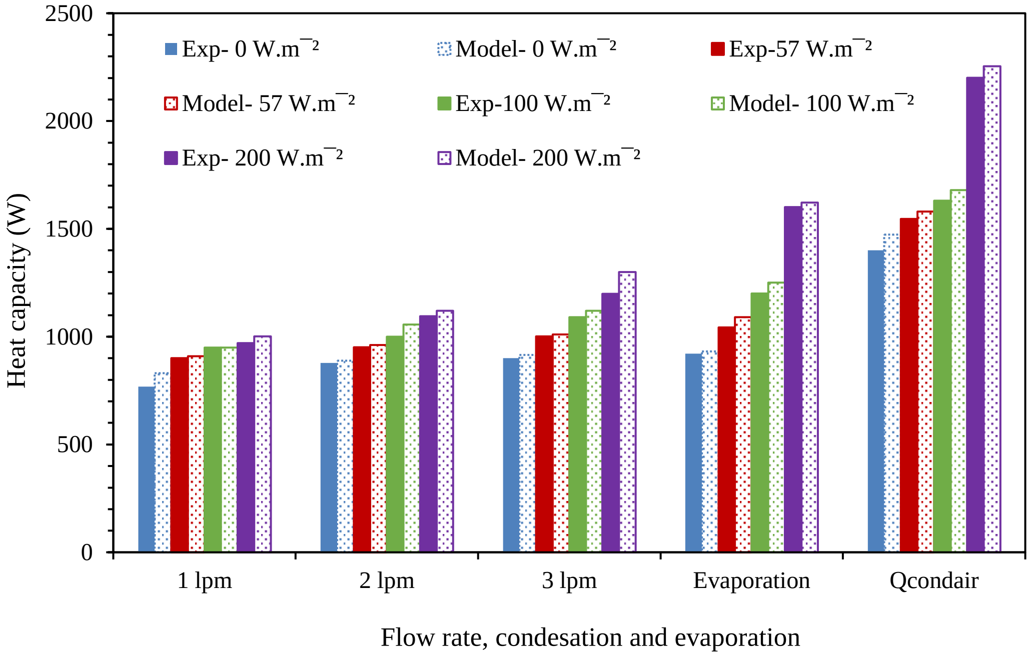

Figure 7.26. Comparison between predicted and experimental results of the DX-SAMHP system

From the graphs, it is obvious that, the experimental $COP_{DX-SAMHP}$ values are in agreement with those from the mathematical modelling of the *DX-SAMHP* system. It is observed that at lower irradiation the system proves satisfactory performance in terms of higher values of COP during cold season, the when indoor and outdoor temperature are lower. This is because the system has the capacity to recover and obtain heat from exhausted and indoor air at low grade heat. The $COP_{DX-SAMHP}$ is responsive to the evaporation temperature as expected. As mentioned before, the $COP_{DX-SAMHP}$ of the system for space heating-only mode was between 3.6 and 3.9 for experimental results whereas the those for space and water heating mode were between 3.7 and 3.8 for both theoretical and experimental findings. Hence, the $COPs$ for both simulation and experiment are in close range.

Figure 7.27 shows the heat capacity at different simulated solar irradiations and water flow rates for each condenser. The heat gain at the two condensers was calculated and plotted against the evaporation heat capacity as illustrated in Figure 7.28.

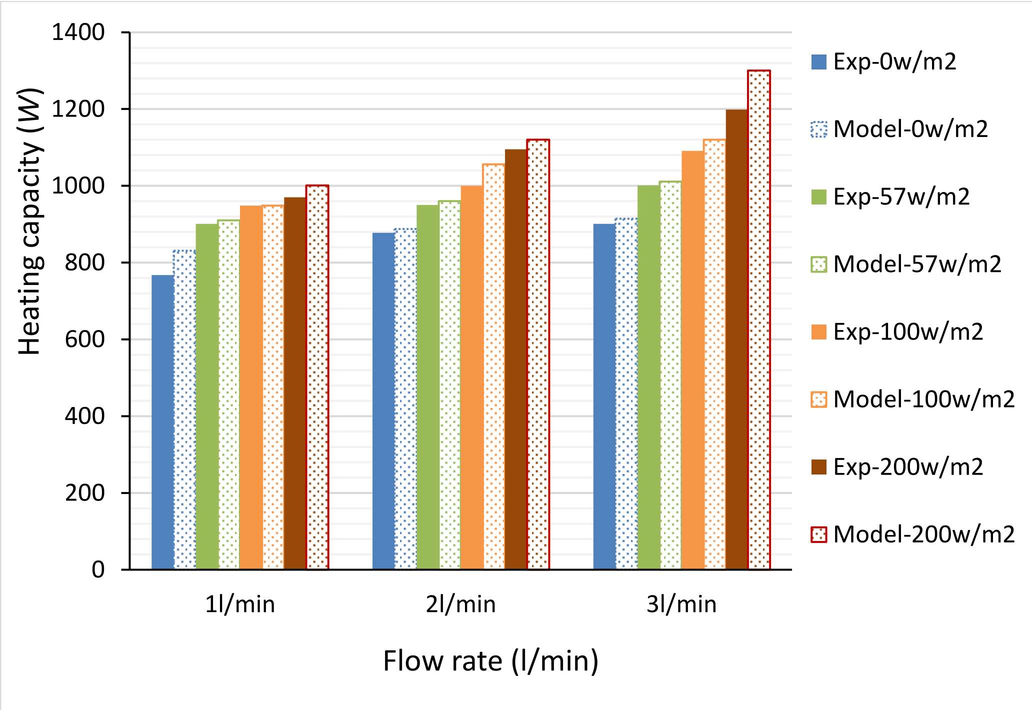

Figure 7.27. Theoretical Vs experimental heat gain of the system under different waterflow rate

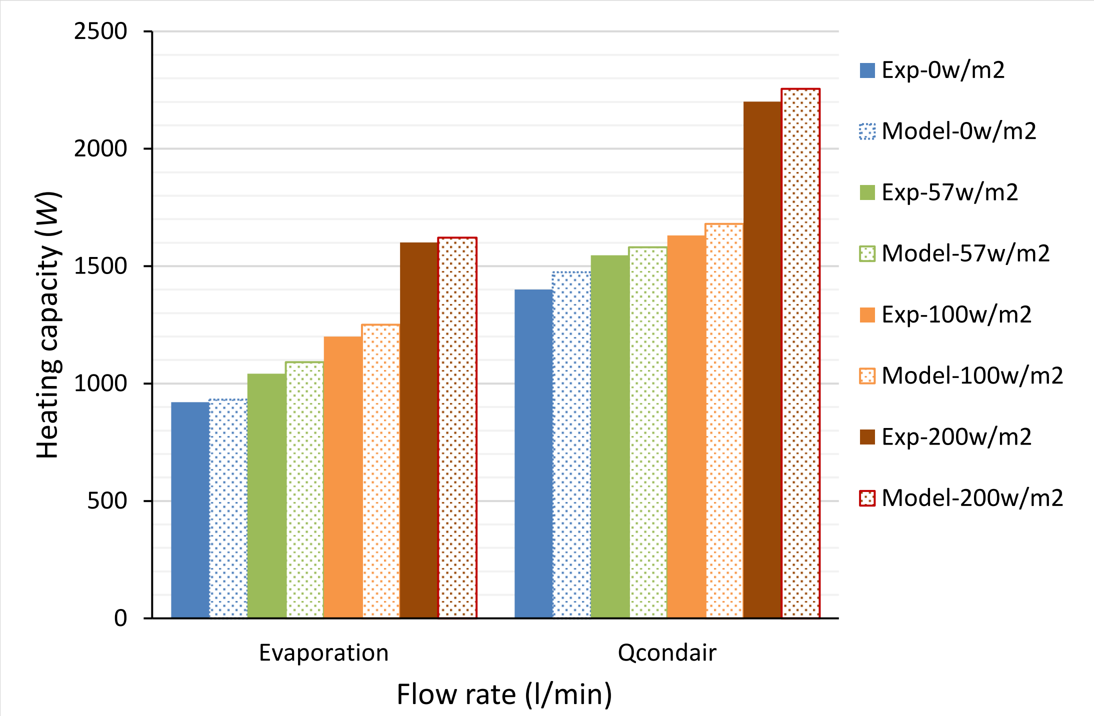

Figure 7.28. Predicted and experimental values of the evaporation and condensation heat capacity

The heat capacity of the system is between 921-1601 *W* and is similarly varying with solar irradiations. This is also attributed to the indoor and evaporation temperature as aforementioned. Figure 7.29 shows that, when solar irradiance is between 0 to 57 $W{\cdot}m^{-2}$, the average experimental water temperatures at the DHWT were lower than the modelled ones by about 2.4°C. But under 100 to 200 $W{\cdot}m^{-2}$, the water temperatures were lower than the modelled results by 2°C (Figure 7.30).

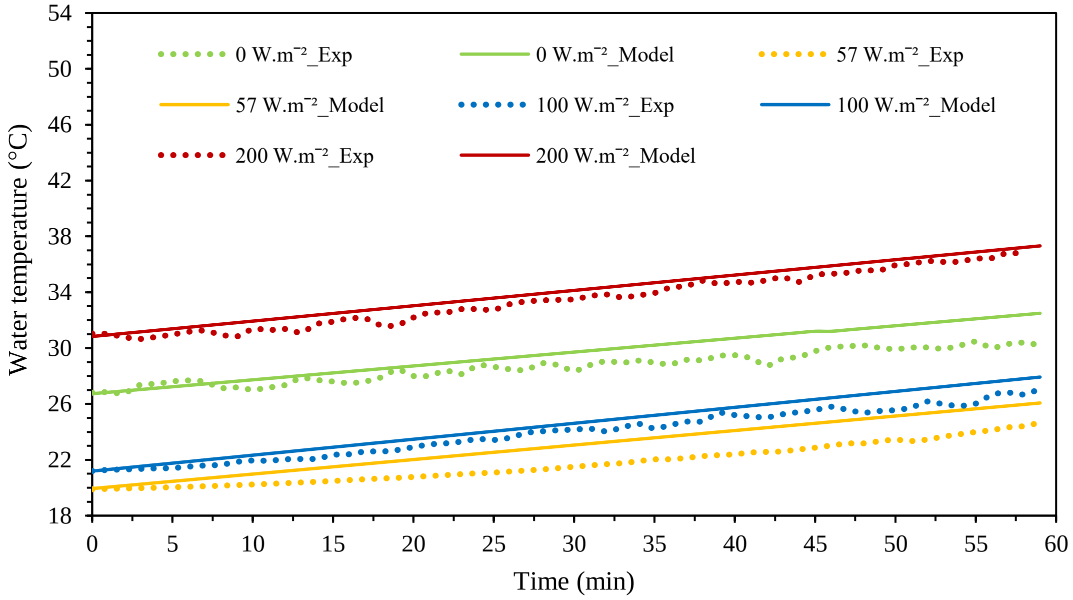

Figure 7.29. Comparison between simulated and experimental water heating values of the system under 1 l/min water flow rate

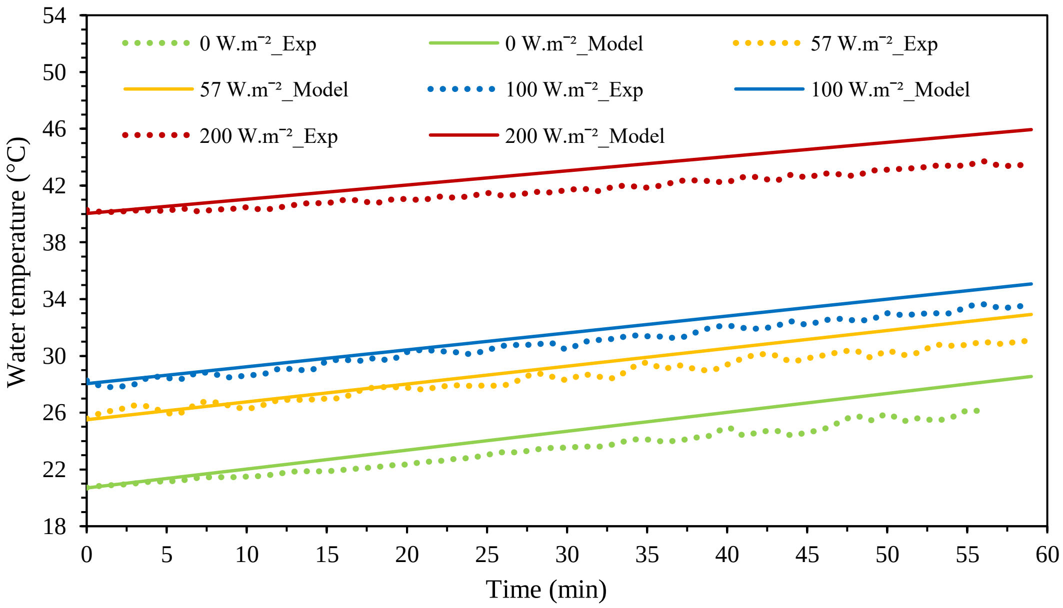

Figure 7.30. Comparison between simulated and experimental water heating values of the system under 2 l/min water flow rate

It is found that the predicted results are slightly higher than the experimental results with average deviations of ±4 % within one hour of operation. The higher the solar intensity and water flow, the higher the system heat losses to surrounding due to a higher possibility of conduction heat transfer. This is also attributed to the instrument uncertainties and the environmental conditons in the laboratory as explained earlier. It is also noticed that at the beginning of the experiment some parameter values are somehow higher than theoretical ones, but they still have the same trend, as indicated in Figure 7.30 and Figure 7.31. This is because of the temperature from the experiment $T_{w,out}$ was measure during transient measured condition.

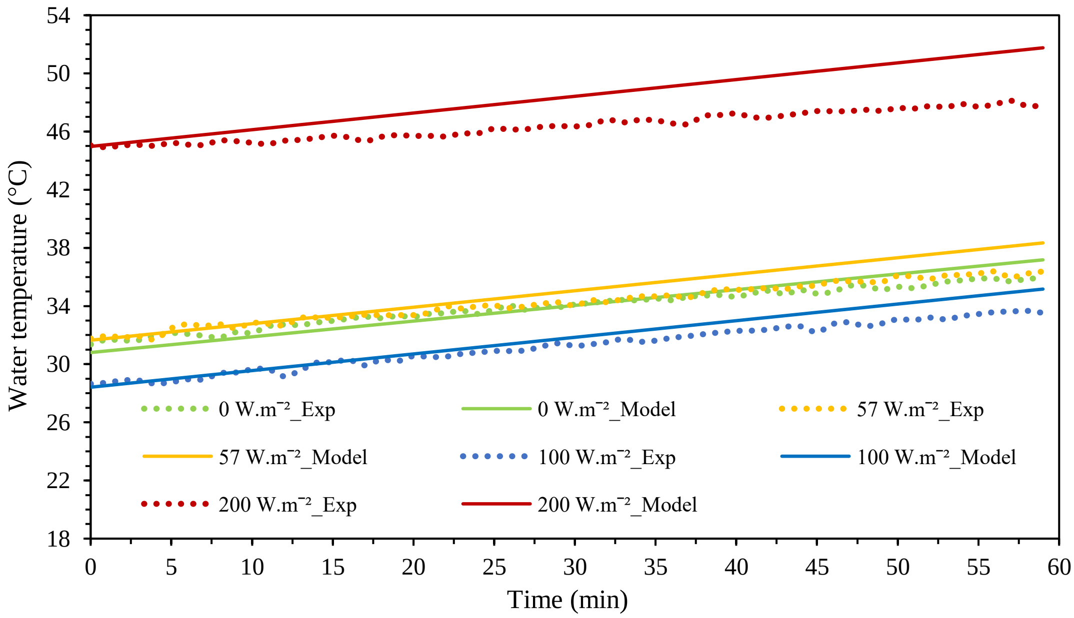

Figure 7.31. Comparison between simulated and experimental water heating parameter values for 3 l/min water flow rate

Figure 7.32 is plotted to show the comparision between the predicted and experimental values for air heating. It is also intended to indicate the time dependence of the performance of the system in both cases.

It should be noted that, due to the limitation of time assigned for each air heating case in the lab, the time frame for the experiment temperature is less than that for the simulation temperature. It was also difficult to predict the cold inlet air temperature since the analysis was based on steady-state modelling of the thermodynamic vapour compression cycle. The comparisons of the air section result reveals that the experimental values are also in agreement with the theoretical values. The experimental hot air temperature deviates no more than 0.6°C from theoretical values after one hour of operation. In conclusion, there is a very good agreement between predicted and experimental results.

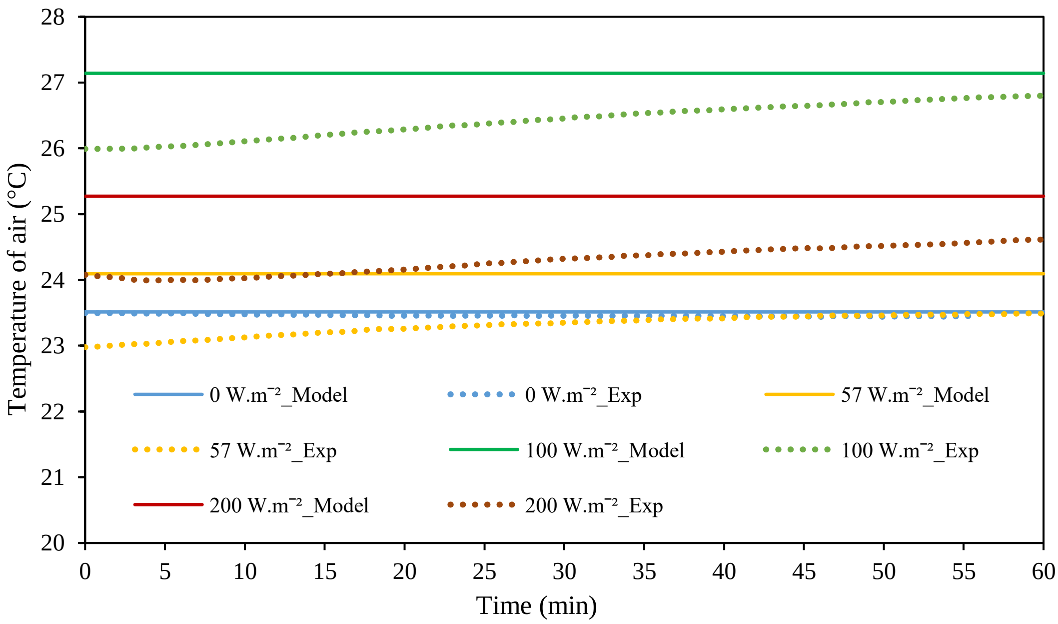

Figure 7.32. Comparison between simulated and experimental results for the system's air heating

7.8. Conclusion of chapter 7

A series of experiments were conducted for two fundamental operating modes under typical Nottingham indoor/outdoor weather conditions for a period of five consecutive months during the cold season. It is important to mention that, due to several experimental tests performed, each test was conducted for one hour to minimize the experimental period and resources. Therefore, the *DX-SAMHP* system was operated between 23:00pm to 06:00am. The experimental parameters were tested for solar irradiations of 0, 57, 100 and 200 $W{\cdot}m^{-2}$ and flow rates of 1, 2 and 3 l/min. The wind speed factor was not considered in this study because it has no significant influence on the system performance. The effect of varying the relative humidity from 26 to 40 % on the *DX-SAMHP* system performance was found to be insignificant since the relative humidity values were reasonably low. Various COP values were obtained for different solar irradiances and water flow rates. The influence of frost formation on the performance of the system was examined. The response of various system parameters such as electrical power consumptions and the heat capacities of the system, on the variation of the water temperature of the heat storage tank, indoor air temperature of the building, were also investigated.

The findings show that the COP of the developed *DX-SAMHP* system is always higher than that of the traditional heat pump systems and the existing multifunctional systems analysed for application in cold region. Finally, the comparision of the simulation and the experimental results shows that there is a very good agreement between predicted and experimental results.

Chapter 8. Design principles, Synthesis and Small Scale Testing of the Selected Thermochemical Storage Materials

8.1. Introduction

There are far-reaching researches concentrating on the exploitation of different energy sources mostly with solar energy for. It is well understood that the combinations of solar and other sources of energy have been applied in various fields of life, For instance, cooling-heating systems, agriculture industries and water treatment. A number of researchers have been assessing and evaluating various thermochemical energy storage materials that can be effectively used in residential homes, based on the open thermochemical heat storage system 'charging and discharging' cycles.

In this chapter, the utilization of thermochemical material jacket has been studied in terms of thermal heat generation, coupled with the operation of *DX-SAMHP* to enhance the household's heating system. In particular, toward improving the thermal energy capacity of the domestic hot water tank so that the heating system operates more efficiently to fulfill the daily heating demands in severe winter period in cold climates.

8.2. Selection of the composite materials for the thermochemical jacket

Material selection is crucial for achieving a high efficiency system. In order to select the appropriate thermochemical materials, three candidate materials capable of producing adequate exothermic thermochemical reactions for 'open' THS were nominated for advance material data analysis (Devrim, 2016). The criterion for selecting the composite material depends mainly on the specific heat capacity of the storage material (energy density), the volume of the materials, porosity, composite discharge, and heat loses. The decomposition of composite adsorbent and water vapour of the materials is also considered. In addition, material synthesis, material testing, and their processes are included. It is also required to examine the porous structure and hygrothermal properties of the materials in order to correlate the material type and behaviour. Therefore, Micrometrics Mercury Auto Pore (MMIP) or Mercury Intrusion Porosimetry (MIP), Micrometrics Helium Pycnometer, and Simultaneous Differential Technique (SDT-Q600 (MIHP)) are used to analyse and determine the composite characteristics. This included differential scanning calorimetry (DSC) for the proposed raw materials and thermogravimetric analysis (TGA) for regeneration temperature, modified transient plane source (MTPS) for thermal conductivity, N_2 and moisture vapour physisorption for meso-pore analysis and moisture uptake. These tests must take place before the decision is taken to select the most effective jacket composite materials. Generally, a robust working pair of materials would have certain applicable properties:

- High attraction of the pair to each other
- High availability and low raw material costs
- Ecologically stable
- High ΔT temperature lift, in exothermic reaction (absorption)
- High storage energy density and thermal conductivity
- High storage volume
- Low regeneration temperature for material charging, in endothermic reaction (desorption) cycle
- Minimal hydrothermal cyclic, or high cyclic efficiency

Therefore, according to the material specifications, the selection processes would consist of three platforms:

- Sample synthesis preparation
- Testing procedure and data recording
- Micrographics data analysis
- Thermodynamic results and analysis of small scale experimental test

8.2.1. Samples synthesis preparation

According to the previous studies about thermochemical heat materials (Devrim, 2016), the most promising composite materials include; V-$CaCl_2$, V-$MgSO_4$, and V-$LiNO_3$. These composites have demonstrated the highest storage density, appropriate water uptake, and the lowest regeneration temperature. However, in such applications where these materials are applied, the (sorbate/sorbent) working pair must be restricted to that the composites are safe for human contact. In this study, water moisture is used as a sorbent in the form of vapour. Generally, the salt and matrix combinations (SIM) have met the requirements for THS listed above. For SIM synthesis, the matrix and solution (salt) were used as supplied. The vermiculite (Micafil) used was obtained from Dupre Minerals UK with a particle size of 2-8 mm. The composite formula of the vermiculite is:

$(Na_{0.21}, K_{0.39}, Mg_{0.19}, Ca_{0.13}, 6H_2O)\ (Mg_5, Fe^{+2}_{0.2}, Fe^{+3}_{0.8})\ (Si_{5.5}, Al_{2.5}, O_{20})\ (OH)_{4}.$

The salts used in this study were obtained from Sigma Aldritch UK. The method used to synthesise the composites was pioneered by Aristov at the institute of Catalysis, Russia(Aristove, 2000). The Insipient Witness Technique (IWT) uses natural wet matrix pore structure to be filled with the selected salt solution. The composite samples of saturated salts solution are added into the matrix with pore volume until the fully wetted visual confirmation occurs The samples are then dried for up to a temperature of 150°C before they are taken for testing as shown Figure 8.1. The saturated salt solution of the matrix pore volume is 100% reliant on the total sample (m_m) and the matrix specific pore volume (V_p). Hence it is prepared as given by $m_m \times V_p$.

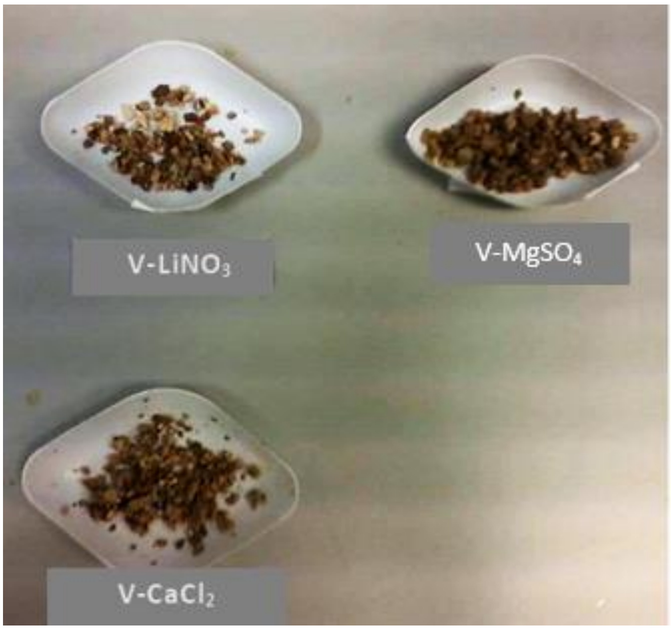

Figure 8.1. Vermiculite-CaCl2 composite sample

A large variant vermiculite matrix sample should be wetted two hours prior to testing so that the sample's relative humidity can reach up to 95 %, and the storage material is holding the maximum amount of water. The first necessary part is the determination of specific pore volume V_p (cm^3/g) of the matrix material for each composite. This can be achieved by using a Mercury Intrusion Porosimetry (MIP) device. In this investigation, the V_p value of the Vermiculite matrix only was found to be about 2.84 ml/g. MIP analysis was performed for samples with m = 0.5g, prepared by furnace heating at T =100°C for a time t =24 hours and hence cooled down to room temperature for T = 20°C before testing. Table 8.1 presents comparision of the results for the three vermiculite base samples.

8.2.2. Testing procedure and data recording

As impregnated salt is a fraction of the pore space V_p, there was a general reduction in the adsorbed volume for the three composites as expected, when matched to the original matrix raw material. V-$MgSO_4$ and V-$LiNO_3$ samples experienced reductions of only 34.2% and 36.6% respectively, but in the V-

$CaCl_2$ sample, the V_p value was reduced by 49.6%. In this range, V-$CaCl_2$ can capture more salt solution within its pores.

Table 8.1. MIP report and data analysis

Porosity factors	**V-$CaCl_2$**	**V-$MgSO_4$**	**V-$LiNO_3$**
Specific pore volume, V_p, (mL/g)	1.4315	1.8687	1.8003
Median Pore diameter (volume), (µm)	1.3737	1.2789	0.0036
Average pore diameter, (µm)	0.6350	0.2789	0.0063
Median pore diameter (area), (µm)	0.2547	0.0487	0.0033
Stem volume used, (%)	58	69	74
Bulk density $\boldsymbol{\rho_{bulk}}$, (g/mL)	0.492	0.340	0.625
Mass uptake 33→ 55 % RH, (kg/kg)	0.146	0.06	0.79
Specific surface area SSA, (m^2/g)	10.9	3.6	2.4

In order to determine the porosity of the materials, it was essential to initially determine the solid density ρ_{solid}, and the bulk density ρ_{bulk}. The ρ_{bulk} value was obtained from MIP testing for the vermiculite based materials whereas theρ_{solid} value was obtained for all samples using MIHP, in accordance with BS ISO 21687 standard while using helium as an inert gas(BSi, 2007). The samples were identically prepared for V_P test. The analysis shows that there was no evidennce of increase in density as it would be expected. The solid densities of the raw matrices and the salts are very close, i.e. the solid density is about 1.88 g/cm^3 and raw matrices density is1.4 g/cm^3. Figure 8.2 shows the range of ρ_{solid} values for all the impregnated vermiculite samples tested.

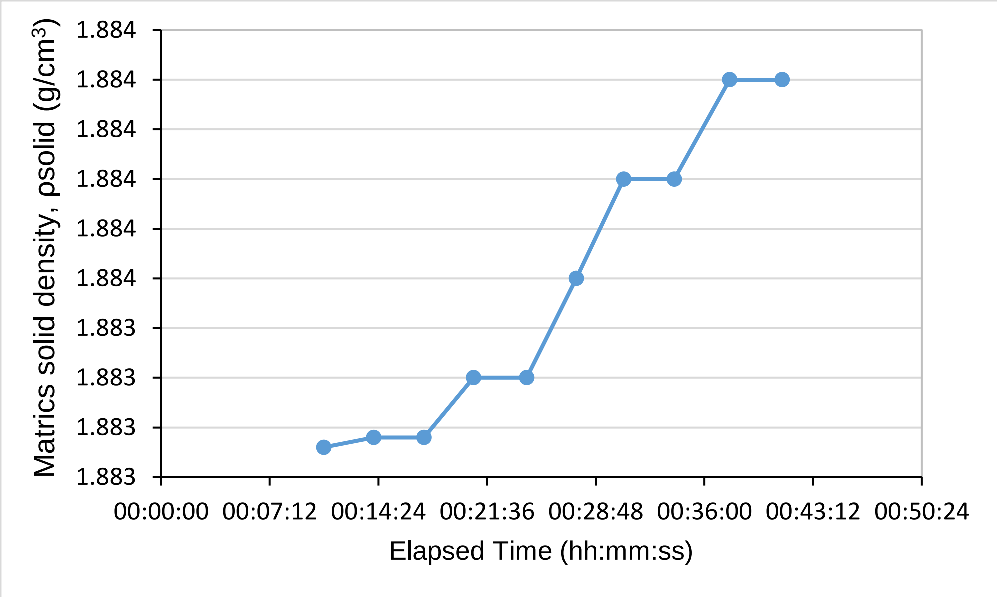

Figure 8.2. MIHP solid density (ρ_{solid}) test for matrices with impregnated salts

To define the composite energy storage and the decomposition of the materials (adsorbent and water vapour), tests were performed on the SIM samples using an SDT Q600 analyser. The analyser was also used to evaluate the specific energy density of the material E_d, and to perform the composite hydration rate through thermo-gravimetric analysis (TGA) in accordance with BS EN ISO 11358 standard. The results obtained from TGA analysis was found consistent with those from the sorption isotherm analysis. A greater rate of water vapour implies grater rate of water loss for a given range of temperature. Before the test is performed, two empty alumina cups are placed onto the balanc, where one is used to hold the sample during the test and the other is a reference cup. The furnace is sealed and the 'tare' function is used repeatedly until the difference in the weight reading of the sample and reference cups are within 0. This process was repeated for every tested sample. The two cups are then heated from ambient temperature up to a range of 30 < T < 140°C at a constant rate of 10°C/minute in an inert argon atmosphere and later cooled by using ambient air. The weight of the cups is continuously measured along with heat flow to obtain a baseline measurement.

One cup is now filled with a sample to approximately halfway, which is then placed onto the balance next to the empty reference cup. Once the balance settles slightly, the furnace is sealed, and the balance is allowed to fully settle inside the closed furnace. The test started while the results are recorded until the tested are completed to plot the required graph. Since the aim of the tests is to get the information about the sample but not the cup, the baseline measurement was subtracted from the total measurement to get the actual weight of the samples. To find the energy density of the sample, the average readings were recorded in (J/g) (Appendix 1,2 and 3). The procedure was repeated three times and the averages computed through the same process as shown in Figure 8.3.

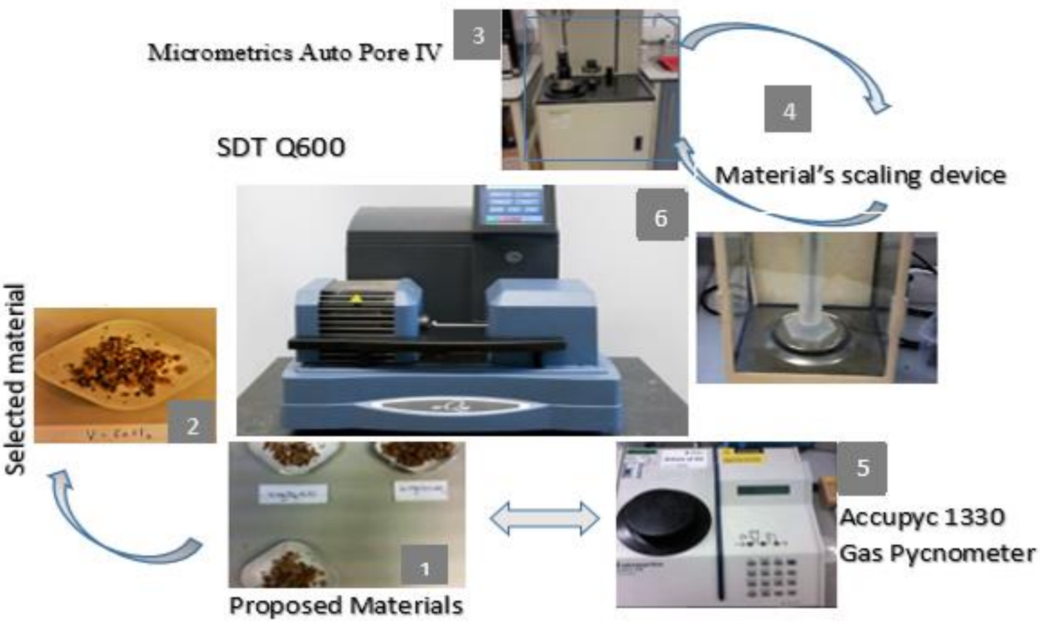

Figure 8.3. THS materials test procedure

The isotherm sorption test for the nominated vermiculite $MgSO_4$, $LiNO_3$, and $CaCl_2$ samples reveals that $LiNO_3$ and $CaCl_2$ are performing better than the others. $CaCl_2$ has a slightly higher advantage than other samples when the V_P, water uptake and the charging temperature are taken into consideration. Conversely, $LiNO_3$ is too expensive compared to V-$CaCl_2$, which has a very limited adsorption potential, hence it is not considered as a prime candidate for use (Table 8.2) (Appendix-C). However, V-$CaCl_2$ generally has a superior performance over the other samples, suggesting that it may be suitable for open THS, due to high specific energy density (E_d) of 538 kJ/kg, good accessibility to moisture transfer in low relative humidity, lower regeneration temperature around 83°C, and larger reduction in specific pore volume V_P as indicated in Table 8.1 and Table 8.2.

Table 8.2. SDT Q600 test results

Samples characteristics	**V-$CaCl_2$**	**V-$MgSO_4$**	**V-$LiNO_3$**
Thermal conductivity (λ) W/ (m·K) Dry state	0.0669	0.0607	0.0659
Water/Moisture uptake, g/g	0.61	0.59	0.60
Specific energy density (E_d)kJ/kg	538.2	535.5	552
Regeneration temperature, °C	82.3	<100	95
Salt material cost, $/kg	0.48	2.1	5.3

8.2.3. Micrographics data analysis

As a result of the tests discussed above, a V-$CaCl_2$ composite was chosen for the proposed 'open' thermochemical heat storage (THS) for further evaluation and parametric analysis (Appendix-C). Therefore, it was selected as the sorption material to be experimented. The vermiculite raw material was subsquently scanned using the Philips XL30 electron microscope (SEM) to provide visual confirmation of the salt presence. Micrographs were recorded and presented the sample with and without the salt using a secondary electron detector (Everhart Thornley type) as indicated in Figure 8.4 (a) and (b). The raw vermiculite material revealed lamellar structure with micro-porous channels (nominal Ø pore = 3.68μm) in between the lamellas, allowing a large amount of salt to be impregnated. This is missing from the sample with a salt solution due to the trapped salt as seen in Figure 8.4 (a). Figure 8.4 (b) illustrates the lamella structure of V-$CaCl_2$, where the SIM-3a, image shows the salt crystals loaded inside the horizontal Nano-scale channels between the lamellas.

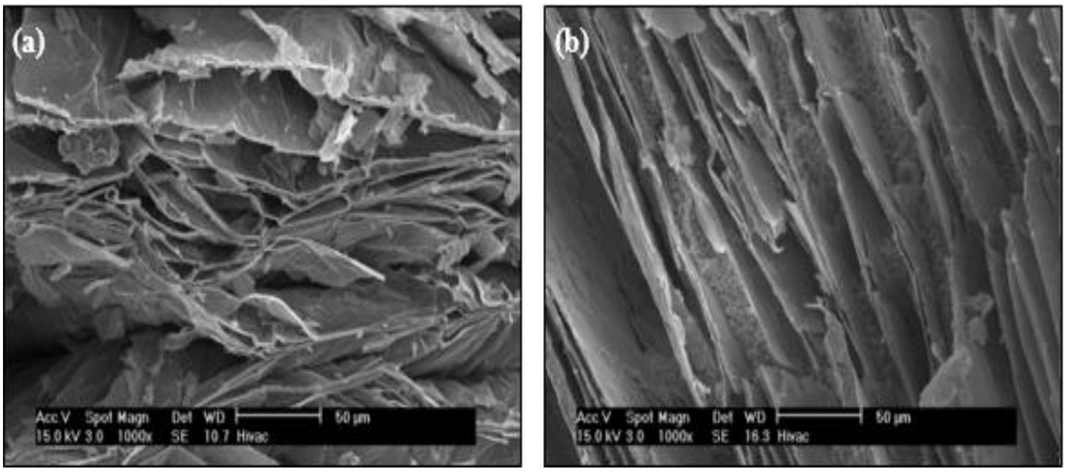

Figure 8.4. (a) SEM micrographs of Vermiculite raw material and (b) SIM-3a: (V-CaCl2) impregnated salt

8.3. Thermodynamic analysis and results of small scale experimental test

To investigate the maximum thermal energy that can be extracted from the Vermiculite$CaCl_2$ as well as providing the insight into the composite hygrothermal behaviour, It is essential to assess the composite performance under controlled experimental conditions. A small testing rig was constructed to study the sorption material comportments to be used in the proposed sorption jacket. This system shown in Figure 8.5 (a) and (b) was mainly designed to examine the hydrodynamic and thermodynamic performance of the sorption materials. A series of experiments under ideal laboratory conditions were undertaken to achieve the set research objectives. Perforated tubes were used to facilitate vapour diffusion to the material so asto reduce the effect of the reaction front and to provide uniform air flow. The reaction chamber

(8) is a rectangular shape of dimensions (500 mm x 250 mm x 200 mm) with a sloping lid to facilitate the post absorbent airflow and is constructed of aluminium sheet with welded seams.

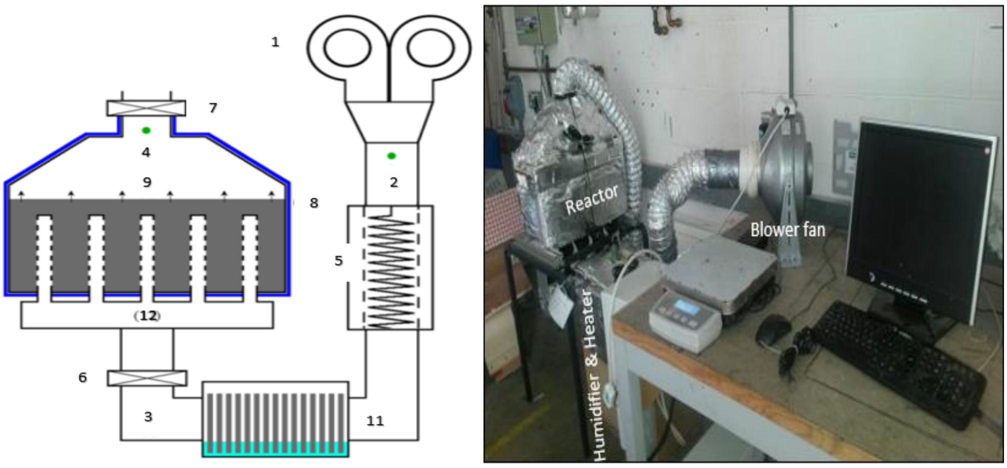

(a) (b)

Figure 8.5. (a) Schematic diagram (b) view of the experimental test rig

Ten perforated tubes, with a diameter of 20 mm and perforated aluminium sheet of 0.55 mm thick were placed vertically inside the reactor in two parallel rows with a horizontal distance of 100 mm between each (x and z direction) (Figure 8.6).

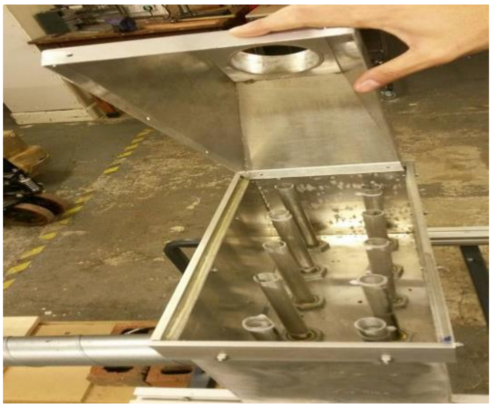

Figure 8.6. Internal view of reactor showing perforated diffuser pipe allocation

The tubes are connected to an external manifold (12) to equalise airflow to each tube, with the top end of the tubes sealed in order to achieve the sufficient internal pressure, providing air flow laterally to the absorbent (9). The humidification of the inlet air is provided using an evaporative pad matrix placed inside a rectangular shaped wick chamber (11). The air flow through the wick chamber is parallel to the evaporative pads, enabling moisture enhancement of the inlet air before entering the reaction chamber. An inline duct fan (1) of type Xpleair (UK) XID series, and d = 150 mm is used to provide air flow and is connected to the ducting (d = 100 mm) via a reducer. To reduce thermal losses to the external environment, the complete system is insulated using a 25 mm thick foil lined with glass wool. The temperature and RH was recorded using thermocouples (K type) and the EK-H4 Eval Kit from Sensiron, AG, Switzerland respectively. The maximum deviation for the quantities measureds were; ±0.3°C for temperature, ± 2 % for RH and ± 2 % for air mass using flow meter. Three sensor locations were used; (2) for ambient temperature, (3) for manifold inlet and (4) for reactor outlet, to measure the required quantities.

The cycle was allowed to run until the condition $T_{out} = T_{in} + 3°C$ was met for about 20 hours for this case. The THS open cycle is based on air temperature lifting due to exothermic thermochemical reaction which causes a steep temperature lifting at the beginning of the reaction. Since the humidifier is connected and the airflow is monitored with the desired humidity level, as the moisture passes inside the THS material, the chamber rises and moisture sorption rate decelerates (i.e. sorption kinetics) which results in temperature drop. Pressure, temperature and humidity are the main factors that govern theTHS performance. As RH_{in} level rises in the reactor, there is instantaneous rise in T_{out} corresponding to the vapour and SIM reaction. This cycle (discharging) is supposed to be completed when $RH_{in} \approx RH_{out}$ or $T_{out} \approx T_{in}$, and in this case, these values were 70 % and 50 °C respectively.

During the test period the total thermal energy output was 2.93 kWh with mass uptake of 1.41 g_{wv}/g_{abs} as shown in Figure 8.7. This suggests that low RH levels

(<50 % RH) are required to fully react with the composite, to rapidly release higher amount of energy (Appendix-D).

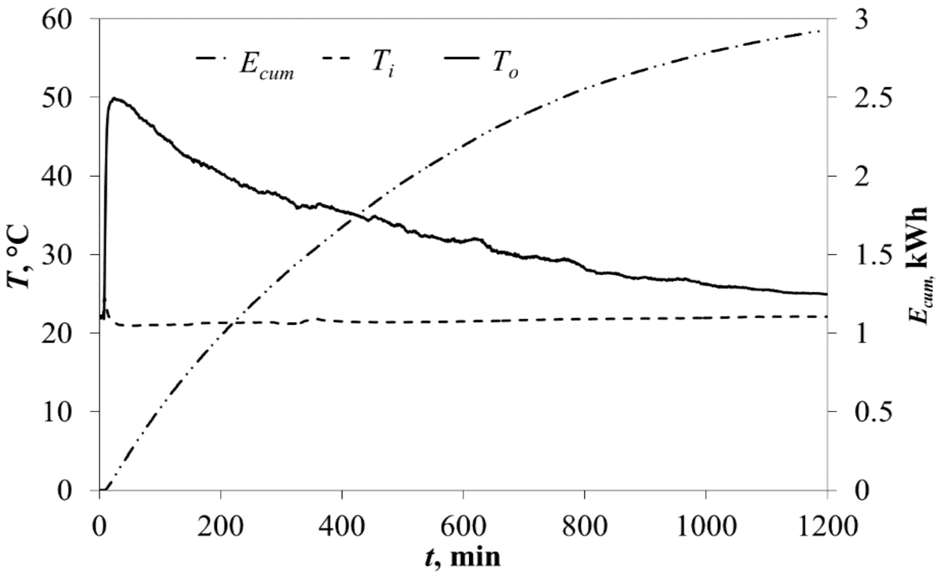

Figure 8.7. The variation of air temperature and heat output

The V-$CaCl_2$ moisture vapour desorption twas measured at 538.2 kJ/kg (based on a bulk, uncompact sample). The moisture vapour adsorption isotherms (at 23ºC) are shown to be Type IV (IUPAC classification). The V-$CaCl_2$ has a highermass uptake in the lower RH bands in the range of 20 to 50 %, when compared to the standard Zeolite 13X material historically used for adsorption storage (Type I) which has minimal initial uptake with no further increase after ≈15 % RH as shown in Figure 8.8. It was also observed that $T_{out,\ max}$ is up to 50°C, and the D_{well} time t_{dwell} (the time from initial temperature increase until $T_{out} \approx T_{ambient}$) is about 20 hours. Interestingly, thermal energy of about 2.93 kWh was achieved from only 0.01 m^3 of storage volume. However, it should be noted that the testing was performed under controlled laboratory climate conditions but during real life operating conditions, it might not be possible to obtain such a high energy storage density due to several reasons. Firstly, as the supply temperature is set to 20°C and RH to 70 % during the testing, moisture supply rate to the sorbent was high (w_{air} equal 10 gr/kg) (Figure 8.9).

In real life operation, low air temperature might limit the water holding capacity of air (i.e. for T = 10°C and RH = 100 %, w_{air} = 7.5 gr/kg) which could lead to lower rate of heat output. Besides, the tested material was initially anhydrous (fully dehydrated); therefore it released high amount of sorption heat. In practical applications, due to the insufficient regeneration, it is highly likely that sorbent remains partially moist (i.e. monohydrate) and it could reduce the heat output. Heat losses would be another important parameter negatively influencing the achievable energy storage density in real applications. In addition, with the increasing heat storage size, heat and mass transfer effectiveness would drop, reducing the heat storage performance. Practically, the energy storage density is expected to be in the range of 150-180 kWh (for average ΔT = 15°C) for a regeneration temperature of 90°C in real life applications. Figure 8.10 illustrates the correlation of Δ*w* and ΔT over 20 hours of testing the V-$CaCl_2$. During the test period (t = 20 hours), it can be observed that the correlation between Δ*w* and ΔT is almost linear and independent of time. Recognizing and using this correlation will enable to design, operate and control the heat storage process with sorption jacket in an effective manner.

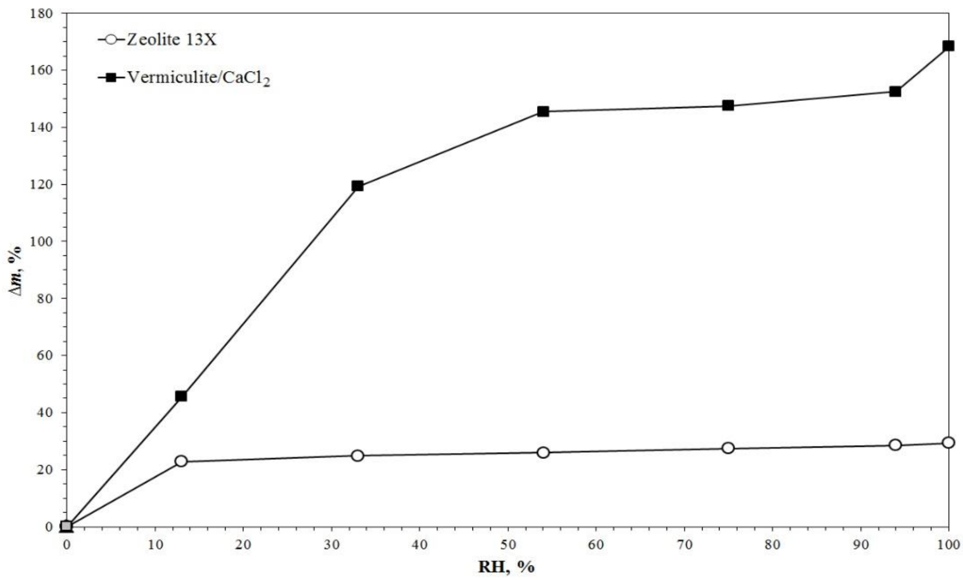

Figure 8.8. Moisture vapour adsorption isotherms at 23 ºC for V-CaCl2 and Zeolite 13X

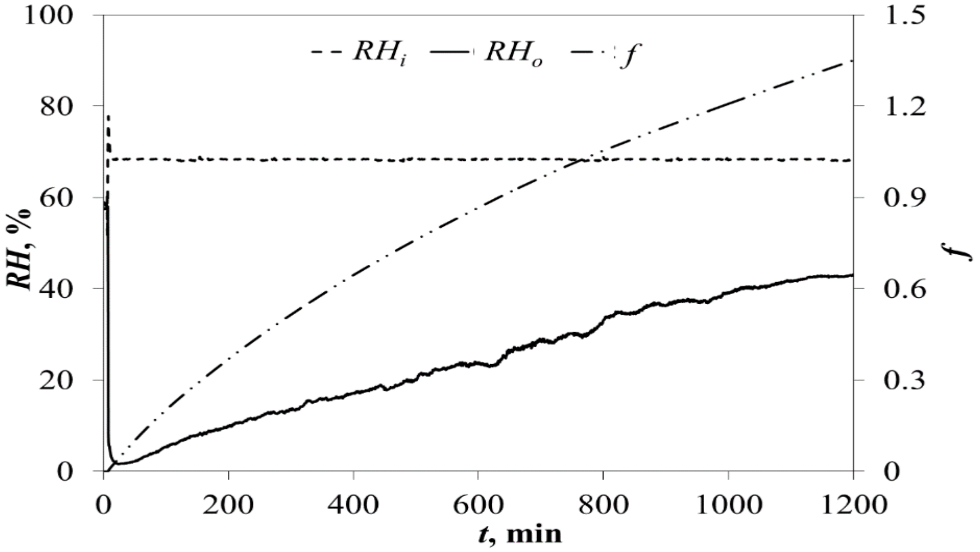

Figure 8.9. The RH variation of air and water/mass uptake of absorbent over the discharging period

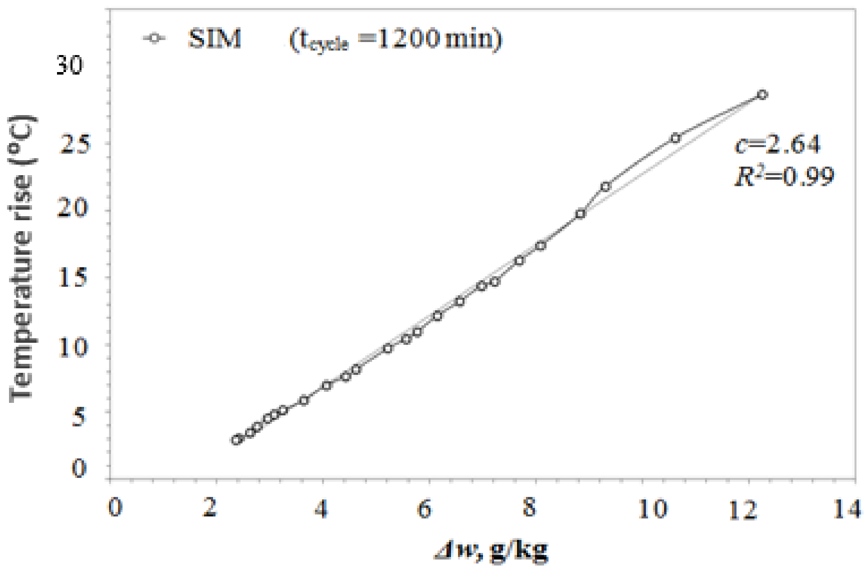

Figure 8.10. Correlation between Δw and ΔT for V-CaCl2 composite

These findings suggests that THS has remarkable potential to be utilized in such applications. It is also indicated that the V-$CaCl_2$ has can potentially be used in sorption jacket to reduce heat losses, increase heat storage duration and reduce the extensive energy consumption in buildings for water heating.

8.4. Conclusion of chapter 8

This chapter has covered the characterization and synthesis of selected matrices and salts for sorption materials. The selection of matrices and salts as prospective candidate materials for thermochemical heat storage systems was based on the literature study on several materials. The comparative properties analysis of all composites in laboratory test devices and determination of the best composites has also been discussed. Design and construction of a small scale sorption reactor as well as the testing of the chosen composite with the purpose of attaining enhanced heat storage performance, have also been elaborated. Scanning Electron Microscopic (SEM) analysis proved the existence of salt in the desiccant matrix after impregnation, which as well confirmed that there was no damage within the Vermiculite pore structure sample due to the increase in Ø pore. Three different absorbents were investigated for thermal performance including the vermiculite (V) $MgSO_4$, $LiNO_3$, and $CaCl_2$ samples. Energy density analysis (E_d) and thermal properties for successful selection of open THS system reveals that V-$LiNO_3$ had the highest E_d of all samples. Nevertheless, as it has a limited adsorption potential and high regeneration temperature, this may not be accessible under UK winter conditions. The V-$CaCl_2$ thermal performance demonstrates the best absorbent performance among the three tested candidates. V-$CaCl_2$ appears to have a very good E_d coupled with excellent equilibrium moisture content (EMC) and relatively low regeneration temperature. According to the experimental results, there is evidence that there is direct and linear correlation between the amount of moisture vapour Δw delivered to the absorbent and the temperature lift ΔT. This is necessary for the proposed open thermochemical heat storage systems control process and design. These findings suggest that V-$CaCl_2$ can potentially be utilised in an open sorption jacket.

Chapter 9. Experimental Study of the Combination between *DX-SAMHP* System and Adsorption Jacket

The purpose of the experiment described in this chapter is to investigate the performance of both solar and thermochemical energy as described in the previous section, in conjunction with the *DX-SAMHP* and novel design of a thermochemical jacket. The objective of the combined system is to enhance the domestic water tank heating capacity in order to deliver mutually air and water heating, and to utilize the stored heat if additional heating is needed.

9.1. Description of the proposed system

The proposed system consists of three main parts; a refrigerant cycle (DX-SAMHP), the water loop, and a DHWT enclosed within a new thermochemical jacket as indicated in Figure 9.1. The system incorporates into a household using the existing DHWT and a central heating pipe system, in addition to the auxiliary components such as a water pump, air heater, blower fan, humidifier, and a radiator.

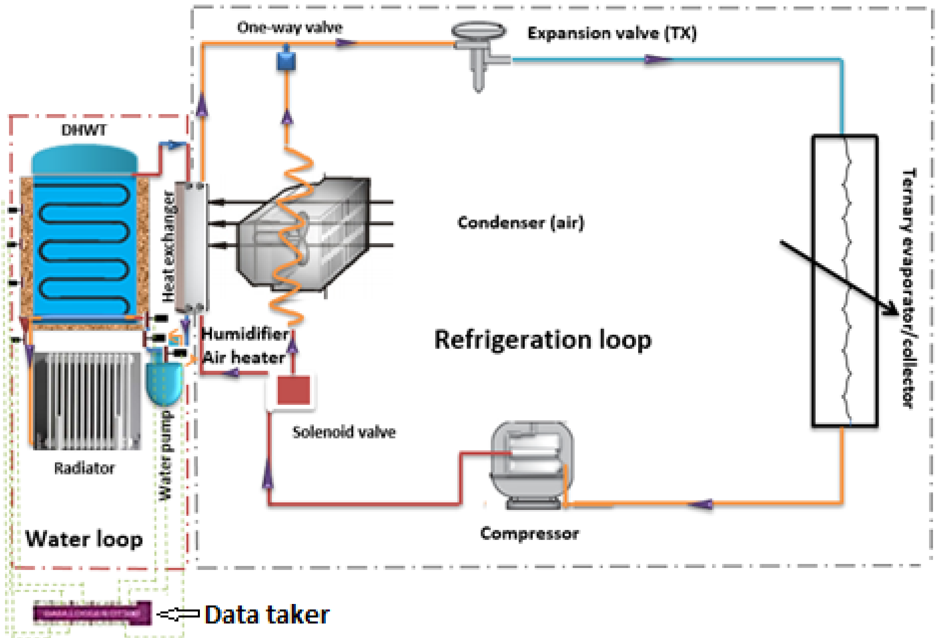

Figure 9.1. Schematic diagram of the experimental set up

9.2. Fabrication and construction of the thermochemical jacket

The jacket unit is made of two metallic vacuity rings with 50 mm depth shielding the bare DHWT. An inlet air entrance is made in the lower ring and an outlet air exit in the upper one as shown in Figure 9.2. The holes of one inch size are also drilled in the upper surface of the lower ring, and the lower surface in the upper one. The function of the holes in the lower ring is to pass the hot-dry or moist-air into the jacket materials while the upper holes are used to extract the moisture from the jacket material when the outlet air is open. Other smaller holes of ½ inch spaced similarly are drilled in the bottom and the top rings to facilitate the airflow.

Fourteen rectangular perforated columns were also fixed on the jacket's rings to enable uniformity of moisture vapour when it is being transmitted to and from the material with minimal pressure drop as indicated in Figure 9.3.

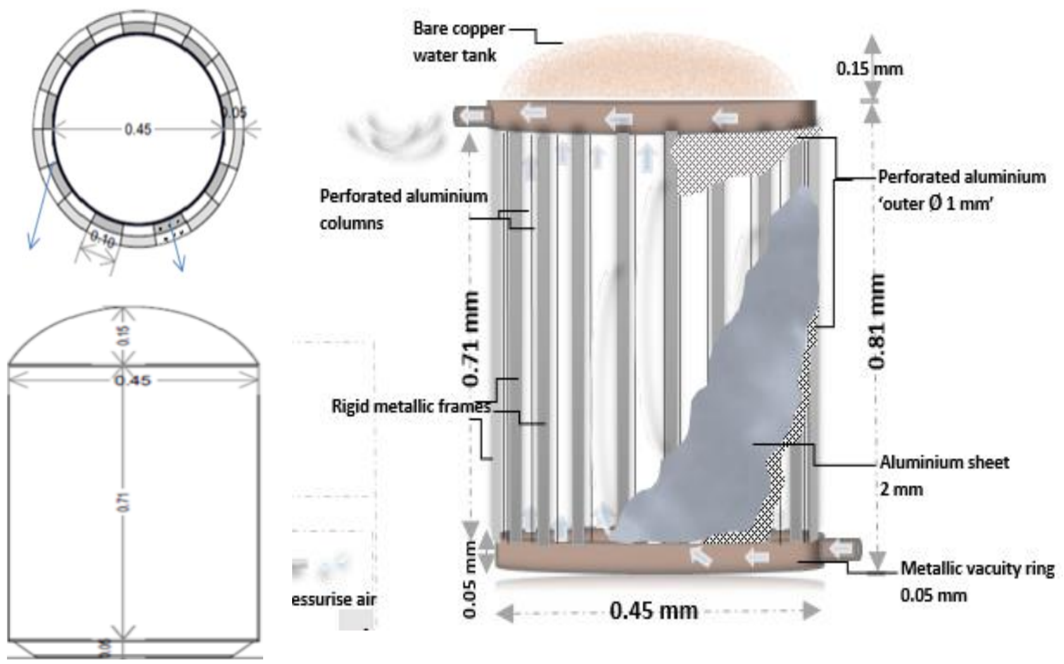

Figure 9.2. The design of a proposed thermal jacket system

Figure 9.3. The fabrication and rigged of proposed thermochemical jacket

A DHWT of 200 litre capacity which is made of Bare copper is used as depicted in Figure 9.2 and Figure 9.3. The outer surface of the bare DHWT and the jacket are twisted by perforated aluminium sheets as shown in Figure 9.3. The reason for using the twisted by perforated aluminium sheets to hold the material firmly together and allow heat transfer between the material and DHWT surface. The frame is also enveloped with an aluminium sheet to secure the material and seize the chemical reaction within the jacket as indicated in Figure 9.4. The jacket is insulated hermally using two layers of thermal protection with rock wool, and is externally covered by cylinder glass fibre filled with insulation (red jacket).

Figure 9.4. The protection of the jacket's outer-skin

The jacket is then connected to an ultrasonic humidifier and the electrical air heater. The heater is a stainless steel air heater with heli-arc welded at the heater outlet, which is used to dry the material in the charging cycle.

9.3. Preparations of the composite materials of the jacket for experimental test

Optimizing the sorption kinetics of $CaCl_2$ is fundamental to enhance the performance of the material. Therefore, the combination of $CaCl_2$ with different salts that have reasonably steadier hygrothermal performance is recommended (Casey, 2014). The mixture of $CaCl_2$ impregnated into the pore structure of a desiccant vermiculite is extensively investigated.

The purpose here is to discuss the preparation of the composite material for field unit testing of a full scale thermochemical heat storage system assisted with a DX-SAMHP system. A moderate quantity of salt ($CaCl_2$) is mixed with vermiculite matrix to enhance the overall energy density of the thermochemical jacket. A simplified sample material synthesis preparation is also carried out, firstly, to characterize the proposed material and secondly to analyze the moisture adsorption capacity of the material.

The composite material is known as salt in matrix (*SIM*). The utilised method to synthesise the *SIM* was based on the procedures initiated by Yuri Aristov as mentioned earlier. However, the prepared composite material for this experiment is described in detail as follow:

1. The refinement and selection of suitable vermiculite particles was done in such a way that the hot matrix was classified according to their grain size. After word, the high-quality properties (i.e. particles sizes, structures, etc.) were specified and analysed by weighing the material particles for the experiment as seen in Figure 9.5.

Figure 9.5. Selection of suitable Vermiculite particles process

2. The hold matrix was dried in the oven at a temperature of 150 °C to remove any absorbed water.
3. The measurements were carried out to determine the mass of the salt samples, by assuming that the matrix pore volume is 100 % filled with the salt.
4. The saturated solution was promptly prepared by mixing two molecules of calcium chloride with one molecule of pure water as a minimum rate, to ensure that water is fully liquidised by $CaCl_2$. The percentage of the

salt within the solution was about 57% by weight. This was executed under 20-30°C room temperature as shown in Figure 9.6 (a) and (b).

5. The Vermiculite was subsequently mixed with the salt solution (CaCl2). Special consideration is given during mixing the dried Vermiculite with the solution. Therefore, the solution was added into Vermiculite in a confined container while being continually stirred, while the solution being sprayed slowly until the matrix was fully soaked (Figure 9.7 (a)). The composite was kept for some time to allow the salt solution to move into the matrix centre. At this stage, the solution volume was estimated to be equal to the pore volume (Figure 9.7 (b)).

(a) (b)

Figure 9.6. The preparation of the solution

(a) (b)

Figure 9.7. Techniques of mixing $CaCl_2$ with Vermiculite

6. The occurrence of fully wetted transition was verified by Visual confirmation to ensure that the Vermiculite has been uniformly impregnated by $CaCl_2$ (Figure 9.8 (a)).
7. To dry the wetted *SIM*, the prepared *SIM* is positioned in an aluminium mesh tray placed in an oven, to make sure that the salt is covered within the evaporated matrix water and energy stored in the hydrated salt (Figure 9.8(b)). A minimum temperature T_{emp} = 150 °C was set to dry the salt for a period of up to 24 hours to ensure complete dehydration of impregnated salt. The salt was subsequently allowed to cool down for up to two hours prior to the next stage.

(a) (b)

Figure 9.8. Mixing and drying processes of the composite

The total mass of impregnated salt into the pore structure of a desiccant (Vermiculite) as a percentage of the total weight of the composite was determined after drying the materials based on equation (9.1).

$$m_{salt} = \frac{m_{SIM} - m_{volume}}{m_{SIM}} \; x \; 100 \; (\%) \tag{9.1}$$

Where, m_{SIM} is mass of the *SIM* composite anhydrous; and and m_{volume} is the mass of the raw vermiculite.

Confinement is the final process of keeping the mixed material without accessing it to ensure that it is in the required state by avoiding more wetness and humidification. The process is repeated till the required quantity of the composite material for use in the experiment is reached. Consequently, the prepared composite material is sealed in a large transparent container ready for use as shown in Figure 9.9.

Figure 9.9. Material's confinement process

9.4. Experimental set up

The components of the system have been described previously except the thermochemical jacket. As explained above, it consists of two parts. The first one is the *DX-SAMHP* with a solar simulator which represents a ternary solar collector connected to a water storage tank of 200 ltrs (Figure 9.10). The water storage tank is linked with a flow meter, a regulator and circulation pump to facilitate the water-flow. The second part is a field scale unit of thermochemical reaction jacket enclosed within the DHWT. Initially and during the trial tests, the water in the tank was set at 20°C, and indoor temperature was between 19-20°C. The RH was 75 % at the inlet of the jacket during the discharging process with mass moist air of 0.30 l/min. Thus, the ultrasonic humidifier device was filled with 3.5 ltrs of pure water.

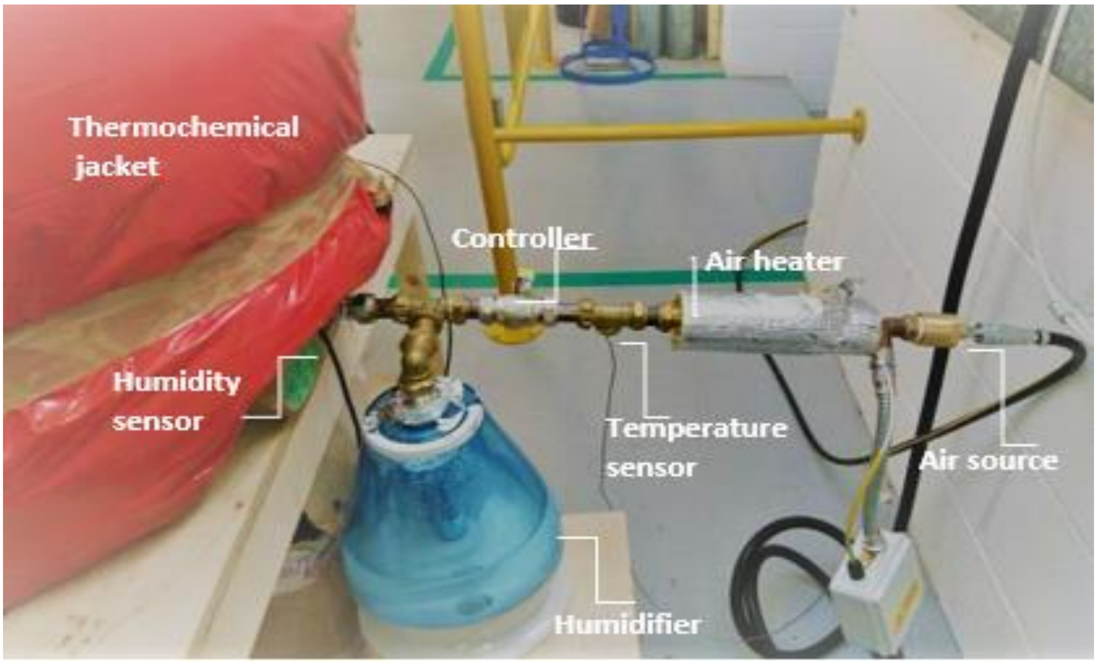

Figure 9.10. The experimental Set-up

The composite material was dried by an electric air heater with constant power input as shown in Figure 9.11. The jacket inlet and outlet air temperatures were measured in addition to associated fan, and the mean average power through the whole running period was recorded. Since the experiment was conducted indoor, hermetical insulation was utilized to protect the composite material from external humidity or wetness.

Figure 9.11. The humidifier and the air heater connections

9.5. The main principles and operating conditions of the system

The adsorption heat storage system operates by using simple design process with more straight forward operational conditions. At the beginning, the heat energy from the *DX-SAMHP* is utilized to heat the water in the tank. In this experiment the *DX-SAMHP* is supposed to be switched off when the cylinder reaches a temperature of about 20°C to examine the influence of the thermochemical jacket on the DHWT temperature in severe cold weather. the thermochemical jacket is required in severe winter where more heat is needed because the *DX-SAMHP* system is not able to deliver a sufficient heat for water in the tank at the desired temperature. Therefore, it is assumed that the water temperature in the storage tank is at the low value, in order to systematically examine the influence of the thermochemical jacket on the proposed system. Hence, the initial water temperature in the storage water tank was set at 20°C.

During the discharging process, the humidifier as source of RH at the entrance of the jacket opens to humidify the incoming air into the adsorbent jacket up to a desired level of RH of 70-80 % (Figure 9.12, 3), This is done an embedded perforated aluminium columns all-round the adsorption jacket with the help of a centrifugal fan (blower). However, in real applications the moist air can be extracted and recycled from the interior of the house for example due to showering or cooking areas, which is transferred into the jacket at air mass flow rate of 0.015 $m^3\ s^{-1}$ and pressure of 30 mbar (Figure 9.12, 4). Due to the reaction between the moisture vapour and composite materials (discharging process), the temperature of the jacket rises. This is attributed to the exothermic nature of the reaction, whereby the moisture is absorbed while heat generated. The hot air is produced and used to heat the outer surface of the tank (TS) by conductional heat transfer which increases the water tank temperature (5,6, and 7 in Figure 9.12). .

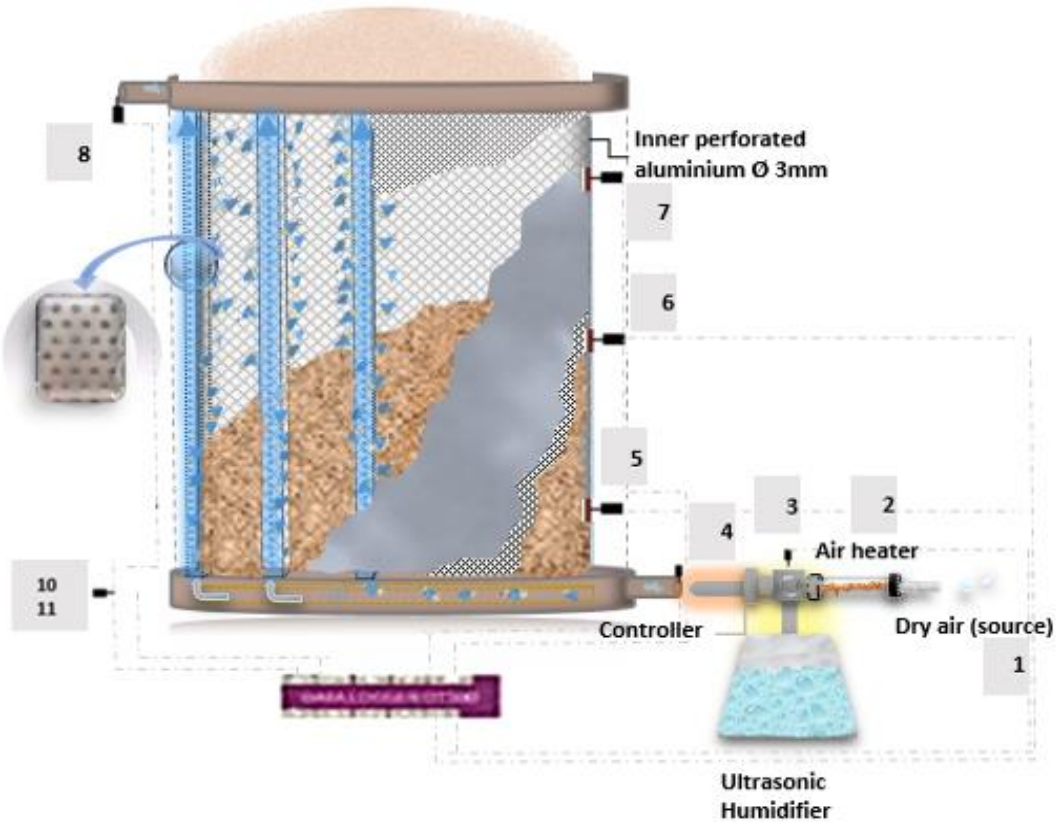

Figure 9.12. Operating process and components of the proposed adsorbent jacket

The jacket is enclosed by perforated aluminium wall to permit easy conduction and heat transfer between the composite and the tank surface and to let air move freely within the material. The jacket also allows moisture vapour to be transmitted to and from the composite materials with minimal pressure drop.

In reverse, to prepare the system for the next discharging process, the charging process started, where the composite materials is heated by external dry air by the heater between 95 and 100°C before entering the jacket so that the energy reversed cycle is completed (Figure 9.12, 2). The heater is powered by cheaper off-peak electricity supply. At this stage, during the charging process, the humidifier is disconnected whereas the adsorbent jacket is heated (Figure 9.12, 1). The absorbed vapour in the composite materials as a results of endothermic reaction is desorbed to emit humid cooled air through pores and small spaces. During the period of drying the material, if the water temperature inside the tank exceeds 65°C, the tank outlet water-flow valve (Figure 9.12, 10) is open, permitting the hot water into a domestic radiator for additional space heating (Figure 9.12, 11). Once the material of the jacket is fully dried (anhydrite), the jacket outlet (Figure 9.12, 8) and inlet (Figure 9.12, 4) are closed while the heater is switched off (Figure 9.12, 2). At this point, the hot water in the DHWT is ready for use. The operating parameters of the test are always controlled by adjusting the humidifier, fan, and the heater controller for inlet air to the desired conditions. The test can then be repeated until the system reaches a steady cyclic performance.

9.6. Experimental Procedures and components

As aforementioned in the literature, ‘open’ THS systems function under atmospheric pressure, without the requiring the use of complex pressure systems. A typical diurnal cycle consists of both charging and discharging stages. The power input was also monitored and recorded. The air flow was also measured using the laboratory central air pressure gauge, connected in line with the air heater.

The measuring points are carefully chosen to monitor the temperatures in different zones including:

- The jacket zone; inside the composite materials from the bottom to the top [5], [6] and [7], at outer surface of the tank [9], and at the outer surface of the adsorbent jacket (Figure 9.12).
- Airflow zone; before the air heater [1], at the jacket inlet [4], and at the exit of the jacket [8] (Figure 9.12)
- Water temperatures zone; at the top and bottom of the DHWT (Figure 9.12).

The data taker was programmed to read and store the measured data on the computer at one second intervals.

The test was prepared to provide data about the perormance of the adsorbent jacket, including the following parameters:

- Temperatures; Ambient ($T_{ambient}$), Input (T_{in}), Output (T_{out}), Water (T_{water}), and Regeneration (T_r)
- Relative Humidity's; Input (RH_{in}), Output (RH_{out}), and Ambient humidity ($RH_{ambient}$).

In the open experiment type, the discharging is obtained when either $RH_{in} = RH_{out}$, $T_{out} = T_{in}$ or $T_{out} = T_{ambient}$. On the onther hand, charging is achieved when either $RH_{out} = RH_{in}$ or $T_{in} = T_{out}$.

Special consideration was given to the insulatation of the jacket from the surrounding humidity and temperatures. Therefore, the jacket was sealed tightly using 35 mm and 80 mm insulation material which was wrapped externally around the jacket as shown in Figure 9.13.

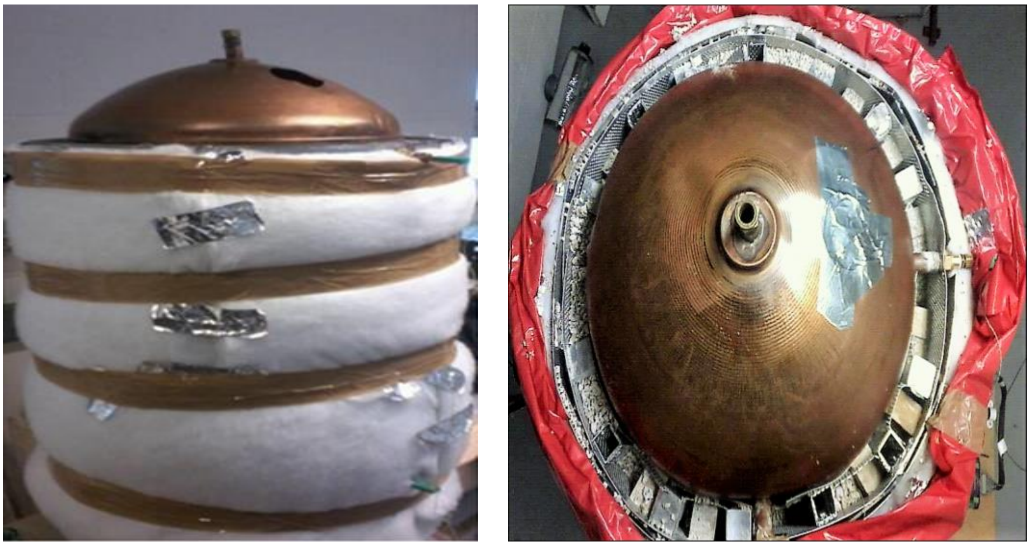

Figure 9.13. Insulation layers of the heating jacket

9.7. Measuring tools and Instruments

The laboratory scale test was equipped with a set of instruments to measure and monitor the system performance throughout the experimental process. K-type thermocouples with an accuracy of 0.1°C and used to measure the temperatures. All the experimental parameters were measured and recorded using data acquisition system (Data Taker DT600). To ensure that all sensors provide approximately accurate reading, they were calibrated and compared to a mercury-in-glass thermometer with ±1 division accuracy. They were all also immersed in a hot water bath and the readings were checked.

The airflow controller was installed in line with the air heater direction to govern the airflow as indicated in the experimental set up. The ultrasonic humidifier (VICKS, 3.5 litre) was chosen to deliver most effective humidity to humidify the air for chemical reaction (Figure 9.14). The RH was recorded using humidifier sensitive sensor (Sensiron EK-H4 Eval kit from Sensiron, Switzerland) with the acuracy of ±3 %,.

(a) (b)

Figure 9.14. The 3.5 ltr humidifier and humidity sensors measurements tool

The sensors are positioned at the tip of the probe, which is secured against damage by a membrane filter. The electric power consumed by the air heater and the blower fan (Figure 9.16) was measured using digital power meter

(Primera-Line) with the accuracy of ±1 % as shown in Figure 9.15. The in-line pressure gauge indicated in Figure 9.17 was used to measure the air pressurre.

Figure 9.15. Power meter used to estimate the power consumption of the system

Figure 9.16. Fan used to facilitate the air mass flow rate from and to adsorbent jacket

A multipurpose pressure gauge was placed at the inlet of the airflow to monitor the air and moisture pressure (Figure 9.17).

Figure 9.17. In-line pressure gauge to measure the air

The in-line air heater used in this study is an Omega (AHP-7562-NF) equipped with a K-type temperature probe which has uncertainty of 0.2°C, and Omega (CN243-R1) controller with the accuracy of ±5 % (Figure 9.18). This heater is connected in line with the pressure gauge and the humidifier device as previously illustrated (Appendix-F).

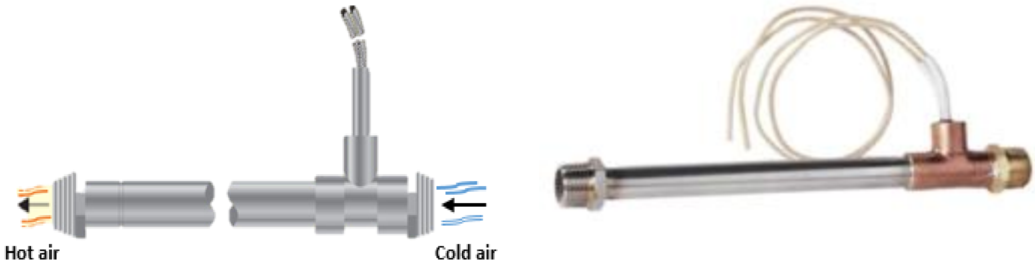

Figure 9.18. In line heat supplier (electric heater)

9.8. Results and analysis of the adsorbent jacket

The aim of this section is to investigate the performance of the adsorbent jacket and its hygrothermal cyclic behaviour. In order to achieve direct and stability operating conditions, the experiment was carried out with two charging/discharging cycles. Both cycles were performed using the same operating conditions and material quantities.

9.8.1. Experiment's observations results

Figure 9.19 shows the output of the composite material for the first discharging (exothermic reaction) cycle. for the results include the RH of the jacket (RH_{in}, RH_{out}), with air mass flow rate m_{air} (temperatures $m_{air,}$ T_{emp} and pressure $m_{air, Pre}$) as well as the temperatures of the material ($T_{air,\ in}$ and $T_{air,\ out}$) in the jacket, with water (T_{tank}) and ambient ($T_{ambient}$) temperatures.

At the beginning of the reaction, the results show sharp temperature increase due to high moisture absorption rate. The discharging process (chemical reaction) lasted for about 75 min, which is the time when the composite materials absorb the moisture air. It is worthy to mention that although at 166 min the outlet and inlet temperature difference is not markedly vast at this moment, this does not mean the hydration reaction is completely terminated. From this point, the hydration reaction continues at a slowr rate. Meanwhile the generated heat is transferred to water tank wall through air.

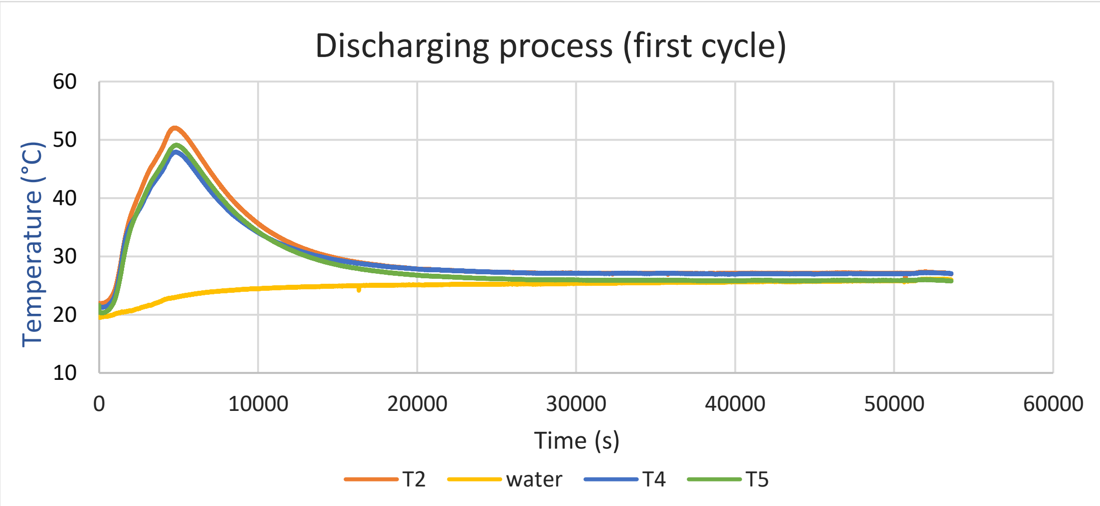

$T_{ambient}$ (°C)	RH_{in} (%)	$RH_{out,initial}$ (%)	m_{air} ($m^3\ s^{-1}$)	$T_{air,\ in}$ (°C)	$m_{air,pres}$ (mbar)	$T_{tank,initial\ temp}$ (°C)
20	75	9.5 %	0.015	23	20	20

Figure 9.19. Behavior of the adsorbent jacket during the first discharging process

As time passes, the moisture content of the reaction rises and the sorption rate drops, causing decrease in the temperature. The value of $T_{air,out\ max}$ below 50°C. The instantaneous output temperature reaches its peak at 50°C in the first cycle but it starts to drop at a rate of 2°C every two hours. In other words, when the RH level rises, $T_{air,\ out}$ also rises which is attributed to the higher reaction between the composite material and the moisture vapour. However, it is noticed that in the subsquent reaction period, the reactor's front becomes wet, allowing moisture to be condensed which causes a pressure drop to prevent the air flow. Subsequently, the jacket's inlet and outlet valves are closed to maintain the heat within the jacket and to allow the heat transfer from the composite materials to the water tank.

After this stage, the composite material starts to loose the temperature slowly towards the water tank. The temperature in the water tank increased from 20°C to the about 28°C at an increasing rate of 4°C in the first two hours due to insulation. It is also observed that the water tank temperature remained constant for more than 14 hours with negligible heat losses as shown in Figure 9.19. This confirms that the jacket released heat is supplied directly for water heating. The operating trend during discharge also demonstrate good agreement between the experiment and initial test results as presented in chapter eight.

In contrast, the performance of the system during the charging process is also analysed by assessing the heating of the materials until anhydrous state is reached. During the regeneration (charging cycle), the inlet air was set at $T_{air,\ inlet}$ =100°C for decomposition process to remove the vapuor as depicted in Figure 9.20. Meanwhile, the outlet valve is also open to blow the moisture away using a blower. The hot and dry airflow pressure and mass flow rates ($m_{air,\ ch}$) are kept constant at 20 mbar and 0.015 $m^3\ s^{-1}$ respectively. RH_{out} at the outlet of the reactor was monitored throughout the charging process, making sure that the material reaches the anhydrous form. As can be observed from Figure 9.20, the composite materials absorbed the maximum amount of heat at 100°C.

However, the dehydration process took more time than expected due to a declining trend in air diffusion within the wet compact materials, triggering serious accumulation phenomenon, and pressure drop which is not conducive for air permeability within the spaces of the material. This prevented sufficient hot air to be transmitted through the composite materials (m_{air}), affected the mass transfer performance as as retarding the drying process. At the end of this stage, the composite materials were fully dried and ready for rehydration cycle.

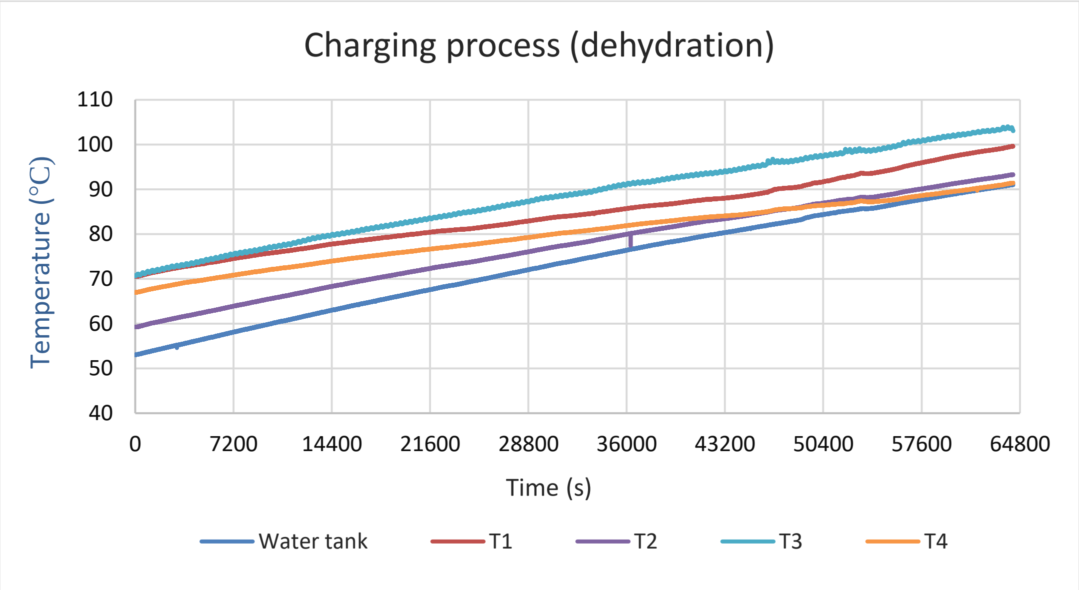

$T_{ambient}$ (°C)	RH_{in} (%)	$RH_{out,initial}$ (%)	m_{air} (m^3 $s^{-1)}$)	$T_{air, in}$ (°C)	$m_{air,pres}$ (mbar)	$T_{tank,initial\ temp}$ (°C)
20	0	9.5	0.015	100	20	29

Figure 9.20. Thermal behavior of the adsorbent jacket during the charging process

In demonstrate the cyclic thermal durability of the materials, a second discharge process was sequentially conducted under the same operating conditions, from which the results appear to be relatively stable as depicted in Figure 9.21.

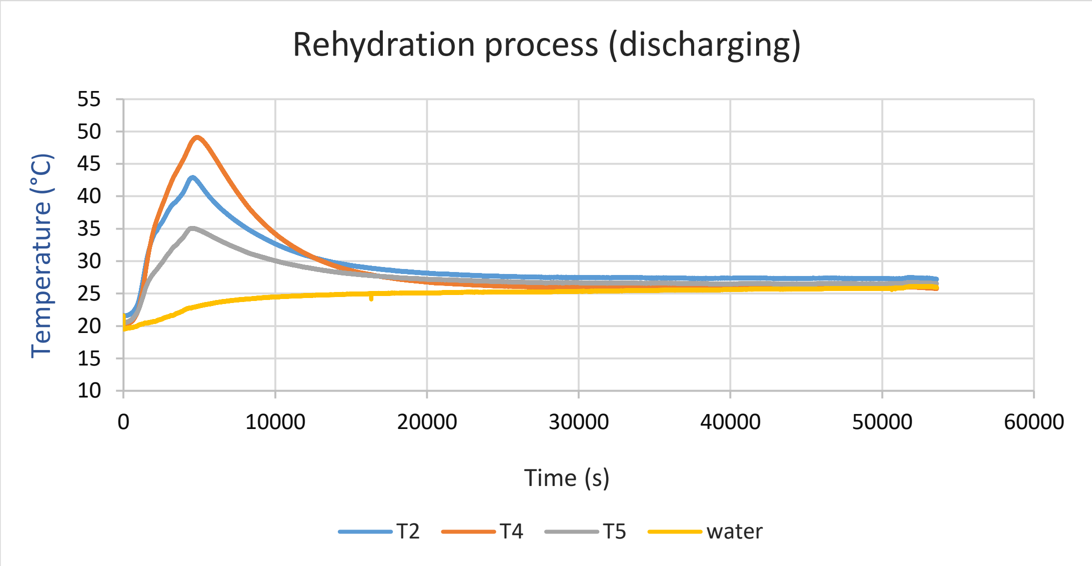

$T_{ambient}$ (°C)	RH_{in} (%)	$RH_{out,initial}$ (%)	m_{air} ($m^3\ s^{-1}$)	$T_{air,\ in}$ (°C)	$m_{\ air,pres}$ (mbar)	$T_{tank,initial}$ (°C)
20	75	75	0.015	23	20	20

Figure 9.21. Cyclic thermal stability performance of the 2nd rehydration process

As stated earlier in the first cycle, the material shows a very good performance, however, the rehydration performance follows the same trend but the pattern was slightly changed and relatively reduced in the repeated cycle with no transition time (time interval for $T_{air,\ out}$ to reach $T_{ambient}$), where '$t_{transition}$' change as shown in Figure 9.21. There is relatively lower average output gain due to either a lower regeneration temperature (T_{rege}) or large hysteresis. Although a maximum temperature of 50°C was obtained in the first cycle , the average decrease of the temperature at the end of the second cycle was about 45°C. This indicates that significant advantage can be gained from the thermo-chemical reaction. Although, $T_{out,\ max}$ ≤ 50°C for V-$CaCl_2$ as stated above in the first cycle, and decreased slightly for the second cycle down to 45°C, the $t_{transition}$ was the same ($t_{transition}$ < 15 hours) for both cycles. The temperature of water in the tank was reduced by less than 2°C (T_{out} =26.7°C), compared to the first discharge cycle as illustrated in Figure 9.21. This indicates that there is a minimal reduction in mass uptake Δm (hysteresis) between the two cycles as a result of regeneration temperatures (T_{rege} = 95°C) being inadequate to entirely eliminate all the absorbed vapour, lendering some materials to remain in monohydrate form. However, the material demonstrated good reversibility reactions and the stability of V-$CaCl_2$ in those tests. According to theresults, the rehydration reaction proves an excellent reversibility which are consistent for the two cycles. The results are also in agreement with the literature and theoretical studies though more tests had to be conducted to extensively analyse the performance of the materials.

To conclude, it is shouns be noted that any heat absorbed by the composite materials during the fast sorption kinetics is directly related to the released sorption heat during the discharging process. This means that the increase in the regeneration heat requirement is relatively related to the heat output from discharging. However, V-$CaCl_2$ is a non-toxic material, has relatively low regeneration temperature compared to the conventional desiccants, and is less costly (≈ 0.48 $/kg) compared tp other materials.

In addition, the jacket plays a significant role in term of providing a good insulation which maintains a constant temperature of the water tank for long period without heat losses. The experimental results demonstrate the feasibility of the new design based on V-$CaCl_2$ composite.

9.8.2. Energy analysis and the effect of heat and mass transfer on the adsorbent jacket

To select a suitable thermochemical adsorbent for the jacket, various aspects must be considered, for instance, regeneration temperature, yield temperature, mass uptake, energy generation, cyclic ability, and energetic efficiency. For example to analysis the energy during the experimental value reference values of the parameters were set for the discharging process i.e. $T_{ambient}$ should be greater than $T_{air,in}$, $T_{air,out}$ = $T_{ambient}$ = 20°C . All tests were performed at the same volume for material of 0.01586 m^3. The humidity, temperature, and pressure were set as the psychometric conditions that determines the performance of the composite materials, namely the difference between inlet and outlet temperature with area integration of $T_{in} \rightarrow T_{out}$ curves gives the energy density of the composite material, E_d. As mentioned before throughout the experiment, the mass of moist air, ($m_{m,\ air,\ dis}$) for discharging process was set at 0.30 l/min, with initial dry weight of 5 kg for the V-$CaCl_2$, and the power consumption of the centrifugal fan was recorded as 5 W. The energy analysis of the system and the overall discharging performance are calculated as follow:

Based on equations (9.2) and (9.3), the instantaneous output heat gain, $\dot{Q}_{gene}$ for the period of hydration can be determined as follows;

$$\dot{Q}_{gene} = \dot{m}_{air,dis}.\left(\dot{h}_{fin,dis} - \dot{h}_{in,dis}\right) \tag{9.2}$$

$$\dot{Q}_{gene} = \dot{m}_{air,dis}.c_p.\left(T_{fin,dis} - T_{in,dis}\right) \tag{9.3}$$

Where $\dot{m}_{air,dis}$ is the mass of the moist air for discharging process; $\dot{h}_{fin,dis}$ and $\dot{h}_{in,dis}$ are the final and initial heat (enthalpies) respectively for the composite materials; $T_{fin,dis}$ and $T_{in,dis}$ are the final and initial air temperatures of the composite materials respectively; while c_p is the specific heat of the moist air.

In this experiment, instantaneous heat output power of 255 W was obtained in the first cycle. For the second cycle the heat output power was 229 W which is 10% less than for the first cycle as indicated in Table 9.1. The volumetric energy storage density, E_d can be experimentally measured using:

$$E_{cumulative} = \dot{m}_{air,dis}.c_p \int_{0}^{t_{dis}} \left(T_{out,dis} - T_{in,dis}\right)dt \tag{9.4}$$

$$E_d = \frac{E_{cumulative,dis}}{\Delta m} \tag{9.5}$$

$$E_d = \frac{E_{cumulative}}{V_{adsorb}} \tag{9.6}$$

Where $E_{cumulative,dis}$, is the cumulative thermal energy generation obtained from the discharging process; t_{dis} is the discharging period; and Δm is the difference between the initial and final mass uptake of the moisture; V_{adsorb} is the volume of the adsorbent.

The effective reaction time of the composite material was greater than 2 hours. However, as time passes, a higher humid water vapour slowly occupied its pore structure at RH ≥ 75 %, resulting in higher cumulative energy output of up to 2.99 kWh. Therefore, the highest volumetric heat energy storage density achieved in this study is 32.156 kWh/m^3 based on the above equations as revealed in Table 9.1. It is worth noting that here that, for the period of the experiment the heat transfer between the adsorption unit and the whole surface of the water tank wall has been noted to be insufficient. This limits the capability of the system to reach the maximum capacity of the composite. It can be attributed to the fact that, when the temperature difference between the composite material and the wall of the tank becomes smaller, the driving force becomes smaller as well as. This causes the temperature of the composite material to rise, so that the released heat transferred.

Table 9.1 Discharging and charging thermal performance of the sorption jacket

<table>
<tr><th>$\dot{Q}_{gene}$ 1ST cycle</th><th>$\dot{Q}_{regen}$ 6th cycles</th><th>$\dot{Q}_{water,gene}$ 1ST cycle</th><th>$\dot{Q}_{water,regen}$ 6th cycles</th><th>COP_{gene} 1ST cycle</th><th>COP_{regen} 4th cycles</th><th>$\eta_{sys,gene}$ 1ST cycle</th><th>$\eta_{sys,regen}$ 6th cycles</th></tr>
<tr><td>255 W</td><td>229 W</td><td>156.5 W</td><td>130.5 W</td><td>7.28</td><td>6.54</td><td>0.761 %</td><td>0.683 %</td></tr>
<tr><td rowspan="5">0. 51 kWh</td><td rowspan="5">0.458 kWh</td><td rowspan="5">0.313 kWh</td><td rowspan="5">0.261 kWh</td><td>E_d (gene) 1ST cycle</td><td>E_d (regene) 6th cycles</td><td>Energy input apparatus</td><td>Consumption W</td></tr>
<tr><td rowspan="4">32.156 kWh/m3</td><td rowspan="4">27.877 kWh/m3</td><td>Air heater</td><td>264 W</td></tr>
<tr><td>Humidifier</td><td>30 W</td></tr>
<tr><td>Blower fan</td><td>5 W</td></tr>
</table>

In the DHWT, to calculate the heat gain $\dot{Q}_{water,gene}$ from the reaction of the adsorbent jacket during the discharging cycle, equation (9.7) can be used:

$$\dot{Q}_{water,gene} = M_w \,.\, c_{p,w} \,.\, (T_{w,gain} - T_{w,initial}) \quad (9.7)$$

Where M_w is the water mass in the DHWT; $c_{p,w}$ the specific heat coefficient of water; and $T_{w,gain}$ and $T_{w,initial}$ are the respective final and initial temperatures of the water in the DHWT.

The total heat transferred to the water tank ($\dot{Q}_{water}$) in the first cycle was 156.5 W out of the initial heat energy generated and extracted of 255 W from the composite material as presented in Table 9.1. In the subsequent steady cyclic process, the heat gain by the water tank reduced by 10 %, which decreased to 130.5 W corresponding to initial generated thermal energy of 229.5 W.

As it can be seen from discharging and rehydration processes above, most of the heat energy generated by the composite material was transferred to the hot water tank. However, it is noted that the adsorbent jacket's metallic structure would be responsible for the heat energy losses, where the upper and lower metal rings dissipate the heat to the surroundingas shown in Figure 9.22.

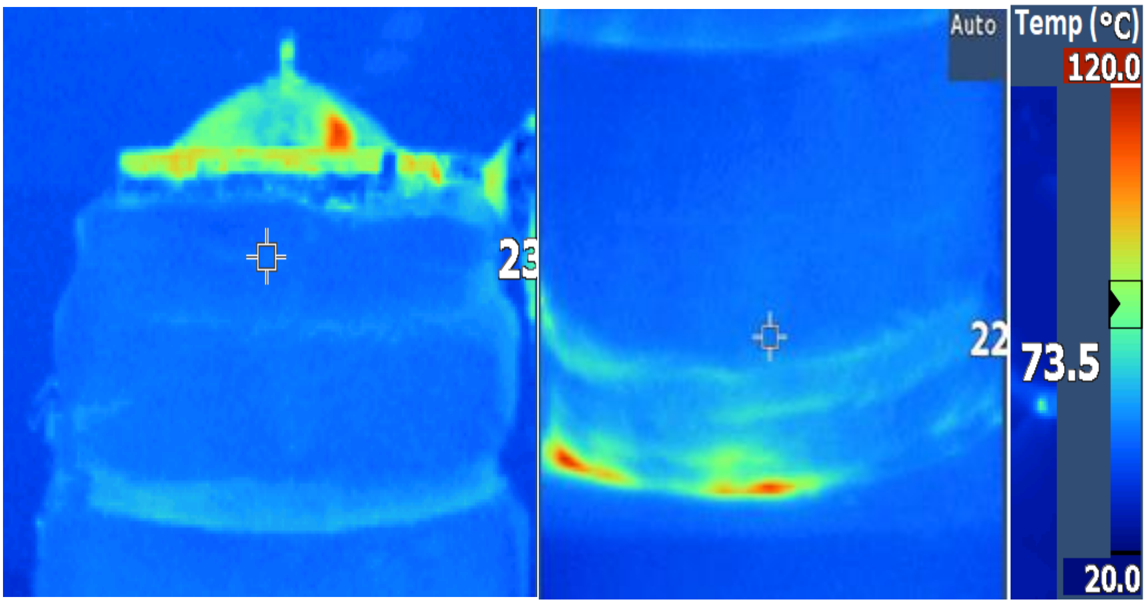

Figure 9.22. Thermal photos of the adsorbent jacket (out-skin) showing the thermal behavior during discharging process

To calculate the energy absorbed by the composite material during the charging cycle, a simple equation is used:

$$\dot{Q}_{\mathrm{material,absorb}} = \mathrm{m}_{\mathrm{sorbent}} * Cp_{\mathrm{sorbent}} * \Delta\mathrm{T} \qquad (9.8)$$

Where $\mathrm{m}_{\mathrm{sorbent}}$ is the mass of the sorbent; $\Delta\mathrm{T}$ is the temperature variation of the sorbent. Thus, to determine the instantaneous heat transfer to the absorbent $\dot{Q}_{rege}$ for regenerate the material equation (9.9) or (9.10) are emploted:

$$\dot{Q}_{rege} = \dot{m}_{ch}.(\dot{h}_{in,ch} - \dot{h}_{out,ch}) \qquad (9.9)$$

$$\dot{Q}_{rege} = \dot{m}_{ch}.c_p.(T_{in,ch} - T_{out,ch}) \qquad (9.10)$$

The cumulative energy transfer to absorbent, $E_{cumulative}$, and the desorption specific heat transfer $E_{tr,s}$ can be obtained as follow:

$$E_{cumulative} = \dot{m}_{ch}.c_p \int_0^{t_{ch}} \left(T_{out,ch} - T_{in,ch}\right)dt \tag{9.11}$$

$$E_{tr,s} = \frac{E_{cumulative,ch}}{\Delta m_{ch}} \tag{9.12}$$

During the decomposition process, the composite material absorbed 264 W, as the highest amount of heat to ensure water vapour is desorbed completely. This emphasizes the influence of the specific heat C_{p} (which is the amount of required heat to raise 1 kg of absorbent temperature by 1°C), and density ρ of the thermochemical heat storage system in regeneration. The values of C_{p} and ρ were high ($C_{\mathrm{p}}$was 565.2 kJ/kg to 792 kJ/kg), where the second discharging temperature declines from 50°C to 45°C under a regeneration temperature of 100°C. Δm, is the removed moisture (mass loss) and can be attained using equation (9.13) as follows:

$$\Delta m_{ch} = M_{water\ vapour} = M_{wet} - M_{ch} \tag{9.13}$$

$$\Delta m_{ch} = \int_0^{t_{ch}} \dot{m}_{ch} * (w_{out} - w_{in})dt \tag{9.14}$$

Where w_{out} and w_{in} are the extracted and delivered moisture content to the absorbent respectively. This indicates that for the volume of 0.01586 m^3, the material absorbs more heat until it reaches the equilibrium with the inlet air temperature ($T_{absorbent} \approx T_{air,\ inlet}$). Since the composite material needs only around a temperature of 85-90°C to dry, the composite material exposed to 100°C air heating will completely since approximately 90°C is the maximum temperature required.

9.8.3. Results and analysis of multiple cycles

In an open THS process, the cyclic stability of the thermochemical material at all times is one of the essential factors to be considered. Repeated cycles would be beneficial for sufficient assessment of hygrothermal cyclic performance. The cyclic behaviour is also one of the fundamental key parameters to attain an efficient system. The purpose of these hydration and dehydration cycles is to obtain the amount of heat released in the generation process (discharging) equivalent to that absorbed in charging process whereby $\dot{Q}_{rege} = \dot{Q}_{gene}$. Hence, several discharge-charge processes were sequentially conducted, from which the results appear to be relatively stable as depicted in Figure 9.23 and Figure 9.24.

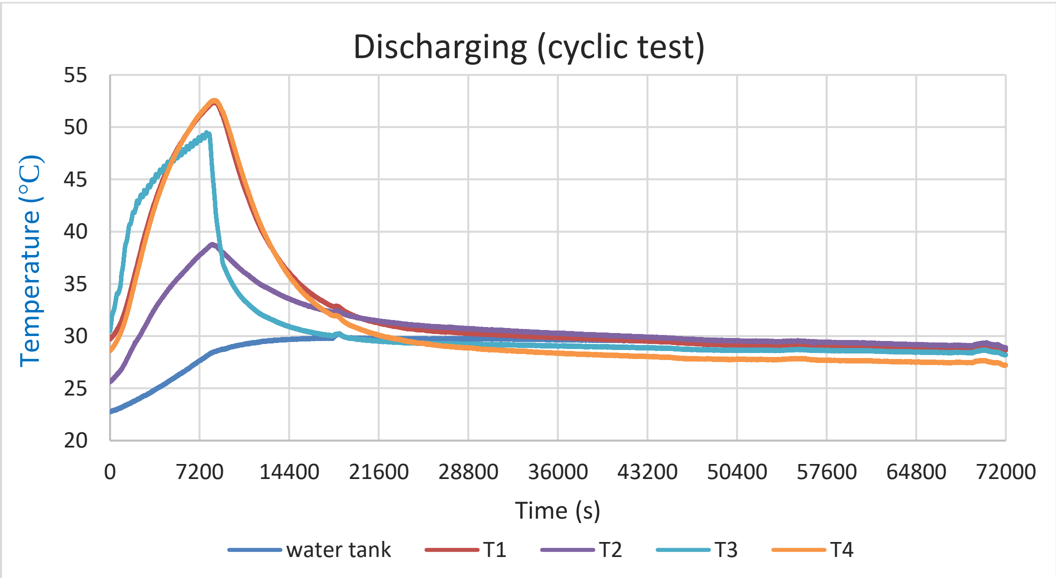

Figure 9.23. Cyclic test of the composite material and tank surface (TS), for the 3rd rehydration process

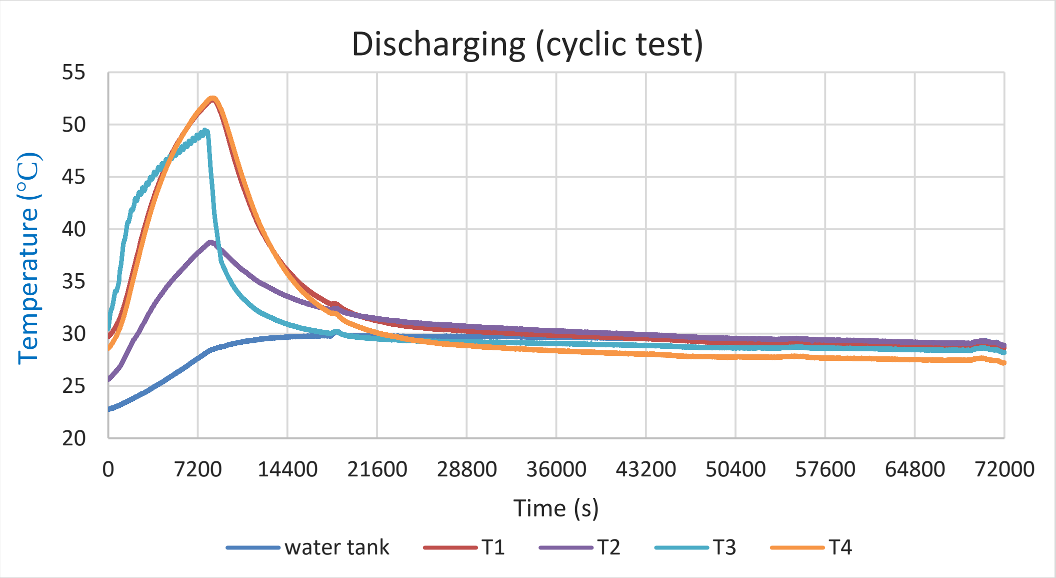

Figure 9.24. Cyclic test of the composite material and the tank surface (TS), for the 4th rehydration process

The values of $\dot{Q}_{rege}$ and $\dot{Q}_{gene}$ are equal for a steady cyclic performance as presented in Table 9.1. With the steady cyclic hygrothermal behaviour, the highest heat output $\dot{Q}_{gene}$ in all the discharging cycles is 0.51 kWh. However, the performance reduces to $\dot{Q}_{gene}$ of 0.459 kWh at the end of the cycles respectively (Table 9.1). It is observed that for all the cyclic tests, the composite did not demonstrate any physical degradation or damage in the jacket materials. Figure 9.23 and Figure 9.24 reveal that the composite material behaves almost the same in multiple cycles with a minimal change. The reduction in the performance is due to drop in mass uptake over cycles, which indicates the relationship between the temperature lifting and moisture supplied as previously discussed. For long periods of cycle testing, V-$CaCl_2$ provided initial temperature lift of 50°C, reducing to 28°C over 14 hour with volumetric heat storage density of 65.35 Wh/g, corresponding to highest THS density of about 565.2 kJ/kg. This exhibited superior performance of the heat storage.

9.8.4. The effect of moisture absorption/desorption of mass uptake and mass release ratio on cyclic performance

The mass uptake ratio f, of the composite material and the removed moisture were calculated using the equations below:

$$f_{dis} = \frac{M_{adsorbent,x} - M_{adsorbent,dis}}{M_{adsorbent,dis}} \tag{9.15}$$

$$f_{dis} = \left[\int_{0}^{t_{dis}} \dot{m}_{dis} * \ (w_{in} - w_{out}) dt \right] / m_{adsorbent,dis} \tag{9.16}$$

$$f_{ch} = \frac{M_{adsorbent,w} - M_{adsorbent,x}}{M_{adsorbent,w}} \tag{9.17}$$

$$f_{ch} = \left[\int_{0}^{t_{ch}} \dot{m}_{ch} * \ (w_{out} - w_{in}) dt \right] / m_{adsorbent,w} \tag{9.18}$$

Where f_{dis}, is the mass uptake ratio (discharging), and f_{ch} is removed moisture mass ratio (charging).

This ratio is the total amount of moisture vapour absorbed by the adsorbent to the initial dry mass of the adsorbent. Although the composite materials absorb a little mass of moisture vapour $m_{m,\ air}$ of about 300 g, it has a reasonable value of f = 0.32 $g_{water,vapour}$ /$g_{absorbent}$ for the initial results, but it reduced to 0.21 $g_{w,v}$/g_{abs} for the last cycle as seen in Figure 9.25. This means from one aspect that some of the vermiculite pore structure is most likely being partially closed, causing Δf = 0.04 g/g which is still considered insignificant.

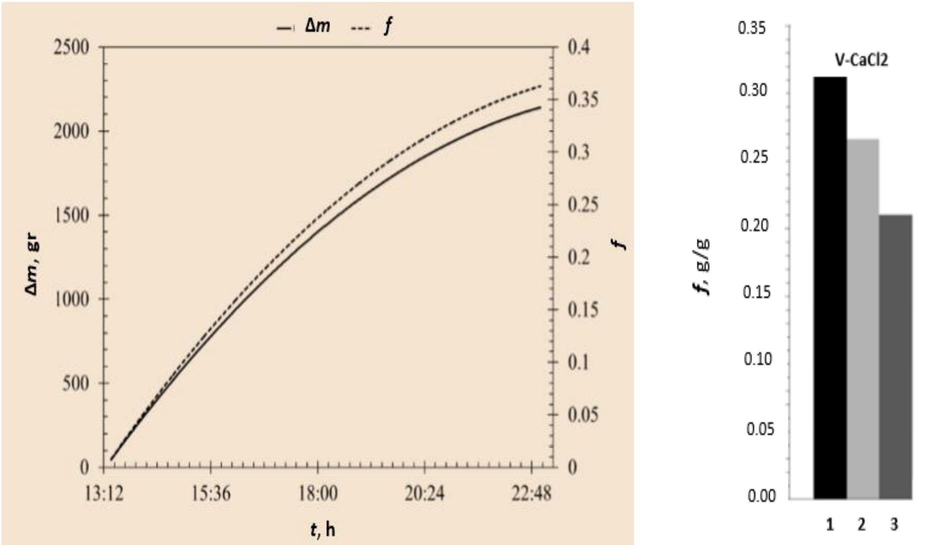

Figure 9.25. (a) Moisture absorption and mass uptake ratio during discharging process, (b) Mass uptake ratio of the materials over three cycles

9.8.5. The effect of the system air mass flowrate

Nevertheless, THS ‘open’ cycle is a reasonably simple process for storing heat, which comprises of multiple absorption processes in terms of mass or heat transfer from air to the adsorbent and vice-versa. This transfer process is dynamic and takes place instantaneously. The air mass flow rate $\dot{m}_{air}$, of the inlet air has thus a considerable impact on the general performance of the heat storage. This encompasses the direct and indirect effect of moist air, all correlated with reachable temperature lift ΔT. As an example, greater mass of moist air ($m_{m,\ air}$) carries more water vapour, which allows higher absorbent heat generation. Increasing RH has a positive impact on temperature lift ΔT, though excessive RH can create a wetting effect of the absorbent which leads to sensible cooling between moisture air and absorbent. Equally, adequate amount of hot-dry air is required to heat the material and contribute to moisture removal. However, increasing the rate of dry air supply has a negative impact in that the matrix pores structure can be damaged. In contrast, a low mass moisture rate ($m_{m,\ air}$) may provide inadequate uniform moisture diffusion and pressure through the absorbent. This can cause several issues such as moisture condensation at the reaction front, non-uniform moisture, low kinetics reaction as well as low temperature lift. To examine the system air mass flow rate Figure 9.26 illustrates three different inlet and outlet mass flow rates of air including; 0.02 $m^3 s^{-1}$, 0.015 $m^3 s^{-1}$ and 0.012 $m^3 s^{-1}$.

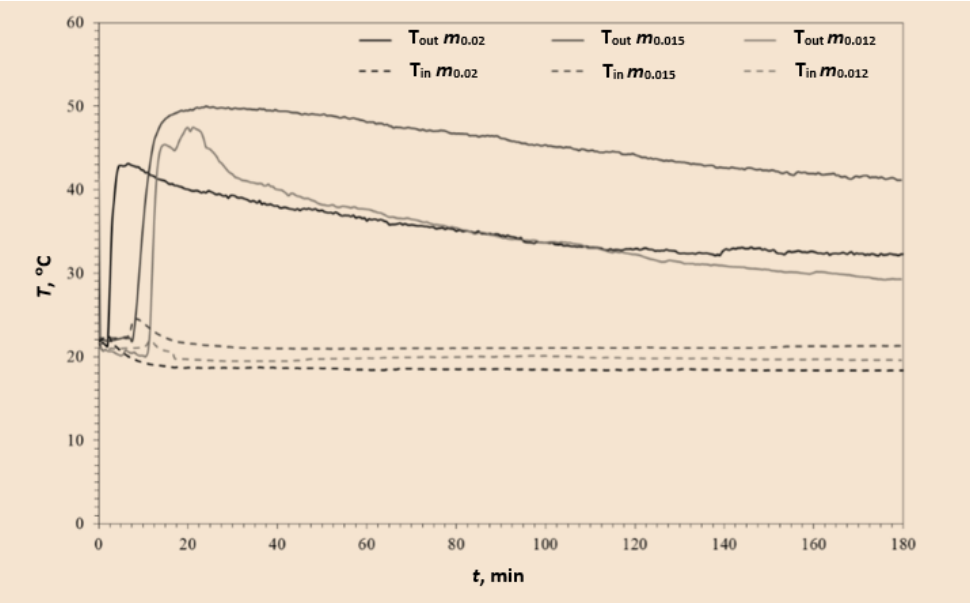

Figure 9.26. Temperature variation of 5 kg V-CaCl2 with different air mass flow rates

It should be mentioned that due to limitation of operating in severe winter environments, it could not be possible to deliver high water vapour level to the absorbent. This may result in a low heat storage performance. For example, with RH of air RH_a, of 50 % and ambient temperature $T_{ambient}$ of 10°C, the corresponding air moisture supply rate to the sorbent w_a, is 3.77 g/kg. In such environment, although the air is fully saturated where RH_a is 100 %, w_a would then be restricted to 7.5 g/kg. This is the maximum amount of moist air that could be delivered to the absorbent. Although the moisture is completely absorbed, the maximum reachable temperature lift value is $\Delta T_{peak} < 10$°C when the absolute humidity and temperature is taken into consideration. Hence, in real applications under similar winter conditions, preheating air prior to entering the humidifier could substantially enhance the performance of heat storage by considerably raising the value of w_a.

The results considerably exhibit enhanced performance at mid flow rate of 0.015 $m^3\ s^{-1}$, with $T_{air,out\ max}$ of 50°C and ΔT of 20°C. It should be noted here that each reactor design would have a specific ideal flow rate which should be experimentally or mathematically determined and carefully analysed in order to obtain the system optimal thermal output.

9.8.6. The energy efficiency of the adsorption system

Several parameters have considered when assessing the open THS system efficiencies including; RH, ambient temperature, absorbent properties, absorbent moisture content, and the amount of regeneration heat supplied, are all indispensable. The storage efficiency is necessary since it reveals the level of thermal performance as well as demosntrating the possibility of thermal energy storage applications.

Exothermic thermochemical reaction period (discharging period) plays a vital role when determining the average output of the absorbent or the heat storage density. As absorbent temperature lifts during the exothermic reaction are not fully at quasi-state condition and increases over time, the measured reaction time is crucial. At RH of 75 %, the composite has the highest energy efficiency which demonstrates that it ejectes highest heat gain. The short-term efficient performance of the composite material ($t < 2$ hours) was investigated as it has the highest temperature lift and the peak output in those 2 hours. On the other hand, due to steady performance, it is estimated that over longer periods ($t > 10$ hours) the composite material would provide the highier average heat output.

The system efficiency is the ratio of the overall energy input to the overall energy output of the system for full cycles (discharging-charging) and is calculated based on equations (9.19) and (9.20):

$$\eta_{dis} = \frac{\dot{Q}_{gene}}{\dot{W}_{humidifier}} \tag{9.19}$$

$$\eta_{ch} = \frac{\dot{Q}_{rege}}{\dot{W}_{fan} + \dot{W}_{heater}} \tag{9.20}$$

V-$CaCl_2$ has energy efficiency of close to 70 % at the end of the experiment as presented in Table 9.1, indicating that the open THS system cycle has outstanding capability for lessening the required space for future heat storage system in buildings.

9.8.7. The COP of the adsorption system

To estimate the performance of the tested composite material in term of COP, it (COP) is defined as the ratio of the energy gain in discharging to the total energy input. Alternatively, COP is the ratio of heat gain to the power consumption (etc. blower fan, humidifier) in charging which is obtained using equation (9.21) and (9.22):.

$$COP_{generation} = \frac{\dot{Q}_{gene,ave}}{\dot{W}_{humidifier}} \tag{9.21}$$

$$COP_{regenerate} = \frac{\dot{Q}_{regenerate,ave}}{\dot{W}_{fan} + \dot{Q}_{heater}} \tag{9.22}$$

As displayed in Table 9.1, the composite material V-CaCl2 with stable cycle have steady COPs for the subsequent cycles with the final cycle being 10 % less, compared to the initial cycles. The highest COP generated was 7.28, whilst the final had a *COP* of 6.54.

9.9. Uncertainty analysis and data accuracy

Since experimental works are subject to errors, differences between the actual experimenal results and the analytical values exist. Hence, errors must be quantified so that the differences in the results be explained appropriately. The most crucial errors in the results is the calibration and accuracy of measuring instruments. In this experimental study, Gauss propagation law was used to determine the uncertainties. The summation of W_R and the calculated values of independent variables x_1, $x_2 \ldots x_n$ and w_1, $w_2 \ldots w_n$ to represent the total uncertainties is achieved by the equation(Moffat, 1988a):

$$W_R = \left[\left(\frac{\partial_R}{\partial_{x1}} w_1\right)^2 + \left(\frac{\partial_R}{\partial_{x2}} w_2\right)^2 + \left(\frac{\partial_R}{\partial_{x3}} w_3\right)^2 + \cdots + \left(\frac{\partial_R}{\partial_{x4}} w_4\right)^2\right]^{1/2} \tag{9.23}$$

In the thermal reaction jacket, three sensor positions were utilised for determining the temperatures of the material including; $T_{material,\ out}$, $T_{water,\ tank}$) electrical heater air temperature $T_{electric}$; the humidity values such as; RH_a, humidifier $RH_{out,\ tank}$, and absolute humidity of air mass flow rate (w_a); and the pressure, were all recorded in both discharging and charging cycles. Experiments were conducted by using following instruments:

To obtain the heat storage efficiency η_i which is a function of T and m_{air} measured during discharging and charging, each is subjected to uncertainty(Moffat, 1988a):

$$W_R = \left[\left(\frac{\partial_{\eta_i}}{\partial_{T_{i,c}}} \mathrm{W}T_{i,c}\right)^2 + \left(\frac{\partial_{\eta_i}}{\partial_{T_{o,c}}} \mathrm{W}T_{o,c}\right)^2 + \left(\frac{\partial_{\eta_i}}{\partial_{T_{i,d}}} \mathrm{W}T_{i,d}\right)^2 + \left(\frac{\partial_{\eta_i}}{\partial_{T_{o,d}}} \mathrm{W}T_{o,d}\right)^2 + \right.$$

$$\left.\left(\frac{\partial_{\eta_i}}{\partial_{m_{a,c}}} \mathrm{W}m_{a,c}\right)^2 + \left(\frac{\partial_{\eta_i}}{\partial_{m_{a,d}}} \mathrm{W}m_{a,d}\right)^2\right]^{1/2} \tag{9.24}$$

By using equation (9.19) and (9.20), the uncertainty rate of the proposed system was computed to estimate the total uncertainty that affects the heat storage efficiency. In the calculation, the η_i value is found to be around 2.61 %.

9.10. Conclusion of chapter 9

This chapter focused on the heat storage capacity of the proposed THS system, and its influence on the performance of the domestic hot water tank in order to evaluate the application of thermochemical jacket. Moreover, different parameters under various operating conditions were correlations to determine the system performance. The study has determined the performance of the open THS system under specific operating conditions as well as analysing the significant parameters for the open THS system performance. The THS system expectations and areas which require future improvements have been clearly identified.

A real domestic water tank of thermochemical heat storage reaction jacket was constructed and tested experimental for the selected operating conditions. The composite materials for the jacket include the Vermiculite as matrix pads, $CaCl_2$ as the reactive salt, and water vapour as the working pair, in which the jacket was used to transfer its thermal energy to heat the water tank. The results have indicated that the performance of the composite materials unit (jacket) is influenced by different air mass flow rates, and discharging temperature. The experimental results show that, with 20 kg of composite materials, the maximum THS density experimentally measured was about 565 kJ/kg, where the discharging temperature was 50°C whereas the corresponding volumetric density of the THS was 65.35 Wh/g. Besides, temperatures in the range of 90-100°C were sufficient for dehydration process in the jacket. The highest THS efficiency obtained was 76 %, while the maximum thermochemical heat output power in the first two hours was about 0.225 W.

The water tank received most of the energy generated by composite materials up to 57 % of the total generated heat. This in return equivalent to 9°C water temperature lift for more than 14 consecutive hours. The jacket was tested under three different air mass flow rates, with the highest performance at 0.015 m^3/s. The $Ca\text{-}Cl_2$ material posesses several advantages as an effective matrix, including high energy density low cost, non-toxic, and high latent heat of water vapour . However, some problems which limit its performance and as such must be addressed, such as the limitation of mass transfer in discharging process which was found to be far lower than the expected, attributed to the low heat transfer between the composite materials and the water tank wall. Also the jacket metallic structure (chemical reactor) is also found to be responsible for some energy losses.

Finally, the findings from this research also demonstrate clearly that intense solar irradiance would be required to enable the use of solar energy for regeneration of $V\text{-}CaCl_2$ in the 85-100°C temperature range, which is not readily available under normal European climate conditions. However, to overcome these technical difficulties, recommendations and improvements are suggested in the next chapter.

Chapter 10. Conclusions and future work

10.1. Conclusions

The aims of this research were to enhance the heating system performance of the exsiting homes in the winter time in cold climates; A solar-air heat pump's evaporator/collector has been developed to make use of the potential domestic waste heat and low grade energy, and to reduce the frost formation. A solar-air source heat pump system has also been developed for multiple use to cover sufficiently the rapid heating demand from the beginning of the heating season to the end of coldest days. In addtion, the thermal storage density of the existing DHWT has also been improved to enhance the COP of the multiple solar-air heat pump and to enable a constant temperature during severe winter period.

To fulfil the research aim and objectives, experiments were carried out in several stages to study the performance of the combination of DX-SAMHP with thermochemical heat storage system under different operating conditions. A single air-to-air heat pump has been tested experimentally and empirically in the first stage, to evaluate the performance of air source heat pump for space heating. The system performance has been assessed based on the results of the first stage. In the second stage, the study mainly concentrated on improving the evaporator/collector area of the heat pump. The modified system has been designed and assembled with one operating mode (space heating only). Meanwhile, ternary evaporator/collector was added to the air source heat pump, from which promising results were obtained and relatively high coefficient of performance is achieved. However, the third stage focused on adding a water loop to the *DX-SAHP* system for water heating purpose in order to operate the system in multi-mode to enable the satisfaction of the household space and water heating demand throughout the year. The developed system has been constructed, fabricated and tested for for residential use to provide two fundamental operating modes: domestic hot water and space heating. The system is experimentally examined using computer simulation. The developed system (*DX-SAMHP*) have been tested under the lowest outdoor ambient temperatures of -1 to 8°C. The system is investigated under varying solar insolation in the range 0 $W{\cdot}m^{-2}$ to 200 $W{\cdot}m^{-2}$. In addition, a sorption jacket made of thermochemical V-$CaCl_2$ composite material has been designed, constructed and integrated with a hot water storage tank. The *DX-SAMHP* system performance has been analysed at different water flow rates with and without a thermochemical reaction jacket.

The experimental results show that a single air-to-air heat pump and the *DX-SAHP* system can produce adequate space heating in space heating only-mode with COPs of up to a vaue of 4. The water temperatures at the condenser tank were varied between 43°C and 55°C within two hours in correlation with available heat energy. The average values of COP for the system ranged from 2.8 to 3.9 and the solar collector efficiency was found to be between 40 % and 75 %. For water-heating-only mode, the modelled multi-functional *DX-SAMHP* system could provide 200 litres of hot water, with a maximum temperature of up to 65°C. This is in agreement with the findings of the theoretical model with a maximum deviation less than 8 %. On the other hand, the results also indicate that the performance of the system is influenced by the collector area, ambient air temperature and the solar irradiation level. It is observed that, in absence of solar irradiation, the system can still operate by making use of the collector plate inside the loft space through absorbing the surrounding heat in the attic area. In this case the system can also provide frost protection. In return, variations of both ambient/indoor air temperatures and solar irradiation result in a large fluctuation in the thermal load imposed on the collector/evaporator of the *DX-SAMHP*. Solar energy utilization raises the collector temperature, leading to lower temperature lift in the heat pumping process. However, the system can also perform appropriatelly without the presence of solar energy or even ancillary traditional sources.

In addition, frosting formation study and its conditions has also been conducted to evaluate the influence of the frost accumulation layers on the system components. It is noticed from the results that the frost becomes less serious with relatively high solar irradiations. Therefore, solar irradiance can considerably reduce frosting formation on multi-functional *DX-SAMHP* system and improve the performance of the whole system. Besides, the system can take advantage of the low off-peak energy rates set by the utility companies which can be utilised to reduce the energy consumption cost of the system. The developed multi-functional heat pump system therefore could guarantee an appropriate operation under low temperature and relatively low running cost. Compared to a traditional *DX-SAHP* water heater, with or without sufficient solar irradiation, the use of a developed *DX-SAMHP* is obviously more advantageous. Not only it is able to provide water and space heating efficiently for residential buildings, but also helps to solve the problem of poor operation of the traditional heat pumps due to absence of solar energy. It can be concluded that, for domestic space and water heating purposes in cold region, the system is suitable for applications in the temperature range of 50-70°C..

Further, the storage system was also integrated with a heat source in conjunction with household water tank, by using reliable material (Vermiculite-$CaCl_2$). The V-$CaCl_2$ was impregnated in matrix-porous structure, and compacted in a jacket using field-scale unit. In this case, the DHWT was replaced with another one made of a bare copper to investigate the viability of the proposed system. Preliminary tests showed that the thermochemical jacket has a considerable impact on maintaining the water tank temperature for around eighteen hours without any heat losses. The revisable nature of the hydration/dehydration reaction, ensures there is no effective low heat loss from the system. This offers a distinct advantage over other systems whereby the thermal production capacity of the DHWT is increased by 0.583 kWh compared to *DX-SAMHP* alone at the same temperature and environmental conditions.

The maximum energy density obtained through the discharging process is 32.156 kWh/m^3. A small-scale-prototype and field-scale tests of the V-$CaCl_2$ composite material reveals that this energy density level is maintained over multiple charge/discharge cycles with a temperature rise of up to 50°C. This system has proved to be a promising thermal heat storage, due to its good thermal properties. It is also possible to achieve economic benefits to reduce the energy cost of the system by charging the material during off-peak periods, when the electricity price is lower. However, during the tests the heat transfer between the adsorption unit and the whole surface of the water tank wall has been noted to be insufficient. This limits the capability of the system to reach the maximum capacity of the composite.

Humidification process has also been noticed to be relatively slow due to low moisture air distribution throughout the materials. Hence, more ways to control the system to meet the user demand have to be thoroughly investigated.

To conclude, the system fulfilled the main objective of generating heat energy for domestic use. By using the existing central heating pipe system, the thermochemical jacket can be placed within the same storage area as the DHWT incorporated into the attic of the household. This firstly maximizes the use of space with minimized cost. Also, the proposed system is capable of providing sufficient water heating, and space heating directly through heat pump or radiator at low grade temperature with minimal heat losses over an extended period of time.

10.2. Future work and advancements

The performance of the combined system can be improved in the future research work through several ways. A combination of *DX-SAMHP* and open THS system has many promising advantages as discussed earlier. The suggested improvements to overcome the system problems, are summarized as follows though not exhaustive:

Since most of the energy consumed in UK building sector goes to space heating, A multifunctional heat pump system with an appropriate solar technology could be a promising option to deliver adequate space and water heating in addition to efficient system operation. This, would help in meeting the heating demand and reduce the energy storage consumption. In contrast, apart from the thermal protection (insulation materials) coupled with a refrigeration system, it is necessary to equip individual components of the heating system with special thermal protection. This could eliminate the condensation and reduce chances of noise in the system. Running length of the refrigeration lines between the evaporator/collector and heat pump components should be reduced. Therefore, it is recommended to position the heat pump system away from living so that the refrigeration lines could provide a reduced amount of heat losses and better performance. A larger or a scroll compressor with high speed can be replaced not only to overcome the mismatch between the collector but also to enhance the system performance. With respect to the thermochemical storage jacket system, uniform airflow through the composite materials is essential for effective performance. One of the key suggested approaches is to improve the internal contact area of the jacket to accelerate the airflow from the composite materials. Therefore, further study on optimizing the size of perforated tubes is needed to enhance the system performance. The inclusion of the new porous fibre capillaries can further improve the reaction rate and energy density. The porous fibres tubes are proposed to raise the thermal conductivity of the consolidated composite materials and to improve the heat transfer performance of the chemical reactive salt. The porous fibre capillaries are indicated in Figure 10.1, which could comprise of long strands of hollow plastic fibre tubes with $Ø_{int}$ of 1 mm and microscopic holes to perforated in the exterior walls of the tube. Embedding the fibres within the composite can effectively increase the vapour permeability of the composite as well as permitting smooth moist vapour transfer to and from the material with minimal pressure drop as demonstarted in Figure 10.2.

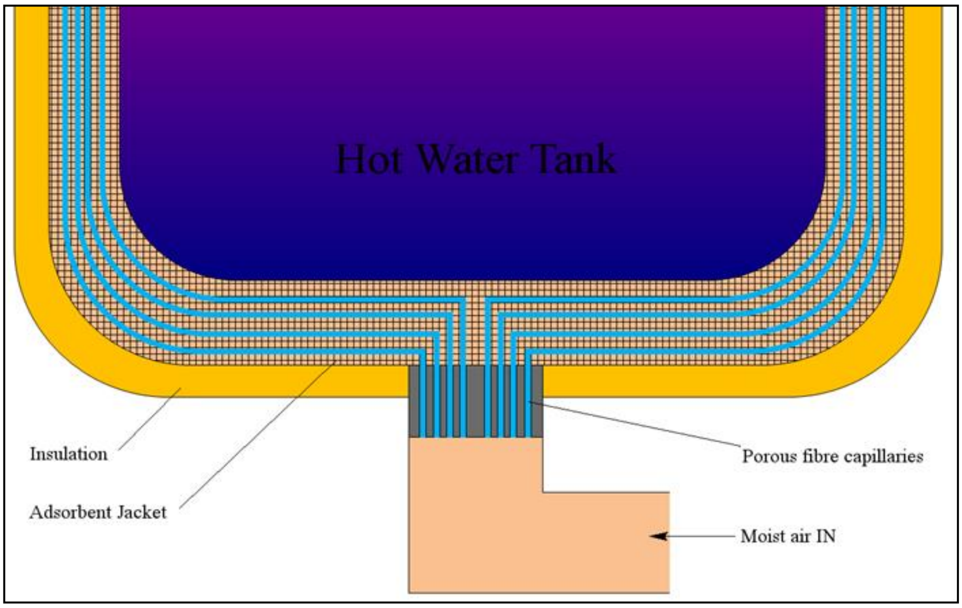

Figure 10.1. Recommended detail of adsorbent reaction jacket showing embedded fibres

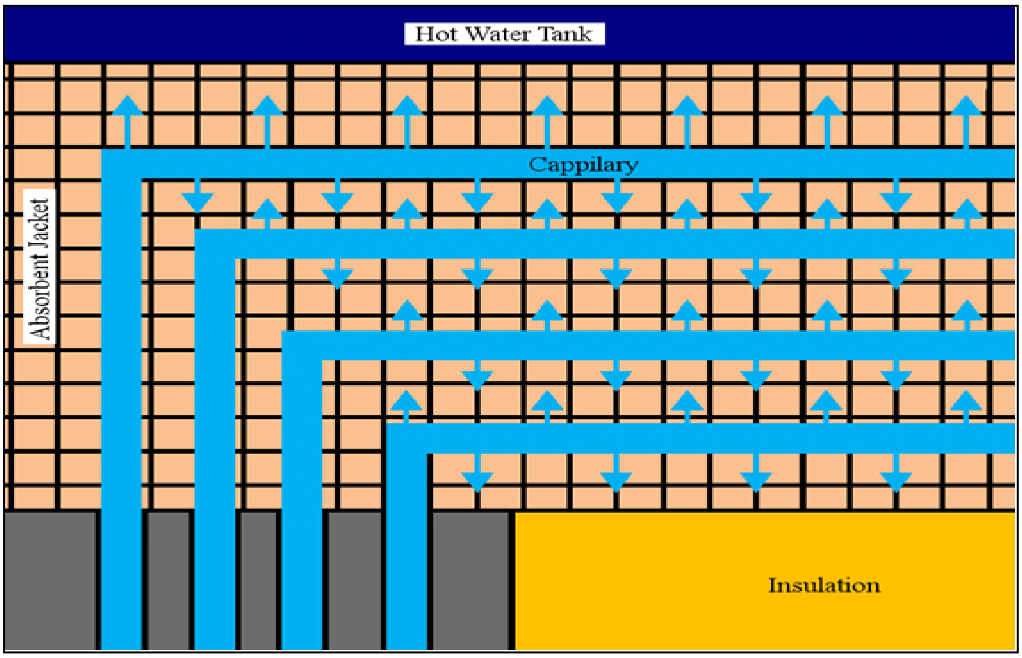

Figure 10.2. Details of recommended embedded fibre capillaries to enhanced mass transfer

The addition of the fibres could also increase the composite density, enabling extra storage volume to be achieved. However, an improved humidification system with low power consumption for delivering the moist air, received from the interior of the house (cooking, showering etc.) is also highly suggested. This would increase the quantity of loaded moisture to the adsorbent materials during the hydration process which could help to achieve higher temperature lifting.

On one hand, another key parameter that could be improved to enhance the system performance is the COP of the system. The integration and optimization of the heat pump and the thermochemical jacket should be carried out further to enhance the performance of THS. Using the combined system for energy heating in charging process would substantially reduce the dehydration consumption, thereby improving the COP of the system.

Finally, if the optimal design of thermochemical reaction jacket is performed in future to achieve smaller system volume for more compact jacket structure, the jacket metallic thermal capacity and sensible heat consumption can be reduced as well. Thus, the thermochemical jacket capacity of the field-scale system could be considerably improved.

References

A, R. 1966. HOLMAN, JP-EXPERIMENTAL METHODS FOR ENGINEERS. NATL INST SCIENCE COMMUNICATION DR KS KRISHNAN MARG, NEW DELHI 110 012, INDIA.

ABHAT, A. 1983. Low temperature latent heat thermal energy storage: heat storage materials. *Solar energy,* 30, 313-332.

AHN, J. H., KANG, H., LEE, H. S., JUNG, H. W., BAEK, C. & KIM, Y. 2014. Heating performance characteristics of a dual source heat pump using air and waste heat in electric vehicles. *Applied Energy,* 119, 1-9.

ALAVY, M., NGUYEN, H. V., LEONG, W. H. & DWORKIN, S. B. 2013. A methodology and computerized approach for optimizing hybrid ground source heat pump system design. *Renewable energy,* 57, 404-412.

ARISTOV, Y. I. 2007. New family of solid sorbents for adsorptive cooling: Material scientist approach. *Journal of Engineering Thermophysics,* 16, 63-72.

ARISTOVE, Y. I. R., G., TOKAREV, M., BUERGER, H. D. & FRENI, A. 2000. Selective water sorbents for multiple applications, 11. CaCl2 confined to expanded vermiculite. *Reaction Kinetic and Catalysis Letter* 71, 377-384.

AVEYARD, R. & HAYDON, D. A. 1973. *An introduction to the principles of surface chemistry*, CUP Archive.

BALASUBRAMANIAN, G., GHOMMEM, M., HAJJ, M. R., WONG, W. P., TOMLIN, J. A. & PURI, I. K. 2010. Modeling of thermochemical energy storage by salt hydrates. *International Journal of Heat and Mass Transfer,* 53, 5700-5706.

BALES, C., GANTENBEIN, P., HAUER, A., HENNING, H.-M., JAENIG, D., KERSKES, H., NUNEZ, T. & VISSCHER, K. 2005. *Thermal Properties of Materials for Thermo-chemical Storage of Solar Heat : Report B2 of Subtask B*, The International Energy Agency (IEA).

BANISTER, C. J., WAGAR, W. R. & COLLINS, M. R. 2014. Validation of a Single Tank, Multi-mode Solar-assisted Heat Pump TRNSYS Model. *Energy Procedia,* 48, 499-504.

BI, Y., GUO, T., ZHANG, L. & CHEN, L. 2004. Solar and ground source heat-pump system. *Applied Energy,* 78, 231-245.

BSI 2007. Carbonaceous materials used in the production of aluminium. Determination of density by gas pyknometry (volumetric) using helium as analysis gas. London: BSI, solid material.

BUREAUE, E. E. 2006. Energy Conservation Building Code.

CABROL, L. & ROWLEY, P. 2012. Towards low carbon homes–A simulation analysis of building-integrated air-source heat pump systems. *Energy and Buildings,* 48, 127-136.

CASEY, S. D. 2014. Salt impregnated desiccant matrices for 'open' thermochemical energy storage-Hygrothermal cyclic behaviour and energetic analysis by physical experimentation. *Energy and Buildings*, 342-355.

CHARTURVEDI, S., CHIANG, Y., ROBERTS, A 1982. Analysis of two-phase flow solar collectors with application to heat pumps. *Journal of Solar Energy Engineering*, p 356-365.

CHATURVEDI, S., GAGRANI, V. & ABDEL-SALAM, T. 2014. Solar-assisted heat pump–a sustainable system for low-temperature water heating applications. *Energy Conversion and Management,* 77, 550-557.

CHUA, K., CHOU, S. & YANG, W. 2010. Advances in heat pump systems: A review. *Applied Energy,* 87, 3611-3624.

CHYNG, J., LEE, C. & HUANG, B. 2003. Performance analysis of a solar-assisted heat pump water heater. *Solar Energy,* 74, 33-44.

CLELAND, A. 1994. Polynomial curve-fits for refrigerant thermodynamic properties: extension to include R134a. *International Journal of Refrigeration,* 17, 245-249.

DCLG 2008. Existing Housing and Climate Change. HC 432-1, HC 432-1.

DEMIR, H., MOBEDI, M. & ÜLKÜ, S. 2008. A review on adsorption heat pump: Problems and solutions. *Renewable and Sustainable Energy Reviews,* 12, 2381-2403.

DEVRIM, A. 2016. Investigation of Innovative Thermochemical Energy Storage Processes and Materials for Building Applications Nottingham: The University of Nottingham, eprint

DIKICI, A. & AKBULUT, A. 2008. Performance characteristics and energy–exergy analysis of solar-assisted heat pump system. *Building and Environment,* 43, 1961-1972.

DING, Y., CHAI, Q., MA, G. & JIANG, Y. 2004. Experimental study of an improved air source heat pump. *Energy Conversion and Management,* 45, 2393-2403.

DING, Y. & RIFFAT, S. 2013. Thermochemical energy storage technologies for building applications: a state-of-the-art review. *International Journal of Low-Carbon Technologies,* 8, 106-116.

DUFFIE, J. A. & BECKMAN, W. A. 1980. Solar engineering of thermal processes.

ECUK, D. O. E. A. C. C. 2014. Domestic energy consumption in the UK between 1970 and 2013. *Energy Consumption in the UK (2014)*

Department of energy and climate change, 1-17.

EUGENE, S. 2014. *Heat Pump Basics* [Online]. Heatinghelp.com. Available: https://heatinghelp.com/systems-help-center/heat-pump-basics/ [Accessed 18/06 2018].

FAN, R., GAO, Y., HUA, L., DENG, X. & SHI, J. 2014. Thermal performance and operation strategy optimization for a practical hybrid ground-source heat-pump system. *Energy and Buildings,* 78, 238-247.

FANINGER, G. 2004. Thermal energy storage. *Faculty for Interdisciplinary Research and Continuing Education, IFF-University of Klagenfurt, Austria*.

FARID, M. M., KHUDHAIR, A. M., RAZACK, S. A. K. & AL-HALLAJ, S. 2004. A review on phase change energy storage: materials and applications. *Energy conversion and management,* 45, 1597-1615.

GOVERNMENT 2008. Government memorandum. *Publication parliament,* EV 277-94.

GRECO, A., MASTRULLO, R. & PALOMBO, A. 1997. R407C as an alternative to R22 in vapour compression plant: an experimental study. *International journal of energy research,* 21, 1087-1098.

GREENING, B. & AZAPAGIC, A. 2012. Domestic heat pumps: Life cycle environmental impacts and potential implications for the UK. *Energy,* 39, 205-217.

HADORN, J.-C. & AGENCY, T. O. T. I. A. O. B. I. E. 2005. *Thermal energy storage for solar and low energy buildings: state of the art*, Universidad de Lleida.

HASNAIN, S. 1998. Review on sustainable thermal energy storage technologies, Part I: heat storage materials and techniques. *Energy Conversion and Management,* 39, 1127-1138.

HAUER, A. Sorption storages for solar thermal energy—possibilities and limits. Proceedings of Eurosun, 2008. 7-10.

HEAP, R. D. 1979. Heat pumps. *London, E. & FN Spon, Ltd.; New York Halsted Press, 1979. 164 p.,* 1.

HEPBASLI, A. & AKDEMIR, O. 2004. Energy and exergy analysis of a ground source (geothermal) heat pump system. *Energy conversion and management,* 45, 737-753.

HEWITT, N. J., HUANG, M. J., ANDERSON, M. & QUINN, M. 2011. Advanced air source heat pumps for UK and European domestic buildings. *Applied Thermal Engineering,* 31, 3713-3719.

HOLMAN, J. P. & GAJDA, W. J. 1994. *Experimental methods for engineers*, McGraw-Hill New York.

HUANG, B. & CHYNG, J. 2001. Performance characteristics of integral type solar-assisted heat pump. *Solar Energy,* 71, 403-414.

INGLEZAKIS, V. & POULOPOULOS, S. 2006. *Adsorption, ion exchange and catalysis: design of operations and environmental applications*, Elsevier.

JÄHNIG, D., HAUSNER, R., WAGNER, W. & ISAKSSON, C. Thermo-chemical storage for solar space heating in a single-family house. Proceedings of ECOSTOCK conference, Richard Stockton College, New Jersey, 2006.

JASON, P. & IAN, C. 2013. United Kingdom housing energy fact file. Department of Energy and Climate Change.

KARA, O., ULGEN, K. & HEPBASLI, A. 2008. Exergetic assessment of direct-expansion solar-assisted heat pump systems: review and modeling. *Renewable and Sustainable Energy Reviews,* 12, 1383-1401.

KHUDHAIR, A. M. & FARID, M. M. 2004. A review on energy conservation in building applications with thermal storage by latent heat using phase change materials. *Energy conversion and management,* 45, 263-275.

KJELLSSON, E., HELLSTRÖM, G. & PERERS, B. 2010. Optimization of systems with the combination of ground-source heat pump and solar collectors in dwellings. *Energy,* 35, 2667-2673.

KLEIN, S., BECKMAN, W., MITCHELL, J., DUFFIE, J., DUFFIE, N., FREEMAN, T., MITCHELL, J., BRAUN, J., EVANS, B. & KUMMER, J. 2006. TRNSYS. *A transient system simulation program*.

KONG, X., ZHANG, D., LI, Y. & YANG, Q. 2011. Thermal performance analysis of a direct-expansion solar-assisted heat pump water heater. *Energy,* 36, 6830-6838.

KUANG, Y. & WANG, R. 2006. Performance of a multi-functional direct-expansion solar assisted heat pump system. *Solar Energy,* 80, 795-803.

LEE, H.-S., KIM, H.-J., KANG, D.-G. & JUNG, D. 2012. Thermodynamic performance of R32/R152a mixture for water source heat pumps. *Energy,* 40, 100-106.

LEE, J. S., PARK, H. & KIM, Y. 2014. Transient performance characteristics of a hybrid ground-source heat pump in the cooling mode. *Applied Energy,* 123, 121-128.

LI, R., OOKA, R. & SHUKUYA, M. 2014. Theoretical analysis on ground source heat pump and air source heat pump systems by the concepts of cool and warm exergy. *Energy and Buildings,* 75, 447-455.

LI, Y., WANG, R., WU, J. & XU, Y. 2007. Experimental performance analysis on a direct-expansion solar-assisted heat pump water heater. *Applied Thermal Engineering,* 27, 2858-2868.

LIU, H., JIANG, Y. & YAO, Y. 2014. The field test and optimization of a solar assisted heat pump system for space heating in extremely cold area. *Sustainable Cities and Society,* 13, 97-104.

MICHEL, B., MAZET, N. & NEVEU, P. 2014. Experimental investigation of an innovative thermochemical process operating with a hydrate salt and moist air for thermal storage of solar energy: Global performance. *Applied Energy,* 129, 177-186.

MOFFAT, R. J. 1988a. Describing the uncertainties in experimental results. *Experimental thermal and fluid science* 1(1): 3-17.

MOFFAT, R. J. 1988b. Describing the uncertainties in experimental results. *Experimental thermal and fluid science,* 1, 3-17.

MOHAMED, E., RIFFAT, S. & OMER, S. 2017. Low-temperature solar-plates-assisted heat pump: a developed design for domestic applications in cold climate. *International Journal of Refrigeration*.

MOLINAROLI, L., JOPPOLO, C. M. & DE ANTONELLIS, S. 2014. Numerical Analysis of the Use of R-407C in Direct Expansion Solar Assisted Heat Pump. *Energy Procedia,* 48, 938-945.

MORENO-RODRIGUEZ, A., GARCIA-HERNANDO, N., GONZÁLEZ-GIL, A. & IZQUIERDO, M. 2013. Experimental validation of a theoretical model for a direct-expansion solar-assisted heat pump applied to heating. *Energy,* 60, 242-253.

N'TSOUKPOE, K. E., LIU, H., LE PIERRÈS, N. & LUO, L. 2009. A review on long-term sorption solar energy storage. *Renewable and Sustainable Energy Reviews,* 13, 2385-2396.

OH, S., CHO, Y. & YUN, R. 2014. Raw-water source heat pump for a vertical water treatment building. *Energy and Buildings,* 68, 321-328.

OZGENER, O. & HEPBASLI, A. 2005. Experimental performance analysis of a solar assisted ground-source heat pump greenhouse heating system. *Energy and Buildings,* 37, 101-110.

QI, Z., GAO, Q., LIU, Y., YAN, Y. & SPITLER, J. D. 2014. Status and development of hybrid energy systems from hybrid ground source heat pump in China and other countries. *Renewable and Sustainable Energy Reviews,* 29, 37-51.

RAD, F. M., FUNG, A. S. & LEONG, W. H. 2013. Feasibility of combined solar thermal and ground source heat pump systems in cold climate, Canada. *Energy and Buildings,* 61, 224-232.

REAY, D. A. & MAC MICHAEL, D. B. 1986. Heat pumps.

SARBU, I. & SEBARCHIEVICI, C. 2016. *Solar Heating and Cooling Systems: Fundamentals, Experiments and Applications*, Academic Press.

SARBU, I. & SEBARCHIEVICI, C. 2017. Chapter 9 - Solar-Assisted Heat Pumps. *Solar Heating and Cooling Systems.* Academic Press.

SHARMA, A., TYAGI, V., CHEN, C. & BUDDHI, D. 2009. Review on thermal energy storage with phase change materials and applications. *Renewable and Sustainable energy reviews,* 13, 318-345.

SIVASAKTHIVEL, T., K.MURUGESAN & SAHOO, P. K. 2014. A study on energy and CO2 saving potential of ground source heat pump system in India. *Science Direct,* 32, 278–293.

STITOU, D., MAZET, N. & BONNISSEL, M. 2004. Performance of a high temperature hydrate solid/gas sorption heat pump used as topping cycle for cascaded sorption chillers. *Energy,* 29, 267-285.

TOUCHIE, M. F. & PRESSNAIL, K. D. 2014. Testing and simulation of a low-temperature air-source heat pump operating in a thermal buffer zone. *Energy and Buildings,* 75, 149-159.

VOCALE, P., MORINI, G. L. & SPIGA, M. 2014. Influence of Outdoor Air Conditions on the Air Source Heat Pumps Performance. *Energy Procedia,* 45, 653-662.

WANG, L., WANG, R. & OLIVEIRA, R. 2009. A review on adsorption working pairs for refrigeration. *Renewable and Sustainable Energy Reviews,* 13, 518-534.

WANG, R., XIE, G., WU, Q., WU, Y. & YUAN, J. 2011. An air source heat pump with an advanced cycle for heating buildings in Beijing. *Energy Conversion and Management,* 52, 1493-1500.

WANG, Y., WONG, K. K., LIU, Q.-H., JIN, Y.-T. & TU, J. 2012. Improvement of energy efficiency for an open-loop surface water source heat pump system via optimal design of water-intake. *Energy and Buildings,* 51, 93-100.

WATMUFFJ, H., WITT, H. T., & JOUBERTP, N. 1985. Developing turbulent boundary layers with in rotating channel flow. *Journal of Fluid Mechanecs*, 130, 377-395. .

WBDG. 2016. *Geothermal heat pumps* [Online]. Department of Energy Federal Energy Management Program (FEMP). [Accessed 18/06/2018 2018].

WEBER, R. & DORER, V. 2008. Long-term heat storage with NaOH. *Vacuum,* 82, 708-716.

WILE, D. 1935. The measurement of expansion valve capacity. *Refrigeration Engineering,* 8, 108-112.

WONGSUWAN, W., KUMAR, S., NEVEU, P. & MEUNIER, F. 2001. A review of chemical heat pump technology and applications. *Applied Thermal Engineering,* 21, 1489-1519.

WRIGHT, A. 2008. What is the relationship between built form and energy use in dwellings? *Energy Policy,* 36, 4544-4547.

WYATT 2004. Renewable heat-the era of ground-source heat pumps.

XU, J., WANG, R. Z. & LI, Y. 2014. A review of available technologies for seasonal thermal energy storage. *Solar Energy,* 103, 610-638.

XUE, Z. & SHI, L. 2010. Modeling and experimental investigation of a variable speed drive water source heat pump. *Tsinghua Science & Technology,* 15, 434-440.

YIQIANG, B. J., YANG, Y. & ZUILIANG, M. 2000. Calculation of the loss coefficient for frosting defrosting of air source heat pumps [J]. *HV & AC,* 5, 010.

YU, N., WANG, R. & WANG, L. 2013. Sorption thermal storage for solar energy. *Progress in Energy and Combustion Science,* 39, 489-514.

YU, Y., ZHANG, P., WU, J. & WANG, R. 2008. Energy upgrading by solid–gas reaction heat transformer: a critical review. *Renewable and Sustainable Energy Reviews,* 12, 1302-1324.

YUMRUTAS, R. & KASKA, Ö. 2004. Experimental investigation of thermal performance of a solar assisted heat pump system with an energy storage. *International journal of energy research,* 28, 163-175.

YUNUS A. CENGEL & BOLES, M. A. 2011. *Thermodynamics: an engineering approach*, McGraw-Hill New York.

ZALBA, B., MARíN, J. M., CABEZA, L. F. & MEHLING, H. 2003. Review on thermal energy storage with phase change: materials, heat transfer analysis and applications. *Applied thermal engineering,* 23, 251-283.

ZHENG, X., YOU, S., YANG, J. & CHEN, G. 2014. Seepage and heat transfer modeling on beach well infiltration intake system in seawater source heat pump. *Energy and Buildings,* 68, 147-155.

Appendices

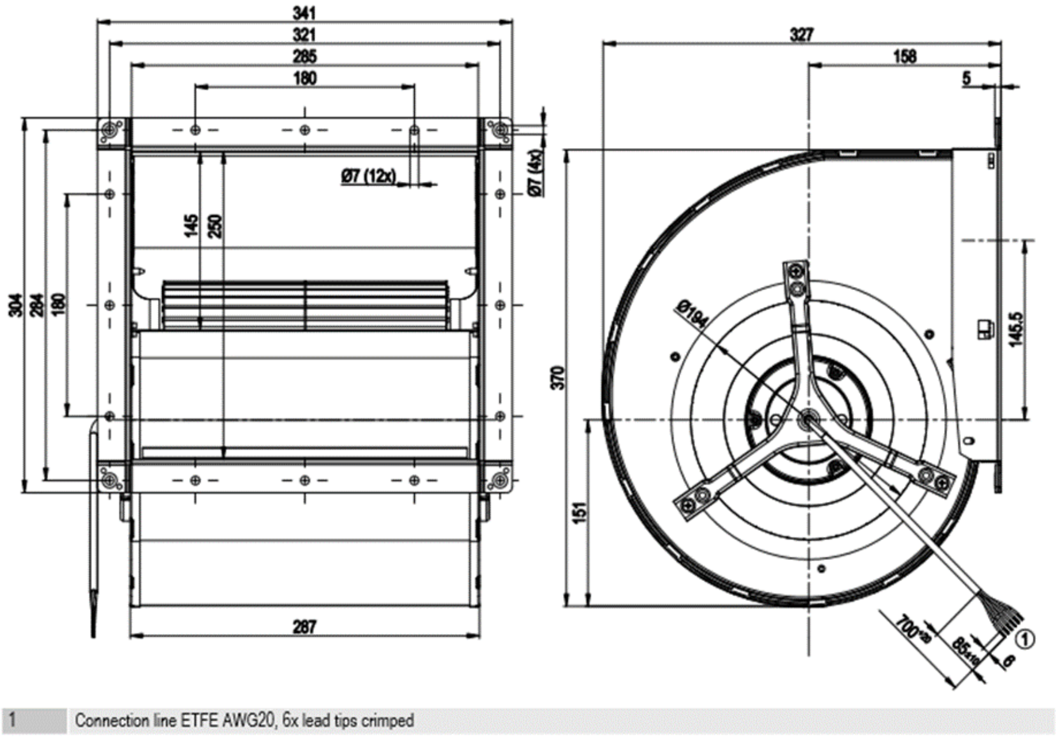

Appendix A (1)

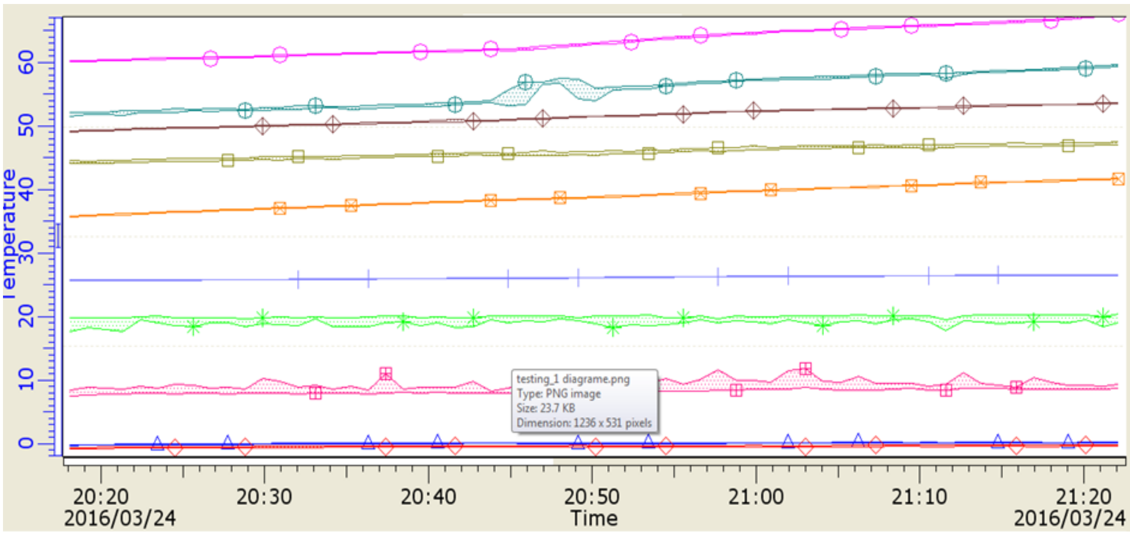

Appendix-B (1): The influnce of 200 W$\cdot$m^{-2} on the system performance

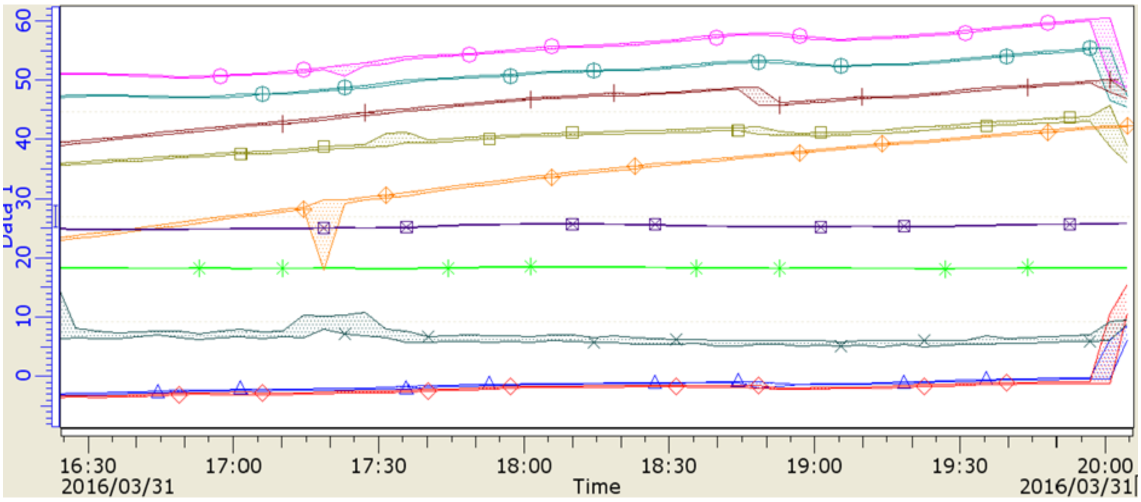

Appendix-B (2): The influnce of 100 W·m^{-2} on the system performance

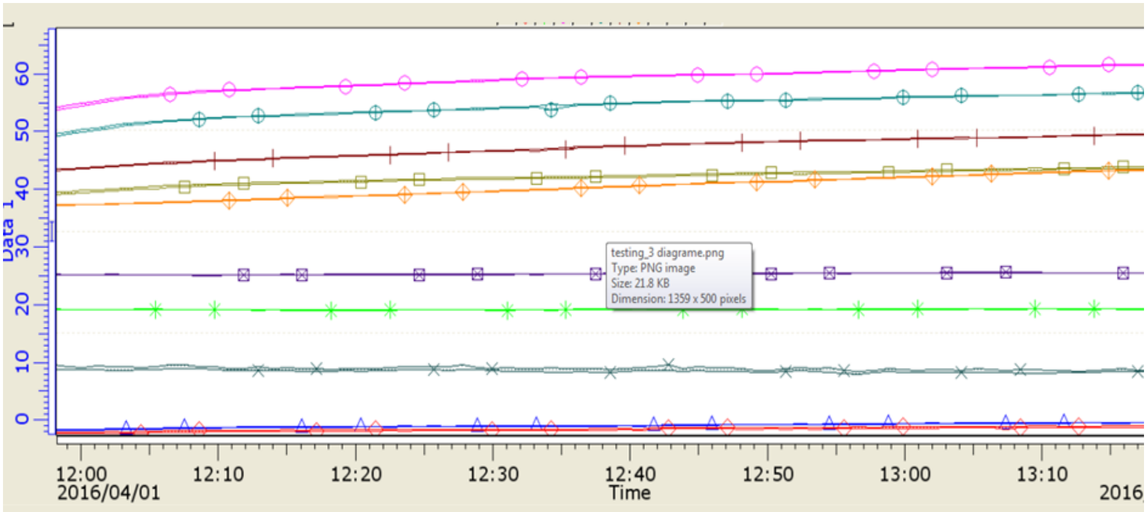

Appendix-B (3): The influnce of 57 W.m-2 on the system performance

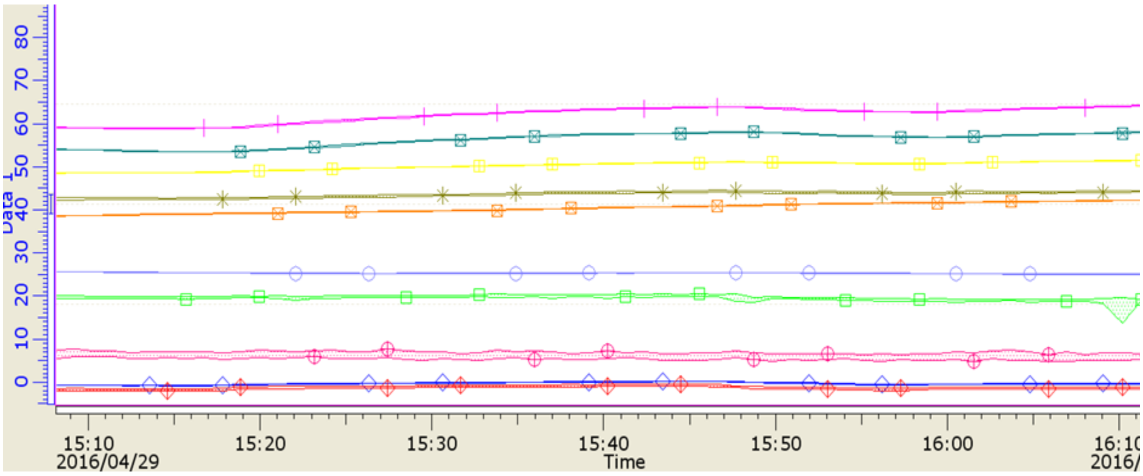

Appendix-B (4): The influnce of 0 W·m^{-2} on the system performance

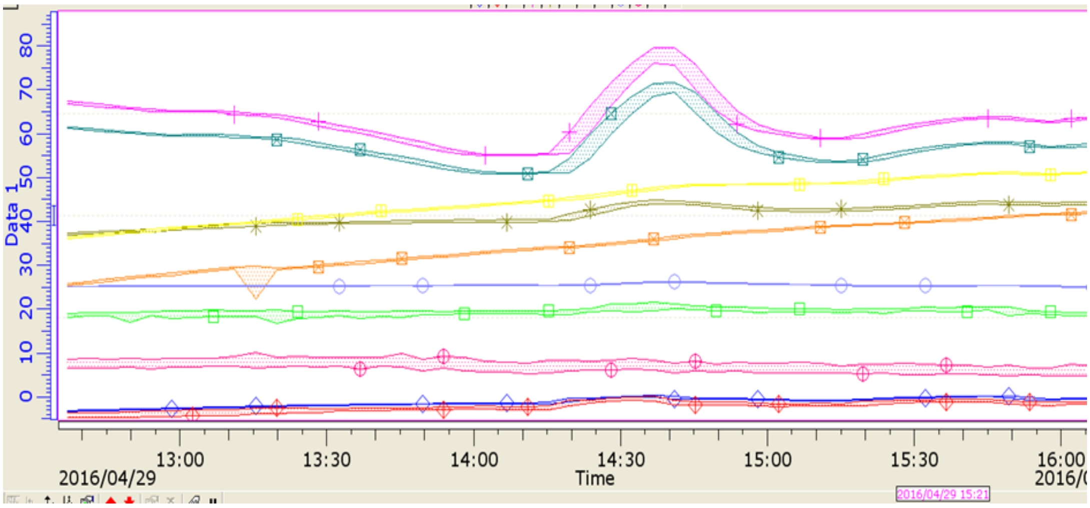

Appendix-B (5): The influnce of 150 W·m^{-2} on the system performance

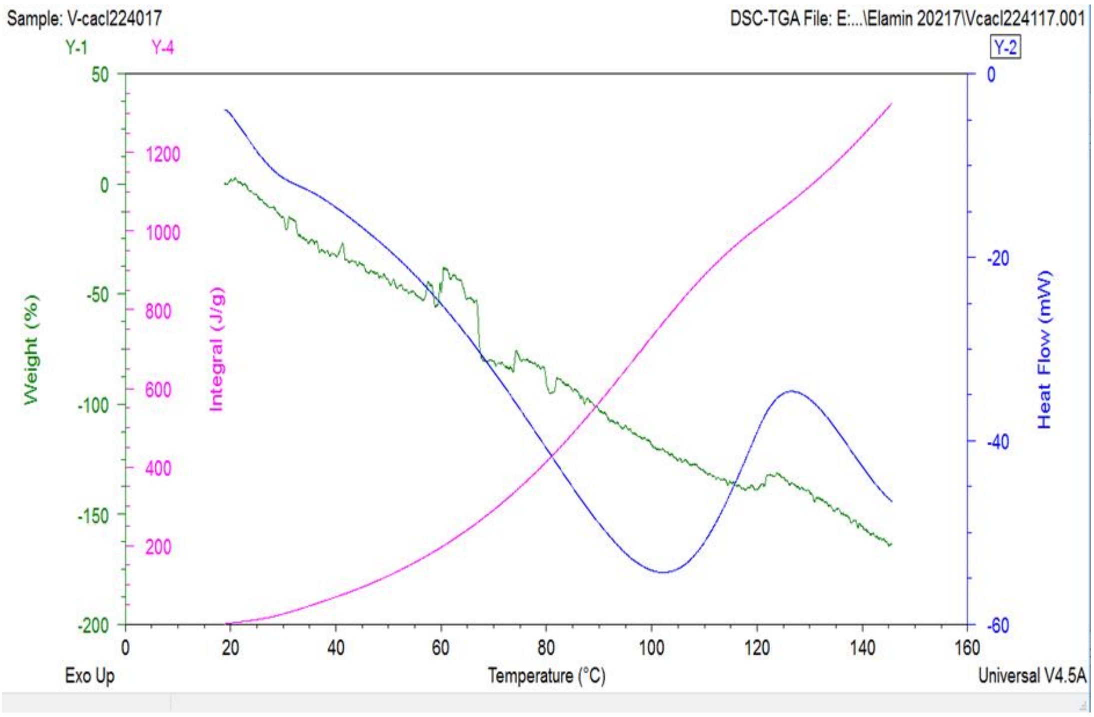

Appendix-C (1)

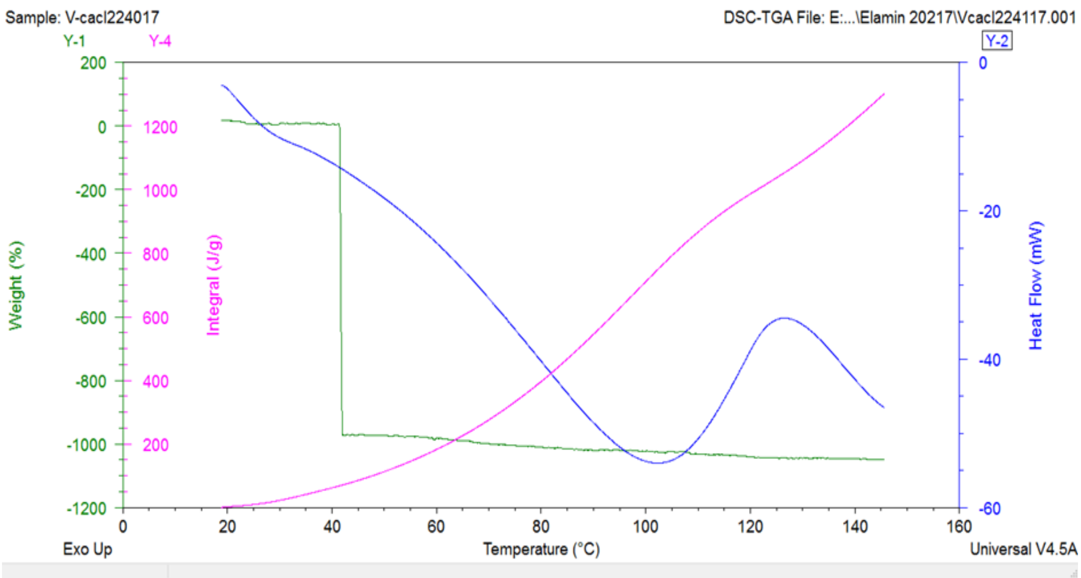

Appendix-C (2)

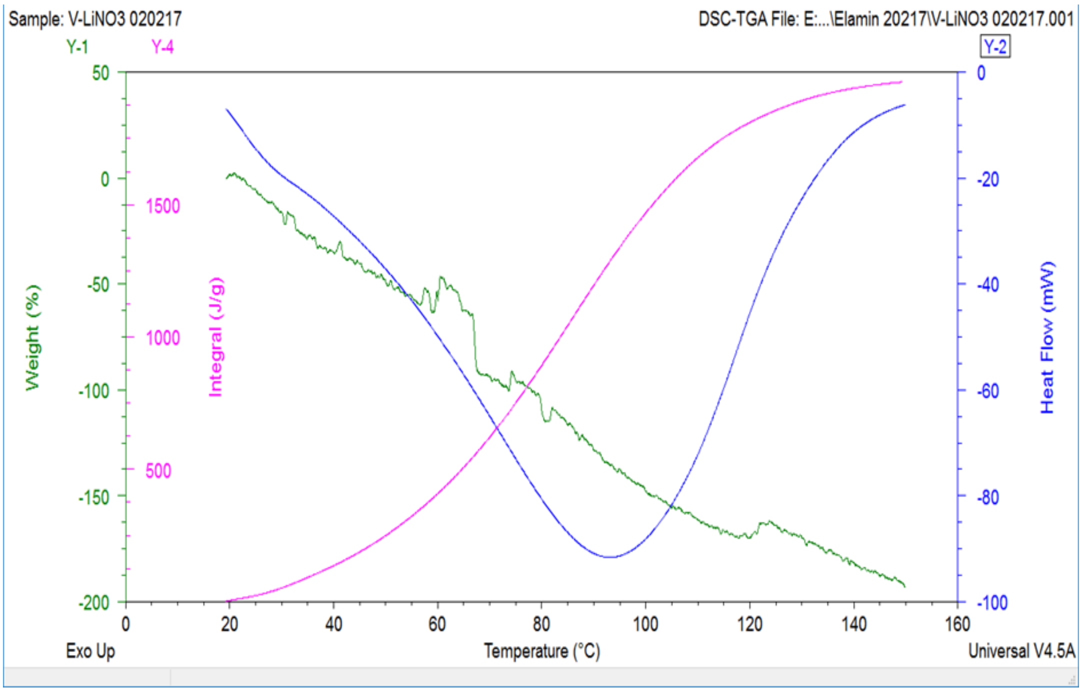

Appendix-C (3)

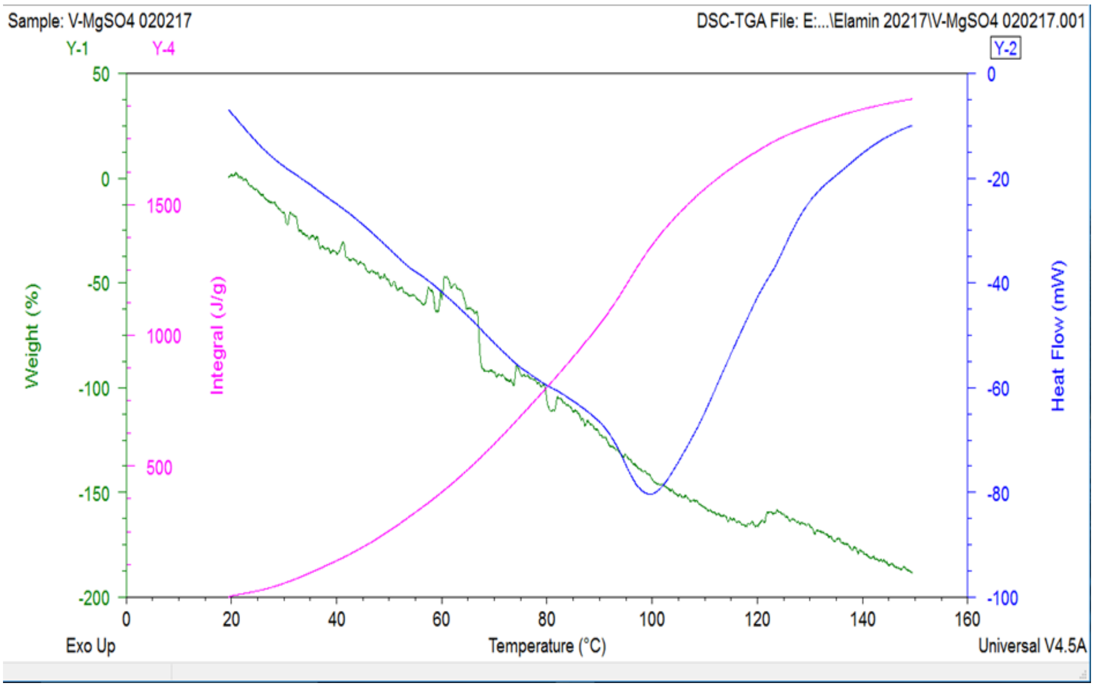

Appendix-C (4)

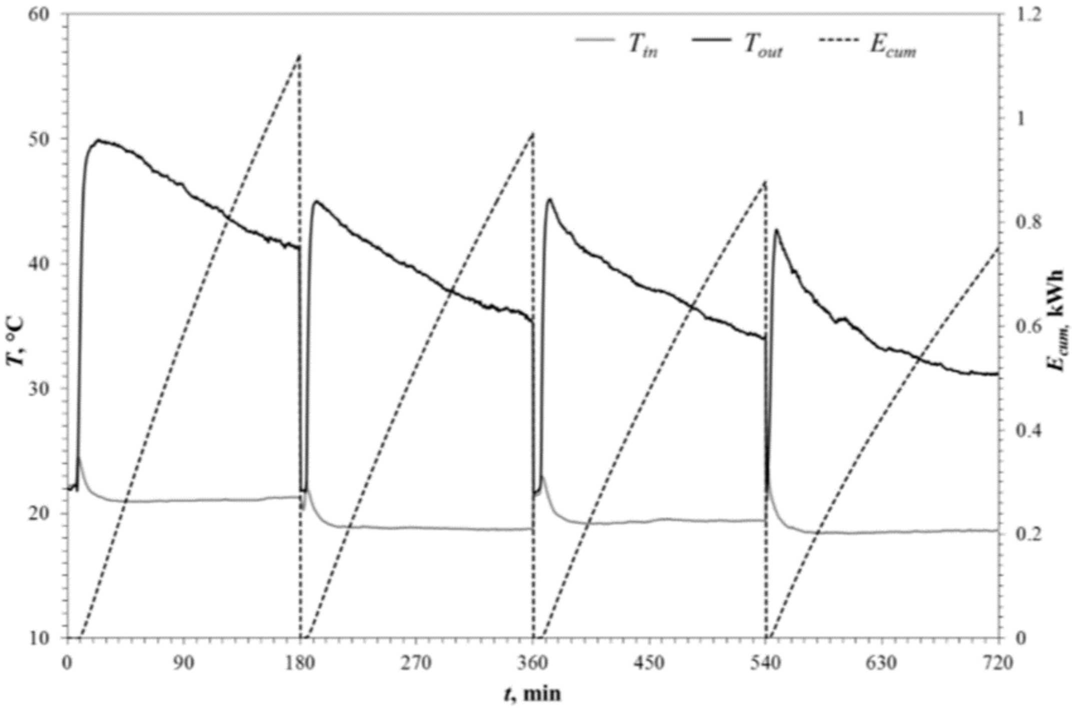

Appendix-D: Cumulative energy and energy output of the small scale test

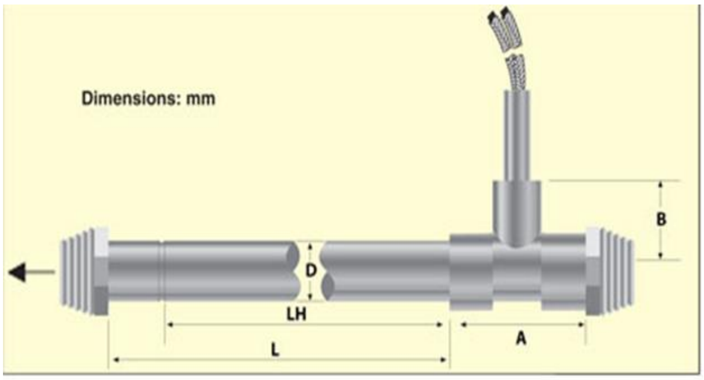

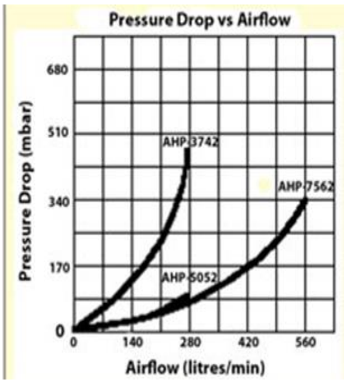

Appendix-F: In line air heater specifications